(1)

DEPARTMENT OF THE AIR FORCE

AIR UNIVERSITY

AIR FORCE INSTITUTE OF TECHNOLOGY

Wright-Patterson Air Force Base, Ohio

AFIT/GE/ENG/88D-61

INVESTIGATION OF THE IMPEDANCE MODULATION OF THIN FILMS WITH A CHEMICALLY-SENSITIVE FIELD-EFFECT TRANSISTOR

THESIS

John M. Wiseman, BSEE
Captain, USAF

AFIT/GE/ENG/88D-6

Approved for public release; distribution unlimited

AFIT/GE/ENG/88D-61

INVESTIGATION OF THE IMPEDANCE MODULATION OF THIN FILMS WITH A CHEMICALLY-SENSITIVE FIELD-EFFECT TRANSISTOR

THESIS

Presented to the Faculty of the School of Engineering

of the Air Force Institute of Technology

Air University

In Partial Fulfillment of the

Requirements for the Degree of

Master of Science in Electrical Engineering

John M. Wiseman, BSEE

Captain, USAF

5 December 1988

Acknowledgements

I would like to thank the many individuals who have provided assistance during this research effort. I am deeply indebted to my thesis advisor, Maj E. Kolesar, for his guidance and support. I greatly appreciate the time he spent in reviewing my work and the many helpful suggestions he provided. I would like to thank James Godfrey for the initial design of the CHEMFET and Kieth Jones and Dave Rapp for their assistance in its redesign. I am grateful for the timely assistance provided by Larry Callahan in mounting and wire bonding the CHEMFET die into the integrated circuit package. I greatly appreciate the technical assistance and equipment maintenance provided by the AFIT Electronics and Materials Cooperative Laboratory Staff.

I would like to thank the EG&G Mound Applied Technology Laboratory, the Armstrong Aerospace Medical Research Laboratory, and the Air Force Flight Dynamics Laboratory support and funds made this research effort possible.

Finally, I wish to express my gratitude and love for my wife [redacted] and my daughters, [redacted] for the support they have given and the sacrifices they have made so that I could pursue my career.

Table of Contents

List of Figures

List of Tables

Abstract

This study resulted in the design and fabrication of a Chemically-Sensitive Field-Effect Transistor (CHEMFET) with an interdigitated gate electrode structure. The electrical performance of the CHEMFET, both in the time-domain and frequency domain, was evaluated for detecting changes in the molecular structure and chemical composition in three thin films: an epoxy, copper phthalocyanine (CuPc), and acetylcholinesterase (ACHE). The change in the chemical state of a film was manifested as a change in the electrical impedance of the interdigitated gate electrode structure. For the epoxy, its molecular structure changed as a result of the curing reaction. To induce a change in the chemical state of the CuPc and ACHE films, they were exposed to part-per billion concentrations of a challenge gas, either nitrogen dioxide (NO_2) or the organophosphorus compound, diisopropyl methylphosphonate (DIMP). The results clearly show that the CHEMFET can detect chemical and structural changes in an epoxy and CuPc film. The sensitivity of the ACHE film was not unequivocally determined due to long term drift in the ACHE film's electrical properties. The most remarkable result of this effort was the demonstration of a unique selectivity feature in the CHEMFET's frequency dependent response to a challenge gas. The examination of the relative changes in

the electrical properties of the CHEMFET at different frequencies showed that the CHEMFET can be used to distinguish between NO_2 and DIMP exposure.

Investigation of the Impedance Modulation of Thin Films with a Chemically-Sensitive Field-Effect Transistor

I. Introduction

Background

The measurement and detection of chemical species and the control of chemical reactions have widespread application. Of particular interest to the military, is the capability to monitor toxic and corrosive chemical compounds (1:1-4; 2:1-28). Two important classes of environmentally-sensitive compounds are chemical warfare nerve agents and oxides of nitrogen. Chemical warfare nerve agents, such as the organophosphorus compounds, are extremely toxic to personnel and may have an ancillary effect on electronic equipment. Oxides of nitrogen are known to evolve from the detonation material of stockpiled munitions as they age, and these compounds cause corrosion of the munition's firing mechanism (3). The military also has substantial interest in the use of composite materials for fabricating military hardware (4). However, the synthesis of a composite material is highly process dependent, and thus, its physical properties may vary within a single batch (5:1). Because of this variability, an in-situ chemical sensor is needed to accomplish

the process control monitoring function. These three applications share a common requirement for a small, sensitive, and selective sensor.

A candidate sensor for the above applications is the Chemically-Sensitive Field Effect Transistor (CHEMFET). In the CHEMFET, a chemically-sensitive film is intimately interfaced with an interdigitated gate electrode of a conventional Metal-Oxide-Semiconductor Field Effect Transistor (MOSFET). Figure I-1 illustrates the CHEMFET structure. The CHEMFET's operation is based on the sensitivity of a field effect transistor's output current to changes in the molecular structure or chemical composition of a thin film that covers the interdigitated gate electrode; the molecular and compositional changes are manifested as changes in the gate impedance. An impedance change in a film can be caused by a chemical reaction (as occurs in the polymerization or cure of an epoxy resin) or by the adsorption of a chemical species (for example, the interaction of a gas with the thin film) (7). An impedance change in the thin film is also anticipated to alter the frequency response of the transistor.

An interdigitated gate electrode CHEMFET has been successfully used to monitor the cure of epoxy films (8). However, this CHEMFET was designed such that the substrate beneath the interdigitated gate electrode was biased , and this situation resulted in the formation of a parasitic capacitance. This parasitic capacitance unnecessarily complicated the analysis of the data collected with this sensor (8).

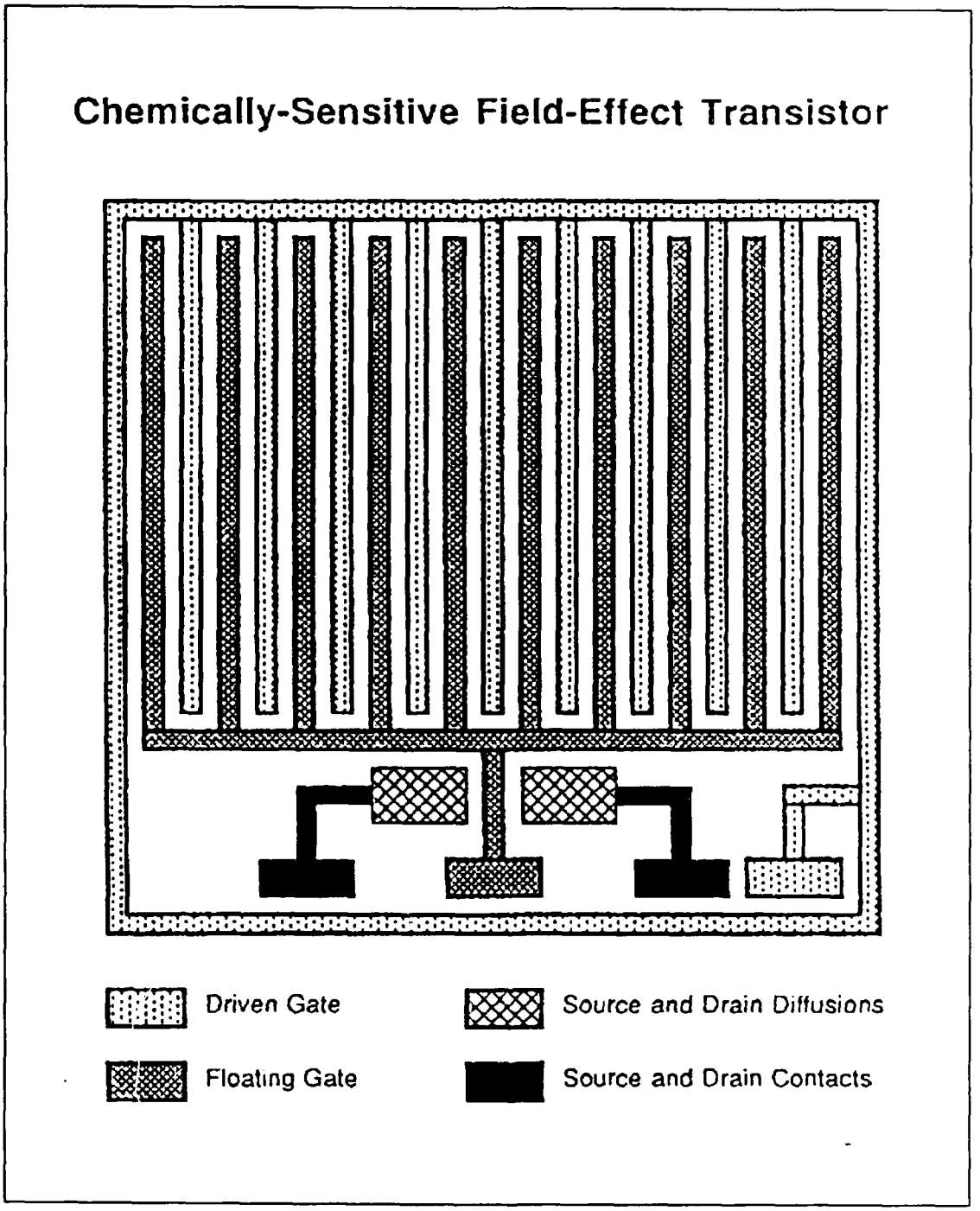

Figure I-1. An Interdigitated Gate Electrode CHEMFET (4).

Problem Statement

The impedance change occurring in thin films resulting from either a chemical reaction or adsorption of a chemical species has not been investigated with an interdigitated gate electrode CHEMFET with an electrically-isolated substrate.

Scope

This project involved the design and fabrication of a CHEMFET with an electrically-isolated substrate for characterizing the impedance properties of thin films. The CHEMFET fabricated was based upon an interdigitated gate electrode CHEMFET designed by a previous thesis student, Capt James Godfrey (GE-87D). The primary modification was the addition of a bond pad to the floating gate to facilitate independent impedance measurements.

The electrical properties of the CHEMFET were investigated with three thin films: an epoxy, a mixture of EPON828 (Miller-Stephenson Chemical Co. Danbury, CT) and VERSAMIDE 40 (Miller-Stephenson Chemical Co. Danbury, CT); the metal-substituted phthalocyanine, copper phthalocyanine (CuPc); and an enzyme, acetylcholinesterase (ACHE). Each film was deposited on the interdigitated gate electrode. No attempt was made to optimize the thin film deposition process for achieving maximum sensitivity or response time to changes in the chemical state of the thin film. Electrical measurements were performed as each film underwent a change in its chemical state.

Assumptions

Throughout this study, it was assumed that the materials used in fabricating the interdigitated gate electrode, including the thin films deposited on the gate, form a linear, and time-invariant system. A condition for linearity is that the superposition principle is applicable; that is, the response of a system to the linear combination of two signals is equal to the sum of the responses produced by each signal applied separately (9:43). This condition implies that the transfer function of the system is independent of the magnitude of the excitation signal. Real systems, in general, are not totally linear. However, any continuous, differentiable function is linear over a range of sufficiently small input values. Thus, a non-linear system may be treated as a linear system provided the excitation signal is sufficiently small that the superposition principle is applicable. A system is time-invariant if its response is independent of the time period over which it is being observed. In this study, since we are investigating the impedance changes resulting from a change in the chemical state of a thin film, the system is not totally time-invariant. However, a time-invariant analysis can be used if the time required to perform any given measurement is short relative to the rate of change of the system's response. This assumption may not necessarily be true for the epoxy cure, especially during the early curing process where the chemical reaction rate is large. For the case where the film's chemical state is reversibly modified by exposure to a gas, the system may be allowed to attain equilibrium before making a measurement.

Approach

CHEMFET Design.

The current interdigitated gate electrode CHEMFET design was modified to incorporate a bond pad to the floating gate electrode structure to facilitate independent impedance measurements. The redesigned CHEMFET was fabricated by the Metal Oxide Semiconductor Implementation Service (MOSIS) (University of California, Berkeley, CA). The devices received from MOSIS were separated into four test groups for analysis with three different thin films, as summarized in Table I-1. The impedance properties of the copper phthalocyanine film were investigated with two different challenge gases: diisopropyl methylphosphonate (DIMP) and nitrogen dioxide (NO_2).

Table I-1. Thin Films and Challenge Gases for the Experimental Test Groups.

Test Group	Thin Film	Challenge Gas
1	Epoxy	----------
2	Copper Phthalocyanine	Nitrogen Dioxide
3	Copper Phthalocyanine	Diisopropyl methyl-phosphonate (DIMP)
4	Acetylcholinesterase	DIMP

Film Deposition.

The thin films were deposited on the interdigitated electrode surface using one of two methods: direct application with a syringe or vacuum electron-beam evaporation. The method of application depended on the type of film to be deposited.

1. Epoxy -- The epoxy was mixed in the desired proportions and directly deposited on the interdigitated gate electrode's surface.

2. Copper Phthalocyanine -- The CuPc was deposited on the interdigitated gate electrode's surface using an electron-beam vacuum evaporation process. To deposit the CuPc film only over the interdigitated gate electrode, a photolithographic mask process was required. This step was complicated by having to perform this process on individual diced integrated circuits (4600 x 6800 μm). Deposition of CuPc by solvent casting was not feasible because of the insolubility of the material in solvents that are compatible with the CHEMFET materials.

3. ACHE -- An aqueous ACHE solution was prepared and directly deposited on the interdigitated gate electrode's surface. The water was then removed by evaporation.

Test and Evaluation of the Chemically-Sensitive Thin Films.

The test and evaluation measurements were accomplished as the films underwent a change in their chemical state. For the epoxy, this was simply the result of the curing reaction. To induce a change in the chemical state of the CuPc films, it was exposed to two challenge gases: nitrogen dioxide (NO_2) or diisopropyl methyl-

phosphonate (DIMP). Nitrogen dioxide was selected to act as a model compound for the nitrous oxides which exist in stockpiled munitions. DIMP was selected to act as the model compound for chemical warfare nerve agents. The sensitivity of CuPc to nitrogen dioxide and dimethyl methylphosphonate (DMMP), a structurally related compound to DIMP, has been reported in literature (7:155-165). DMMP was not selected as the model compound because of its greater toxicity. The challenge concentration range differed for the two gases. The NO_2 concentration spanned 20-400 parts-per-billion (ppb). The DIMP concentration spanned 40-4000 ppb. The measurements were performed at a temperature of 105°C. Similarly, to induce a change in the ACHE film, it was exposed to DIMP in a high humidity environment at 105°C. The DIMP challenge concentration was in the range of 0.5 - 10 parts-per-million (ppm). To deliver these gaseous challenges, a gas generation and delivery system, along with a test fixture for the device under test, were designed and fabricated. Since water affected the impedance of all three films, the humidity of the gases delivered to the test fixture was monitored and controlled.

Electrical Measurements.

The electrical measurements were similar for all three films. For the CuPc film, these measurements were repeated at each NO_2 and DIMP gas exposure concentration. During a given experiment, the ACHE film, was exposed to a single DIMP concentration and the measurements were made as a function of exposure time. The initial range of NO_2 and DIMP concentrations selected for the CuPc film were based upon the published sensitivity to these gases (7:155-165; 10). The

impedance of a film and its gain-phase response were measured at selected frequencies spanning 5 Hz-13 MHz. Additionally, the resistance was measured using an electrometer. The gain-phase measurements were made separately across the interdigitated gate electrode, across the entire device from the driven gate to the output drain voltage, and across the FET from the floating gate to the output drain voltage. These measurements were used to determine the effect of the individual CHEMFET components (the interdigitated gate and the transistor) on the overall response of the CHEMFET sensor.

The frequency spectrum of the input and output time-domain waveforms of the CHEMFET was measured using a FFT analyzer. For these measurements, the driven gate of the CHEMFET was excited with a 4 V, 50 μs voltage pulse at 256 Hz.

Plan of Development

Chapter II reviews the current research literature concerning solid state sensors for detecting organophosphorus compounds, nitrogen oxides, and the cure monitoring of epoxy films. Chapter III discusses the theory concerning impedance measurements using a CHEMFET. Chapter IV describes the experimental methodology and includes a discussion of the CHEMFET design, film deposition, gas generation and delivery system design, and the electrical measurements. The findings and results are presented in Chapter V, and the recommendations and conclusions are given in Chapter VI.

II. Literature Review of Solid State Sensors for Organophosphorus Compounds, Nitrogen Oxides and Epoxy Cure Monitoring

During the past decade a number of solid state chemical sensors have been developed (6,7,11:109-127) which are based on measuring some electrical property that is a function of the chemical state of a thin film. The chemical state of the film changes when it undergoes a chemical reaction (as occurs with the polymerization or cure of an epoxy resin) or when it interacts with another chemical species. The purpose of this paper is to review the current research in solid state sensors for detecting organophosphorus compounds, nitrogen oxides, and cure monitoring of epoxy films. The solid state sensors that have been developed for each application are treated in separate sections. Within each section, the thin films investigated and the different types of solid state sensors are discussed.

Organophosphorus Compound Sensors

There are four types of solid state sensors which have been investigated for detecting organophosphorus compounds: the piezoelectric sorption detector (12:1764-1768; 13:43-47; 14:2057-2060), the notch filter detector (15), the chemiresistor (7:155-165; 15:410-413), and the Chemically-Sensitive Field-Effect Transistor (CHEMFET) (17:666-671; 18). In this section, a description of each of these sensors and the films used to detect organophosphorus compounds are presented.

Piezoelectric Sorption Detector.

When an electric field is applied to a piezoelectric crystal, a force is exerted on the bound charges within the crystal (19:424). This force causes small deformations in the size and shape of the crystal. Depending on the polarity of the applied field, the crystal experiences either compressive or tensive forces. If a time-varying electric field is applied, the bound charges will oscillate.

In 1964, King (20:1735-1739) developed a sensitive and selective gas detector using a piezoelectric crystal coated with a material capable of selectively interacting with various gases. The interaction may involve both adsorption and absorption, and hence the term "sorption". The oscillation frequency of the crystal depends on the mass of the coating and the mass of the vapor which interacts with the coating. The relationship between the total mass of the coating, and the change in the crystal's resonant frequency is given by (12:1764-1768):

$$\delta F = -2.3 \times 10^6 F^2 (\delta mf/A) \qquad (2.1)$$

where δF = the change in the crystal's resonant oscillation frequency due to the coating (Hz)

F = the fundamental frequency of the piezoelectric crystal (MHz)

δmf = the mass of the coating (grams)

A = surface area of the coated crystal (cm^2).

A change in the mass of the coating due to sorption or desorption of a vapor, will result in a change in the crystal's resonant frequency. The mass sensitivity of a piezoelectric detector with a 9 MHz fundamental resonant frequency was estimated to be approximately 400 Hz/microgram (12:1764-1768). King estimated the detection limit of the piezoelectric detector to be approximately 1 picogram (20:1735-1739).

A number of coatings have been investigated for detecting organophosphorus compounds using the piezoelectric detector. In 1972, Schiede and Guilbault (12:1764-1768) evaluated a piezoelectric crystal detector that was coated with various inorganic salts for sensitivity and selectivity toward the organophosphorus compounds, diisopropyl methylphosphonate (DIMP) and paraoxon (O,O-diethyl-o-p-nitrophenol phosphate). The inorganic salt with the highest sensitivity (ferric chloride) could detect organophosphate concentrations less than 10 ppm with a response time less than 15 minutes for both DIMP and paraoxon. In order to obtain a reproducible response, the ferric chloride film was preconditioned with repeated exposure to the organophosphorus compound under evaluation. The response of the ferric chloride coating to interferences from dry air, laboratory air, nitrogen dioxide, carbon dioxide, and water were shown to be negligible. More recently, Guilbault and his co-workers (13:43-47; 14:2057-2060) have reported additional piezoelectric crystal detector coatings with sensitivities to organophosphorus compounds in the parts per billion (ppb) range.

Notch Filter Detector.

A notch filter detector for organophosphorus compounds has been developed by Kolesar (15). A notch filter is an electrical network which has a null in its transfer function. When a sinusoidal excitation signal at the null frequency is applied to the input of the network, it is not transmitted to the output of the network (15). The notch filter sensor's operation is based on detecting changes in the null frequency and the depth of the null resulting from changes in the conductivity of discontinuous metallic thin films upon exposure to a gas. A notch filter consists of a highly conducting electrode, a dielectric layer, and a resistive electrode. In the notch filter detector for organophosphorus compounds, a discontinuous copper and cuprous oxide films were used for the resistive electrode. Kolesar presents a review of the theoretical models for the conduction processes in discontinuous metallic thin films and a discussion of the possible mechanisms for the change in the conductivity of the films upon exposure to a gas (15).

Chemiresistor Detector.

The chemiresistor detector measures the change in the conductivity resulting from the interaction of a chemical species with a semiconductor (21:1170-1174). The structure of a chemiresistor is illustrated in Figure II-1. Barger and co-workers (16:410-413) evaluated a number of organic derivatives of phthalocyanine (Pc) and metal-substituted phthalocyanines (MPc) for sensitivity to dimethyl methylphosphonate (DMMP). The nickel-Pc film showed the greatest sensitivity to DMMP by manifesting a 128 percent change in its conductivity after exposure to a

10 μg/ml DMMP challenge. The Pc derivative films were deposited via the Langmuir-Blodgett technique over interdigitated gold electrodes supported on a quartz substrate. The authors reported that films deposited by sublimation took 5-25 minutes to respond to the test gas and several hours to return to their initial conductivity after removal from the gaseous challenge. By comparison, the Langmuir-Blodgett films were exposed for only 100 seconds prior to measuring the steady-state conductivity change, and were completely reversible within 60 seconds.

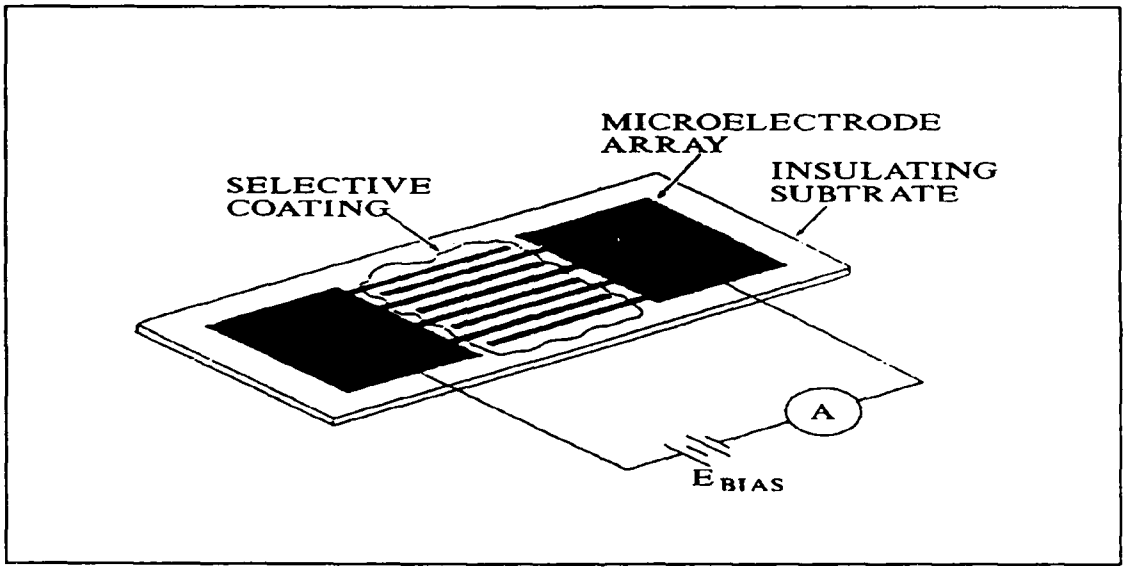

Figure II-1. Chemiresistor Structure (21).

Chemically-Sensitive Field-Effect Transistor (CHEMFET) Detector.

The CHEMFET is a chemical sensor whose operation is based on the sensitivity of a field-effect transistor's channel resistance to changes in the chemical composition of its gate electrode (22:107-174). In the CHEMFET, a chemically sensitive film replaces the metal gate of a conventional Metal-Oxide-Semiconductor

Field-Effect Transistor (MOSFET). The film selectively interacts with a chemical species, and through an electrochemical process, generates a voltage across the film which modulates the channel of the MOSFET through the field-effect mechanism.

The potential application of a CHEMFET for detecting organophosphorus compounds was recently assessed (17:666-671). Four types of CHEMFET structures were evaluated: enzyme-coupled, galvanostatic, catalytic, and work-function. The evaluation criteria were a sensitivity of 1-10 ppb, a response time of less than 10 seconds, complete reversibility in 30 seconds, a shelf-life of 6 months, and an operational life of 10 days of continuous use. Based on these criteria, the work-function CHEMFET was ascertained as the optimum candidate.

The work-function CHEMFET requires a gate material whose work- function, or Fermi energy level, can vary over several orders of magnitude in response to absorbing small concentrations of a chemical contaminant. A material possessing this property is likely to be a semiconductor. Furthermore, to interact specifically with an organophosphorus compound, the material will probably have to be an organic compound (17:666-671). Recently, the role of semiconducting polymers as sensitive elements in physical and chemical sensors has been reviewed (23:129-144). The electrical properties of the organic semiconductors can be changed by several orders of magnitude in a process analogous to doping (17:668). Doping is achieved by modifying the polymer chain in such a way that electrons are donated to, or accepted from, the polymer's conduction band.

A semiconducting polymer membrane composed of 39 percent poly(vinyl pyrrolidone), 39 percent poly(vinyl alcohol), and 22 percent Cu(II)(bipyridyl) was investigated as a potential gate electrode coating for a CHEMFET (18). Although the resistance of this membrane was shown to decrease upon exposure to DIMP, it could not be used as the gate material for a CHEMFET because the resistance change was due to changes at the metal-polymer contact and not to changes in the bulk resistivity of the membrane. However, the material could be used as the gas-sensitive element in an impedance bridge. The detection limit for DIMP using the impedance measurement technique was 1 ppm with a response time of 25 seconds. The sensitivity of the impedance measurement technique was found to decrease with increasing frequency.

Nitrogen Oxide Sensors

Solid state sensors for nitrogen oxides reported in the literature include: chemiresistors, surface acoustic wave (SAW) chemosensors, and CHEMFETs. These sensors detect changes in the electrical impedance, acoustic transport properties, or work-function of a chemically-sensitive film. Both inorganic and organic semiconductor thin films have been investigated for use in nitrogen oxide sensors. However, most of the current research has been directed towards one class of organic semiconductors, the phthalocyanines (Pc) and their metal-substituted phthalocyanine derivatives (MPc). Since the phthalocyanines are tetrabenz derivatives of tetra-azoporphyrins (24:852-854), other porphyrins have also been investigated for this application: mesoporphyrin IX and tetra-arylporphyrin complexes (25:151-156).

In this section, each type of nitrogen oxide sensor and the films used with each configuration are reviewed.

Chemiresistor Detector.

Chang and Hicks (7:58-70) developed a chemiresistor using the inorganic semiconductor, tin oxide. When the device was heated to 250°C and exposed to nitrogen oxides, the resistance of the tin oxide film increased. This device, when operated at 250°C, was capable of detecting nitrogen oxides at a concentration of 10 ppm.

Jones and Bott (10:27-37) conducted a study concerning the conductivity of MPc films using a chemiresistor. Lead Pc (PbPc), cobalt Pc (CoPc), copper Pc (CuPc), zinc Pc (ZnPc), and nickel Pc (NiPc) were deposited on an interdigitated platinum electrode array by thermal evaporation. Each of these films were exposed to five concentration levels of nitrogen dioxide mixed with air spanning 2.8 to 44 ppb; each sensor's response was documented for eight different temperatures spanning 100 to 170°C. Figure II-2 shows the effect of temperature on the response of several of the MPc's to a 44 ppb NO_2 challenge. At 170°C, the sensitivity of the films to a 44 ppb nitrogen dioxide decreased in the following order: PbPc > ZnPc > CuPc > CoPc. The sensitivity of PbPc, expressed as a percentage change in the film's conductivity, was 185 percent at 170°C and 44 ppb nitrogen dioxide. There are a number of possible interferents for this sensor. Barger and his co-workers (7:155-165) reported on the relative sensitivity of Pc and MPc films to sulfur dioxide, benzene, air, ethanol, water, dimethyl methylphosphonate, and

ammonia. The conductivity of the chemiresistors increased or decreased depending on the Pc variant, and on the particular challenge vapor and its concentration. The results are summarized in Table I-1. The response of the metal-free phthalocyanine (H_2) enclosed in parentheses in Table I-1 were extremely variable.

Chemiresistor nitrogen oxide detectors using Pc and other porphyrin films, deposited using the Langmuir-Blodgett technique, have also been developed (7:155-165; 21:1170-1174; 25:151-156; 26:260-263). The phthalocyanines were chemically modified to increase their solubility in organic solvents, such as chloroform. Chemiresistors fabricated with Langmuir-Blodgett films have greater sensitivity, and faster response and recovery times (7:155-165). The chemiresistor, using the Pc film, could detect less than 10 ppm concentration levels of nitrogen dioxide at room temperature (26:260-263). Furthermore, the device had a 30 second response time to a 120 ppm nitrogen dioxide challenge concentration. By comparison, the chemiresistors which used other porphyrin films could also detect nitrogen dioxide in the ppm range at room temperature (25:151-156). As shown in Figure II-3, the porphyrin chemiresistors required a minimum of 100 minutes for the conductivity to reach a steady-state value after exposure to nitrogen dioxide. The response times were shown to depend on the film's thickness. For the chemiresistors discussed above, the conductivity of the film was measured using a direct current (DC) excitation signal. An alternative approach is to measure the change in the harmonic content of an alternating current (AC) excitation signal that passes through the chemiresistor during gas exposure. A nitrogen oxide chemiresistor utilizing this

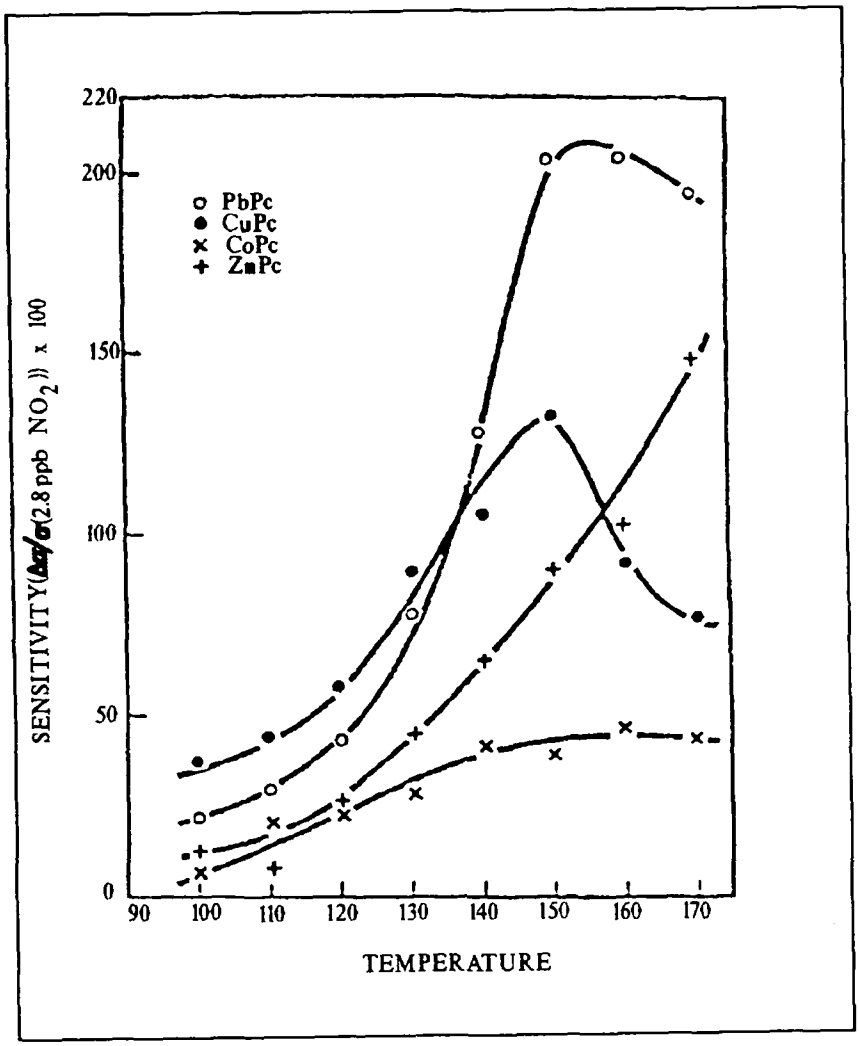

Figure II-2. Sensitivity Variation of MPc as a Function of Temperature (10).

Table I-1. Maximum Percent Change in Relative Conductivity for Sublimed Phthalocyanine Films Exposed to Vapors (7:159).

Vapor	Concentration (ppm)	Phthalaocyanine Type					
		H_2	Fe	Co	Ni	Cu	Pb
Ammonia	100	-41	-36	-72	-51	-81	-24
Dimethyl methyl-phosphonate	100	+23	-10	-7	-5	-21	-51
Sulfur Dioxide	100	+10	+28	-9	+11	+3	-8
Ethanol	1000	(+18)	-11	-5	-1	-15	-4
Water	1000	(+21)	-11	-5	-5	-15	-6
Air	1000	(+25)	-4	-5	+2	0	-8
Benzene	1000	(+11)	-1	-2	+6	-2	+4

concept was investigated by Khanna and his co-workers (25). Their device was a multilayer, thin-film structure consisting of an aluminum/aluminum oxide/cobalt Pc (CoPc)/gold sandwich. A 200-300 Å CoPc film was deposited by thermal evaporation. Upon exposure to nitrogen dioxide, the current in the first harmonic increased, while the current in the second harmonic decreased. A response could be measured for nitrogen dioxide concentrations as low as 1 ppb. The response time was on the order of 1 minute.

Surface Acoustic Wave Detector.

The principle of operation for the surface acoustic wave detector can be explained utilizing the same theoretical principles discussed relative to the piezoelectric sorption detector (28:45-62). The change in mass resulting from the

absorption of a chemical species by a coating on the SAW sensor changes the propagation properties of the surface acoustic waves traveling across the device's surface.

Nieuwenhuizen and his co-workers developed a dual delay line oscillator SAW sensor for detecting nitrogen oxides (29:148-154). Two identical delay lines were fabricated on a piezoelectric quartz substrate. On the acoustic path of one delay line, a Pc film was deposited by thermal evaporation. Interaction of the Pc film with a

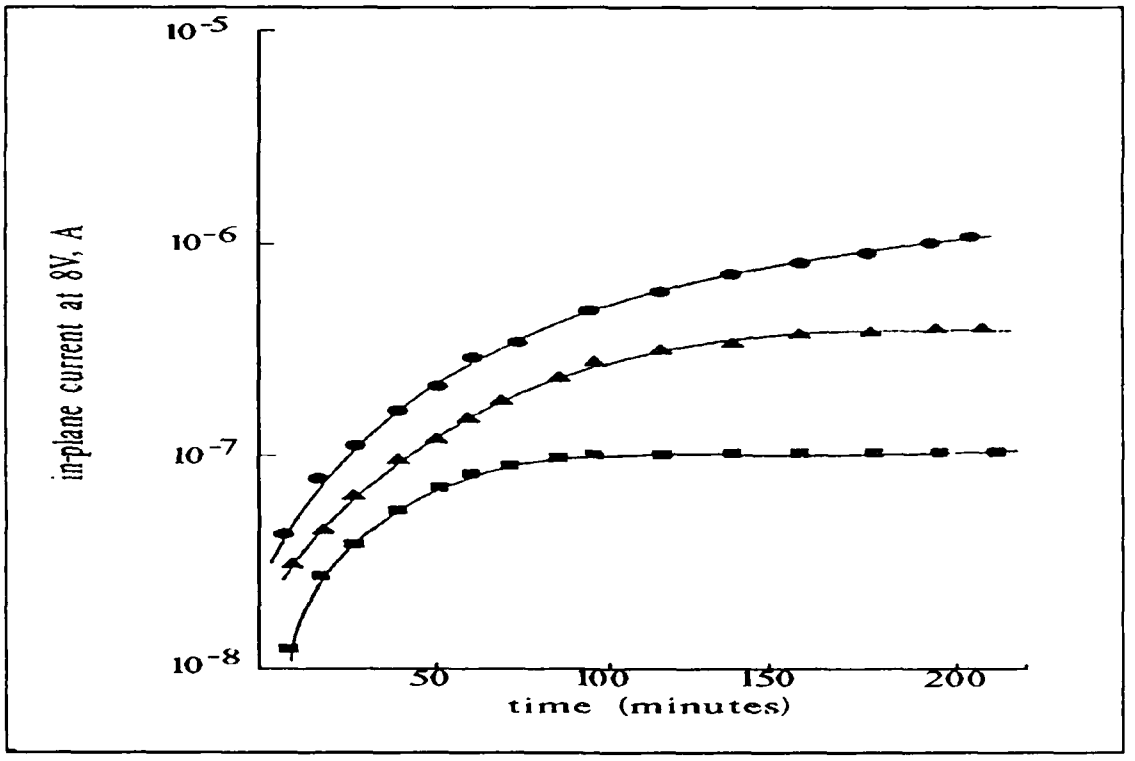

Figure II-3. Current at an Applied Voltage of 8 Volts Across a Meso-porphyrin Film: a) 7, b) 15, c) 25 Layers Thick (25).

nitrogen dioxide challenge caused a change in the phase velocity of the acoustic signal, which was detected as a change in the frequency of an oscillator circuit containing the sensor. The detection threshold for nitrogen dioxide with this sensor design was 0.5 ppm, and the sensitivity to nitrogen dioxide was 100 Hz/ppm. In a separate report (30:230-235), a SAW sensor coated with different MPc films were evaluated using a number of gases (nitrogen dioxide, carbon monoxide, methane, ammonia, sulfur dioxide, water and toluene). The results revealed that cobalt Pc possessed the greatest selectivity and sensitivity for nitrogen dioxide at 150°C, and copper Pc possessed the best response time.

CHEMFET Detector.

A CHEMFET sensitive to nitrogen dioxide has been developed (31:L111-L113). In this device, lead Pc was deposited by thermal evaporation directly onto the gate oxide of a field effect transistor. A change in the threshold voltage was observed when the device were equilibrated at 60°C for 8 hours with several concentration levels of nitrogen dioxide. A linear relationship between the threshold voltage and the logarithm of the nitrogen dioxide concentration was observed over the concentration range of 20-100 ppb. The detection limit for this device was below 20 ppb, and the response time was several days for nitrogen dioxide concentrations below 10 ppb.

Epoxy Cure Sensors

Only one solid state sensor for monitoring the cure of epoxy resins was found in the current literature: the charge-flow transistor (CFT) or microdielectrometer

(7:166-176). The monitoring of epoxy cure with the CFT is based on the change in the material's complex dielectric constant during its cure (32:22-36).

The first CFT was a conventional MOSFET with a split metal gate electrode over which a resistive material was deposited as shown in Figure II-4 (33:106-108;34:17). Since the metal gate rapidly charges when a voltage is applied, the turn-on characteristic of the MOSFET is determined by how rapidly the resistive material can be charged to the device's threshold voltage. The electrically-conductive channel

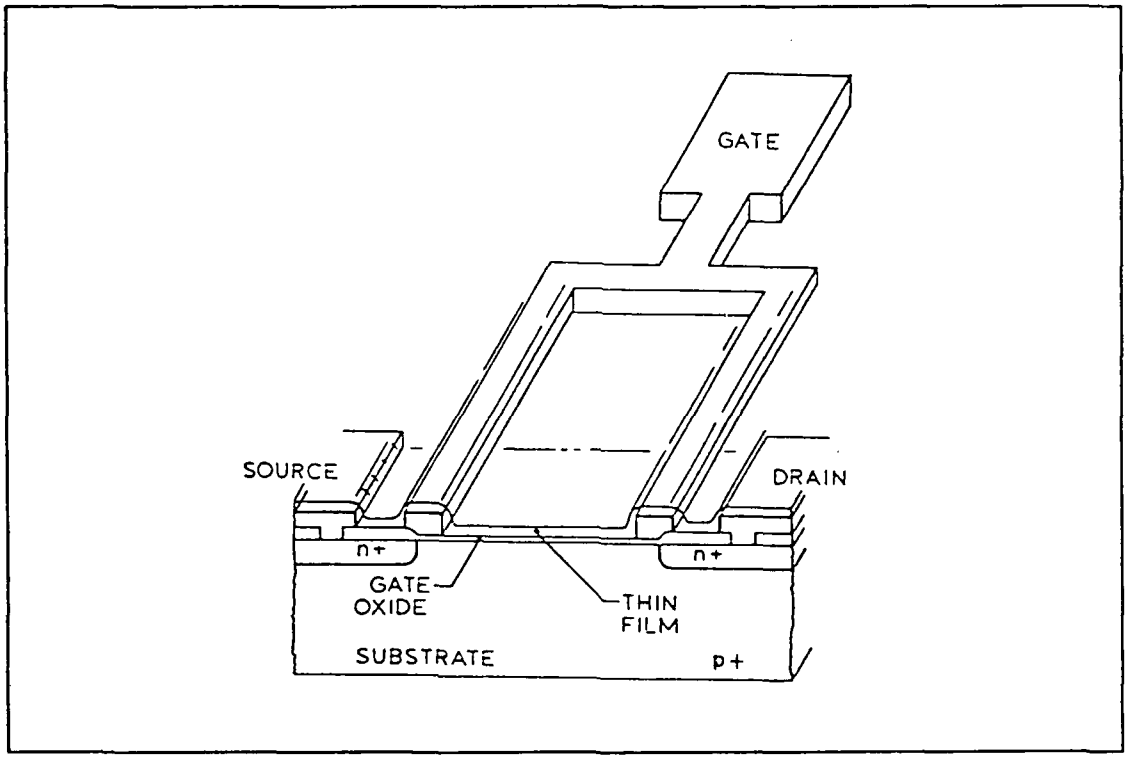

Figure II-4. Structure of Original Charge Flow Transistor (34).

will not form under the gate oxide until both the metal and the resistive film are uniformly charged to the threshold voltage. Thus, there is a time delay between the application of a voltage to the gate electrode and the formation of the conductive channel. This CFT design has an asymmetric switching characteristic. Device turn-on is delayed by the requirement for a complete channel, but it may be turned-off when the voltage on the metal gate structure is reduced below threshold. A second CFT design eliminates the asymmetric switching characteristics by isolating the driven gate outside of the channel region. A cross-section of this device is shown in Figure II-5.

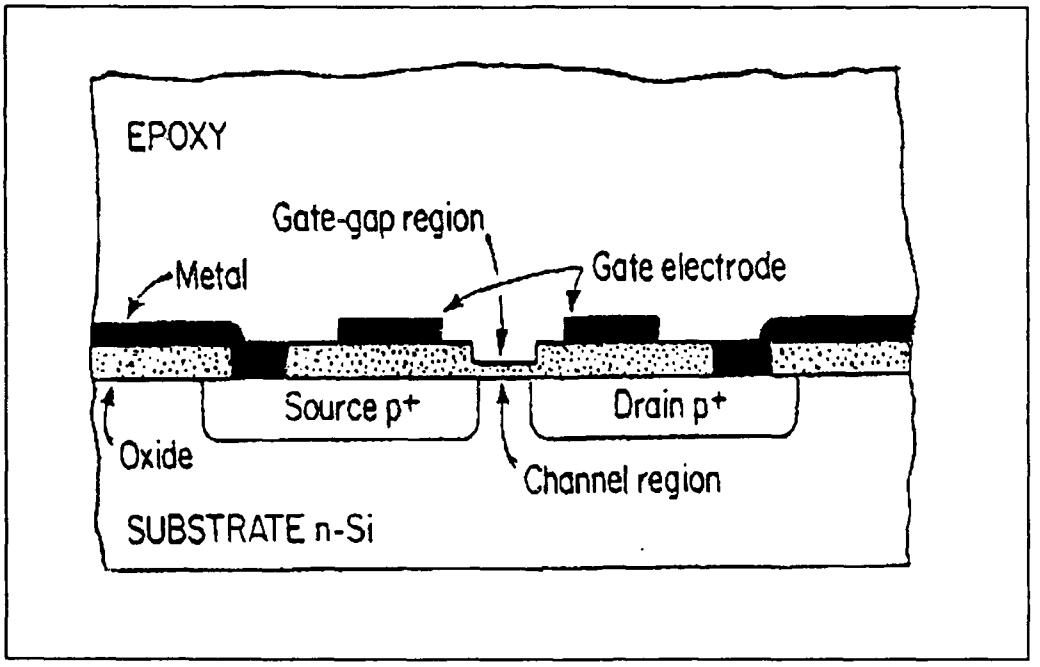

Figure II-5. Modified CFT Design to Eliminate Asymmetric Switching Characteristics (35).

The feasibility of applying the CFT to dielectric cure monitoring was investigated by Senturia and his co-workers in 1979 (35). In this study, the cure of a commercial epoxy was monitored with each CFT design. The epoxy was applied to the gate of a CFT and the change in the drain current's time-domain waveform, as shown in Figure II-6, for the modified CFT, was observed as the epoxy hardened. In addition to the CFT, an interdigitated electrode was fabricated to measure the low frequency dielectric constant, ϵ', and loss factor ϵ" (see Chapter III for a definition of these terms). During the first ten minutes of the cure cycle, ϵ' and ϵ" were large, and they decreased sharply as the chemical reaction proceeded. The change in the drain current's waveform was related to the change in the complex dielectric constant using a lumped element RC circuit model. The authors assumed that the film's resistance (R) in the model behaved like $1/\epsilon$", and that the film's capacitance (C) behaved like ϵ'. Since both ϵ' and ϵ", as measured with the interdigitated electrode, behaved similarly during cure, it was further assumed that their product (RC) would be constant. Using these assumptions, current waveforms were calculated and shown to be similar to the measured waveforms. The CFT was redesigned to eliminate nonlinearities in the device characteristics (36:65-76). The redesigned CFT combines an interdigitated electrode array with a field effect transistor. A commercial microdielectrometer became available in 1983 which combines this sensor with some external electronics for determining the transfer function of the interdigitated gate electrode (37:14). The complex dielectric constant

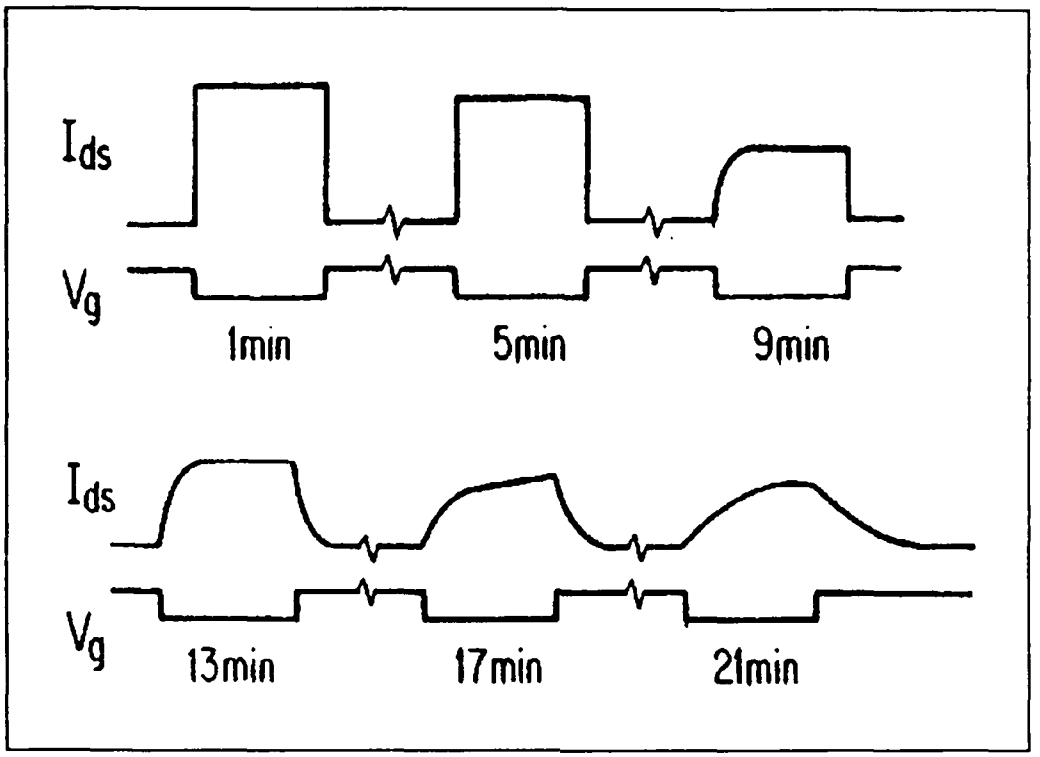

Figure II-6. Typical CFT Current Waveforms Obtained During the Epoxy *Cure using Pulse Excitation* (35).

can be extracted from the gain and phase of the transfer function using calibration curves (8).

Summary

Several types of solid state sensors have been investigated for detecting organophosphorus compounds and nitrogen oxides. Detection of organophosphorus compounds has been accomplished with piezoelectric sorption sensors, notch filter detectors, chemiresistors, and CHEMFETs. Nitrogen oxides have been detected with chemiresistors, SAW sensors, and CHEMFETs. The films used for detecting organophosphorus compounds include: inorganic metal salts (ferric chloride),

discontinuous metal films, and semiconducting polymers. The films used for detecting nitrogen oxides include: inorganic (tin oxide) and organic (phthalocyanines) semiconducting films. Since the tin oxide sensors must be heated to hundreds of degrees Celsius, most of the current research concerning nitrogen oxide sensors involves various phthalocyanine and metal-substituted phthalocyanine films whichoperate at lower temperatures. The detection limit for the most sensitive organophosphorus and nitrogen oxide sensors is in the ppb range.

A solid state sensor developed for monitoring the cure of epoxy and polymer resins is the charge flow transistor (CFT). The CFT combines an interdigitated electrode array with a field effect transistor. The change in the complex dielectric constant resulting from the cure of an epoxy resin changes the transfer function of the interdigitated electrode. The complex dielectric constant can be extracted from the transfer function's gain and phase using calibration curves.

III. Theory of CHEMFET Impedance Measurements

This chapter describes the theory of the impedance measurements of materials using an interdigitated gate electrode CHEMFET design. The first section discusses the fundamental behavior of materials in electric fields. The admittance (or equivalently, the impedance) is defined in terms of the complex permittivity (ϵ^*), and the frequency-dependency of ϵ^* is related to the alignment of microscopic electric dipoles. The second section describes the methods available for measuring electrical impedance. The last section discusses the analysis of the interdigitated gate electrode response.

Behavior of Materials in an Electric Field

The total electric current density (J_T) which flows in a material as the result of an applied electric field consists of two components: a conduction current density (J_c) and a displacement current density (J_d). The conduction current density results from the transport of free charges, such as electrons and ions, within the material. The displacement current density results from the motion of electric dipoles, which are produced by bound charges within the material as they align with the applied electric field. The alignment of the dipoles is referred to as polarization (36:35-39).

The polarization of a material is composed of four components (36, 31): electronic, atomic, orientational, and interfacial polarization. Electronic polarization results from the slight displacement of an atom's electrons with respect to the positively charged nucleus. The magnitude of electronic polarization is small since

a large intra-atomic field allows only a small displacement of the electrons. Atomic polarization results from the distortion of atoms within a molecule or crystal lattice. The magnitude of atomic polarization is usually small, since the inter-atomic bond strength allows only small displacements. Orientational polarization results from the alignment of randomly oriented, permanent dipoles existing within a material so as to produce a net polarization in the direction of an applied electric field. Interfacial polarization is the result of the movement of free charge carriers within a material. These charge carriers, while under the influence of an applied electric field, will be transported through the material until they become trapped in a crystalline defect such as a vacancy, impurity center, or dislocation (38:52). The trapped charge will then induce an image charge on an electrode and produce a dipole moment. The time required for a given polarization mechanism to manifest itself depends on how easily and how far the charge is displaced. As shown in Figure III-1, electronic and atomic polarization occurs at frequencies above 10^{12} Hz, while orientational and interfacial polarization occurs at frequencies below 1 GHz (36:32).

The complex permittivity can be defined by analyzing the response of a homogeneous, isotropic material to an externally applied, sinusoidal electric field (E). The electric field may be described mathematically as:

$$E = E_o \sin\omega t \tag{3.1}$$

where E_o is the amplitude of the applied field,

ω is the frequency and,

t is the independent variable, time.

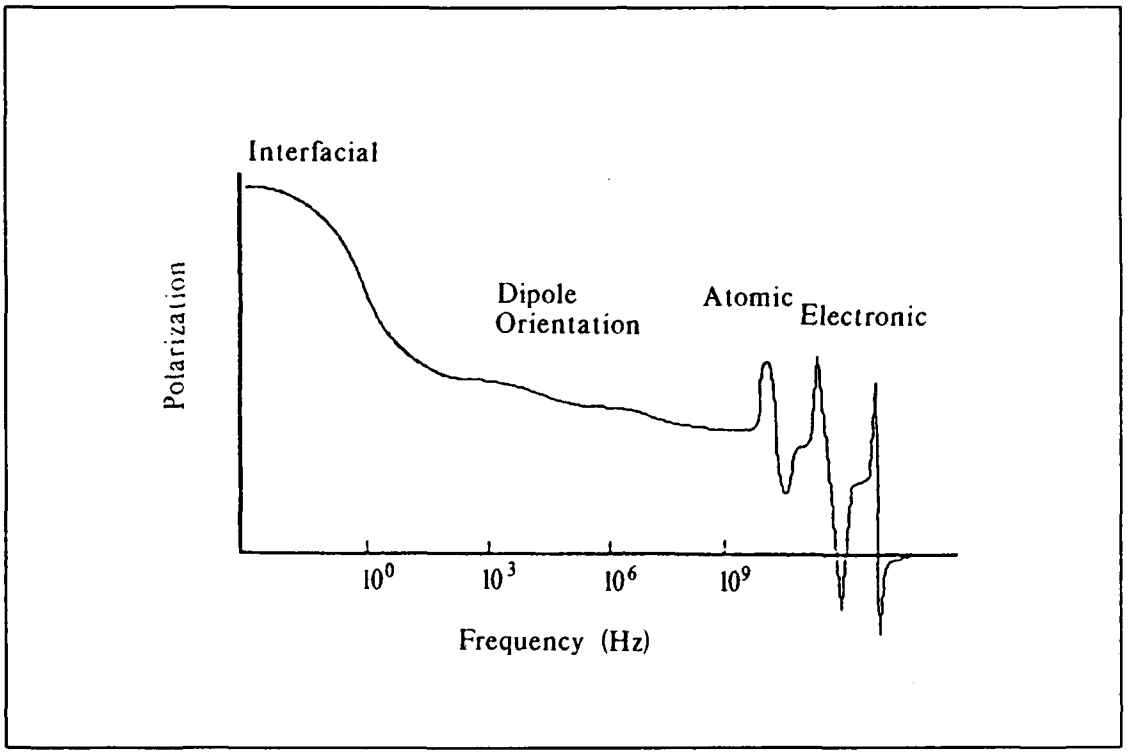

Figure III-1. Dispersion of Polarization in a Dielectric Material (9:32).

By the constitutive relationship, the electric flux density (D) is given by:

$$D = \epsilon' \epsilon_0 E_0 \sin\omega t \tag{3.2}$$

where ϵ' is a material property called the relative permittivity, and ϵ_0 is the permittivity of free space. Converting the electric field and electric flux density

expressions to phasor notation (**E** and **D**), equations 3.1 and 3.2 may be rewritten as follows:

$$\mathbf{E} = E_o \exp(j\omega t) \tag{3.3}$$

$$\mathbf{D} = \epsilon' \epsilon_o E_o \exp(j\omega t) \tag{3.4}$$

The displacement current density (expressed in phasor notation as $\mathbf{J}_d$) in the material is defined as the time rate of change of the electric flux density, d**D**/dt and it is 90^o out of phase with respect to the applied electric field. Thus,

$$\mathbf{J}_d = d\mathbf{D}/dt = j\omega \epsilon' \epsilon_o E_o \exp(j\omega t) \tag{3.5}$$

In addition to the displacement current density, there is a conduction current density (expressed in phasor notation as $\mathbf{J}_c$) in phase with the applied electrical field, resulting from the transport of free charge carriers and ions within the material. By Ohm's law, the conduction current density is proportional to the applied electric field.

$$\mathbf{J}_c = \sigma E_o \exp(j\omega t) \tag{3.6}$$

where σ is the conductivity. Therefore, the total current in the material is given by:

$$\mathbf{J_T} = \mathbf{J_d} + \mathbf{J_c} = j\omega\epsilon'\epsilon_0 E_0 \exp(j\omega t) + \sigma E_0 \exp(j\omega t) \tag{3.7}$$

Factoring out $j\omega\epsilon_0 E_0 \exp(j\omega t)$ yields

$$\mathbf{J_T} = j\omega\epsilon_0(\epsilon' - j\epsilon'')E_0 \exp(j\omega t) \tag{3.8}$$

where $\epsilon'' = \sigma/\omega\epsilon_0$, is a material property called the loss factor or AC conductivity, since it accounts for resistive losses in the material. Equation 3.8 can be rewitten as:

$$\mathbf{J_T} = j\omega\epsilon_0\epsilon^* E_0 \exp(j\omega t) \tag{3.9}$$

where $\epsilon^* = \epsilon' - j\epsilon''$ is defined as the complex permittivity. Thus, the total current density in the material is related to the electric field by the complex permittivity:

$$\mathbf{J_T} = j\omega\epsilon_0\epsilon^* \mathbf{E}. \tag{3.10}$$

Using Ohm's law the admittance, Y, is defined in terms of the complex permittivity as:

$$Y = \mathbf{J_T}/\mathbf{E} = j\omega\epsilon_0\epsilon^* = j\omega\epsilon_0\epsilon' + \omega\epsilon_0\epsilon''. \tag{3.11}$$

In general, both ϵ' and ϵ" are frequency dependent. If one assumes an exponential convergence toward equilibrium with a single time constant (τ), along with the principle of linear superposition, it can be shown that the complex permittivity can be written as (39:42):

$$\epsilon^* = \epsilon_\infty + (\epsilon_S - \epsilon_\infty)/(1+j\omega\tau) \tag{3.12}$$

where ϵ_∞ is the instantaneous polarization of a material due to electronic and atomic polarization, ϵ_S is the maximum permittivity obtained when the material has attained equilibrium after the application of an electric field, ω is the frequency of the applied electric field, and τ is the dipole relaxation time constant. Equation 3.12 is referred to as the Debye dispersion relation. Separating this equation into its real and imaginary parts yields:

$$\epsilon'(\omega) = \epsilon_\infty + (\epsilon_S - \epsilon_\infty)/(1+\omega^2\tau^2) \tag{3.13}$$

and

$$\epsilon''(\omega) = (\epsilon_S - \epsilon_\infty)\omega\tau/(1 + \omega^2\tau^2). \tag{3.14}$$

Figure III-2 depicts the frequency dependence of ϵ' and ϵ". The orientation of molecular dipoles in an electric field is a continuous process. The process starts with

only a few dipoles aligned in the direction of the applied field. As time proceeds more dipoles align with the applied electric field, and the result is a net increase in the polarization. Given sufficient time, all the dipoles in the material will align with the electric field to produce a polarization maximum. At low frequencies, the permittivity is a maximum since the dipoles have sufficient time to align themselves with an applied electric field. Since the electric field is slowly varying, the dipoles are changing their orientation slowly and dissipating very little energy, and ϵ" is small. However, as the frequency increases, the dipoles are moving faster, but fewer dipoles reach full orientation, and the result is a net decrease in the permittivity and an

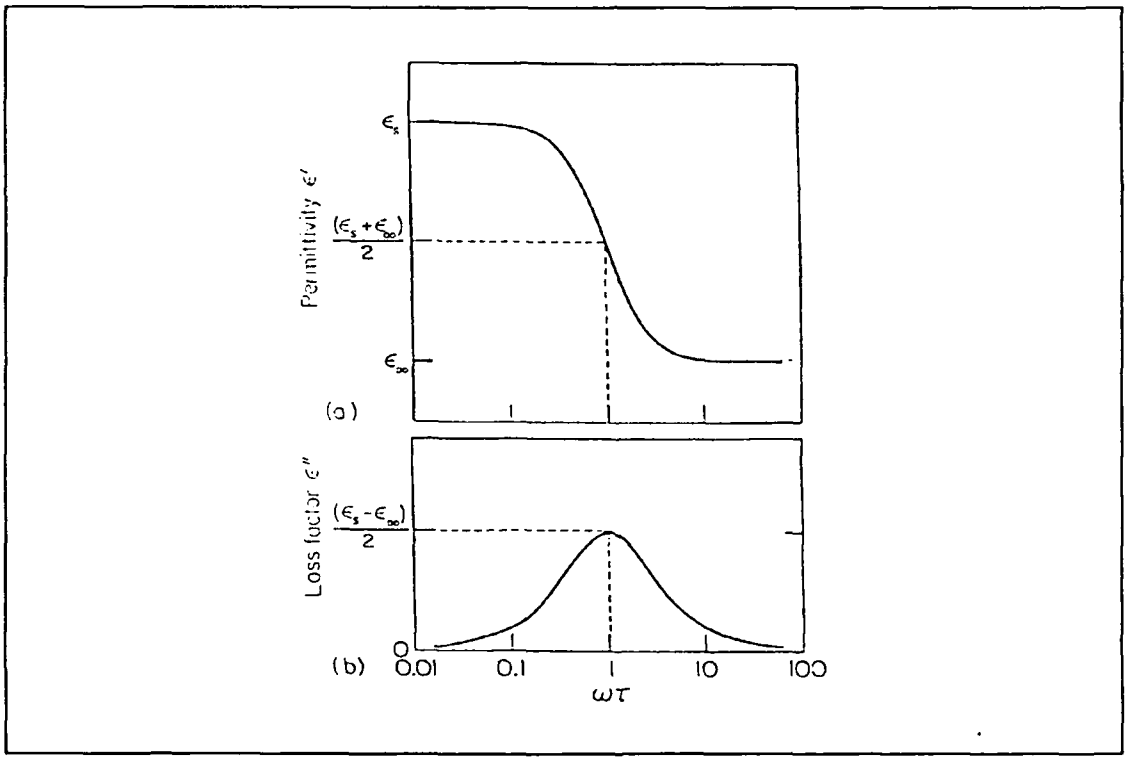

Figure III-2. Frequency Dependence of the Relative Permittivity, ϵ', and the Loss Factor, ϵ"(9:37).

increase in the loss factor. At still higher frequencies, the dipoles have insufficient time to respond to the electric field, and little reorientation occurs, and the observed permittivity is due to electronic and atomic polarization. Accordingly, the loss factor decreases since the dipoles are essentially stationary.

By combining equations 3.13 and 3.14 and eliminating ($\omega\tau$), the relationship between ϵ' and ϵ" describes a semicircle given by (39:43):

$$[\epsilon' - (\epsilon_s + \epsilon_\infty)/2]^2 + (\epsilon'')^2 = [(\epsilon_s - \epsilon_\infty)/2]^2. \tag{3.15}$$

In real materials, where there is a distribution of relaxation times, the experimental data form an arc of a circle whose center is below the ϵ" axis. As a consequence of this behavior, Cole and Cole proposed an empirical modification to the Debye relation of the form (39:43; 36:39):

$$\epsilon^* = \epsilon_s + (\epsilon_s - \epsilon_\infty)/[1 + (j\omega\tau)^\beta] \tag{3.16}$$

where β is a parameter ($0<\beta\leq1$) which accounts for an assumed distribution of relaxation times within a material. A graph of ϵ" versus ϵ', referred to as a Cole-Cole plot, is shown in Figure III-3 for two different values of β. Because of the relationship between the complex permittivity and the admittance (impedance) of

a material, a plot of the admittance (impedance) in the complex plane is also semicircular.

The Debye dispersion relationship describes the frequency dependence of ϵ' and ϵ" resulting from dipole orientation, but it does not account for bulk

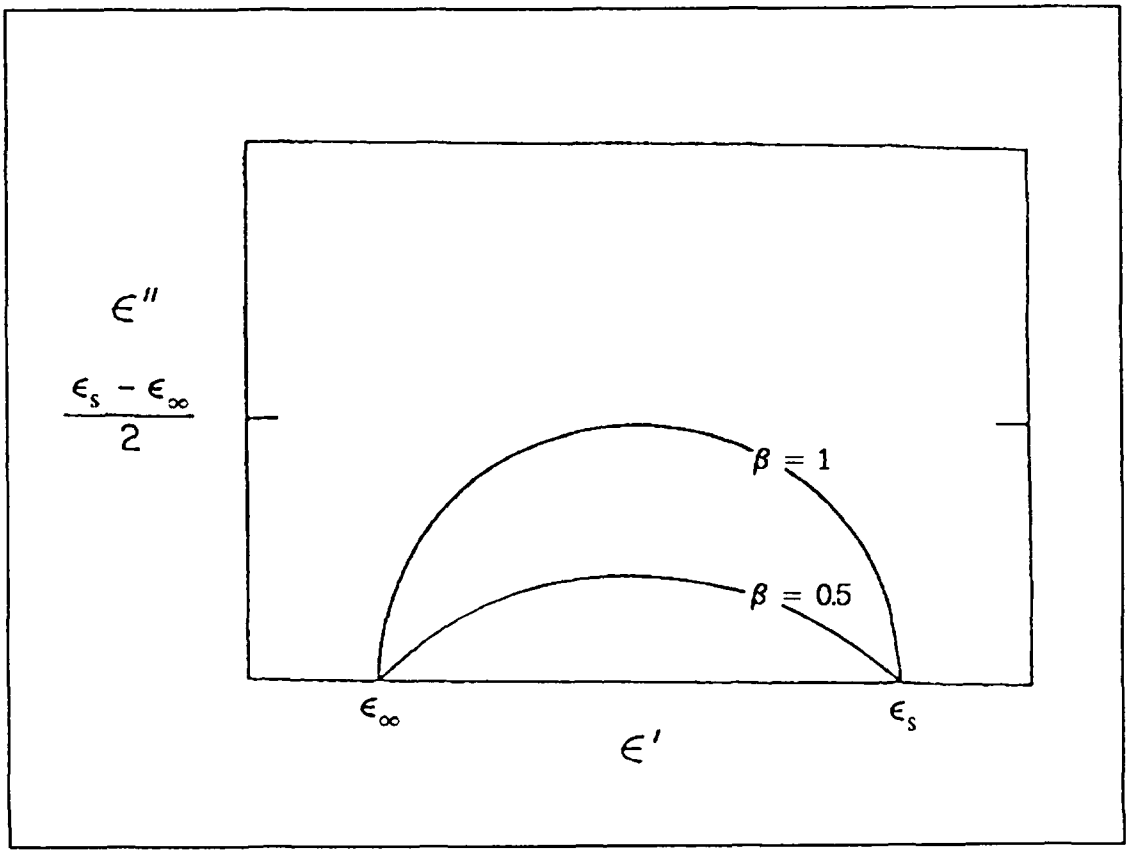

Figure III-3. Cole-Cole Plot of Debye Dispersion Relation for a) β=1 and b) β=0.5 (9:40).

conductivity. From equation 3.11, the $\omega\epsilon_0\epsilon$" term represents a conductance which, neglecting skin effects, is independent of frequency since ϵ"= $\sigma/\omega\epsilon_0$. When there is

mobile charge to produce a net bulk conductivity (σ) in addition to dipole orientation, ϵ" consists of two terms:

$$\epsilon'' = \epsilon''_d + (\sigma/\epsilon_o\omega) \tag{3.17}$$

where ϵ''_d is the loss factor due to dipole orientation. A graph of equation 3.17 , as shown in Figure III-4, where ϵ''_d is given by the Debye single relaxation time model discussed above illustrates the effect that the bulk conductivity has on ϵ". At one extremum , when σ=0, the Debye dispersion curve is obtained; and for the other extremum of large values of conductivity, the loss factor becomes inversely proportional to the frequency.

Electrical Impedance Measurement Methods

The most common approach for measuring the impedance of a material is to apply a voltage across the material at the frequency of interest and directly measure the resulting phase shift and amplitude of the signal which can be related to the real and imaginary parts of the complex impedance. Commercial impedance analyzers are available which automatically sweep the frequency of the applied voltage so that automated measurement of the impedance can be accomplished over the frequency range of interest. Theoretically, the DC impedance or resistance of a material can be measured with a DC applied voltage. However, in materials with very low conductivities ($\sigma < 10^{-9}\ \Omega^{-1}m^{-1}$), when a step voltage is applied, the initial current is dominated by a displacement current due to the polarization of the

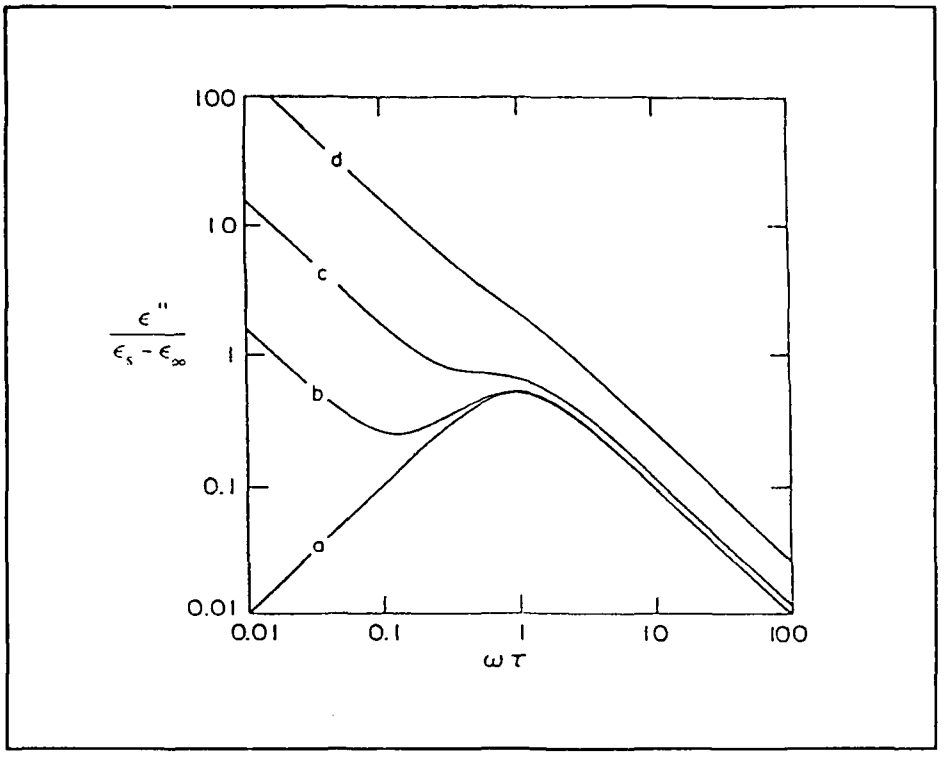

Figure III-4. The Effect of Bulk Conductivity (σ) on the Frequency Dependence of the Loss Factor (ϵ"). a) σ=0, ,b) $\sigma/[(\epsilon_S - \epsilon_\infty)\epsilon_O]$ = 0.1, c) 1, d) 10 (9:44).

material. Since dipole orientation may occur very slowly, the displacement current may dominate the conduction current for a long period of time. A steady-state current reading may not be practically achieved, thus making a direct current measurement of the resistance impossible. However, the DC conductivity may be extrapolated from the low frequency impedance measurements of the loss factor and calculated using the relation $\epsilon'' = \sigma/\epsilon_O\omega$.

An alternative approach for obtaining the impedance is to apply a step voltage across the material and computing the Fourier transform of both the input voltage and the resulting current, to generate the harmonics of each signal. The

frequency dependent impedance is obtained by dividing each harmonic of the input voltage by the corresponding current harmonic. The Fourier transform [$F(\omega)$] of a time-varying signal [$f(t)$] is given by (40:160)

$$F(\omega) = (2\pi)^{-1} \int_{-\infty}^{\infty} f(t) \exp(-j\omega t)\, dt. \tag{3.18}$$

It can be shown that the Fourier transform of a periodic signal is given by a series of impulses located at the harmonic frequencies of the signal. The weight of each impulse is equal to 2π times the value of the corresponding Fourier coefficient in the exponential Fourier series. If $f(t)$ is a periodic signal with period T, it can be expressed as an exponential Fourier series given by (41:89):

$$f(t) = \sum_{n} F_n \exp(jn\omega_o t) \tag{3.19}$$

where $\omega_o = 2\pi/T$, and F_n are the Fourier coefficients given by:

$$F_n = 1/T \int_0^T f(t)\exp(-jn\omega_o t)\, dt. \tag{3.20}$$

By utilizing Euler's identity and taking the real part of the result, the exponential Fourier series can be expressed as a trigonometric Fourier series given by:

$$f(t) = a_o + \sum_{n} a_n \cos(n\omega_o t) + \sum_{n} b_n \sin(n\omega_o t). \tag{3.21}$$

Thus, any arbitrary periodic function $f(t)$ can constructed from a linear combination of sinusoids. This concept is illustrated in Figure III-5 for a square pulse when the first three harmonics are considered.

In practice, the computation of a Fourier transform is performed by first, digitizing the signal waveform over a fixed time period (referred to as the window), and then computing a digital approximation of the Fourier transform of the data collected within the window. The algorithm for computing the digital approximation is called the Fast Fourier Transform (FFT). In this algorithm, the data collected within the window is assumed to be periodic, and it is extended over all time so that the infinite Fourier transform can be computed. The process utilized to digitize the signal and the extension of the sampling window are two primary sources of error in FFT analyses. These two sources of error can be minimized by ensuring that the digitizing process obeys Shannon's sampling theorem, and by applying an appropriate sampling window weighting function.

Shannon's sampling theorem states that the highest harmonic component that can be accurately measured must have a frequency less than half the sampling rate (41:53). The error which results from sampling a signal with harmonic components whose frequency is greater than the sampling rate is called aliasing. This error results from the high frequency components being included in the lower frequency harmonics. Aliasing errors can be avoided by low-pass filtering the signal prior to sampling. In addition to aliasing errors, the accuracy of the digitization process also

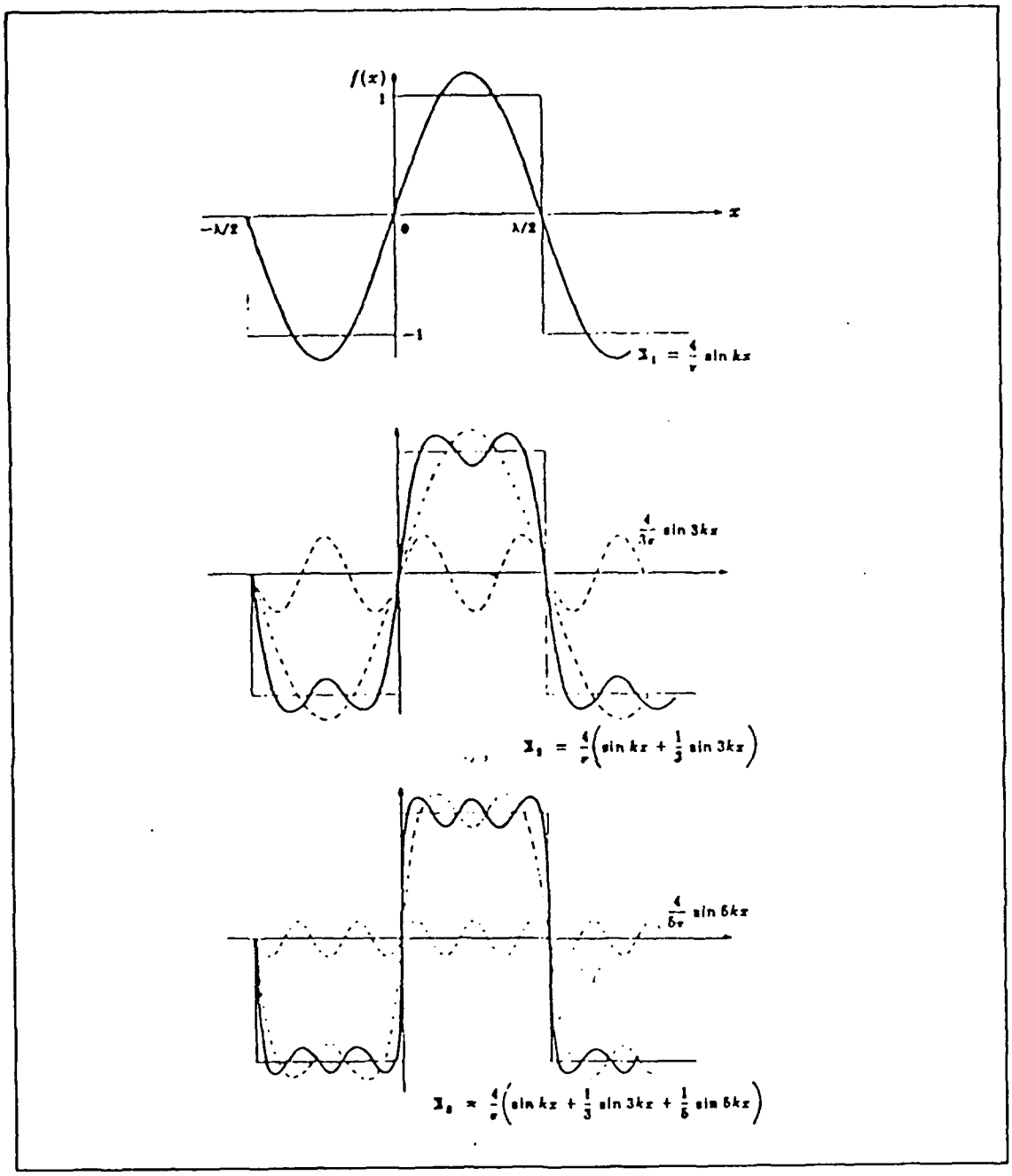

Figure III-5. Approximation of a Square Pulse by the First Three Harmonics of the Trigonometric Fourier Series (4).

depends upon the number of bits available to represent an analog value.

The other primary source of error in a FFT analysis results from assuming that a finite data record within the sampling window is repeated over all time. This error is illustrated in Figure III-6. When the signal's period (T) is larger than the window, the resulting waveform possesses considerable distortion. Even when the signal's period is shorter than the window, discontinuities may result in the waveform produced by the periodic extension of the window. To avoid this type of error, the data records are multiplied by a weighting function. A number of weighting functions have been described, and the use of any particular function depends upon the signal characteristics and the analysis (42:14-22).

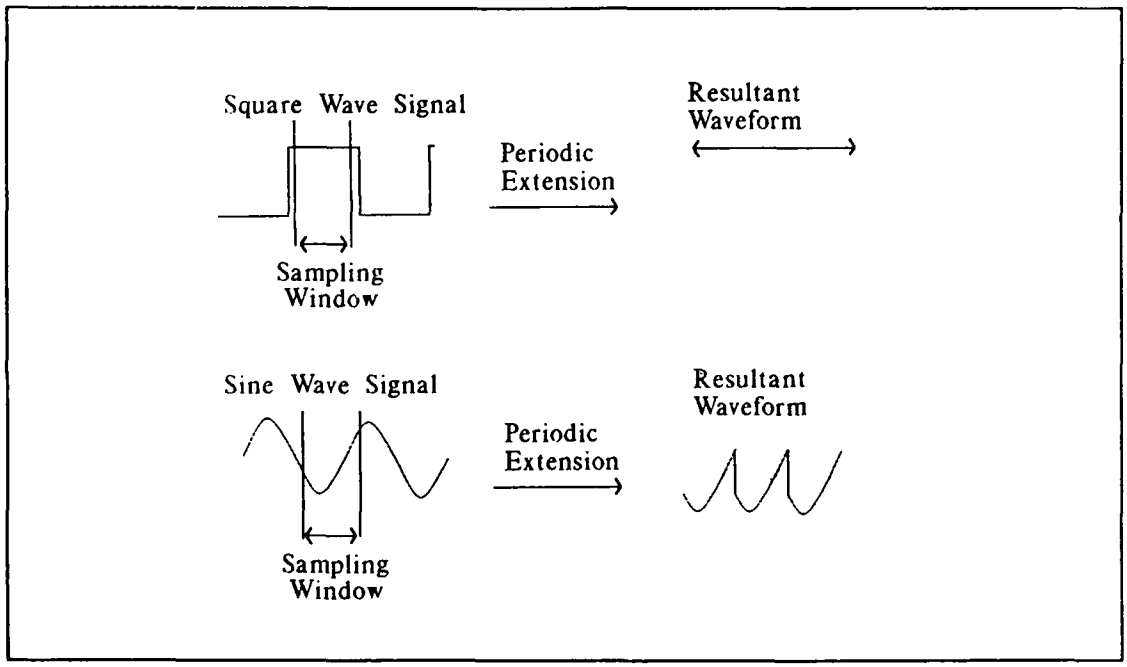

Figure III-6. Examples of the Error Introduced by the Periodic Extension of a Finite Time Record Associated with a Particular Signal.

Analysis of the Interdigitated Gate Electrode Response to Sinusoidal Excitation

A detailed analysis of an interdigitated gate electrode has been performed by Lee (34). Lee briefly describes an oversimplified lumped-element circuit model of the interdigitated gate electrode structure shown in Figure III-7. The capacitor C_{12}, represents the capacitive coupling between the electrodes, and the resistance, R_{12}, represents the losses due to the film's conductance. The capacitance, C_{11}, represents the electrode-to-ground capacitance. When the electrode is uncoated, R_{12} is large, and the output voltage is given by the capacitive voltage divider arrangement. In this case, the gain is minimized and there is no phase shift. However, when a highly conductive coating is applied, the two electrodes are effectively shorted, and the gain is unity and there is no phase shift. For intermediate conductance values, the gain will obviously be less than unity, and the phase shift is negative. This model, although qualitatively correct, does not take into account the distributed nature of the electrode's impedance.

In order to more accurately model the interdigitated gate, Lee has further developed a more complex analysis based upon a two-dimensional numerical solution of Poisson's equation applied to the geometry of the interdigitated gate electrode. This analysis accounts for the interface charge which may exist at the interface of the silicon dioxide and any arbitrary thin film coating covering the interdigitated gate. Using a finite difference algorithm to compute the potential distribution within the gate electrode, the gain and phase of the interdigitated gate was obtained. Thus, the simulation also accounts for the effect of an arbitrary load on the interdigitated gate

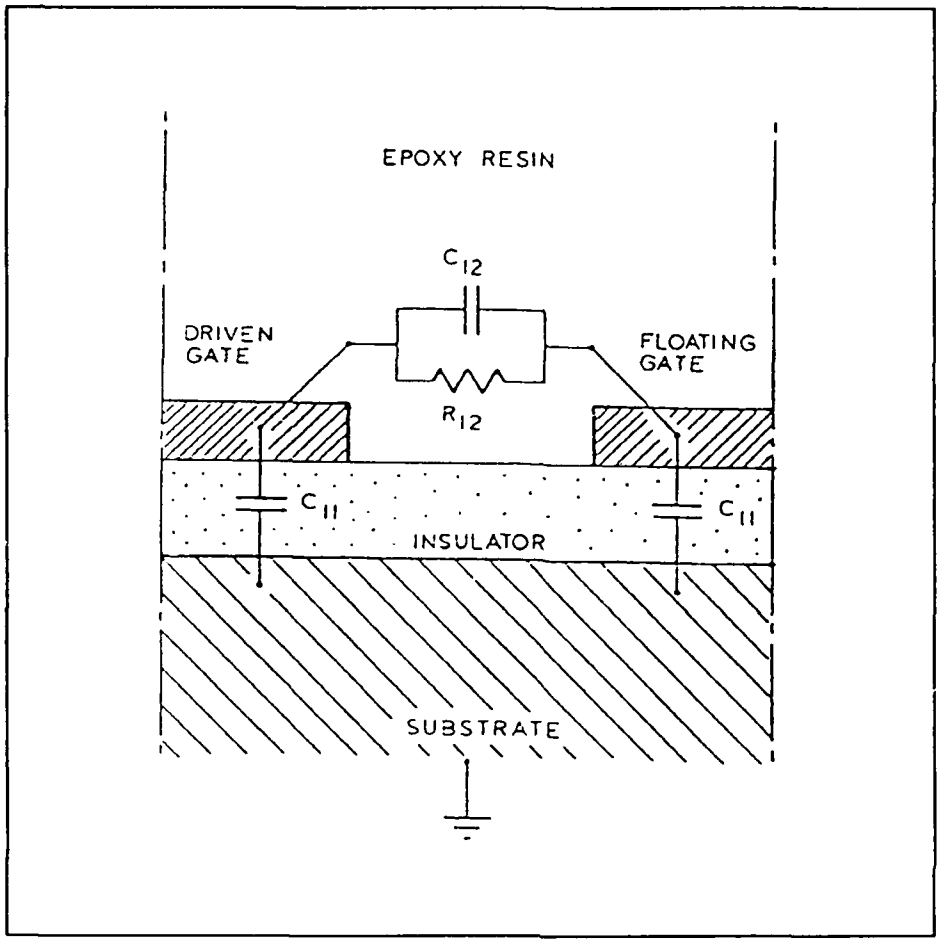

Figure III-7. Lumped-Element Circuit Model for Interdigitated Gate Electrode (34).

with respect to the gain and phase response. The simulation requires the following parameters to perform the analysis: the electrode geometry, the film's relative permittivity (ϵ') and conductance, and the excitation signal's frequency. The electrode geometry determines the inter-electrode and electrode-to-ground coupling. Since a change in the length of the electrodes or the number of interdigitated fingers increases both the inter-electrode and the electrode-to-ground coupling in the same proportion, the voltage division which accounts for the floating gate potential is left

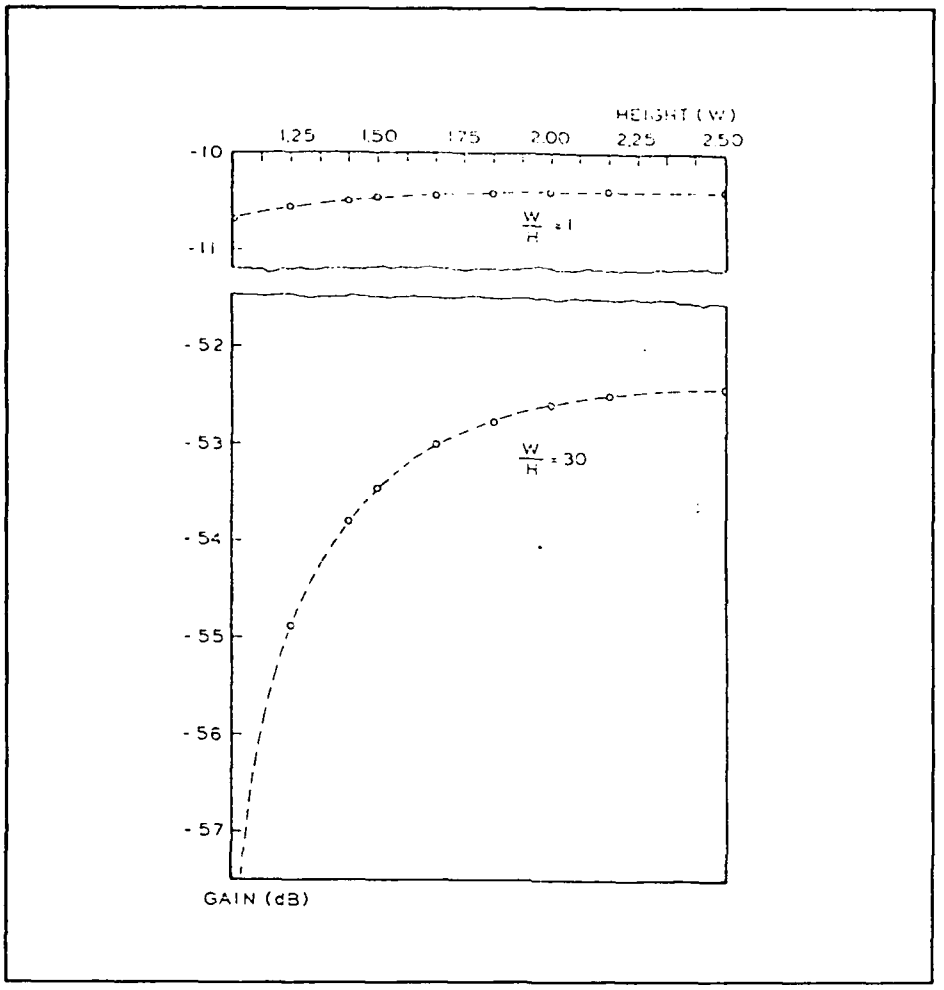

Figure III-8. Gain of an Interdigitated Gate Electrode as a Function of the W/H Ratio (34).

unchanged. The critical geometric parameter is the ratio of the electrode's width (W) to their separation distance as measured with respect to the ground plane (H). The effect of the W/H ratio is shown in Figure III-8. Lee used a fixed W/H ratio of 12.5 to generate a set of calibration curves, shown in Figure III-9, for coatings possessing various relative permittivities and conductivities (represented by the loss factor, ϵ")

(34). Inspection of Figure III-9 demonstrates that the simulation results agree with the qualitative model discussed earlier.

The lumped-element circuit model of the interdigitated gate and the qualitative results of the finite difference model are directly applicable to the present study. However, the finite difference results reported by Lee were for a specific electrode configuration. The interdigitated gate electrode of the sensor reported by Lee had 10 fingers on the floating gate, and the finger width and lateral separation were both 12.5 μm. One of the critical parameters in the finite difference model was the thickness of the dielectric separating the interdigitated electrodes from the ground plane. Lee designed four sensors with 0.45, 0.75, 0.85 μm separation. In addition, Lee assumes that dielectric above the interdigitated electrodes was semi-infinite with a height 2.25 times the thickness of the electrode fingers (28 μm) above the electrode array. This geometry is considerably different from the geometry of the sensor designed for this research (see Table IV-1). Furthermore, the assumption that the dielectric above the electrode array is semi-infinite is not true in the current study for the 0.1 μm thick CuPc films deposited on the interdigitated gate. As a result of these differences in sensor geometry, Lee's analysis only qualitatively applies to the performance of the interdigitated gate CHEMFET evaluated in this research effort.

Summary

The theory of the impedance measurement of materials using an interdigitated gate electrode CHEMFET design was described in this chapter. This

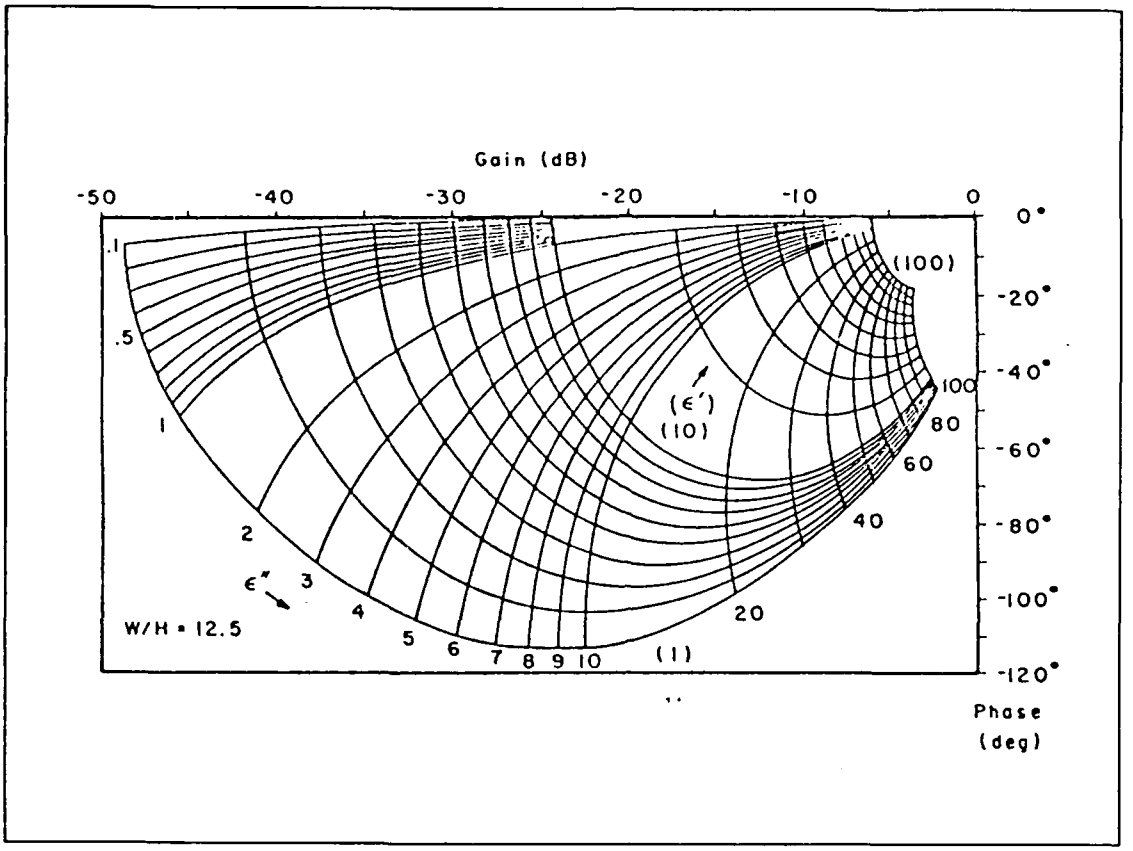

Figure III-9. Calibration Curves for an Interdigitated Gate Electrode with a 1.6pF Load (34).

was accomplished by discussing the microscopic interaction of the electric dipoles and free charge carriers within a material with an externally applied electric field. The material's admittance (or equivalently, its impedance) was defined in terms of the complex permittivity. The frequency dependency of the complex permittivity was then related to the alignment of the microscopic electric dipoles. A change in the microscopic properties of the material produces a change in the electrical impedance. Thus, electrical impedance measurements can be used to probe the chemical state of a film. Two methods for measuring the electrical impedance of

materials were described: i) direct measurement of the phase shift and amplitude of an applied signal as a result of the complex impedance, and ii) Fourier transform techniques for measuring the harmonic changes within a signal as a result of the complex impedance. In the last section, two electrical models for the interdigitated gate were described: a lumped-element circuit model and two-dimensional finite difference model. Although the lumped-element circuit model can be used to qualitatively analyze of the behavior of the interdigitated gate of the CHEMFET used in this research, the more detailed finite difference model is not directly applicable to the current study because of significant differences in electrode geometry.

IV. CHEMFET Sensor Design, Instrumentation, and Evaluation Procedures

The CHEMFET design, and the instrumentation configuration and performance evaluation procedures used to measure the electrical properties of the CHEMFET in response to chemical changes induced in the interdigitated gate coatings are presented in this Chapter. The CHEMFET design and its preliminary electrical performance characterization is discussed in the first section. In the second section, the challenge gas generation and delivery system required to expose the CHEMFET to known concentrations of the challenge gases (NO_2 and DIMP) is described. The third section describes the electrical performance instrumentation configuration used to evaluate the CHEMFET. The fourth section discusses the specific test procedures developed for evaluating each film deposited on the interdigitated gate electrode structure of the CHEMFET. In the final section, the software developed for data analysis and reduction is described.

CHEMFET Design and Characterization

As part of this overall research thrust, Capt James Godfrey (GE87-D) designed several CHEMFETs using n-channel enhancement mode MOSFETs with three different gate electrode structures: a ring gate, a split-gate and an interdigitated gate (unpublished results). Of the three designs, the interdigitated gate electrode structure was postulated to possess the greatest gas sensitivity for a given polymeric membrane because it distributed the polymeric thin films such that their

surface area to volume ratio was maximized. The interdigitated gate electrode structure also required the least amount of post-MOSIS (Metal Oxide Semiconductor Implementation Service) processing. In order to measure the interdigitated gate electrode structure impedance and provide a DC bias to the gate of the n-channel enhancement mode transistors, the interdigitated gate structure was modified.

Four modifications were made to improve the design of the interdigitated gate CHEMFET. To facilitate the measurement of the impedance properties of the thin film membranes and provide a DC bias signal, a bond pad connected to the floating gate was added. The other changes made to the design included: a re-arrangement of the bond pads, the positioning of the transistor's active region, and the method for making contact to the active p-well. The bond pads were rearranged to incorporate the additional bond pad which was connected to the floating gate, to allow bonding to one side of the die only, and to better isolate the bond pads from the interdigitated gate structure. The placement of the bond pads along one side of the integrated circuit, far away from the interdigitated gate, minimized the potential for breaking bond wires or shorting the bond pads during application of the thin film to the interdigitated gate electrode structure. The transistor's active area was also repositioned to better isolate the transistor from the interdigitated gate structure. The method for contacting the active p-well was modified to minimize accidental shorting of the drain or source to the p-well, which may occur by penetrating the

bond pad during probing. This modification involved placing each pad in its own (isolated) p-well.

The basic design of the CHEMFET was obtained by extracting the interdigitated CHEMFET designs contained in the magic cells (arraydig2.31 and arraydig2.15) from the second pass design of Capt Godfrey's CHEMFET (called Chemfet2). The design was implemented using the MOSIS 3μm CMOS double-level metal design rules. Each cell contains a reference transistor with a solid metal gate and two transistors with interdigitated gate electrodes. The interdigitated gate structures were implemented in the second-level of aluminum. The main difference between the two cells is the number of fingers in the interdigitated gate electrodes. The cell arraydig2.31 contains 29 fingers on the floating gate, and arraydig2.15 possesses 15 fingers. As shown in Figure IV-1, the finger separation for both arrays is 9μm, and the finger width is 7.5 μm for the large array and 6 μm for the small array. The arrays were connected to the polysilicon gate of an n-channel enhancement mode transistor with a metal1 line. The threshold voltage of the enhancement mode transistor is more reproducible than in the depletion mode devices. The active region of the transistor is shown in Figure IV-2. The transistor's active gate length is 12μm and its width is 15μm. The critical dimensions of the transistors in each cell are summarized in Table IV-1. Except for the differences in the gate structures, all of the transistors, including the reference and interdigitated FETs, in both cells are identical. Each transistor can be biased above its threshold value by applying a sufficiently large positive bias between the floating gate and the

Table IV-1

Critical Dimensions of CHEMFET Transistors

Structure	Large Array	Small Array
Interdigitated Gate Electrode Structure		
Number of Fingers on Floating Gate	29	15
Number of Fingers on Driven Gate	31	17
Finger Width (μm)	7.5	6.0
Finger Separation (μm)	9.0	9.0
Overall Array Length (μm)	3792	3792
Overall Array Width(μm)	921	459
MOSFET Structure		
Active Gate Length (μm)	12	12
Active Gate Width (μm)	15	15

active-area, p-well contact, without having to make contact with the substrate. However, biasing of the substrate, which is the method used by Senturia (43:72) for biasing the microdielectrometer, may be of interest to compare the performance of the sensor. The discrete bond pad to the substrate, although not used in the present

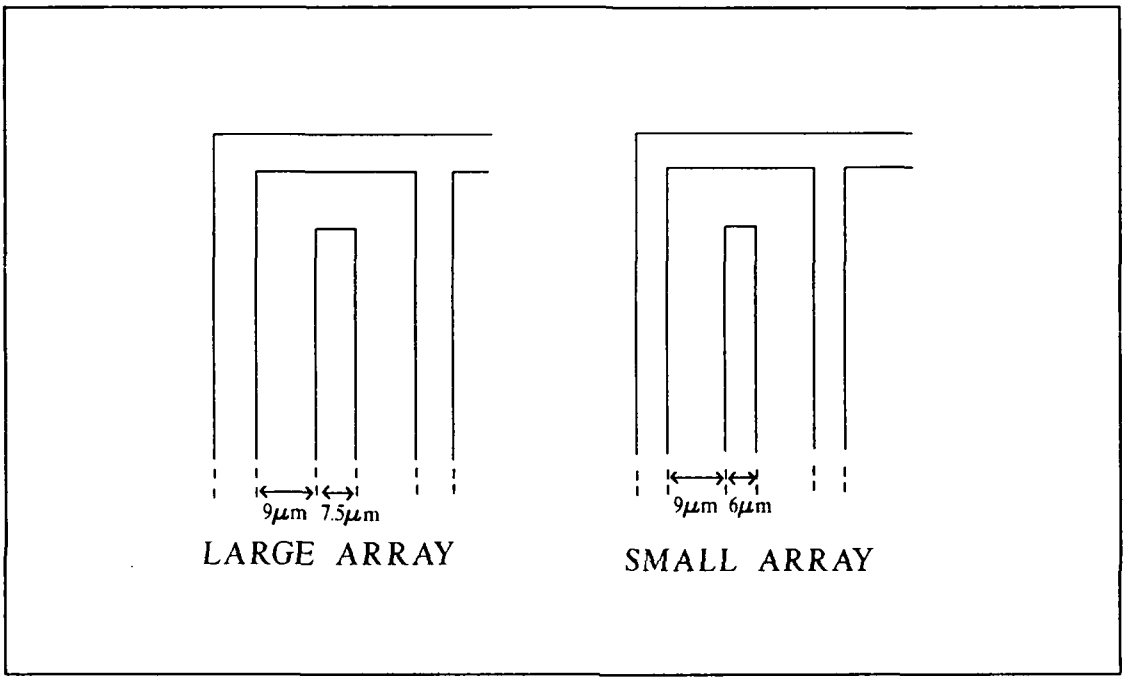

Figure IV-1. Schematic Diagram of the Finger Geometry of the CHEMFET's Large and Small Interdigitated Gate Electrode Structures.

work, was kept for this reason.

Upon extraction from the Chemfet2 file design, the two cells, arraydig2.31 and arraydig2.15, were placed in new cells (called new_arraydig2.31 and new_arraydig2.15) so that they could be subsequently modified. The modifications discussed above were implemented on the new_arraydig2.31 cell. A metal2 line connects the additional bond pad to the metal1 line running between the polysilicon

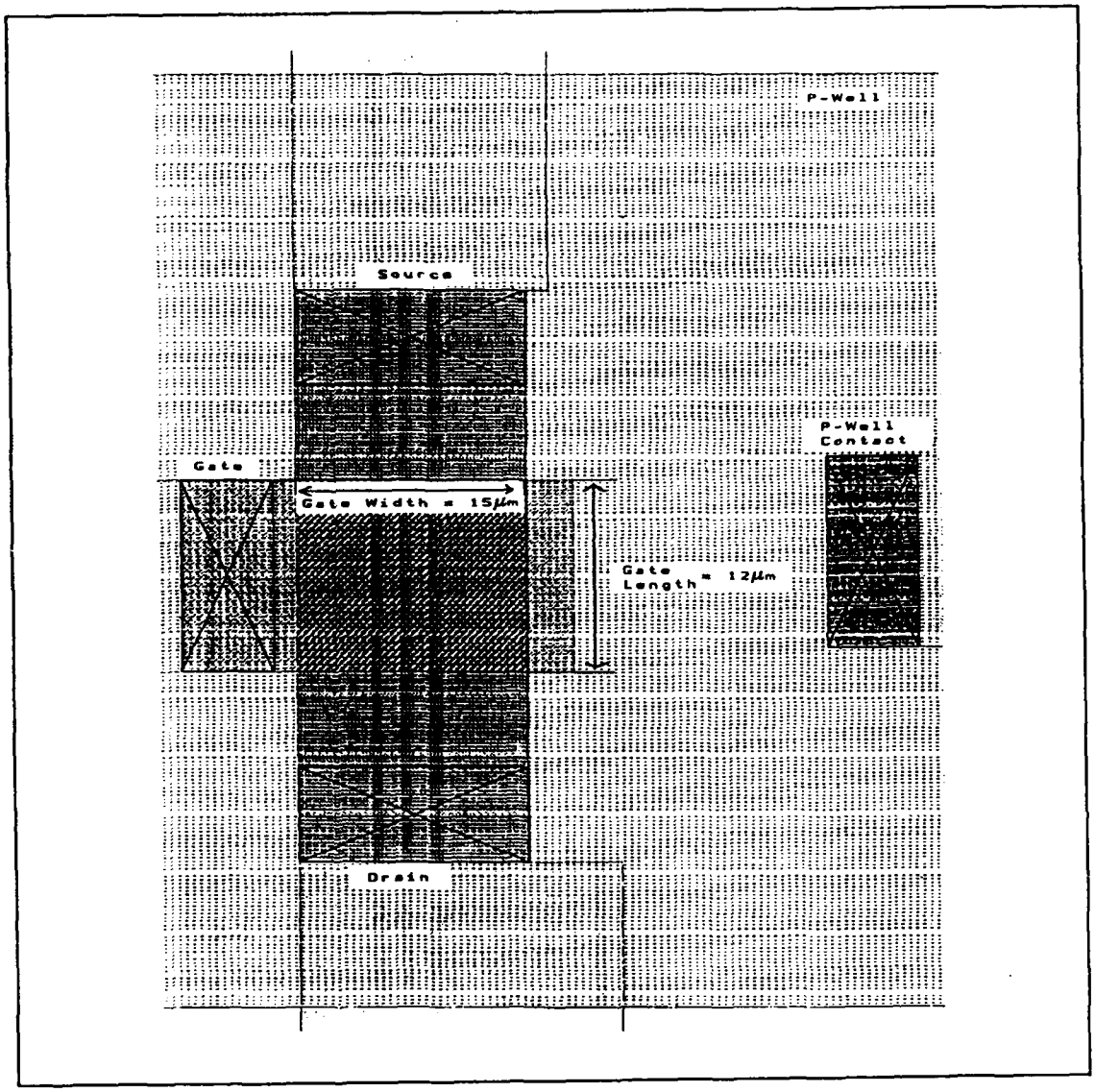

Figure IV-2. Layout of the CHEMFET's Active Area.

gate and the metal2 floating gate. After modification of the new_arraydig2.31 cell was complete, a new cell (called pads) was created which contained the entire structure of one of the CHEMFET transistors in new_arraydig2.31 cell, except for the interdigitated gate electrode. This new cell (called pads) was then used, after

adjustments were made with respect to the position of the bonding pads, to replace the transistor and pads in the cell referred to as new_arraydig2.15. These three cells, new_arraydig2.31, new_arraydig2.15, and pads, were used to produce the complete design, as shown in Figure IV-3. The overall dimensions of the CHEMFET integrated circuit was 4466 x 6755 μm. This size is a subset of the 4600 x 6800 μm die constraint size that minimizes MOSIS fabrication costs. The function of each bond pad, numbering from left to right in Figure IV-3, is summarized in Table IV-2.

Preliminary CHEMFET Physical and Electrical Performance Characterization.

The CHEMFET design was submitted to MOSIS for fabrication. Unpackaged die were received 8 weeks after submission to MOSIS. The MOSIS process characterization data sheet is provided in Appendix A.

The preliminary physical characterization of the integrated circuits involved a visual inspection for fabrication defects (in particular, inter-electrode shorts or fractures in any of the conductors within the interdigitated gate structure). Next, the electrical performance was investigated via an impedance test for short circuits between the driven and floating gates, and measurement of the MOSFET I-V characteristics, gain at different gate biases, and its frequency response. The visual inspection, impedance evaluation, and measurement of the I-V characteristics were made on unpackaged die using a Micromanipulator probe station (The Micromanipulator Company, Model 6200, Carson City, NV). The discrete die could not be held in place by the probe station's vacuum port; and therefore, it was affixed

Table IV-2

CHEMFET Bond Pad Function Summary

Pad Number	Function
1	Large Array, Driven Gate Transistor Number 1 (LT1)
2	Floating Gate LT1
3	Drain or Source LT1
4	p-Well LT1
5	Substrate LT1
6	Drain or Source LT1
7	Driven Gate LT2
8	Drain or Source LT2
9	p-Well LT2
10	Substrate LT2
11	Drain or Source LT2
12	Drain or Source LT3
13	Substrate LT3
14	p-Well LT3
15	Drain or Source LT3
16	Floating Gate LT3
17	Driven Gate LT3
18	Small Array, Driven Gate Transistor Number 1 (ST1)
19	Floating Gate ST1
20	Drain or Source ST1
21	p-Well ST1
22	Substrate ST1
23	Drain or Source ST1
24	Driven Gate ST2
25	Drain or Source ST2
26	p-Well ST2
27	Substrate ST2
28	Drain or Source ST2
29	Drain or Source ST3
30	Substrate ST3
31	p-Well ST3
32	Drain or Source ST3
33	Floating Gate ST3
34	Driven Gate ST3

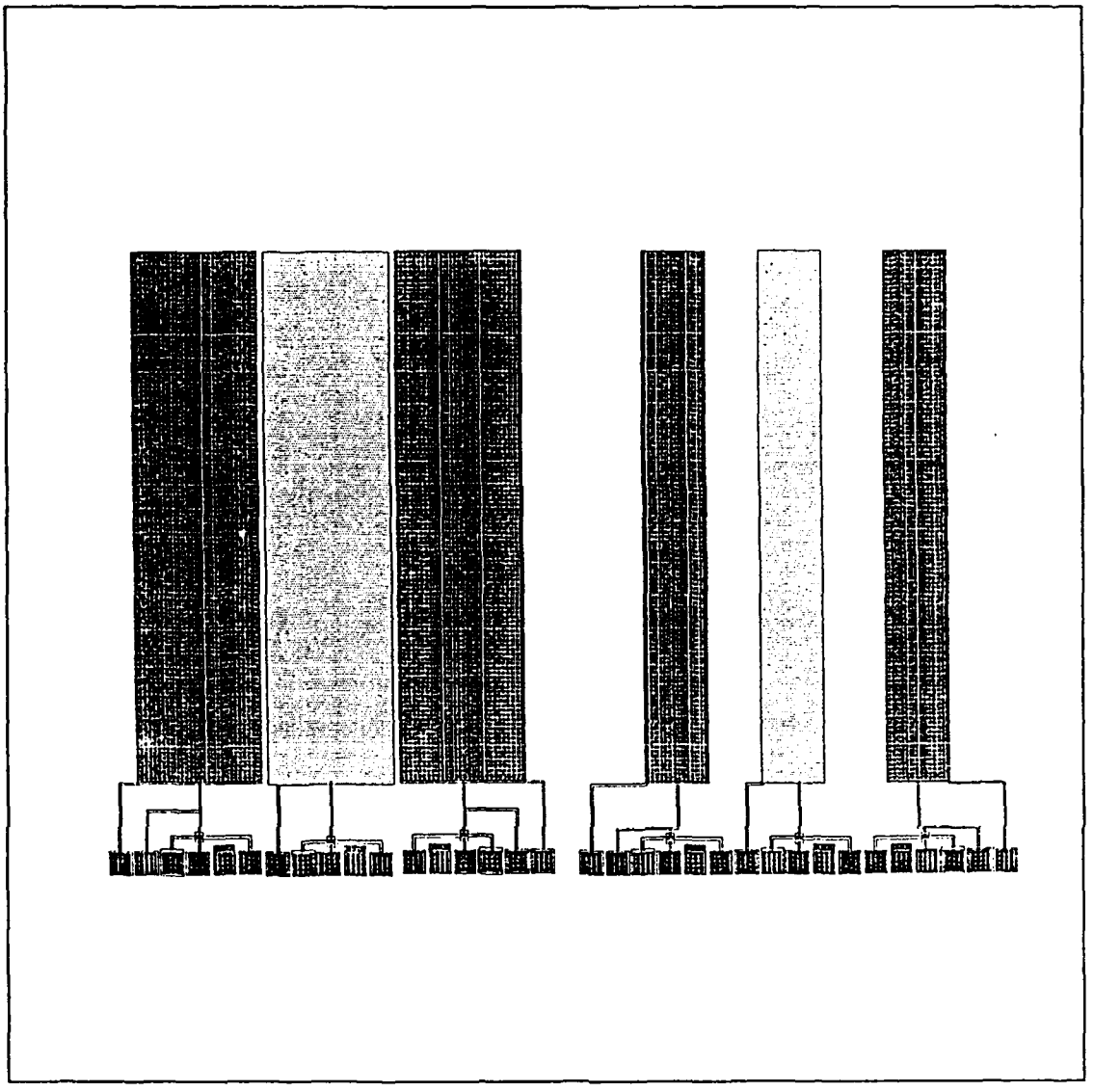

Figure IV-3. CHEMFET Design.

to a blank silicon wafer with double sided tape. The visual inspection was accomplished using the probe station's microscope. Figure IV-4 shows a photomicrograph of the CHEMFET die. No visual defects were detected in the lot of 10 that were examined. The impedance measurement was made with a Fluka

digital multimeter (John Fluke Mfg. Company, Model 77/AN, Everett, WA). All of the interdigitated gates had completely open circuits (>30MΩ) between the driven and floating gates. The output I-V characteristics of the MOSFET were measured with a Tektronix curve tracer (Tektronix Corp. Model 577, Beaverton, OR) (data not shown). The measurement of the output I-V characteristics was repeated, along with the measurement of the MOSFET transfer characteristics, with a semiconductor parameter analyzer (Hewlett Packard Corp., Model HP4145B, Palo Alto, CA) and are shown in Figures IV-5 and IV-6. Identical characteristics were obtained for the lot of 10 transistors that were examined.

The discrete die were then packaged in standard 64 pin dual-in-line (DIP) packages (Kyocera Corp. Part Number KD-83578, Edina, MN) having a square die cavity 300mils on a side. Before packaging, two die had a CuPc film applied to the interdigitated gate prior to packaging (See CuPc Test Procedures). In order to reduce the number of pins required to package the device, the substrate connection was left floating, and the source and p-well of each transistor were connected to the same pin. Since there are only 16 bond pads along any given side of the die cavity, and twenty-two wire bond connections were required, the die was mounted against one edge of the die cavity (Figure IV-7). The placement against one side of the die

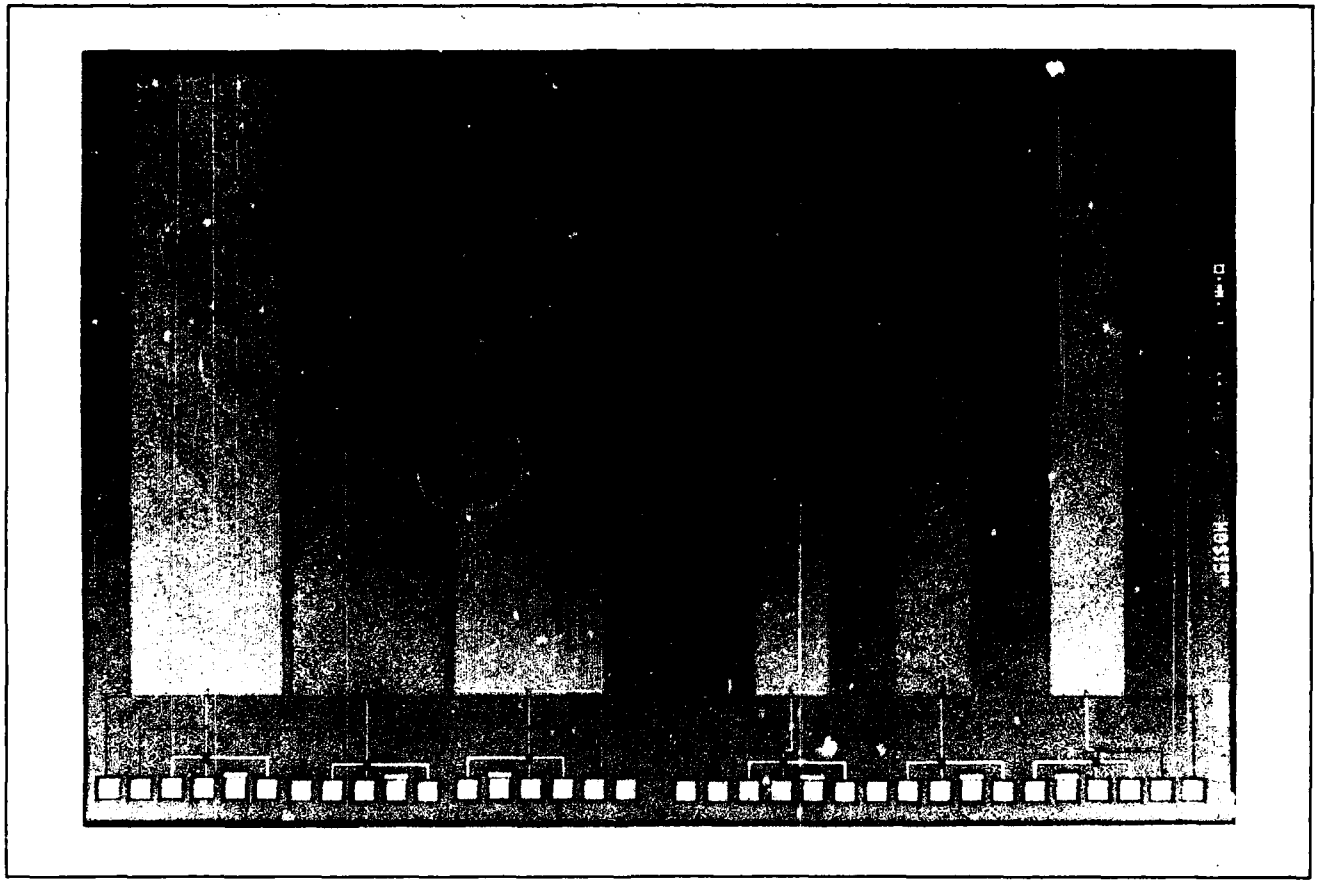

Figure IV-4. Photomicrograph of CHEMFET Integrated Circuit.

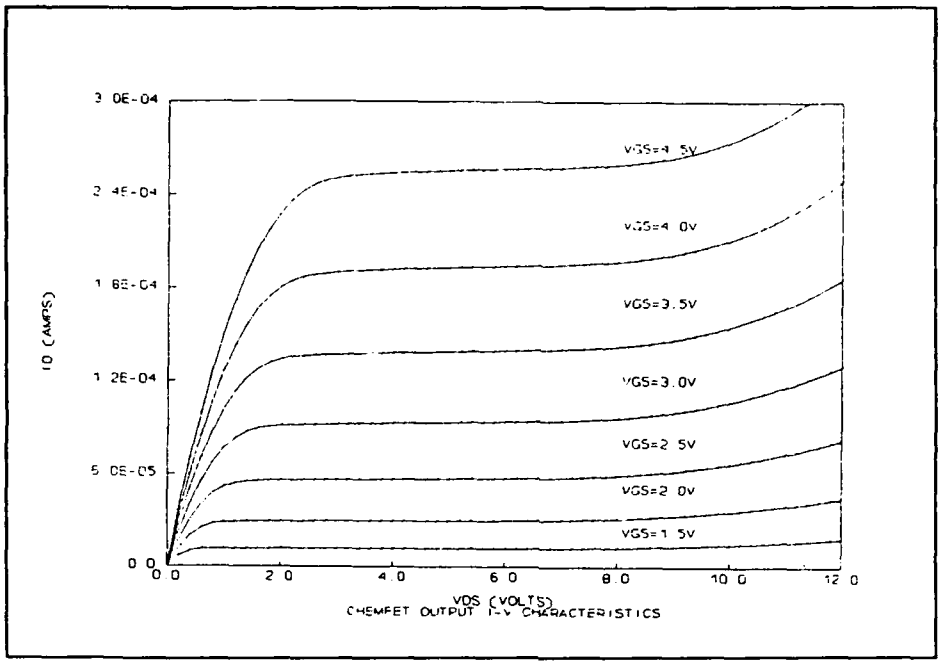

Figure IV-5. CHEMFET Output I-V Characteristics

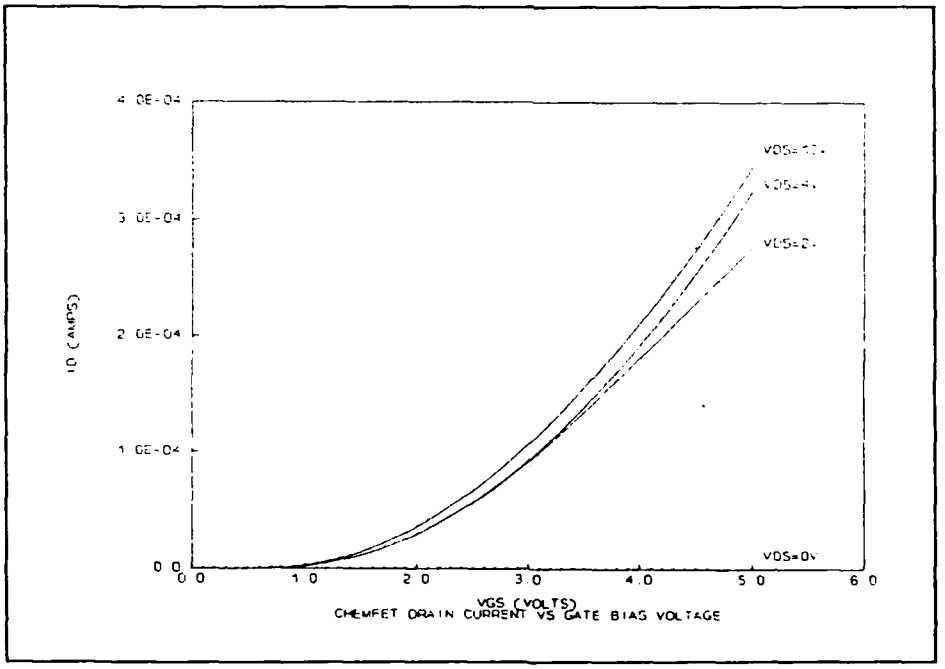

Figure IV-6. CHEMFET Transfer Characteristics.

cavity facilitated wire bonding along two sides of the die cavity, starting at pin2 of the DIP (Figure IV-7). Nevertheless, this die placement required long bond wires.

Biasing Experiments and Frequency Response.

Two experiments were performed to determine the best biasing arrangement for the transistors. In the first experiment, the circuit shown in Figure IV-8 was used to measure the response of the transistor to a square wave and sinusoidal excitation at low (10 Hz - sinusoidal, 100 Hz - square wave), medium (1 KHz), and high frequencies (100 KHz - sinusoidal, 10 KHz square wave). The capacitor value was empirically chosen to maximize the low-frequency response. The 100 Kohm gate resistance was the maximum resistance available on the decade resistance box. Although this gate resistance results in a low input impedance to the amplifier, it was adequate for these preliminary experiments. As shown in Figure IV-9, there is considerable distortion of the square wave at 100 Hz and 10 KHz with a constant gain of approximately 4. The response to a sinusoidal excitation reveals a small degradation in the gain at 10 Hz, and a large degradation of approximately -10 dB at 90 KHz. For comparison, a second experiment was accomplished to measure the gain for different gate bias voltages using a gain-phase analyzer (Hewlett-Packard Corp., model HP4194A, Palo Alto, CA). A representative plot of the gain and phase is shown in Figure IV-10, and the results of this experiment are summarized in Table IV-3. The highest midband gain was measured with an applied gate voltage

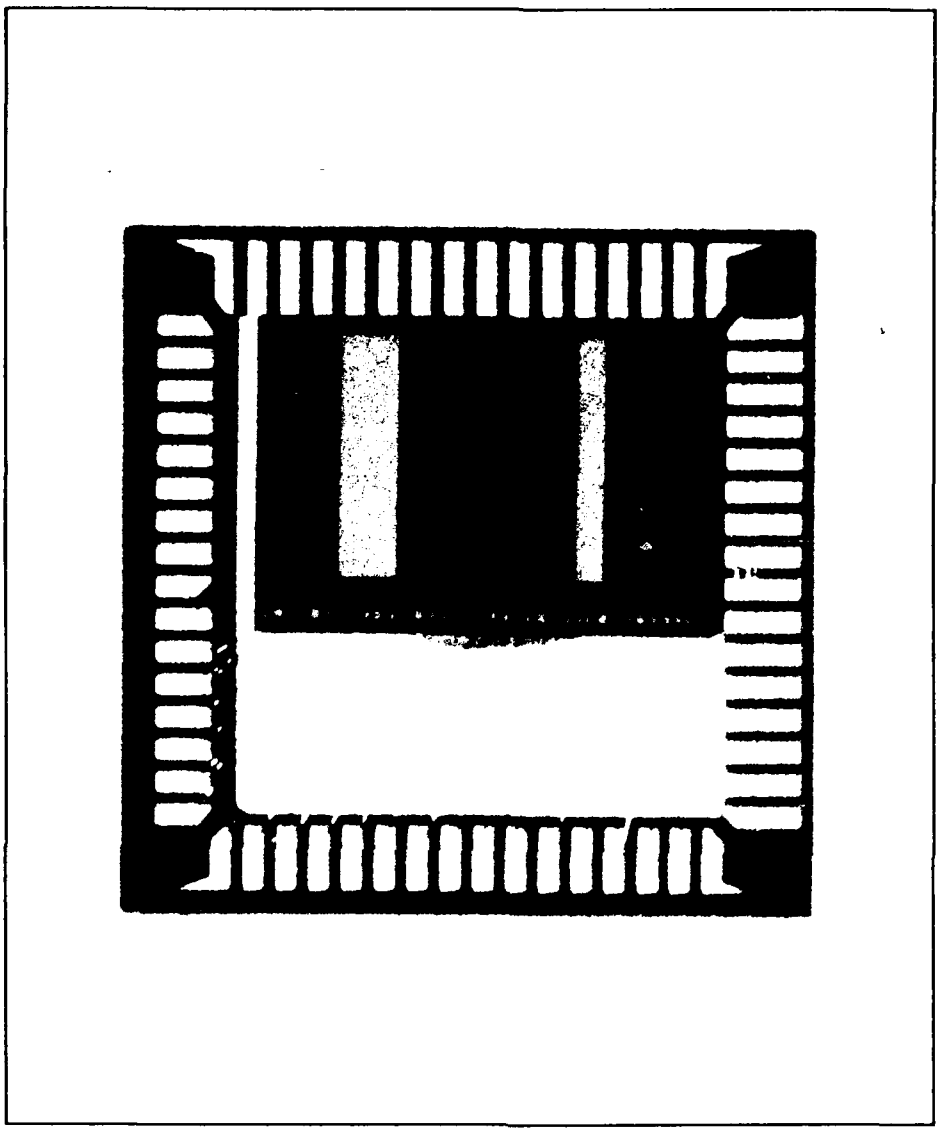

Figure IV-7. Photograph of the Wire-Bonded CHEMFET Integrated Circuit.

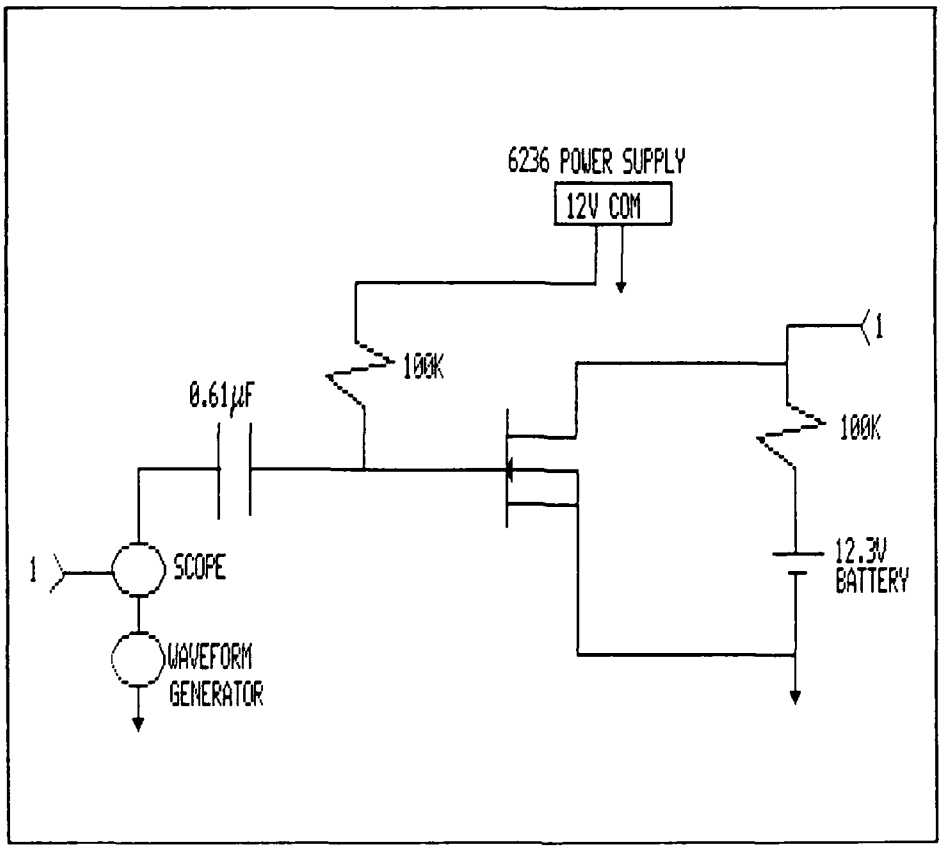

Figure IV-8. Circuit Schematic for Testing the CHEMFET with Square Wave and Sinusoidal Excitation.

(V_{gg}) of 12 V. However, the measured gate to source voltage (V_{gs}) was 3.84 V. The large voltage drop across the gate bias resistor resulted from a gate leakage current on the order of 80 μA. This leakage current was determined from the voltage drop measured across the gate bias resistor. At this applied voltage, the electric field across the gate's dielectric is (8×10^5 V/cm) would not normally cause breakdown since silicon dioxide has a dielectric strength of 1×10^7 V/cm (44:852). The fact that a large leakage current was observed suggests the oxide quality was poor. When

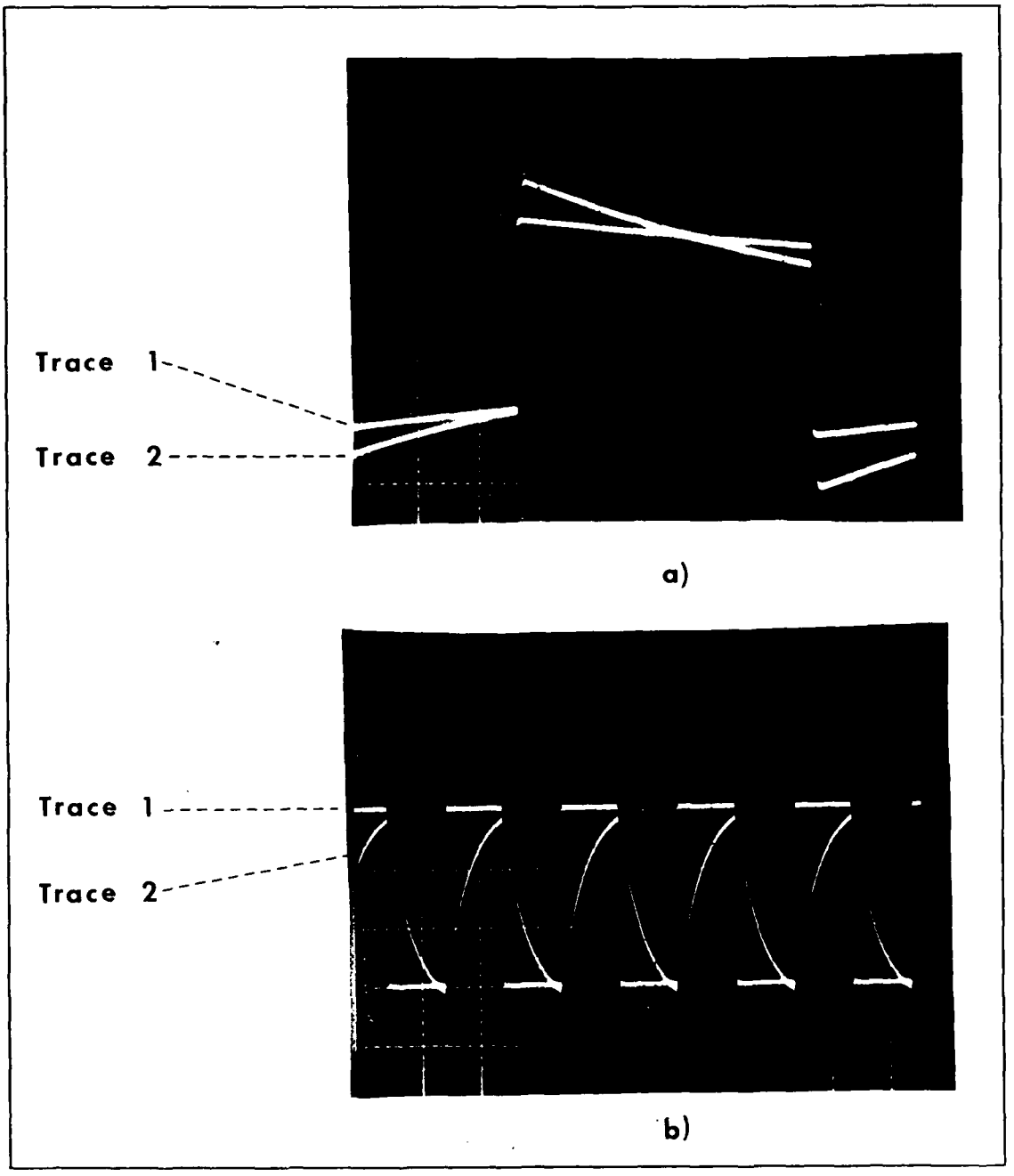

Figure IV-9. CHEMFET Response to Square Wave Excitation.

a) Trace 1 = 10 Hz Excitation Signal, 50 mV/div, Trace 2 = CHEMFET Drain Voltage, 0.2 V/div., Horizontal Scale = 1 ms/div. b) Trace 1 = 10 KHz Excitation Signal, 50 mV/div, Trace 2 = CHEMFET Drain Voltage, 0.2 V/div, Horizontal Scale = 50 μs/div.

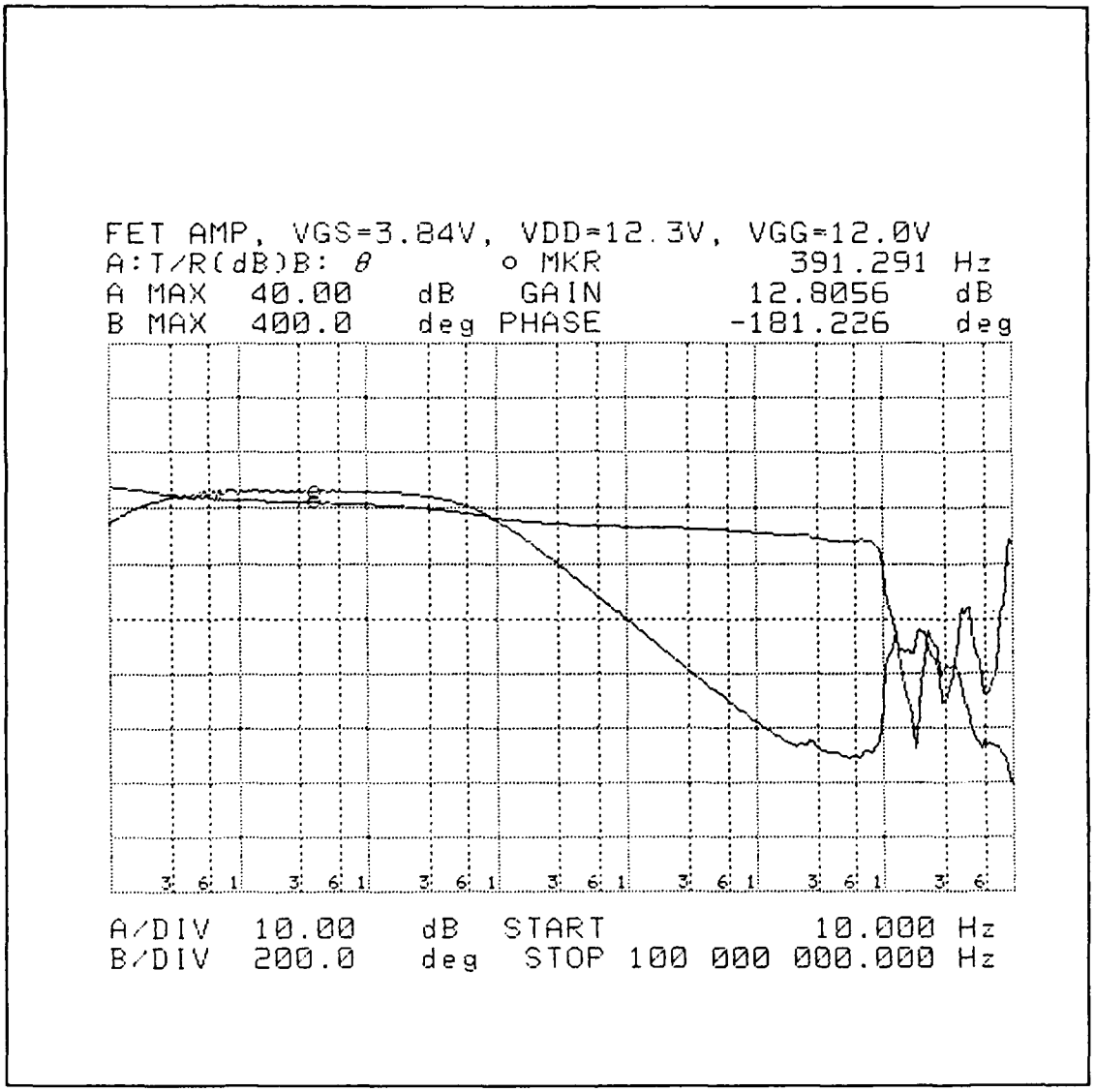

Figure IV-10. Representative Plot of the Gain and Phase of the CHEMFET as a Function of Frequency.

V_{gg} = 2 V, the leakage current was reduced to less than 5 μA. As part of this experiment, a FFT analyzer (Bruel and Kjaer, model 2032, Marlborough, MA) was used to independently measure the transistor's gain with V_{gg} = 12 V. A 500 Hz, 50 μs wide pulse with a 5 V amplitude was applied to the floating gate. The harmonic content of both the input and output waveforms were measured with the FFT analyzer and are shown in Figure IV-11. Figure IV-12 depicts the transistor's gain as a function of frequency, as computed from each of the harmonics. The small excursion in the gain at approximately 20 KHz was a result of noise at a null in the frequency spectrum.

Based on the results of these preliminary experiments, some of the electrical operational conditions for evaluating the performance of the CHEMFET sensor were identified. The transistor bias conditions were established with an applied drain bias (V_{dd}) of 12.3 V and a gate bias (V_{gg}) of 3.1 V. These operational bias voltages were utilized to construct the load-line shown in Figure IV-13. The relatively flat load-line maximizes the output voltage swing for small changes in the gate voltage. The input impedance of the transistor was also increased by replacing the decade resistance box with a discrete 20 Mohm carbon resistor. These experiments also established the test signal used in the FFT analysis. Although a shorter pulse width more evenly distributes the amplitude of the harmonics, the amplitude of each harmonic fell below 1 mV. It was observed that by increasing the fundamental frequency of the pulse signal, the amplitude of the harmonics increased, but it also had the effect of reducing the number of harmonics in the frequency range of

Table IV-3
Gain/Phase Characteristics of CHEMFET Transistors as a Function of Gate Bias Voltage (V_{gg}).

Gate Bias Voltage (Volts)	Midband Gain (dB)
2.0	-2.9
6.0	7.0
9.9	11.3
12.0	12.3

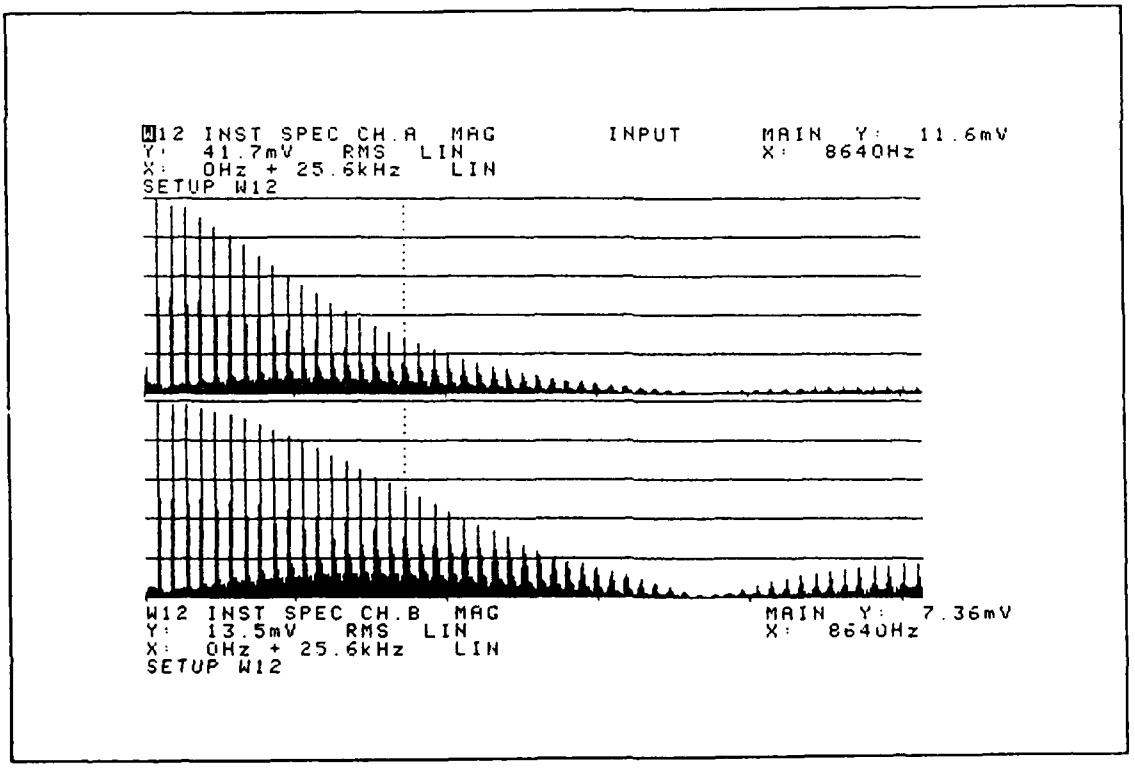

Figure IV-11. Fast Fourier Transform (FFT) Spectra of the CHEMFET Output Signal (above) and the Pulse Excitation Signal (below).

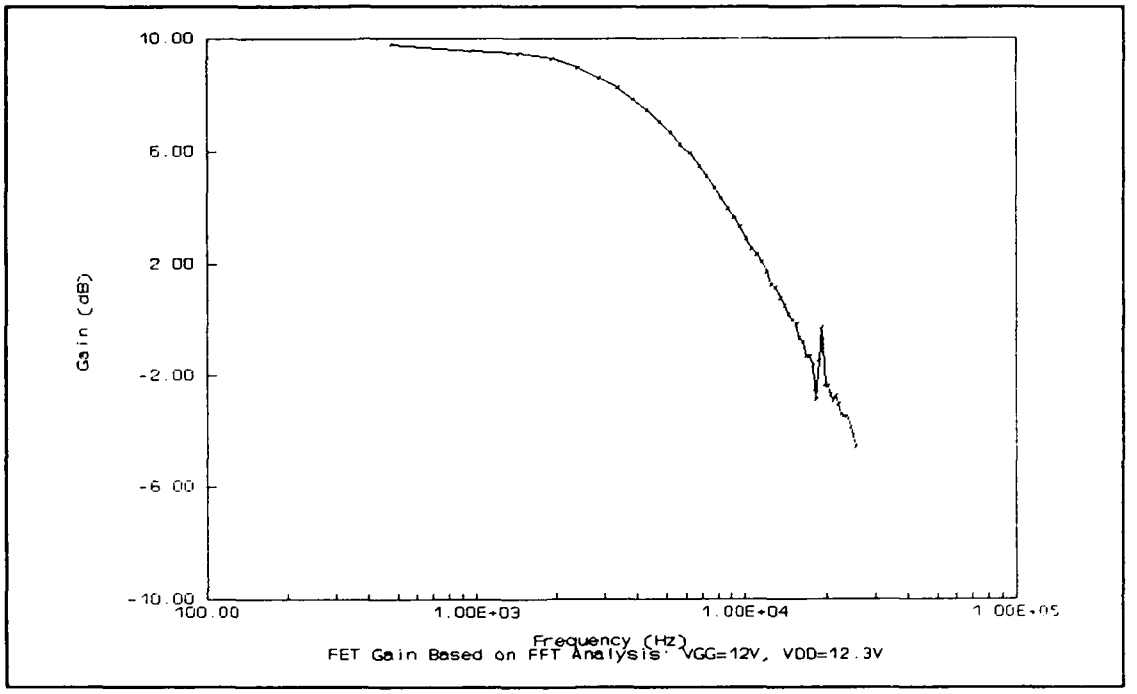

Figure IV-12. CHEMFET Transistor Gain Computed From the Fast Fourier Transform Spectra of the Excitation and Output Waveforms.

interest (below 25.6 KHz). Considering these tradeoffs, the test signal established had a pulse width of 50 μs with a frequency of 256 Hz and an amplitude of 4 V (Figure IV-14).

Gas Generation and Delivery System

This section describes the fabrication and operation of the challenge gas generation and delivery system used to evaluate the performance of the CHEMFET sensor. The challenge gas generation and delivery system was required for two reasons. First, the gas system was necessary to generate, dilute, control, and exhaust known concentrations of the challenge gases (NO_2 and DIMP). Second, the gas

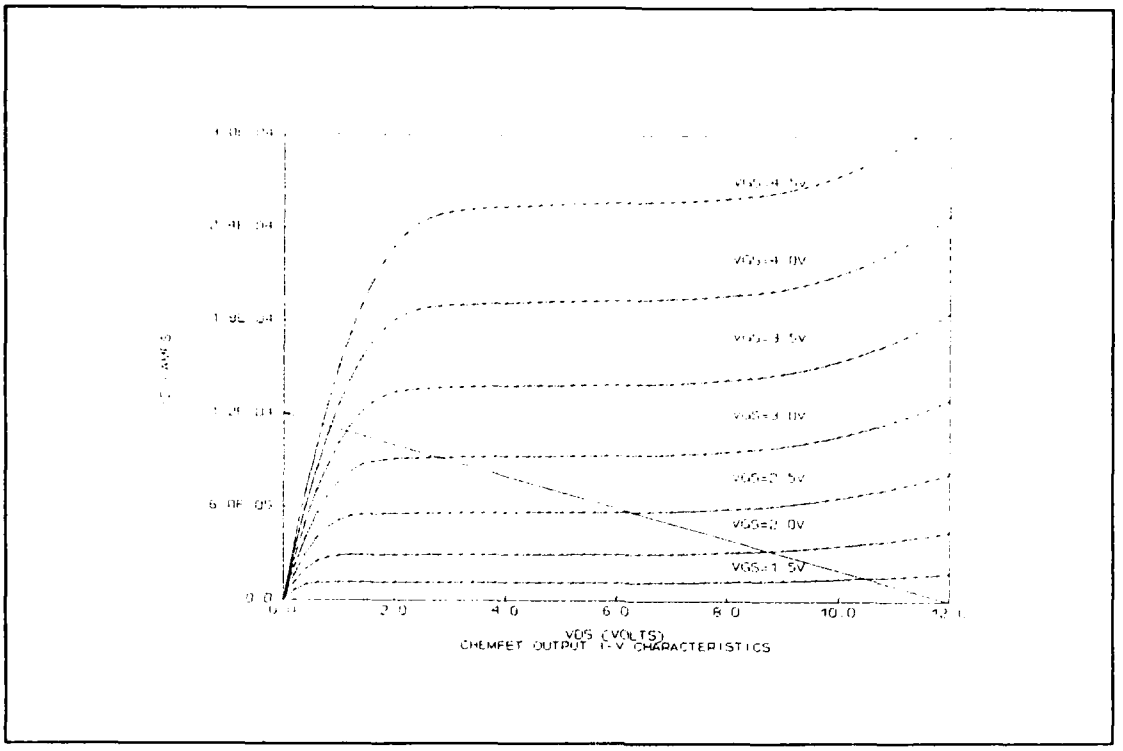

Figure IV-13. CHEMFET Load Line Established for Operational Bias Voltages.

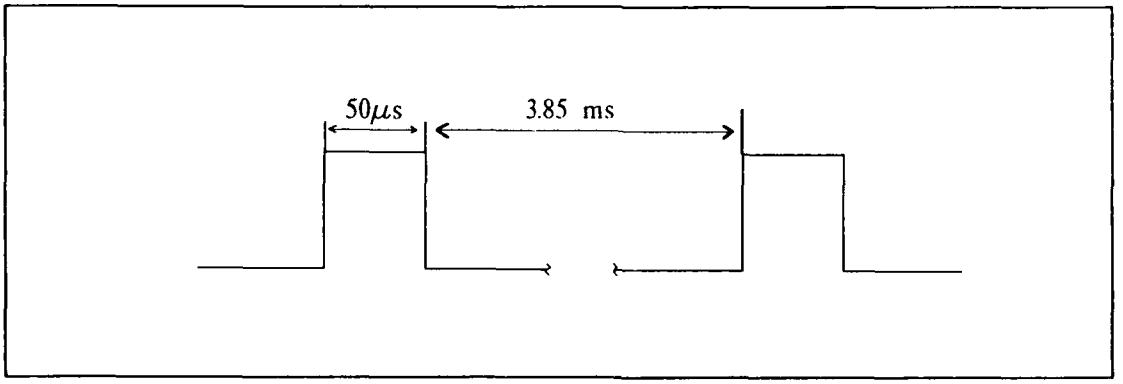

Figure IV-14. Excitation Signal Established for Fast Fourier Transform Spectrum Measurements of the CHEMFET.

system provided a means for controlling the cell's humidity and temperature during an experimental performance evaluation. As part of the challenge gas generation and delivery system, a sensor cell was fabricated such that the electrical properties of the CHEMFET could be monitored simultaneously during exposure to a challenge gas. A schematic of the challenge gas generation and delivery system is shown in Figure IV-15.

Fabrication and Operation of the Gas Delivery System.

The expected gas concentration levels required to produce a measurable electrical change in the CHEMFET's thin films ranged from 1 ppb to 100 ppm, depending upon the film and challenge gas combination. To generate the challenge gases at these concentrations, commercial gas permeation devices were purchased (GC Industries, model 23-7392 for DIMP and model 23-7502 for NO_2, Chatsworth, CA). The permeation devices are calibrated by the manufacturer to generate a stable gas permeation rate when the temperature is carefully thermostatted. The manufacturer's calibration curves for each permeation device are posted in Appendix B. To achieve a desired challenge gas concentration, the permeated gas is diluted with a carrier gas. The manufacturer also supplied the following relationship for determining the gas concentration, in ppm (by volume), given a known carrier gas flow rate (See data sheets in Appendix B):

$$C_{ppm} = K\ P\ F^{-1} \qquad (4\text{-}1)$$

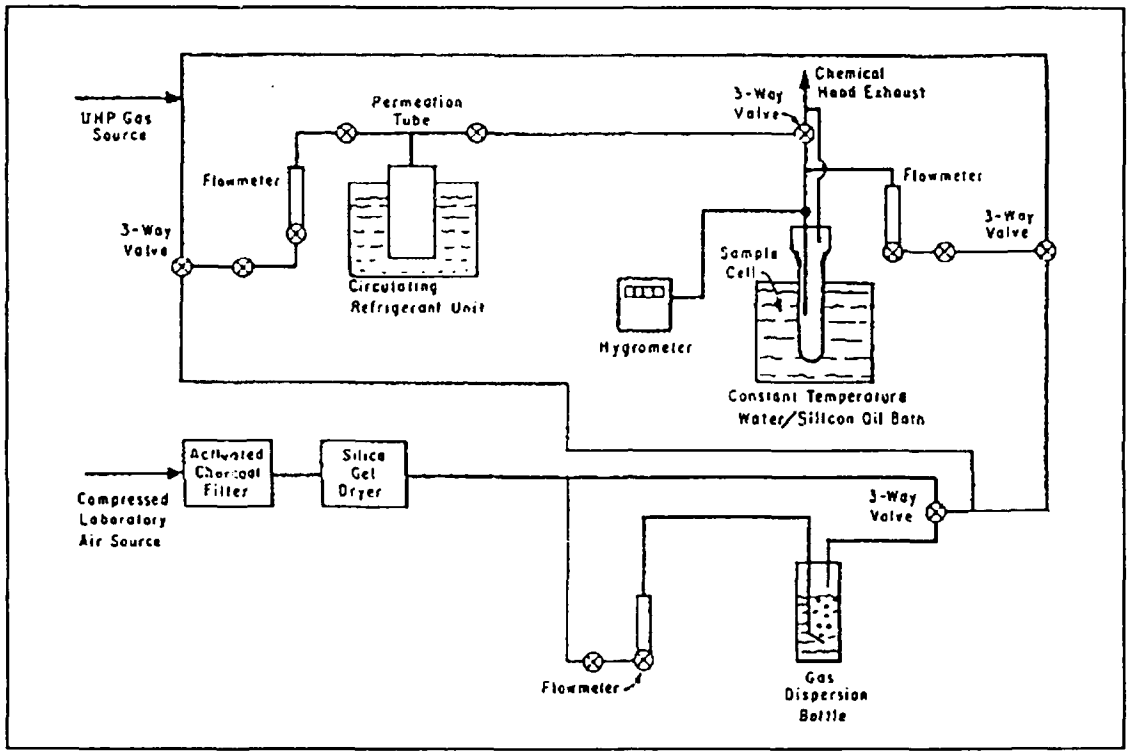

Figure IV-15. Diagram of Gas Generation and Delivery System (49).

where C_{ppm} is the challenge gas concentration in ppm

P is the permeation rate of the device in nanograms-per-minute (ng/min) from the calibration charts in Appendix B

K is an empirically determined gas constant provided by the manufacturer:

K is 0.532 for the NO_2 permeation device

K is 0.136 for the DIMP permeation device

F is the carrier gas flow rate in ml/min.

The challenge gas generation and delivery system utilized was modeled after the system developed by Kolesar (49:1731-1736) for measuring the effect of DIMP on the impedance of discontinuous metallic films. The system had three carrier gases: dry nitrogen (N_2), and dry or humidified filtered laboratory air. The laboratory air was filtered to remove organic contaminants via an activated-charcoal bed. Similarly, water was removed from the laboratory supply air by filtering it through a bed of silica gel beads. When required, the air stream was passed through a deionized water bubbler to rehumidify the carrier gas. The humidity of the carrier gases was monitored with an in-line digital display hygrometer (Thunder Scientific Corporation, model HS-1CHDT-2A, Albuquerque, NM). The hygrometer was calibrated at the factory to measure relative humidity from 0-100 percent over the temperature range 0-50 ^{o}C with an accuracy of $\pm$ 2 percent. To generate the desired challenge gas concentrations, the temperature of the permeation device was held constant in a thermostatically-controlled water bath (Neslab Corp. Refrigerated Circulating Water Bath, model RTE-88D, Newington, NH) and the carrier gas flow rate was controlled with precision flowmeters fitted with micrometer valve assemblies (Gilmont Instruments, model F-7660, Great Neck, NY). The manufacturer's calibration curves for the flowmeters are provided in Appendix B. To minimize absorption effects, all interconnections were made using 316 stainless steel tubing, fittings, and valves. The tubing was purged with trichloroethylene, followed with a rinse with acetone, and then with methanol, and finally flushing it with dry, ultra-high purity N_2. A three-way valve was used to vent the challenge gas into a

chemical hood until needed for delivery to the sensor cell. The temperature of the sensor cell was thermostatted by submerging it in a constant temperature bath. A constant temperature water bath (Lufran Corp., Superbowl, Macedonia, OH) was used to provide a constant temperature environment for bath temperatures below 50 °C. For temperatures above 50 °C, a constant temperature oil bath (Soiltest Corp, model L-114, Evanston, IL) was used.

The operational conditions of the challenge gas generation and delivery system depended upon the film material being investigated. For the epoxy cure experiments, the gas system was used to maintain a dry, constant temperature environment during the cure cycle. The relative humidity within the sensor cell was reduced to 2 percent (± 2 percent) by purging the sensor cell with dry nitrogen at a flow rate of 1 liter/minute throughout the experiment. The constant temperature water bath was set to 30°C (± 1 °C) such that the exhaust temperature of the carrier gas leaving the sensor cell was 25°C. For the CuPc and ACHE experiments, the gas system was used to deliver controlled concentrations of the challenge gases to the sensor cell, in addition to providing a constant temperature and humidity environment.

The sensor cell design was based on three considerations: 1) chamber volume, 2) the required number of external electrical connections, and 3) ease of sensor insertion and removal. A minimum chamber volume facilitates rapid equilibration of the sensor and reduces the potential for absorption of the challenge gas on the chamber walls. To simplify installation and removal of a sample, all electrical

connections were made to it via a DIP socket. To keep the overall size of the sensor cell small, the number of coaxial cables which entered the sensor cell was minimized. This objective was accomplished by capitalizing on the symmetry of the die layout, and connecting the transistors' drains and sources in parallel. As shown in Figure IV-3, the bond pad layout is identical between the large array and small array transistors. This arrangement permitted the DIP socket to be wired for just one set of transistors. The large array transistors or the small array transistors could be selected for evaluation by positioning the DIP with respect to its socket. With this approach, only 10 coaxial cables were required. A schematic of the electrical connections made within the cell is shown in Figure IV-16.

The sensor cell was constructed from a 1 liter pyrex beaker and a specially fabricated stopper, such that a sensor under evaluation could simultaneously be exposed to a gas mixture of interest, while its electronic behavior was monitored (Figure IV-17). A size 15 rubber stopper was sandwiched between two stainless steel plates. An Allen-head bolt was inserted into a hole drilled through the center of the sandwich and screwed into a threaded hole in the bottom plate. Tightening the Allen bolt compresses the rubber stopper against the beaker wall forming a gas tight seal. Fourteen 0.25 inch holes were drilled into the sandwich. Stainless steel tubes were inserted into twelve of the holes to produce 1 inch nipples on top of the sandwich

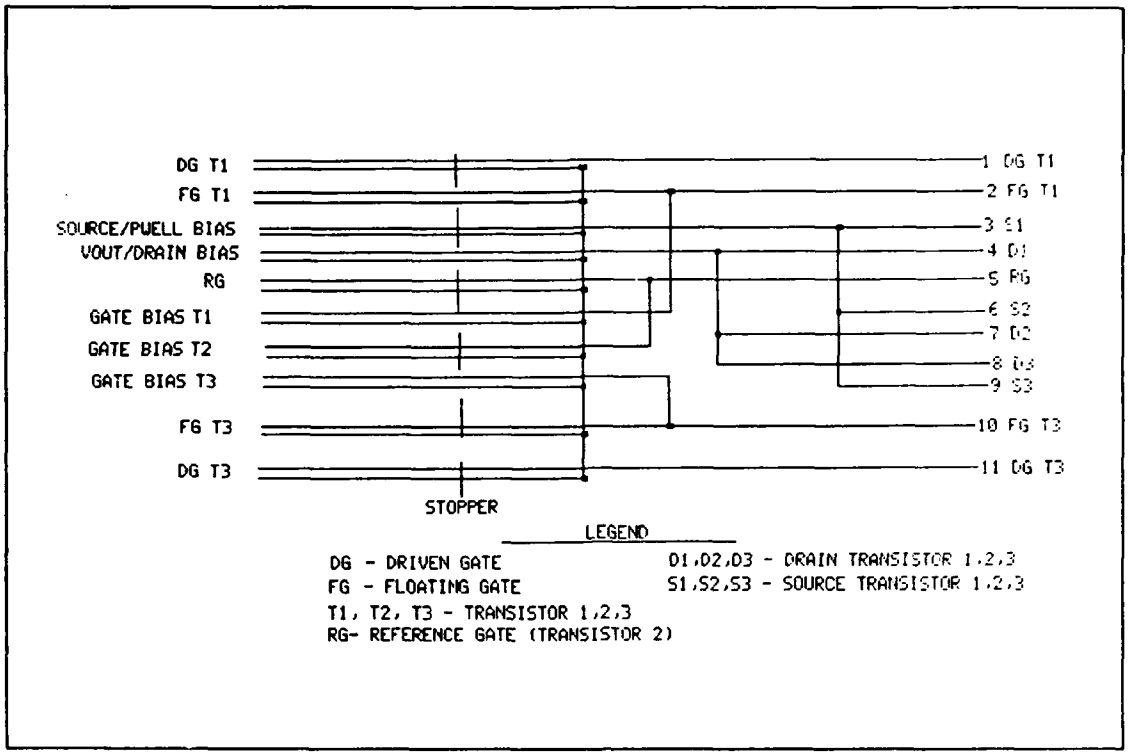

Figure IV-16. Schematic of Electrical Connections Within Sensor Cell.

which served as ports for the electrical connections. The other two holes were used as inlet and exhaust ports for the challenge gas generation and delivery system. Ten RG-58A/U coaxial cables were inserted through the ten stainless steel lined ports and sealed by tightly wrapping teflon tape around each nipple. Inside the stopper, the center conductors of the coaxial cables were soldered to a DIP socket pin with short lengths of aluminum wires. The outer shields of the coaxial cables were shorted together inside the sensor cell. A Type-K thermocouple (Omega Engineering Corp., model 175-KCL, Stanford, CT) was inserted into one of the electrical access ports for monitoring the sensor cell's temperature. The remaining port was not used, and

it was sealed with teflon tape. The sample was shielded from electrical noise by wrapping the beaker with aluminum foil and connecting the foil to a common electrical ground.

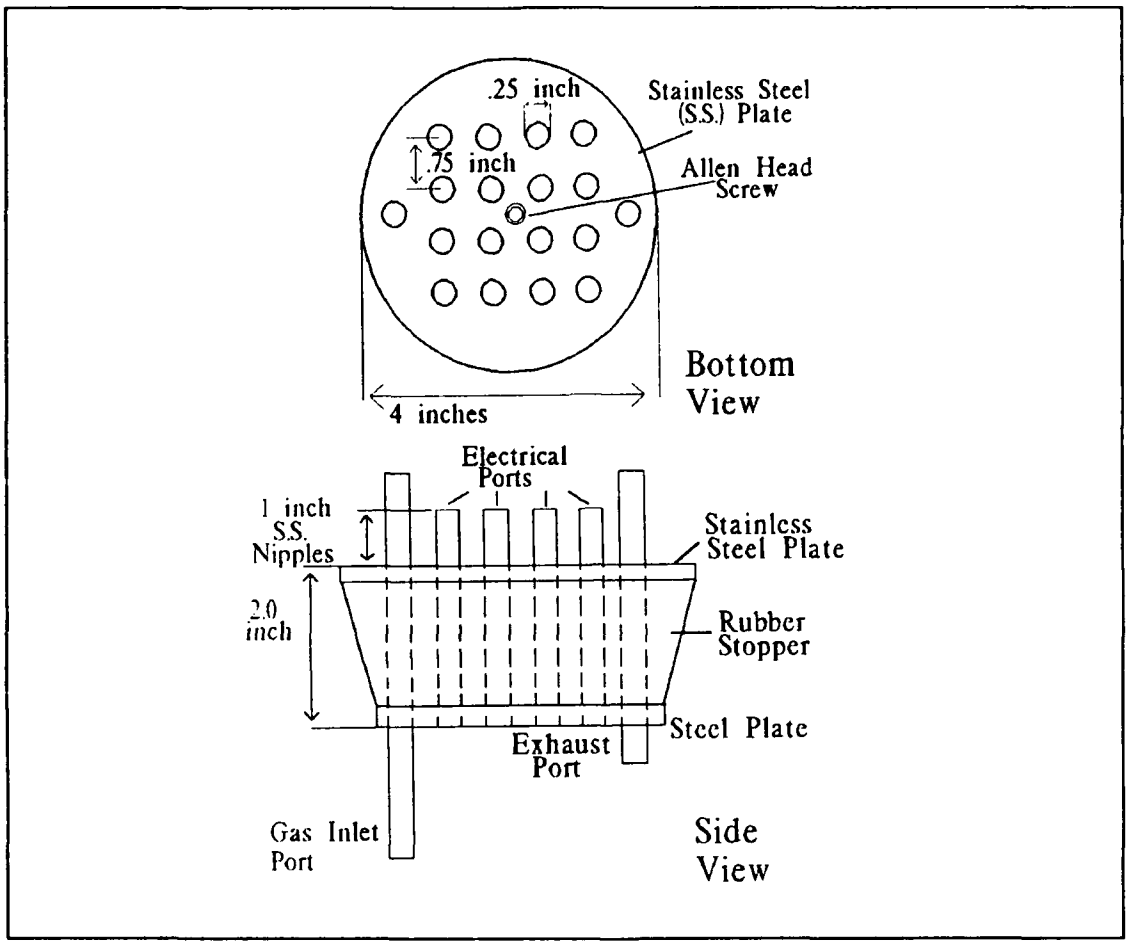

Figure IV-17. Sensor Stopper Cell Design.

CHEMFET Electrical Performance Instrumentation Configuration

This section describes the instrumentation configuration and the baseline test procedure used to evaluate the electrical performance of the CHEMFET with all three thin film coatings (epoxy, copper phthalocyanine, and acetylcholinesterase).

Any variations from the baseline test procedure are explicitly discussed in the sections concerned with the performance evaluation of a particular film. As described in the previous section, only one set of three transistors, either the large array or small array transistors, are connected in the sensor cell at any given time. Of these three transistors, only one interdigitated gate transistor (CHEMFET sensor) and the reference transistor are evaluated during an experiment. The gate bias of the interdigitated transistor not under test is connected to ground throughout the experiment. Similarly, when measurements were made on the interdigitated gate (reference) transistor, the gate bias of the reference (interdigitated gate) transistor was grounded.

A set of eight different electrical measurements were made on the CHEMFET as the coating on the interdigitated gate underwent a chemical change. This set is referred to as the baseline electrical measurements. This set includes:

1) Resistance of the Interdigitated Gate

2) Impedance of the Interdigitated Gate

3) Gain and Phase of the Interdigitated Gate

4) Gain and Phase of the CHEMFET Sensor

5) Gain and Phase of the CHEMFET Sensor Transistor

6) Gain and Phase of the CHEMFET Reference Transistor

7) Frequency Response of the Interdigitated Gate to a Pulse Excitation

8) Frequency Response of the CHEMFET Sensor to a Pulse Excitation.

The instrumentation scheme utilized to accomplish these electrical performance measurements is shown in Figure IV-18. A detailed schematic of the instrumentation scheme is provided in Appendix C. Automated instrument configuration and data collection was controlled via a Z-248 microcomputer and an IEEE-488 interface plug-in card (Capitol Equipment Corp., model 01000-60300, Burlington, MA). The controller computer program, written in BASIC and IEEE-488 interface code, is listed in Appendix D.

The resistance and impedance measurements of the interdigitated gate electrode structure were performed with the transistor's gate bias lead floating. The measurement of the interdigitated gate resistance was accomplished with an electrometer (Kiethley Instruments, model 617, Cleveland, OH). The electrometer was operated in its V/I mode. This mode of operation minimizes the effects of leakage resistances and distributed capacitance, and it permits the measurement of resistances as large as 10^{16} ohms (45:2-19). When making a measurement, the electrometer was manually enabled and allowed to stabilize. After a stable reading was achieved, the resistance data was collected via the data collection software. Swept frequency measurements of the interdigitated gate impedance were made with a low frequency impedance analyzer (Hewlett-Packard Corp., model HP4192A, Palo Alto, CA). The impedance was measured over a frequency range of 5 Hz-13 MHz.

The impedance analyzer uses a four-wire measurement technique to make high-accuracy impedance measurements. As shown in Figure IV-19, the four terminal connections were made external to the sensor cell. A zero-short calibration was

performed at the beginning of each experimental run. A short circuit was created between two unused bonding pads on the sensor DIP. The DIP was inserted into the

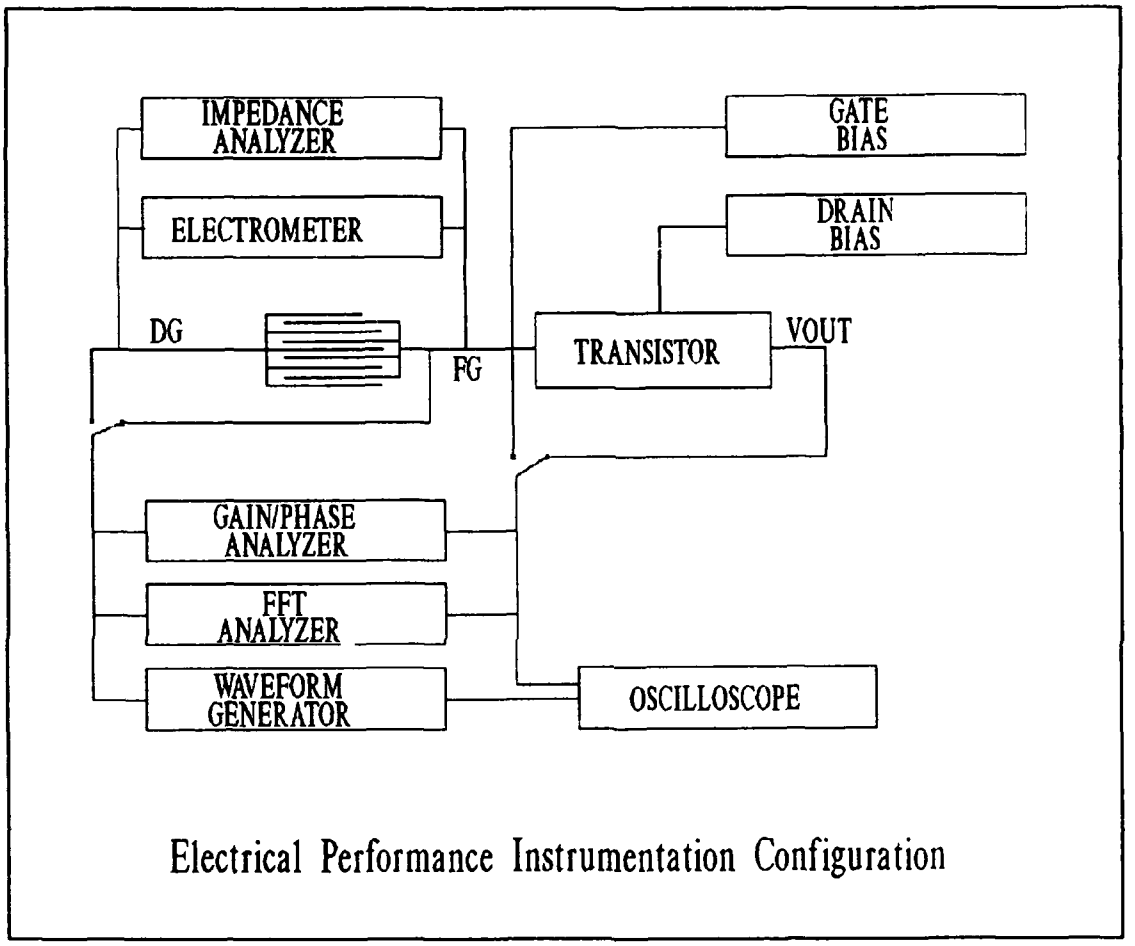

Figure IV-18. CHEMFET Baseline Electrical Performance Instrumentation Configuration.

sensor cell to accomplish the zero-short calibration measurements. The zero-short calibration result was collected via the data collection software at every test

frequency. The corresponding zero-short calibration impedance was subtracted from all subsequent measurements of the unknown's interdigitated gate impedance. The impedance analyzer was configured to measure the real and imaginary components of the unknown's impedance/admittance. The analyzer automatically selects between the impedance and admittance mode to maximize accuracy. The data collection software checks the measurement mode and converts all admittance data to the equivalent impedance.

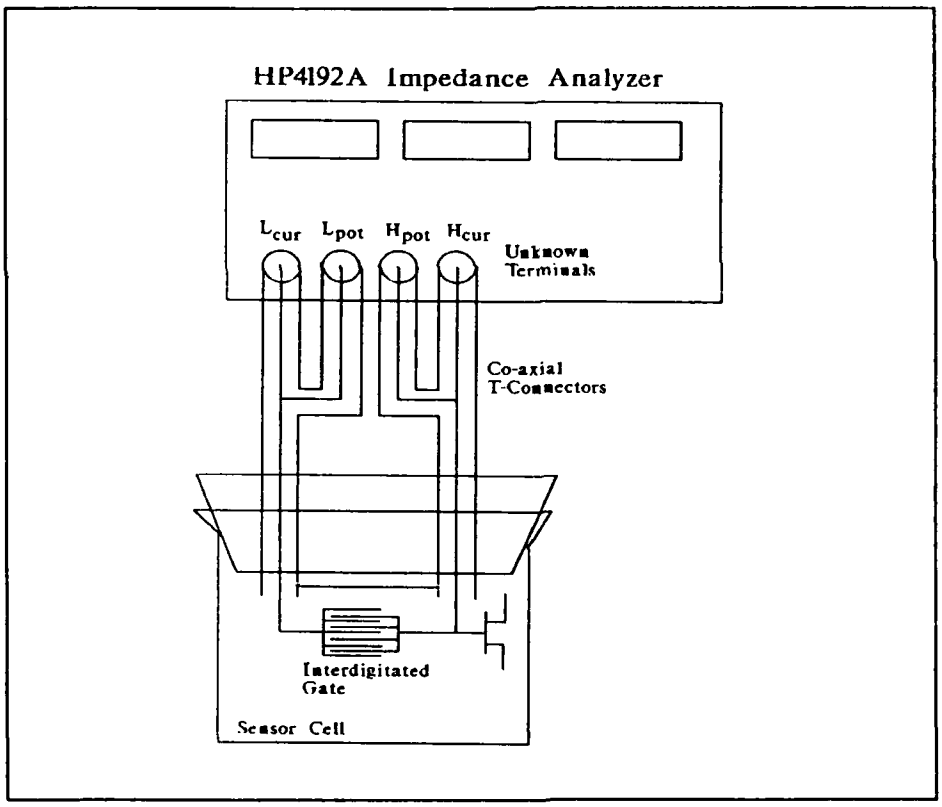

Figure IV-19. Connections for the Four-Terminal Impedance Measurement with the HP4192A Impedance Analyzer.

All other electrical measurements were performed with an applied gate bias (V_{gg}) of 3.1 V on the test transistor. As discussed earlier, the gain/phase analyzer (Hewlett-Packard Corp., model HP4194A, Palo Alto, CA) was utilized to measure the voltage gain (V_{out}/V_{in}) and phase delay (ϕ_{out}-ϕ_{in}) of several different sub-structures within the CHEMFET sensor. The input signal, $V_{in}\angle\phi_{in}$ is provided by the dual-output sweep-generator of the HP4194A. One output of the sweep generator was connected to the reference channel input of the analyzer, and the other output was applied to the input of the structure under test. The output signal from the structure ($V_{out}\angle\phi_{out}$) was applied to the test channel of the analyzer. The input and output connections for testing each structure is summarized in Table IV-4. The gain and phase of each structure was measured with a sinusoidal test signal whose frequency spanned 10 Hz-10 MHz. The signal's amplitude was set to -20 dBm. For the gain/phase measurement of either the CHEMFET sensor transistor or the reference transistor, the test signal was applied through a 0.61 μF capacitor to prevent shorting the gate bias through the 50 ohm output impedance of the gain/phase analyzer's signal generator.

The frequency response of the CHEMFET to a pulsed excitation was measured with the B&K 2032 FFT analyzer. A 256 Hz, 50 μs wide pulse excitation waveform was applied via a function generator (Wave-Tek Corp., model 148, San Diego, CA) with internal triggering. The test signal was adjusted to 4 V and applied to the driven gate of the CHEMFET sensor, and the output was measured at both

Table IV-4
Input and Output Connections for Measuring
the Gain/Phase of the CHEMFET's Sub-Structures

Structure	Input	Output
Interdigitated Gate Electrode Structure	Driven Gate (DG)	Floating Gate (FG)
CHEMFET Sensor System	DG	Drain (V_{out})
CHEMFET Sensor Transistor	FG	V_{out}
CHEMFET Reference Transistor	Reference Gate (RG)	V_{out}

the floating gate and the drain of the CHEMFET sensor. The frequency spectra of both the test signal and the output waveform were measured simultaneously with the dual-channel FFT analyzer. The FFT analyzer's configuration and a representative spectrum of the floating gate output signal, with no coating on the interdigitated gate, is shown in Figure IV-20. An alternate configuration produces the display of both the input and output spectra. A copy of this display is shown in Figure IV-21. Although both the input and output waveforms are measured throughout the experiment, the data for the input was collected only at the beginning of each performance evaluation experiment. The input FFT spectrum was collected only

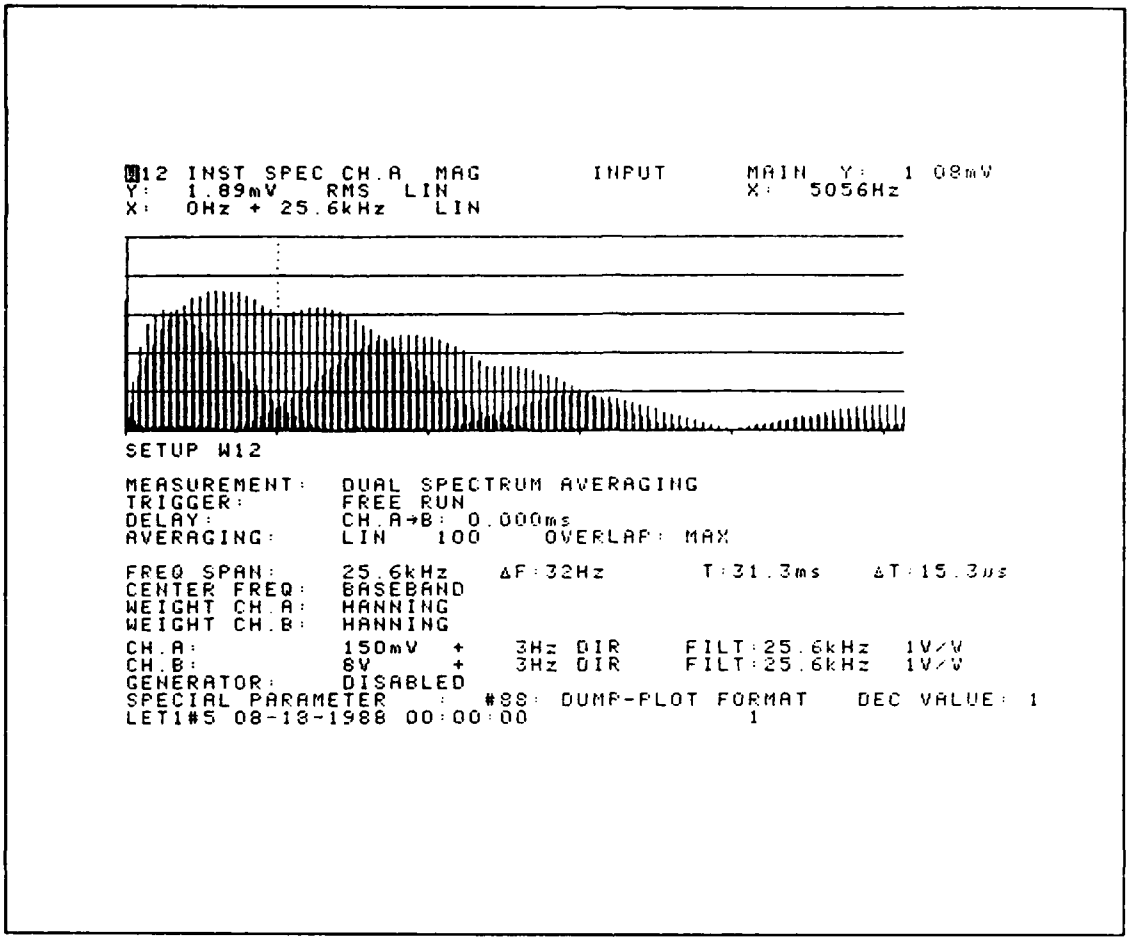

Figure IV-20. Representative Fast Fourier Transform (FFT) Analyzer Configuration and Spectrum of the Floating Gate Signal.

once because the input signal was not varied throughout the experiment. The frequency range of the analysis was limited to 25.6 KHz (the upper limit of the FFT analyzer). In addition to calculating the spectra, the applied test waveform and the measured output waveform were captured on a dual-trace oscilloscope (Tektronix Corp., model 475, Beaverton, OR).

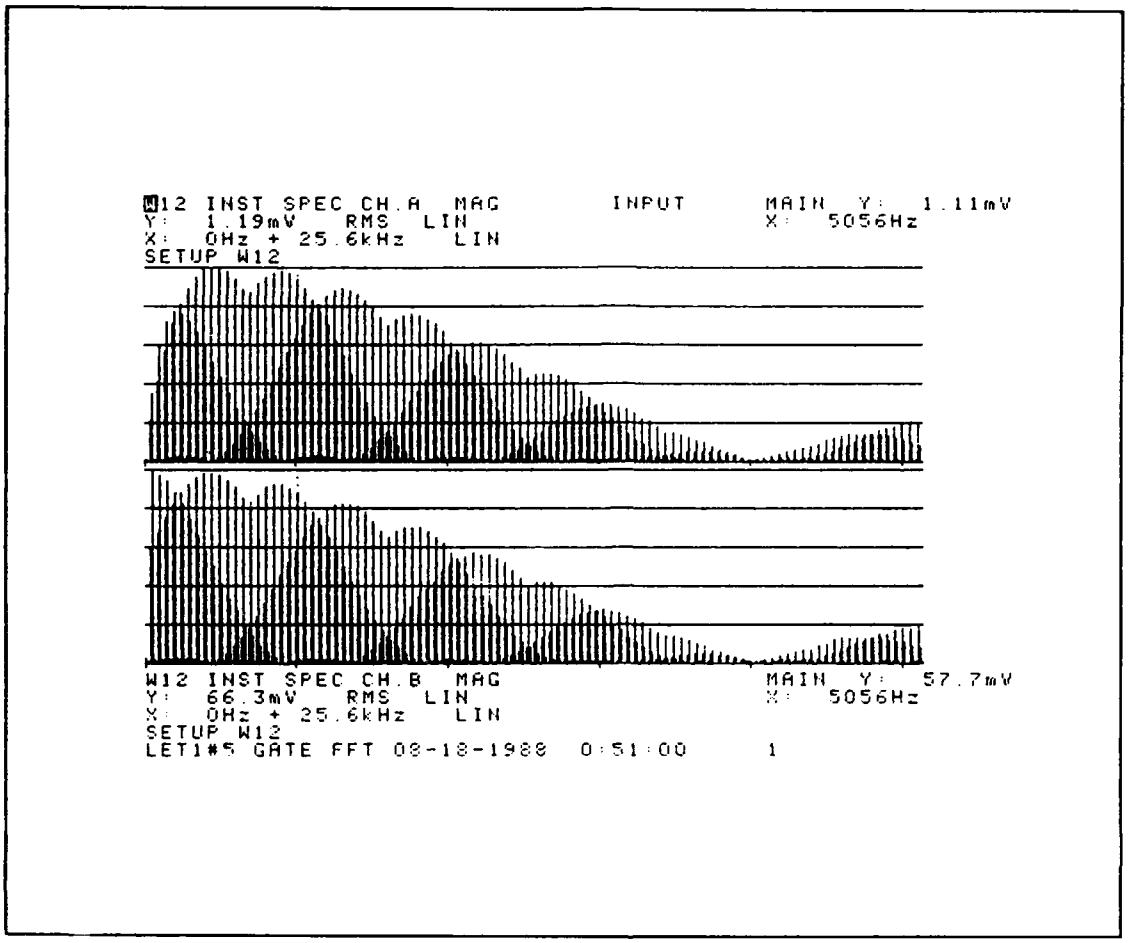

Figure IV-21. Alternate Configuration Display of the Fast Fourier Transform Analyzer Which Shows Both the Excitation and Output Signals Spectra

Experimental Test Procedures

As discussed earlier, the impedance properties of three different films were investigated with the CHEMFET: an epoxy, copper phthalocyanine (CuPc), and the enzyme, acetylcholinesterase (ACHE). The evaluation procedures for these films differ because of the unique properties of each film. This section is divided into three sections corresponding to the evaluation of the three different films. Within

each section, a brief discussion of the film properties and the experimental procedure for its evaluation with the CHEMFET are presented.

Epoxy Test Procedures.

The cure of an epoxy involves a cross-linking chemical reaction between an epoxy resin and a curing agent (46). EPON 828, a bisphenol A - epichlorohydrin epoxy resin (46), was used in this experiment. The structure of the epoxy is shown in Figure IV-22 (46). The average value of the subscript "n" in Figure IV-22 is 0.1 for EPON 828 (46). Epoxies with small values of "n" are typically liquids, like EPON 828. A polyamide curing agent, Versamide 40 (V-40), was used to cross-link the epoxy. EPON 828 and V-40 are recommended for room temperature cure (46).

The cross-linking reaction which occurs between a bisphenol A - epichlorohydrin resin and a polyamide is shown in Figure IV-23. Initially, the epoxy/curing agent mixture is a liquid. As the reaction proceeds, the epoxy resin is cross-linked into a network of increasing molecular weight. When a sufficient number of cross-links have been formed, the mixture forms a solid gel. This condition is referred to as the gelation point (34). The chemical reaction continues past the gelation point to form a rigid, glassy solid. The reaction rate slows and eventually stops as the mobility of the reactants is decreased by the increasing viscosity of the glassy solid. The formation of the glassy solid is referred to as vitrification (34).

The performance evaluation procedure for the epoxy cure was implemented as follows:

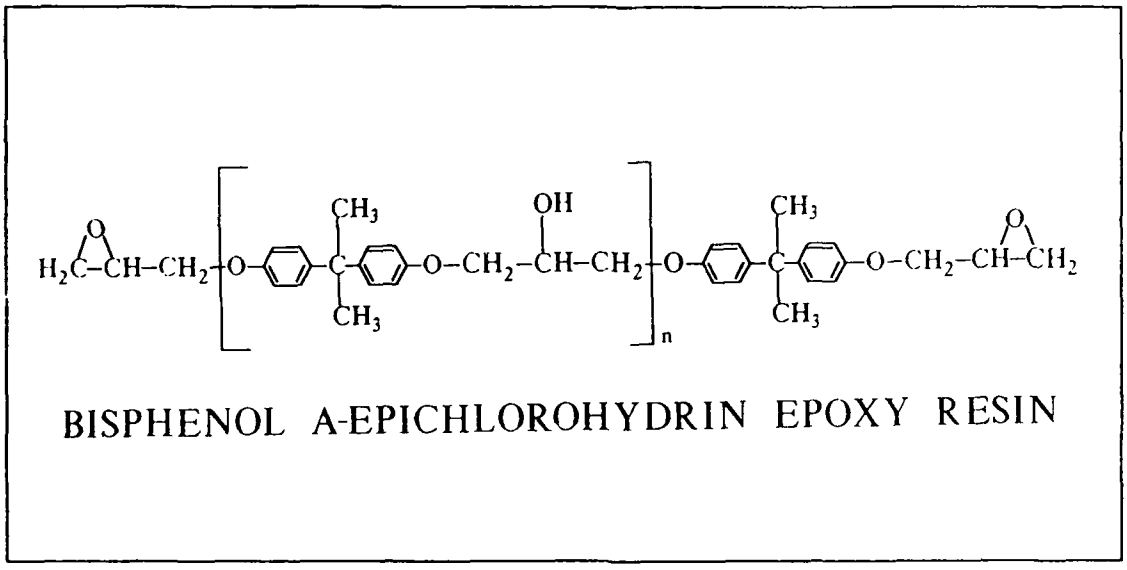

Figure IV-22. Structure of a Bisphenol A-Epichlorohydrin Epoxy Resin (46).

1) The baseline set of electrical measurements was initially performed on the uncoated CHEMFET at a temperature of 25°C (constant water bath temperature of 30°C) in the dry nitrogen environment (relative humidity approximately zero percent) of the gas sensor cell. The nitrogen flow rate was regulated at 1 liter/minute. For the resistance measurement, the internal voltage source of the electrometer was set at 100V.

2) An equal volume of EPON 828 and Versamide 40 were mixed and deposited on the interdigitated gate of the CHEMFET sensor. A 3cc syringe with a 25 gauge hypodermic needle was used to apply the epoxy. The beveled edge of the needle was cut off to improve control of the deposition rate. Small amounts of the epoxy were applied at several points along the length of the array to reduce its

lateral spread across the chip and to prevent it from contacting adjoining interdigitated arrays. Approximately 30 minutes was required to apply the epoxy.

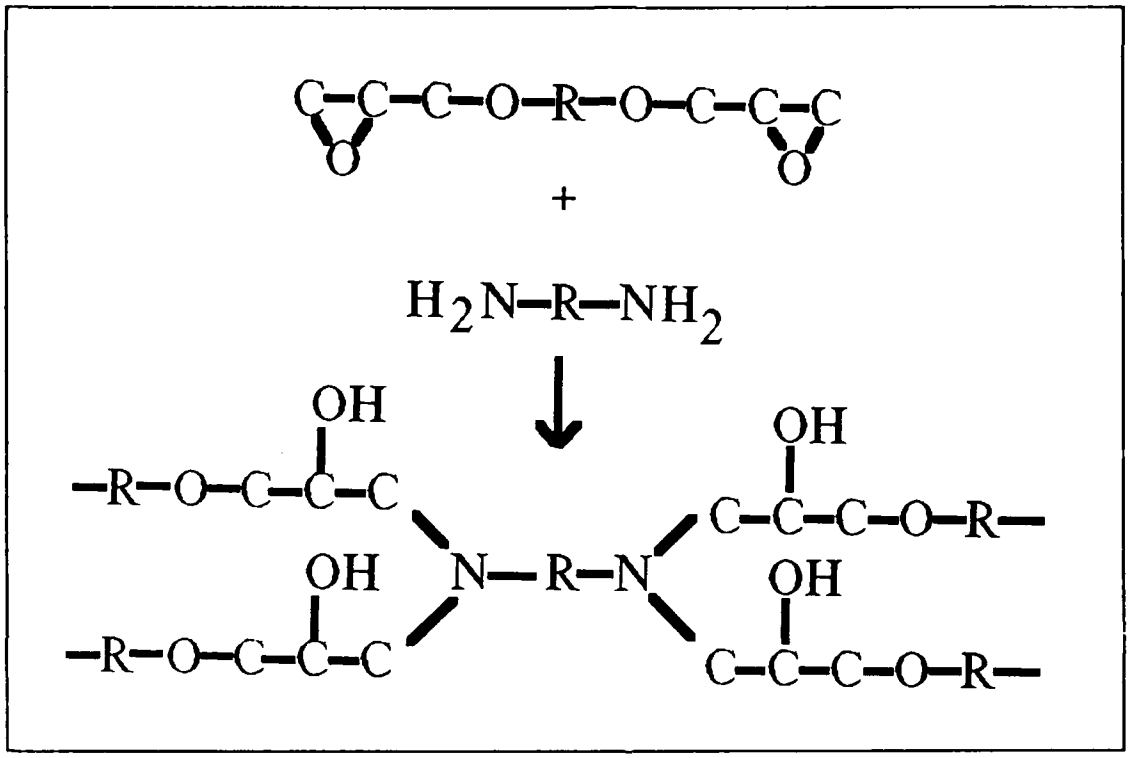

Figure IV-23. Cross-Linking Reaction Between a Bisphenol A-Epichlorohydrin Epoxy Resin and a Polyamine Curing Agent (46).

3) The sample was reinstalled within the sensor cell and purged with dry nitrogen at a flow rate of 1 liter/minute. Electrical performance measurements were initiated when the relative humidity within the sensor cell dropped below 10 percent (approximately 5 minutes).

4) Early in the cure cycle, the baseline electrical measurements were repeated continuously. Two hours into the cure cycle the measurements were repeated less often, approximately every hour.

CuPc Test Procedures.

Copper phthalocyanine is one of several metal-substituted phthalocyanines whose conductivity is highly sensitive to a number of different gases. Phthalocyanine is an azoporphyrin which is similar in structure to the heme-group in the hemoglobin protein, and the cytochromes, a class of electron-transfer proteins. The phthalocyanines are also well known organic semiconductors. The phthalocyanine structure is shown in Figure IV-24. Chemiresistors using metal-substituted phthalocyanines as the gas-sensitive film have been reported to detect part-per-billion concentration levels of NO_2 and DMMP (10:27-37;7:155-165). Temperature studies with copper phthalocyanine have shown that the greatest sensitivity to NO_2 was achieved at 170°C (10:27-37). Furthermore, both the response and recovery times of the phthalocyanines to a transient gas challenge is shortened at higher temperatures and with thin film thickness (25:151-156).

In this research, a 1000Å CuPc film was deposited on the interdigitated gate electrodes of the CHEMFET using the electron beam thermal evaporation process described in Appendix E. The film thickness was monitored with a pre-calibrated piezoelectric quartz microbalance detector. The calibration of the piezoelectric film thickness detector is described in Appendix F.

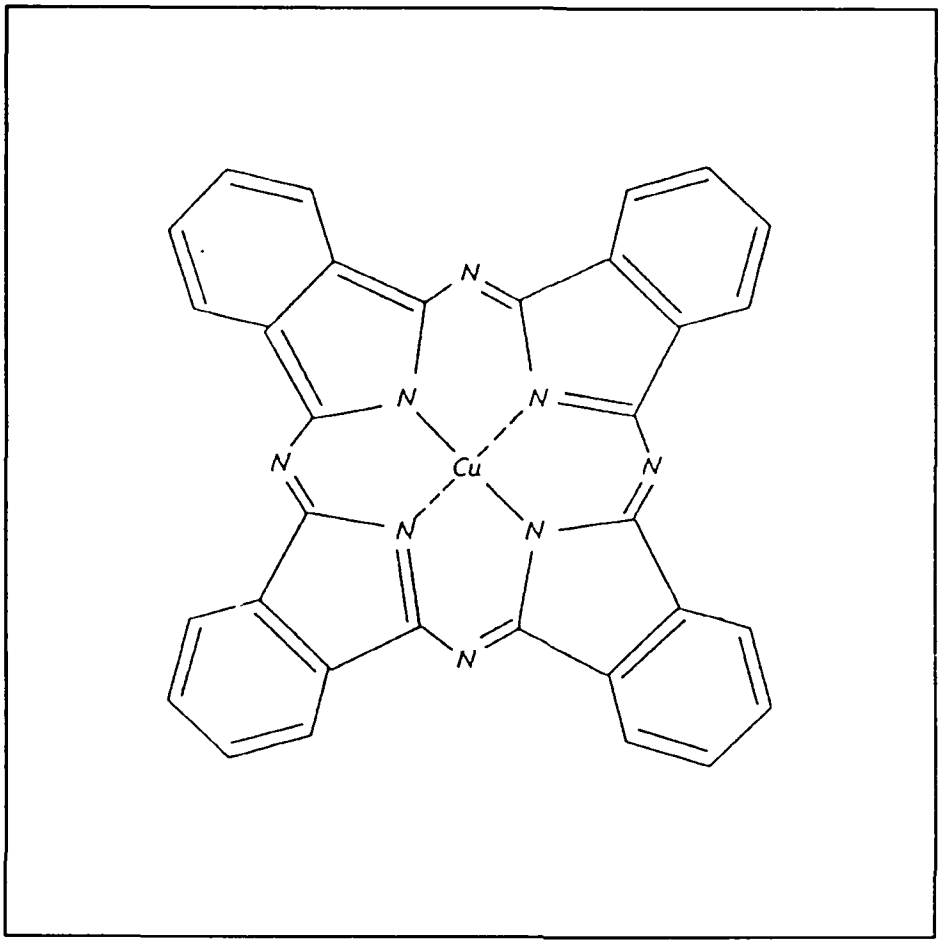

Figure IV-24. Chemical Structure of Copper Phthalocyanine (50:304)

The experimental approach was to perform the baseline set of electrical measurements on the CHEMFET with a thin film of copper phthalocyanine deposited on the interdigitated gate electrode, as the sensor was exposed to increasing concentrations of the challenge gas (either NO_2 or DIMP). The CHEMFET was exposed to five NO_2 concentrations in two separate experiments. In the first experiment, the NO_2 challenge concentrations were 40, 100, 200, 300, and

400 ppb. The large response observed at the 40 ppb concentration motivated a reduction of the challenge concentrations in the second experiment (20, 30, 40, 70, and 100 ppb). The DIMP challenge concentrations were 100, 200, 300, 800, and 4000 ppb. To generate these concentrations, the temperature of the NO_2 permeation device was cooled to 13°C to achieve a permeation rate of 500 ng/min, and the temperature of the DIMP permeation tube was heated to 50°C to realize a permeation rate of 7600 ng/min. The carrier gas (filtered and dry laboratory air), was mixed with the challenge gas at the flow rate required to achieve the desired challenge concentrations. A silicon oil filled constant temperature bath was thermostatted at 125°C to heat the submerged sensor cell. Preliminary experiments revealed that the coaxial cables within the sensor cell could not withstand bath temperatures greater than 150°C. Between successive challenge gas exposures, the sensor cell was purged with the carrier gas while the challenge gas was adjusted to the next concentration level and allowed to equilibrate on a continuous flow basis by venting it to the exhaust hood. The purge flow rate was regulated at 8 liters/minute. The baseline set of electrical measurements were started after a 30 minute exposure to the challenge gas, or after purging it with the carrier gas for 30 minutes. The exposure or purge test condition was continued during the 30 minute time period required to perform the baseline electrical performance measurements. The baseline electrical performance measurements were modified to provide a DC bias voltage during the resistance, impedance, and the interdigitated gate and CHEMFET sensor FFT measurements. For the resistance and impedance

measurements, a 10 V DC bias was supplied by the internal voltage sources of the electrometer and impedance analyzer, respectively. For the FFT measurements, a 10 V DC bias was supplied by the DC bias offset feature of the function generator.

In addition to the baseline electrical measurements, three other electrical measurements were performed. The FFT spectra of the CHEMFET sensor and the reference transistor were measured once prior to exposure to a particular challenge gas. The third electrical measurement was the resistance of the interdigitated gate electrode during the 30 minute exposure and purge times. This data revealed the time response of the CHEMFET sensor to exposure and purge cycles of the challenge gas. The collection of the film's resistance during the exposure or purge cycle was performed manually.

ACHE Test Procedures.

Acetylcholinesterase is an enzyme which catalyzes the hydrolysis of acetylcholine and plays a role in nerve impulse transmission (47:866-870). The molecular weight of the enzyme is approximately 250,000, and it has two binding sites for the substrate, acetylcholine (47:866). The positively charge quaternary ammonium group of acetylcholine binds to an anionic site and positions the substrate such that the acetyl group can react with a serine residue at the esteratic binding site (47:866). Figure IV-25 illustrates the chemical reaction which occurs at the active site of the enzyme. Organophosphorus compounds, such as chemical warfare nerve agents and common pesticides, irreversibly bind to the active site of the enzyme by phosphorylation of the serine residue (47:867).

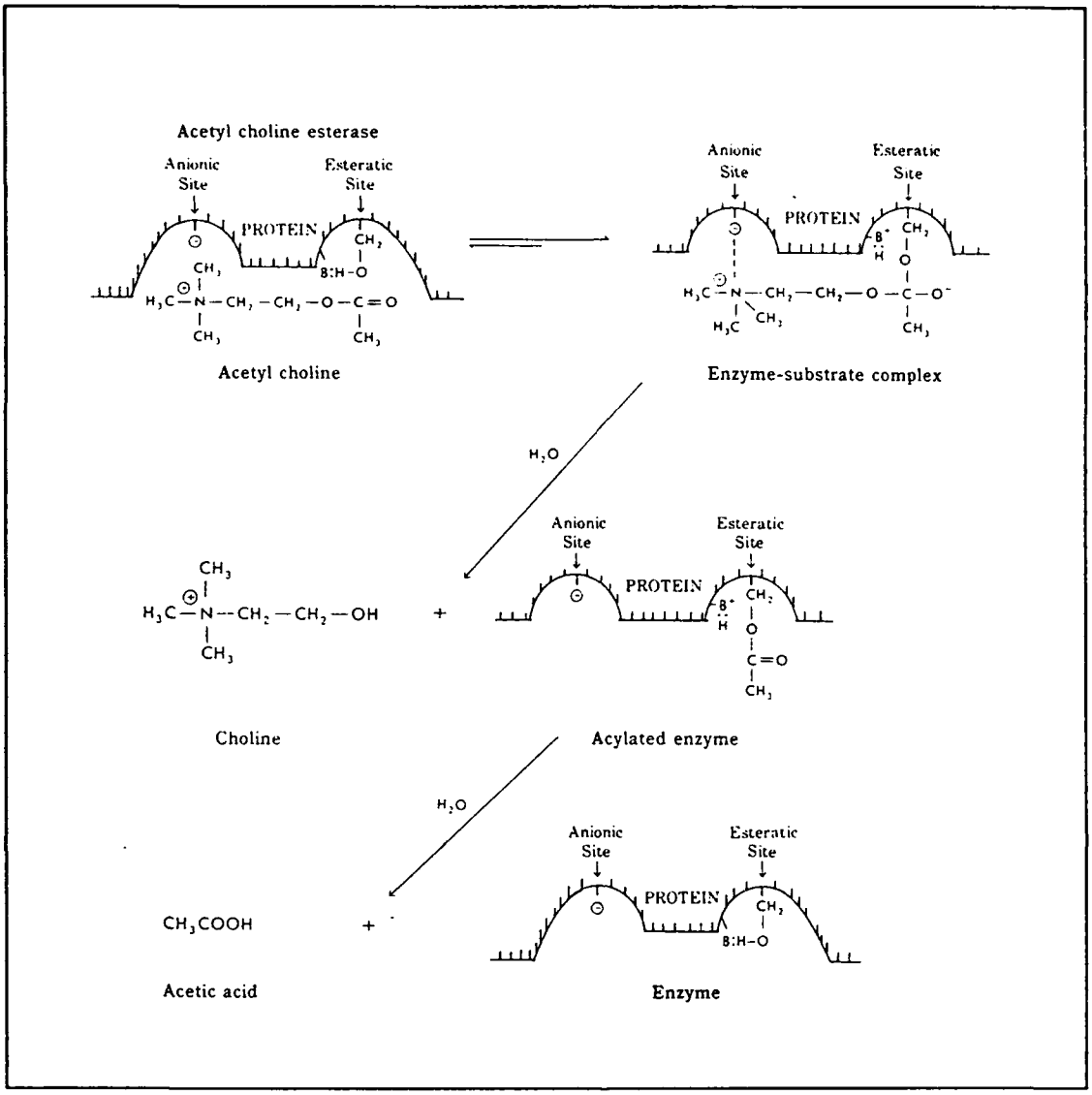

Figure IV-25. Enzymatic Reaction Catalyzed by Acetylcholinesterase (47).

The activity of enzymes is strongly dependent on their three-dimensional structure. Enzymes are composed of a sequence of amino acids connected by single bonds, and folded into a specific configuration to achieve their biological activity.

The three-dimensional structure of the enzyme is stabilized by hydrogen bonds, hydrophobic interactions, and ionic interactions. Thus, the normal biological environment for enzymes requires tightly controlled temperature and ionic (pH) conditions. However, this does not preclude enzymatic activity in the crystalline state. Ribonuclease, chymotrypsin, and carboxypeptidase have been shown to retain their catalytic activity in the crystalline state (48:141).

In this study, an ACHE film was deposited on the interdigitated gate of the CHEMFET, and it was exposed to the organophosphorus compound, diisopropyl methylphosphonate (DIMP). The DIMP structure is shown in Figure IV-26. The chemical change in the ACHE film was anticipated to be reflected in the electrical properties of the film.

A set of four experiments were performed to evaluate the impedance modulation characteristics of the ACHE film upon exposure to DIMP. In the first two experiments, the baseline electrical measurements were performed on a CHEMFET coated with an ACHE film during its exposure to DIMP. The first experiment used a DIMP challenge concentration of 500 ppb that was delivered at a constant relative humidity of 56 percent. Since no DIMP related change in the ACHE impedance properties was detected under these conditions, the second experiment increased both the challenge concentration and the relative humidity. A long term drift in the resistance was observed during both the first and second experiment. To collect more data on this drift phenomenon, the sensor cell was purged with carrier gas at the end of the second experiment, and the resistance was

measured overnight. In the third experiment, an ACHE solution was deposited on the CHEMFET interdigitated gate electrode structure and the film's resistance was measured as the water evaporated. This measurement was repeated during successive applications of the ACHE solution. In the fourth experiment, the ACHE solution was exposed to the DIMP challenge gas prior to deposition on the interdigitated gate of the CHEMFET. The resistance of both an unexposed ACHE solution and the DIMP exposed ACHE solution was measured on the CHEMFET interdigitated gate electrode structure. The detailed test procedure for each of these experiments is outlined in the following four sub-sections.

ACHE Experiment Number 1.

1) The acetylcholinesterase (1000 activity units) was dissolved in deionized water at a concentration of 5 mg/ml and stored at 4°C. A 5 μl aliquot of the enzyme solution was deposited on the interdigitated gate of the packaged CHEMFET and allowed to dry at 4°C.

2) The baseline set of electrical measurements were performed in a manner similar to the CuPc experiments. That is, a 10 V DC bias was applied during the measurement of the resistance and impedance, and during the measurement of the interdigitated gate and CHEMFET sensor FFT spectra. The FFT spectra of the CHEMFET sensor and the reference transistor were also made once prior to exposure with the challenge gas. The resistance was measured manually during exposure and purge of the sensor cell. The internal sensor cell temperature was kept

constant at 37°C (constant water bath temperature of 40°C). The relative humidity and temperature were measured throughout the experiment.

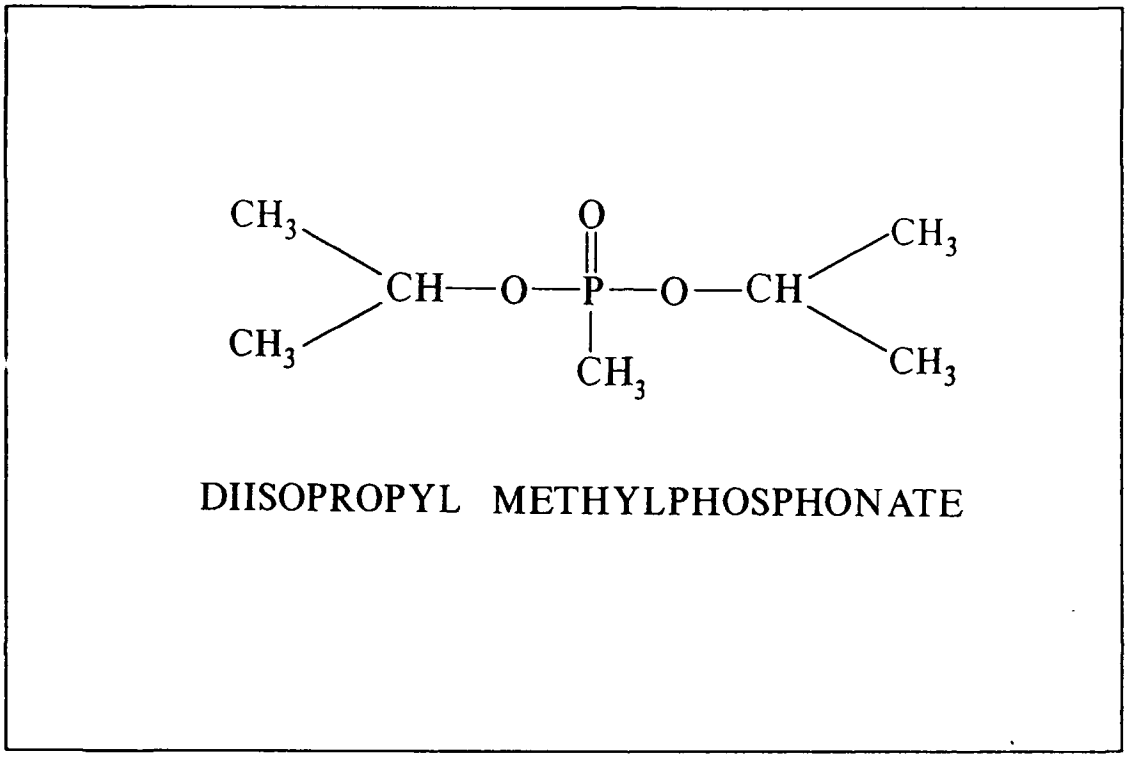

Figure IV-26. Structure of Diisopropyl Methylphosphonate (4).

3) The CHEMFET was installed in the sensor cell and purged for 30 minutes with the carrier gas (humidified laboratory air) at a flow rate of 2 liters/minute. Following this purge, the baseline set of electrical measurements were performed. The purge flow rate was established at the same flow rate necessary to achieve a challenge gas concentration of approximately 500 ppb. Initially, the challenge gas was

vented during the purge. However, this increased the flow rate through the bubbler which increased the humidity of the carrier gas. In addition, when the purge to the sensor cell was turned off and the challenge gas was applied, the flow through the bubbler would decrease, and this arrangement decreased the humidity of the carrier gas. As a result, the decreased humidity level caused the resistance to slowly increase. After a 10 minute exposure to the challenge gas, the challenge gas was vented to the hood and the sensor cell was purged. The relative humidity was again increased. To maintain a constant relative humidity, the challenge gas was turned off during exposure to carrier gas. After an additional 30 minutes of purging, a second set of baseline electrical measurements were performed.

4) To equilibrate the challenge gas prior to delivering the challenge gas to the sensor cell, the purge flow was turned off and the challenge gas was vented to the chemical hood at a flow rate of 2 liters/minute for 10 minutes. The temperature of the DIMP permeation tube was held constant at 50°C to provide a permeation rate of 7600 ng/min. During this time, with no flow through the sensor cell, the relative humidity in the sensor cell was observed to increase slightly.

5) The challenge gas was delivered to the sensor cell at a flow rate of 2 liters/minute. The relative humidity within the cell quickly attained its equilibrium value of 56 ± 1 percent. The baseline electrical measurements were performed after 30, 90, and 150 minutes of exposure to the challenge gas.

ACHE Experiment Number 2.

1) A 5μl aliquot of the enzyme solution prepared in the ACHE Experiment Number 1 was deposited on the interdigitated gate of a packaged CHEMFET and allowed to dry at 4^{o}C.

2) To increase the humidity within the sensor cell, the gas delivery system was modified to position the output of the water bubbler adjacent to the sensor cell.

3) Two independent gas delivery lines were installed on the gas sensor cell: one line provided humidified laboratory air, and the second line delivered the challenge gas. The temperature of the DIMP permeation device was held constant at 50^{o}C to generate a permeation rate of 7600 ng/min. Dry laboratory air was passed over the permeation device at a flow rate of 250 ml/min to produce a challenge concentration of 4 ppm.The flow rate of the humidified air was set at 1 liter/min and kept constant throughout the experiment. The two gas flows were mixed within the sensor cell to produce a final challenge concentration of 1 ppm.

4) The ACHE coated CHEMFET was installed in the sensor cell and was purged with carrier gas for 90 minutes prior to performing the baseline electrical measurements. The purge consisted of the 1 liter/minute humidified air mixed with the dry air source flowing at 250 ml/min. The challenge gas was vented to the hood during the purge.

5) The sample was exposed to the DIMP challenge. The baseline electrical measurements were performed after 30, 90, and 150 minutes of exposure to the challenge gas.

6) The challenge gas was turned off and the sensor cell was purged as discussed above. The DC resistance of the interdigitated gate was measured overnight at 25 second intervals.

ACHE Experiment Number 3.

1) An adapter was constructed so that the packaged CHEMFET was positioned upright when placed in the sensor cell. The adapter is shown in Figure IV-27.

2) The CHEMFET was placed in the adapter and inserted into the sensor cell. The sensor cell was left at room temperature (22°C) without any gas flow. The ambient relative humidity was 85 percent.

3) A 5μl aliquot of the enzyme solution prepared in ACHE Experiment Number 1 was deposited on the interdigitated gate of the CHEMFET. Additional 5μl aliquots of the enzyme solution were applied to the interdigitated gate after the previously deposited aliquot had dried.

4) The resistance of the interdigitated gate was measured prior to the ACHE deposition and throughout the repeated applications of the enzyme solution. The resistance was measured with the electrometer operated in the V/I mode using a 10 V DC bias.

In the fourth experiment, the ACHE solution was exposed to the DIMP challenge gas prior to deposition on the interdigitated gate of the CHEMFET. The resistance of both an unexposed ACHE solution and the DIMP exposed ACHE solution was measured on the CHEMFET interdigitated gate.

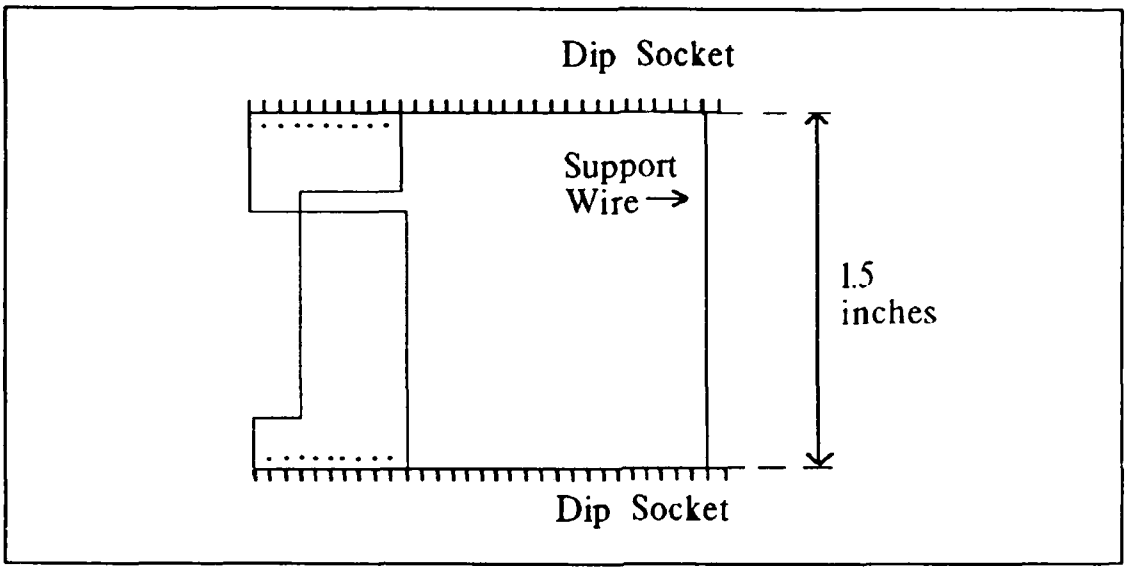

Figure IV-27. Adapter to Position the Packaged CHEMFET Upright when Inserted into the Sensor Cell.

ACHE Experiment Number 4.

1) A 50 μl aliquot of the ACHE solution prepared in ACHE Experiment Number 1 was placed in a Eppendorf microcentrifuge tube, inserted into the gas sensor cell and exposed to a DIMP challenge for 30 minutes. The DIMP challenge was delivered to the sensor cell using the modified gas delivery system described in ACHE Experiment Number 2. Dry laboratory air was passed over the DIMP permeation tube (T=50^{o}C) at a flow rate of 22 ml/minute to achieve a challenge concentration of 47 ppm. The challenge was mixed in the sensor cell with humidified laboratory air flowing at 100 ml/min. The resulting DIMP challenge concentration was approximately 8.5 ppm. The sensor cell temperature was held constant at 37^{o}C.

Under similar conditions, a second 50 μl ACHE aliquot was exposed for 30 minutes to just the carrier gas. These two ACHE solutions are referred to as "exposed" and "unexposed" ACHE, respectively.

2) A CHEMFET was placed in the sensor cell using the adapter described in ACHE Experiment Number 3. A 5μl sample of the unexposed ACHE was applied to the interdigitated gate. The resistance of the gate was measured for 60 minutes following the ACHE deposition.

3) The ACHE solution was removed by rinsing the interdigitated gate electrode structure in 400 ml of distilled water for 10 minutes. The CHEMFET was then dried in an 80^{o}C oven for 10 minutes.

4) The cleansed CHEMFET was returned to the sensor cell. A 5μl aliquot of the exposed ACHE film was applied to the interdigitated gate electrode structure. The resistance of the gate was measured for 60 minutes following the ACHE deposition.

Data Reduction and Analysis Software

The automated data collection software generates seven data files (called IMP, GP12, GP13, GP23, GP43, FFT12, and FFT13). The IMP file contains the electrometer and impedance analyzer data. The GPxx files contain the gain/phase data measured across the interdigitated gate, the CHEMFET sensor, the sensor transistor, and the reference transistor, respectively. The file FFT12 contains the interdigitated FFT data. The first two data sets in this file are the FFT spectra of the sensor and reference transistors which were measured only once during each

experiment. The third data set in this file is the initial interdigitated gate spectra and the corresponding excitation signal spectra. The remaining data sets in FFT12 possess only the interdigitated gate spectra. The FFT13 file contains the CHEMFET sensor FFT spectra. The following BASIC programs (listed in Appendix D) were written to reduce the large amount data contained in the above files:

1) IMPCOMP.BAS -- This program calculates the magnitude and phase of the impedance from the resistance and reactance data contained in the IMP file. The program stores each data set within IMP as a separate output file. To reduce the amount of data in each output file, the program stores every sixth frequency measurement in the output data files. The electrometer resistance measurements are separated from the impedance analyzer data and stored in a file called DCRES.

2) GPCOMP.BAS -- This program simply separates the data sets within the GPxx files and stores them in separate files. To reduce the output data file size, every sixth frequency measurement within each data set was stored in the output files.

3) DFFT13.BAS -- This program calculates the difference spectra for the epoxy experiment. The calculation is a direct substraction of each reference harmonic amplitude from each harmonic in the CHEMFET sensor spectra. The approximate fundamental harmonic frequency was assumed in the program to be 256 Hz. However, as a result of the finite resolution (32 Hz) of the analyzer, simple multiples of the 256 Hz did not accurately locate the harmonic components at larger frequencies. Thus, a local search routine was used to determine the location of each

harmonic. The harmonic selected was based on the greatest amplitude within the search area of ± 32 Hz.

4) NDFFT12.BAS -- This program was used to calculate the normalized difference spectra between the interdigitated gate spectra at each challenge gas exposure/purge concentration with respect to the spectrum of the interdigitated gate prior to exposure. Each spectrum was normalized with respect to the greatest harmonic amplitude contained within the spectrum. Thus, the normalization process generates a spectrum of identical shape to the measured spectrum, but the amplitude of each harmonic has a value between 0 and 1. The location of the harmonic components within the data set were located with the same local search process used in the DFFT13.BAS program.

5) NDFFT13.BAS -- This program calculates the normalized difference spectra between the CHEMFET sensor FFT spectra measured after each challenge gas exposure or purge with respect to the unexposed CHEMFET sensor spectra. Excluding the changes required to account for data structure differences, this program is identical to the NDFFT13.BAS program.

Summary

The CHEMFET design and its preliminary characterization, and the instrumentation and performance evaluation procedures used to evaluate the electrical properties of the CHEMFET in response to chemical changes in the interdigitated gate coatings were discussed in this chapter. The CHEMFET design was accomplished by modifying an earlier interdigitated gate CHEMFET design. The

purpose of each modification and the process by which the modifications were made were discussed in the first section. This section also presented the results of the preliminary electrical performance characterization of the re-designed CHEMFETs. The results obtained were used to establish some of the operational conditions for evaluating the performance of the CHEMFET sensor. The second section described the gas generation and delivery system required for the exposure of the CHEMFET to known concentrations of the challenge gases. The third section described the instrumentation configuration and the baseline test procedures used to evaluate the electrical performance of the CHEMFET. The fourth section details the experimental test procedures specific for a given film and challenge gas. The software developed for data analysis and reduction were described in the final section.

V. Results and Discussion

This chapter contains the results and analysis of the electrical measurements performed with the CHEMFET sensor coated with the three different films investigated: epoxy, copper phthalocyanine (CuPc), and acetylcholinesterase (ACHE). The results for each film are treated in separate sections. Before discussing the results obtained with each film, the gain and phase of the CHEMFET sensor and reference transistors, that was observed in the experiments as a common characteristic with all three films, are discussed in the first section. The second section discusses the results obtained with the epoxy coating. Since the epoxy experiment served only to demonstrate and validate the CHEMFET sensor concept and performance, an abbreviated subset of the electrical measurements is discussed. The third section discusses the electrical measurements performed on the copper phthalocyanine film upon exposure to both nitrogen dioxide (NO_2) and diisopropyl methylphosphonate (DIMP). The complete set of baseline electrical measurements performed with the copper phthalocyanine coated CHEMFET sensor are discussed only for the NO_2 exposure. The fourth section discusses the electrical measurement results associated with the acetylcholinesterase film upon exposure to DIMP.

CHEMFET Sensor and Reference Transistor Characterization

The transfer characteristics of the CHEMFET sensor and reference transistors were measured throughout the duration of an experiment. For the

experiments involving the CuPc and ACHE films, the transfer functions of the FETs (the floating gate, source, and drain structure) did not change during an experiment. Representative plots of the gain and phase of the transistor transfer functions are shown in Figures V-1, V-2. The low frequency gain of the FETs was 9 dB ± 3 dB. The FET transconductance (g_m) was estimated from the slope of the drain current vs gate voltage plot at V_{gs} = 10V to be 0.133 mS (Figure IV-6). A 130 Kohm drain-to-source on-resistance (r_d) was estimated from the slope of the drain current versus drain voltage plot with V_{gs} = 2.5V (Figure IV-5). Using the g_m and r_d values, along with an externally connected 100 Kohm drain bias resistance, the gain of the FET was estimated to be 16 dB. The reference transistor gain was generally 1-2 dB greater than the gain of the adjacent CHEMFET sensor transistor, reflecting the differences between the two gate electrode geometries. The -3 dB cutoff frequency of all the transistors was about 8 KHz. The phase lag decreases from 180° at low frequencies to about 90° at 100 KHz.

The transfer function of the CHEMFET used for the epoxy experiment initially showed similar characteristics to the FETs discussed above. However, when the epoxy was applied, the gain of the CHEMFET dropped from +11.7 dB to -8.9 dB. The reference transistor characteristics did not change, nor did the phase and cutoff frequency of the CHEMFET. These results are shown in Figures V-3, V-4. Three possible explanations for this change were considered. First, since the epoxy

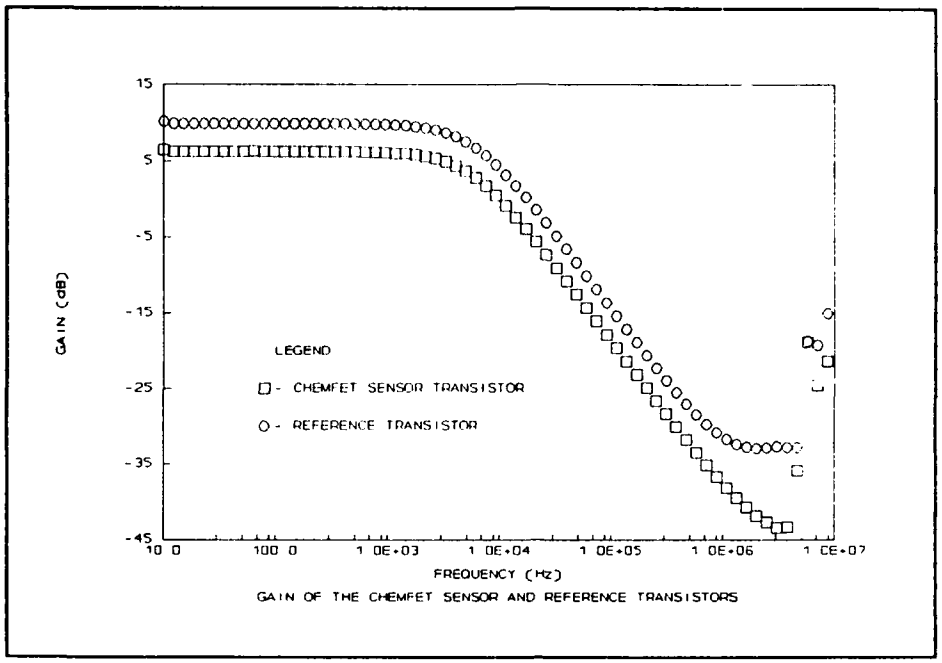

Figure V-1. Gain of the CHEMFET Sensor and Reference Transistors.

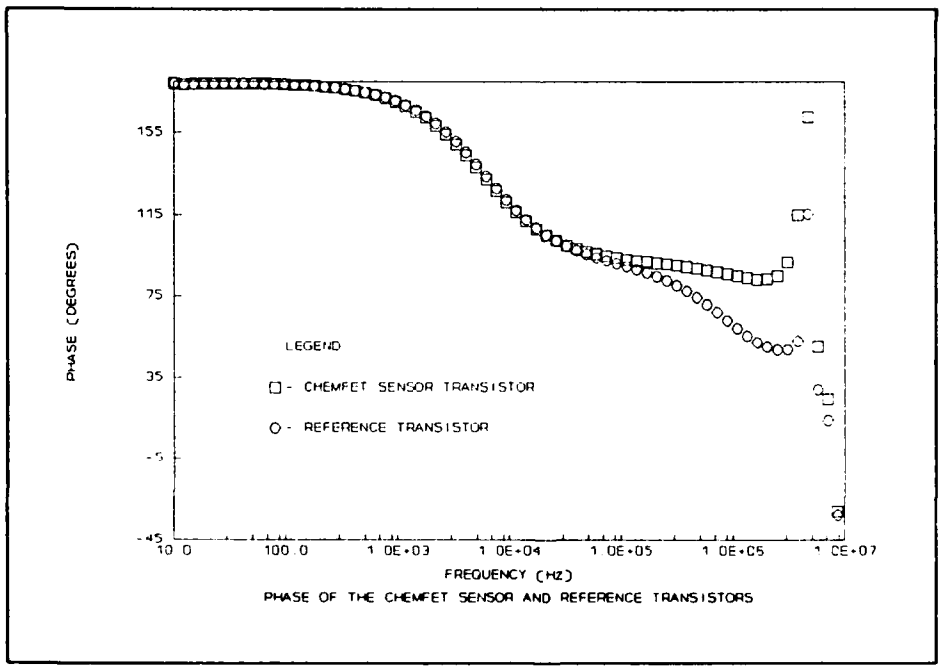

Figure V-2. Phase of the CHEMFET Sensor and Reference Transistors.

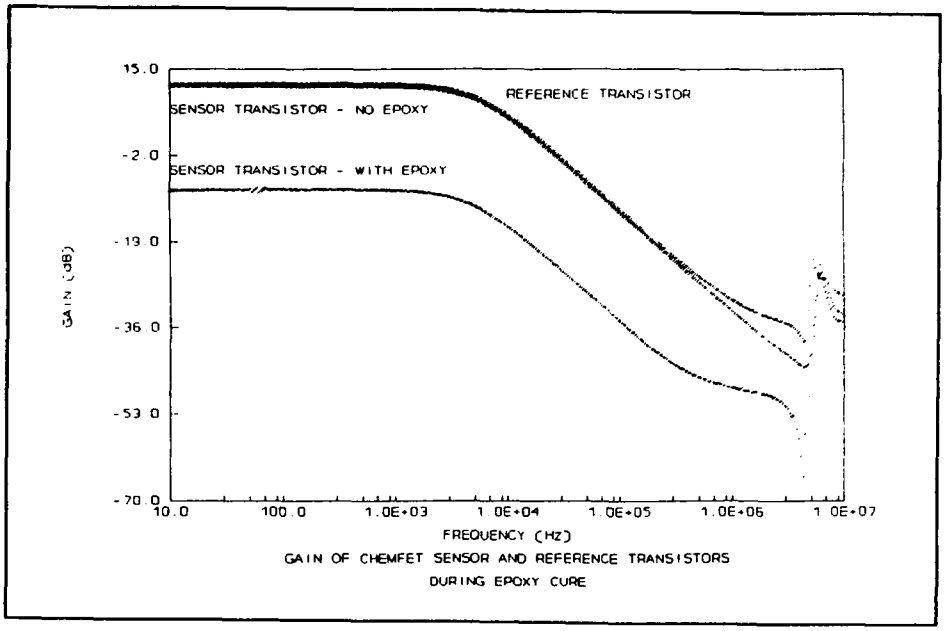

Figure V-3. Gain of the CHEMFET Sensor and Reference Transistors During Epoxy Cure.

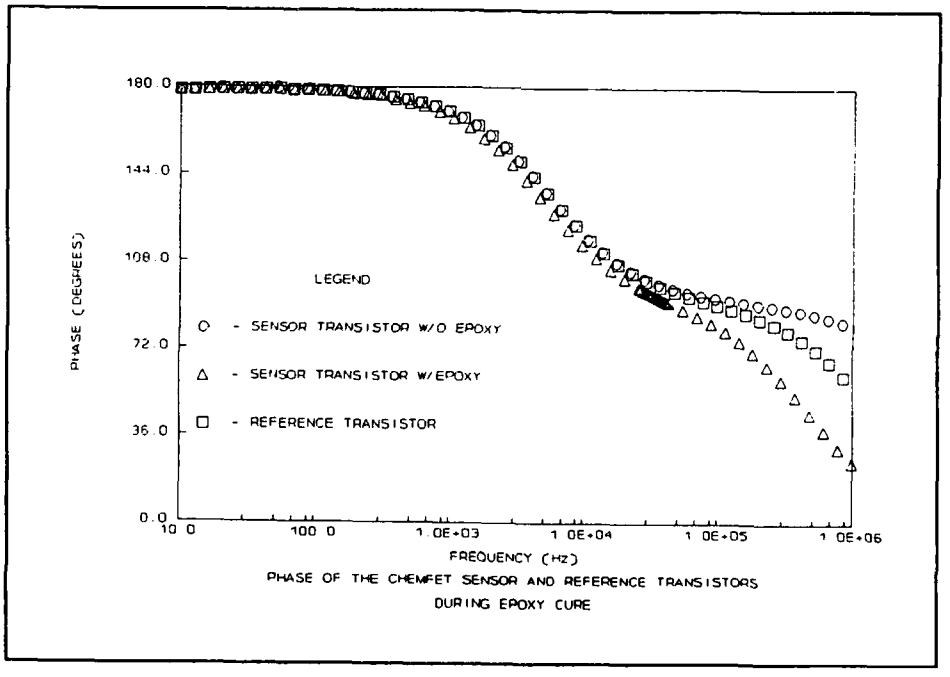

Figure V-4. Phase of the CHEMFET Sensor and Reference Transistors During Epoxy Cure.

is relatively conductive when initially applied, less of the 100 V bias used to measure the interdigitated gate resistance was dropped across the gate, and the resulting higher voltage on the floating gate caused a gate oxide short. However, had the gate oxide shorted, the phase of the transistor would also have been affected, and this was not observed. An alternative explanation is that the epoxy created a high resistance path to ground relative to the larger gate bias voltage. If this were the case, the change in the epoxy's electrical properties during cure, would also change the gate bias voltage. However, after the initial drop in gain, no further changes in the transistor's characteristics were observed. The third explanation is that the large DC voltage used for the resistance measurement, damaged the field oxide and created a high resistance path to ground, that is, a finite oxide leakage current (See Chapter IV: Biasing Experiments and Frequency Response). As a consequence, the voltage on the floating gate would decrease and reduce the gain of the transistor without affecting the phase of the output signal.

Epoxy Cure

Impedance of the Interdigitated Gate.

The electrical measurements performed on the CHEMFET sensor revealed that the epoxy was initially conductive and then became progressively more resistive during cure. The magnitude and phase of the interdigitated gate impedance during cure is shown in Figures V-5 and V-6. The phase data below 100 Hz is not shown since the magnitude of the impedance (admittance) was not measurable (Hewlett-Packard Corp., model 4192A, Palo Alto, CA). When the epoxy was initially applied,

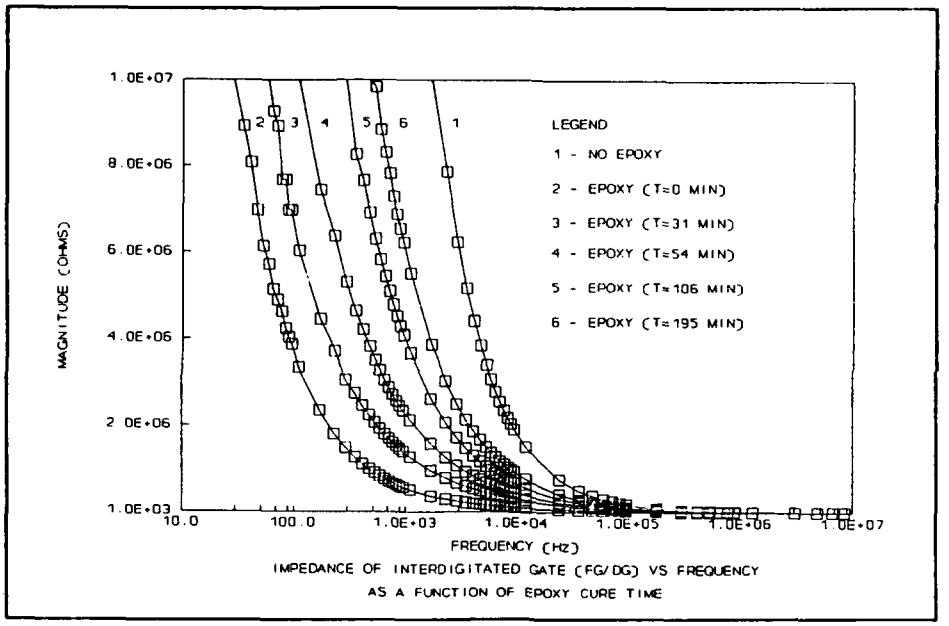

Figure V-5. Impedance of the Interdigitated Gate vs Frequency as a Function of Epoxy Cure Time.

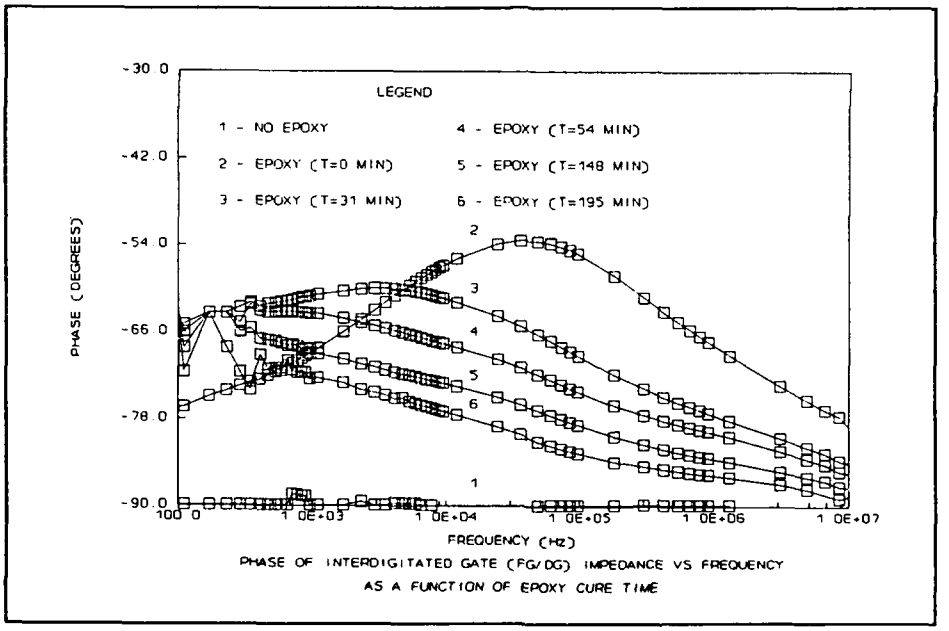

Figure V-6. Phase of the Interdigitated Gate Impedance vs Frequency as a Function of Epoxy Cure Time.

the impedance at any given frequency, decreased several orders of magnitude, and the phase increased. As time progressed and the epoxy cured, the impedance increased and the phase decreased, approaching the initial impedance and phase of the uncoated interdigitated gate. The peak phase shift occurred at approximately 30 KHz when the epoxy was first applied. This peak was observed to decrease and shift to lower frequencies as the epoxy cured.

The trends observed in the impedance data agree with the qualitative model discussed in Chapter III. That is, with no epoxy on the interdigitated gate, the impedance is large because of the extremely low conductivity of the air and the silicon dioxide dielectrics which separate the interdigitated electrodes. The phase shift attains its maximum since the current which flows between the electrodes is a displacement current which lags the applied voltage by 90^{o}. Since the epoxy that was deposited on the electrodes was initially conductive, it was responsible for reducing the phase shift and decreasing the magnitude of the impedance. As the epoxy cured, its conductivity decreased, and in turn, the impedance and phase shift increased.

Gain and Phase of the CHEMFET Sensor.

Although the FET's performance was less than optimal, the trends observed in the interdigitated gate impedance were, nevertheless, reflected in the output response of the CHEMFET sensor. For example, the CHEMFET sensor's gain (VOUT/DG), shown in Figure V-7, correlated with the gate impedance changes; that is, the gain increased when the epoxy was applied and then decreased as the epoxy cured. The reduction in the transistor gain, resulting from the performance of the

FET, caused the CHEMFET sensor's gain, measured during epoxy cure, to decrease below the gain of the uncoated CHEMFET. The CHEMFET sensor's phase also correlates with the impedance phase change which occurred during the epoxy's cure. Figure V-8 shows the CHEMFET sensor's phase over the entire frequency measurement range. Similar to the interdigitated gate phase change, the CHEMFET sensor's phase had a maximum change at approximately 100 KHz. Figure V-9 shows the CHEMFET sensor phase near 100 KHz on an expanded scale. In contrast to the interdigitated gate phase change, the CHEMFET sensor's phase change was a minimum when the epoxy was applied, and increased during the epoxy's cure.

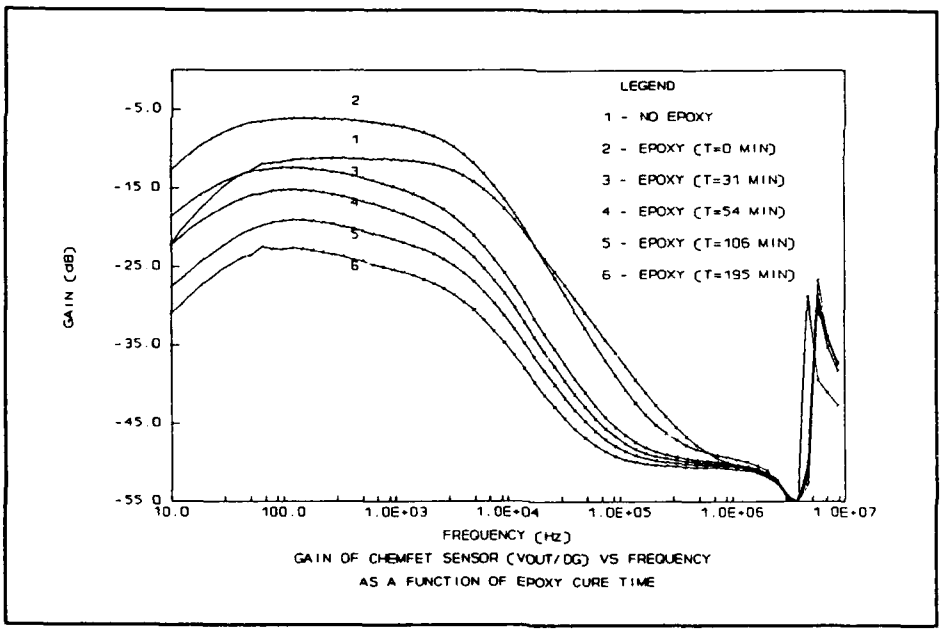

Figure V-7. Gain of the CHEMFET Sensor vs Frequency as a Function of Epoxy Cure Time.

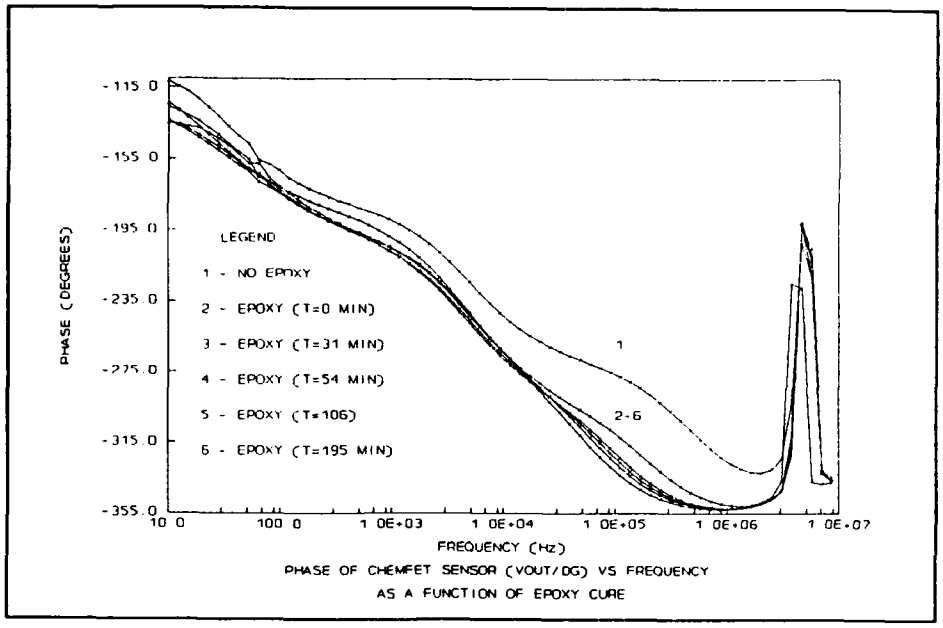

Figure V-8. Phase of the CHEMFET Sensor vs Frequency as a Function of Epoxy Cure Time.

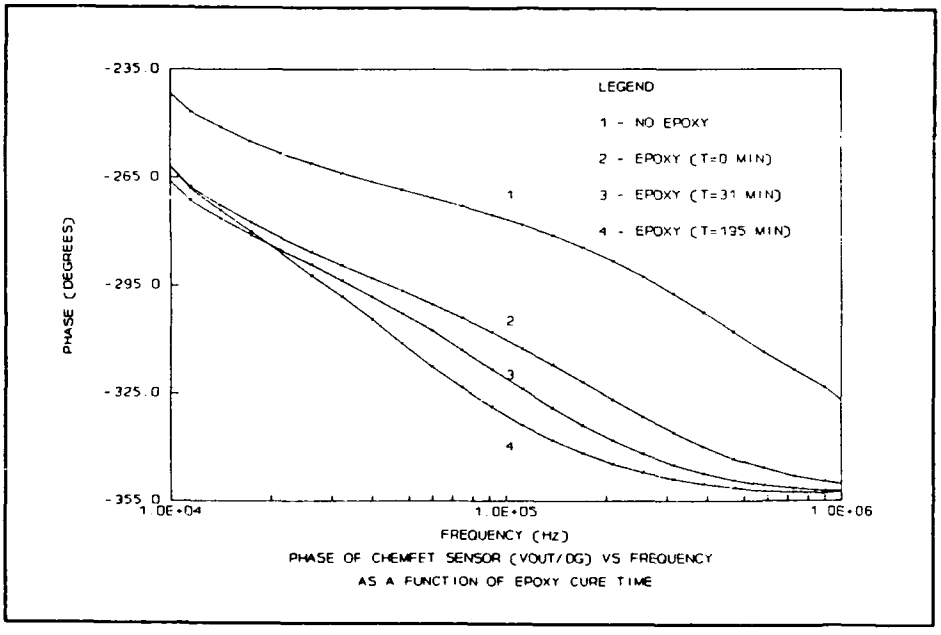

Figure V-9. Phase of the CHEMFET Sensor over the Frequency Range Spanning 10-1000 KHz as a Function of Epoxy Cure Time.

Frequency Response of the CHEMFET Sensor to a Pulse Excitation Signal.

The time-domain response of the CHEMFET sensor to a pulse excitation signal before and during the cure of the EPON 828 epoxy is shown in Figures V-10(a)-(d). The upper trace in Figures V-10(a)-(d) represents the 256 Hz, 50 μs wide pulse excitation signal that was applied to the CHEMFET's driven gate, while the lower traces represent the CHEMFET sensor's response prior to, after, and during the epoxy's cure (0, 106, and 240 minutes). The amplitude of the excitation pulse was 4 V. As shown in Figure V-10(a), the uncoated CHEMFET sensor highly attenuates the excitation signal, especially at higher frequencies, because of the 8 KHz cutoff frequency of the transistor. The distortion that results is characteristic of a low pass filter response. When the epoxy was deposited, less of the excitation voltage was dropped across the interdigitated gate. Thus, a larger signal reached the floating gate. The larger signal on the floating gate was amplified by the transistor, and thus, the transistor's output voltage increased, as shown in Figure V-10(b). As the epoxy cured, its impedance increased. This behavior resulted in a larger voltage drop of the excitation signal across the interdigitated gate. Since the voltage on the floating gate decreased, the CHEMFET sensor's output voltage decreased. The decrease in the CHEMFET sensor's output voltage is shown in Figures 10(c)-(d).

The corresponding FFT difference spectrum (calculated as the difference between FFT spectrums associated with the a specific epoxy cure time with respect to the reference signal; See Chapter IV: Data Analysis and Reduction Software) were computed for each of the corresponding time-domain measurements collected

during the cure process, and they are shown in Figure V-11. The uncoated CHEMFET's spectra revealed that the largest amplitude difference with respect to the reference signal occurred at low frequencies. This characteristic indicates that the CHEMFET sensor is acting like a high pass filter. When the epoxy was applied, the CHEMFET's output increased, since less signal was dropped across the interdigitated gate. In turn, this reduced the amplitude difference between the CHEMFET's output and the reference signal. The largest change in the difference spectra occurs at low frequencies which corresponds to the relatively large conductivity of the epoxy, that is manifested early in its cure cycle. As the epoxy cured, less signal reached the gate, and the transistor's output decreased, and the amplitude difference increased. The reduction in the transistor gain discussed earlier caused the amplitude difference, measured during epoxy cure, to become greater than the amplitude difference between the uncoated CHEMFET and the reference signal.

CuPc Response to NO_2 and DIMP Exposure

The response of the CHEMFET coated with a CuPc film to NO_2 and DIMP was measured over a large span of challenge concentrations. The sensitivity of CuPc to NO_2 reported in the literature (10) ranges from 1 ppb to 1 ppm. In the first experiment, the NO_2 concentration spanned 40 to 400 ppb. A large change in the film's impedance was observed even at the lowest challenge concentration (40 ppb), and the response had saturated with a second challenge concentration level of 100 ppb (complete data set provided in Appendix G). In a second experiment, the NO_2 challenge concentration spanned 20 to 100 ppb. The sample temperature during

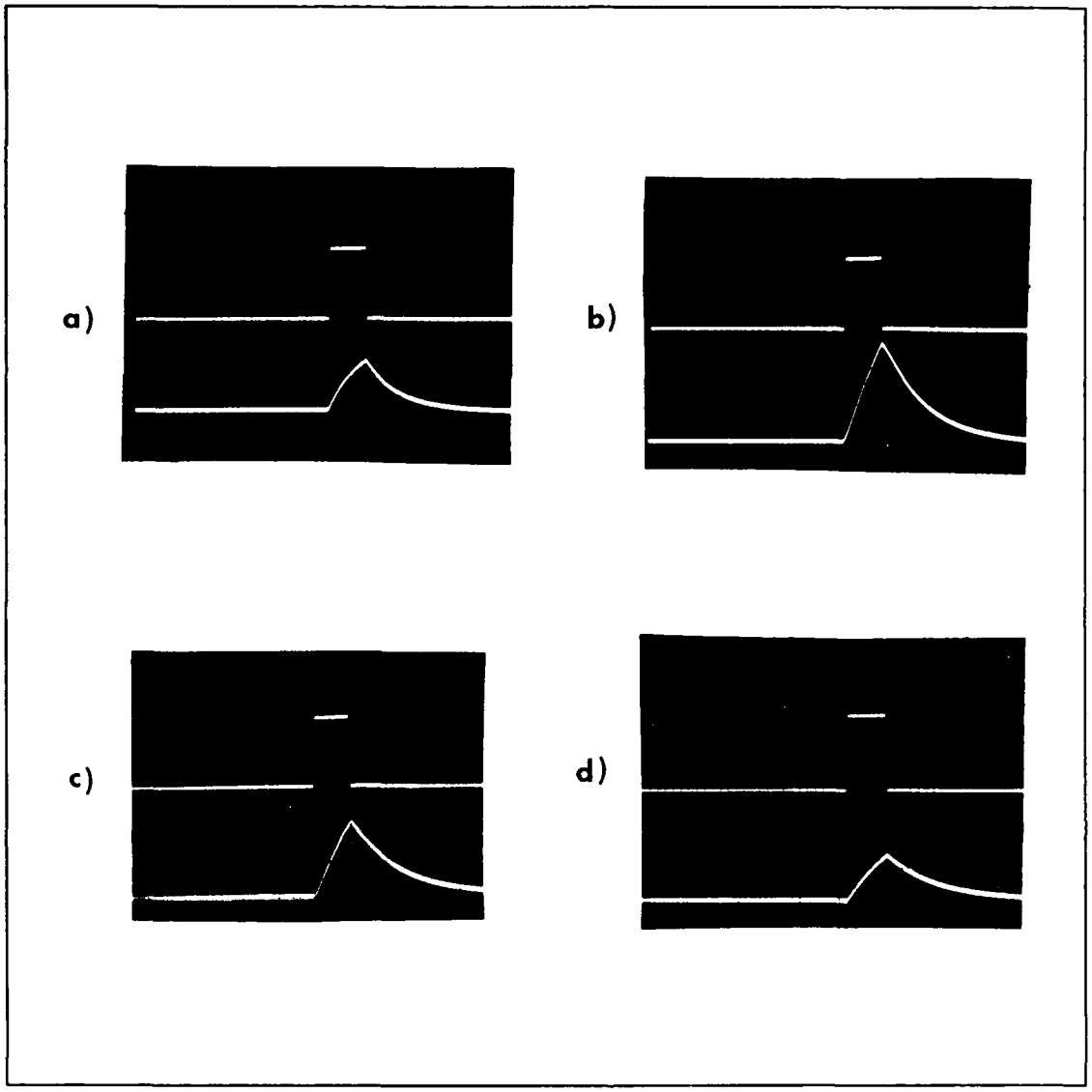

Figure V-10. CHEMFET Sensor Time-Domain Response to a Pulse Excitation Signal during Epoxy Cure.

a) No Epoxy, b) Epoxy Applied (T=0), c) T=106 minutes, d) T=240 minutes. Upper trace: Excitation Signal (2V/div). Lower Trace: Sensor Output Voltage: a) and b) 0.5V/div, c) and d) 0.1V/div. Horizontal Scale: 50μs/div.

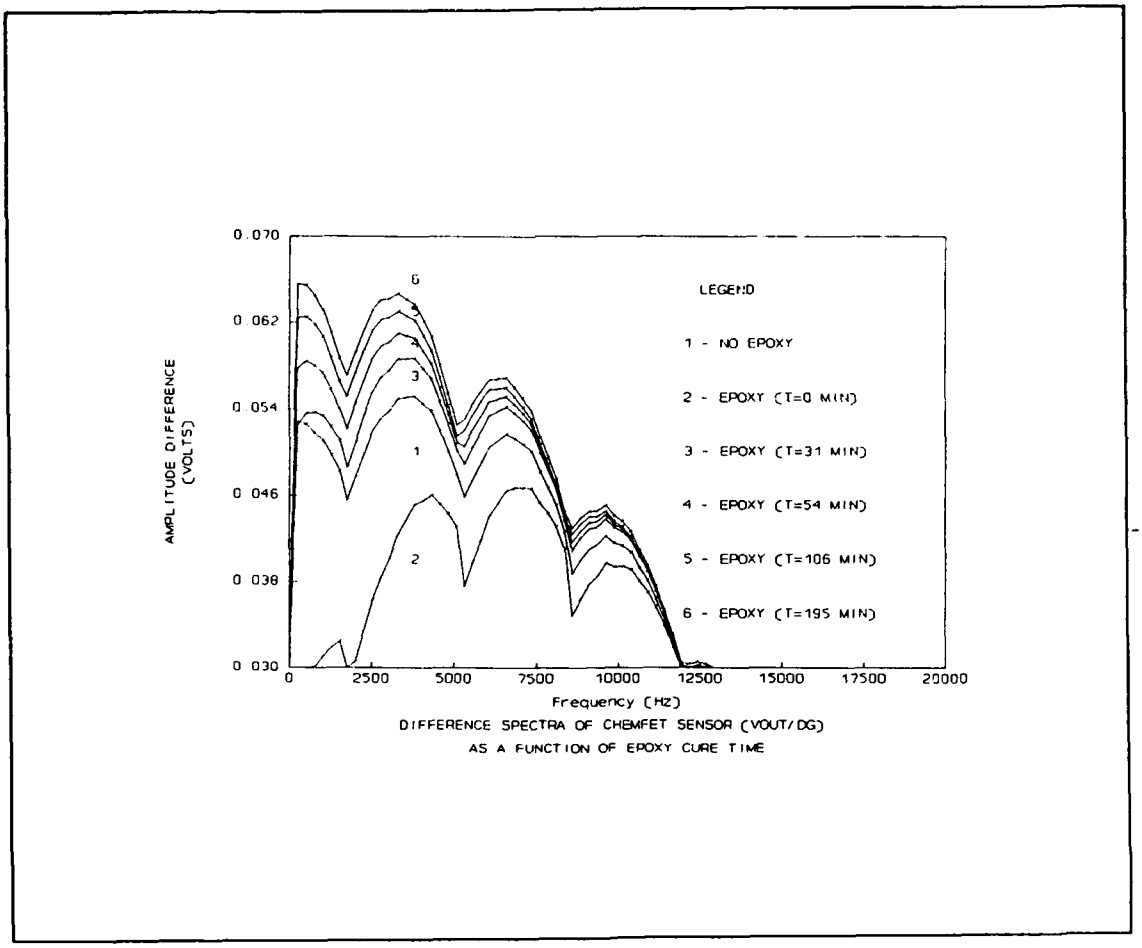

Figure V-11. Difference Spectra of the CHEMFET Sensor as a Function of Epoxy Cure Time.

exposure was thermostatted at 103 ± 5 °C. The observed response was similar, but not identical, to that observed in the first experiment. Following the exposure to 100 ppb NO_2, the CHEMFET was purged overnight with carrier gas (filtered room air), and then used in an experiment to measure the response of the film to DIMP. The sample temperature was thermostatted at 109 ± 5 °C. The sensitivity of CuPc to organophosphorus compounds reported in the literature is much less than that for NO_2 (7). Consequently, the DIMP challenge concentration was adjusted to span 100 to 4000 ppb. An 800 ppb DIMP challenge concentration was required to induce the equivalent percent change in the resistance resulting from exposure to a 30 ppb NO_2 challenge concentration.

Resistance of the Interdigitated Gate.

All three experiments were performed by exposing the film for 30 minutes to the challenge concentration, and then purging it with carrier gas for thirty minutes. The baseline electrical measurements were performed after each exposure and purge. In addition, the resistance of the film was monitored during the thirty minute exposure and purge cycles. Figures V-12 and V-13 reveal that the resistance changes during the cyclical exposure and purge of the CHEMFET to NO_2 and DIMP challenge concentrations, respectively. The resistance of the film rapidly decreased with exposure to the challenge gas. After the first 5 minutes of exposure, the resistance continues to decrease, but at a much slower rate. When the challenge gas was purged, the film's resistance increased, but it did not return to its value prior to the exposure. The failure of the electrical resistance to return to its prior value was

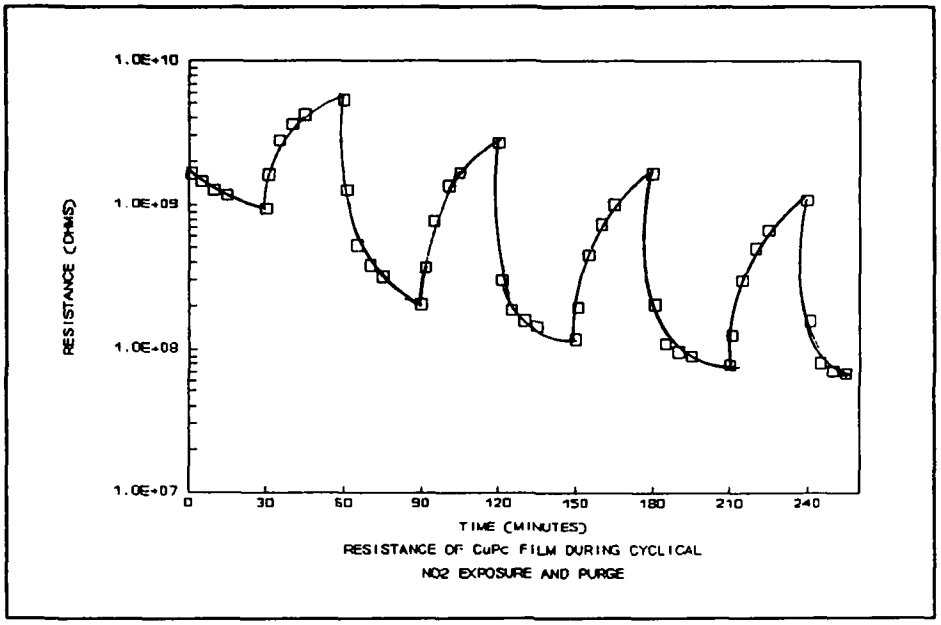

Figure V-12. Resistance of the Copper Phthalocyanine (CuPc) Film During Cyclical Nitrogen Dioxide (NO_2) Exposure and Purge.

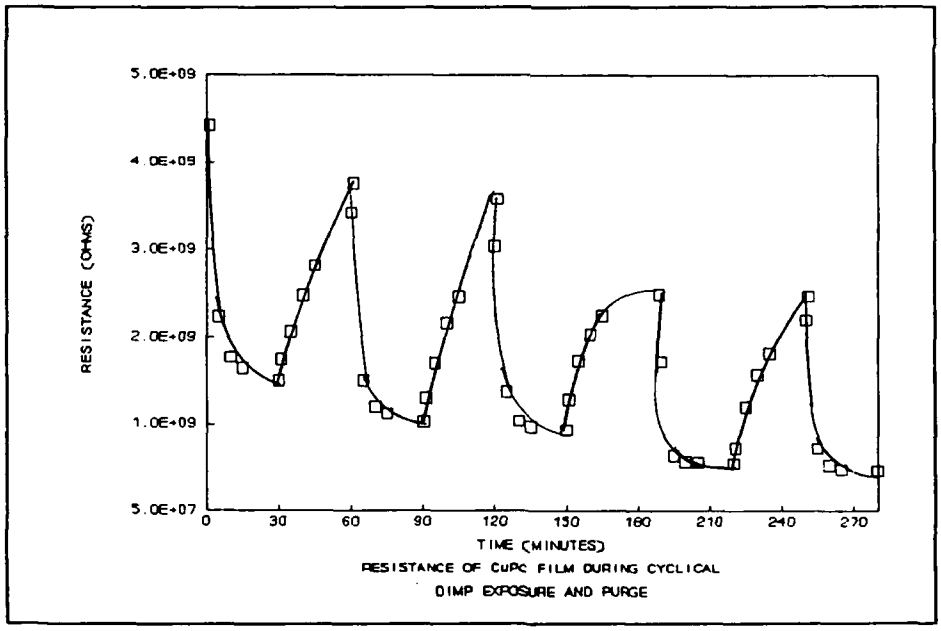

Figure V-13. Resistance of the Copper Phthalocyanine (CuPc) Film During Cyclical Exposure to Diisopropyl methylphosphonate (DIMP) Exposure and Purge.

observed in all of the electrical measurements performed with the CHEMFET. The significant difference between the NO_2 and DIMP exposures was the lower sensitivity manifested by the CuPc film to DIMP exposure. The change in the interdigitated gate resistance as a function of challenge gas concentration is shown in Figure V-14.

Impedance of the Interdigitated Gate.

The increased conductivity of the film after exposure to a challenge gas was also observed in the magnitude of the impedance of the interdigitated gate (Figure V-15, V-16). Similar to the epoxy results, the largest change in the magnitude of the impedance occurs at low frequencies when the CuPc was exposed to either NO_2 or DIMP, and once again, the impedance fails to return to its pre-exposure value after a 30 minute purge (Figures V-17, V-18). In contrast to the behavioral similarity of the impedance magnitude curves with respect to the epoxy measurements, the phase of the interdigitated gate impedance was significantly different (Figures V-19, V-20). That is, as illustrated in Figure V-6, the phase of the uncoated interdigitated gate remained constant at -90^{o} over all frequencies. In contrast, the phase of the CuPc-coated gate, however, increased at low frequencies and approached -90^{o} only at frequencies greater than 100 KHz. Additionally, the CuPc-coated gate impedance possessed a region of constant phase (-82^{o}) spanning 1-10 KHz. These changes were attributed to the impedance of the unexposed CuPc film. In the first NO_2 experiment, the phase of the CuPc-coated interdigitated gate developed two peaks (one at 15 KHz and the other at 100 KHz) when exposed to NO_2 (see Appendix G). In the second NO_2 experiment, as shown in Figure V-19, the double peak was not

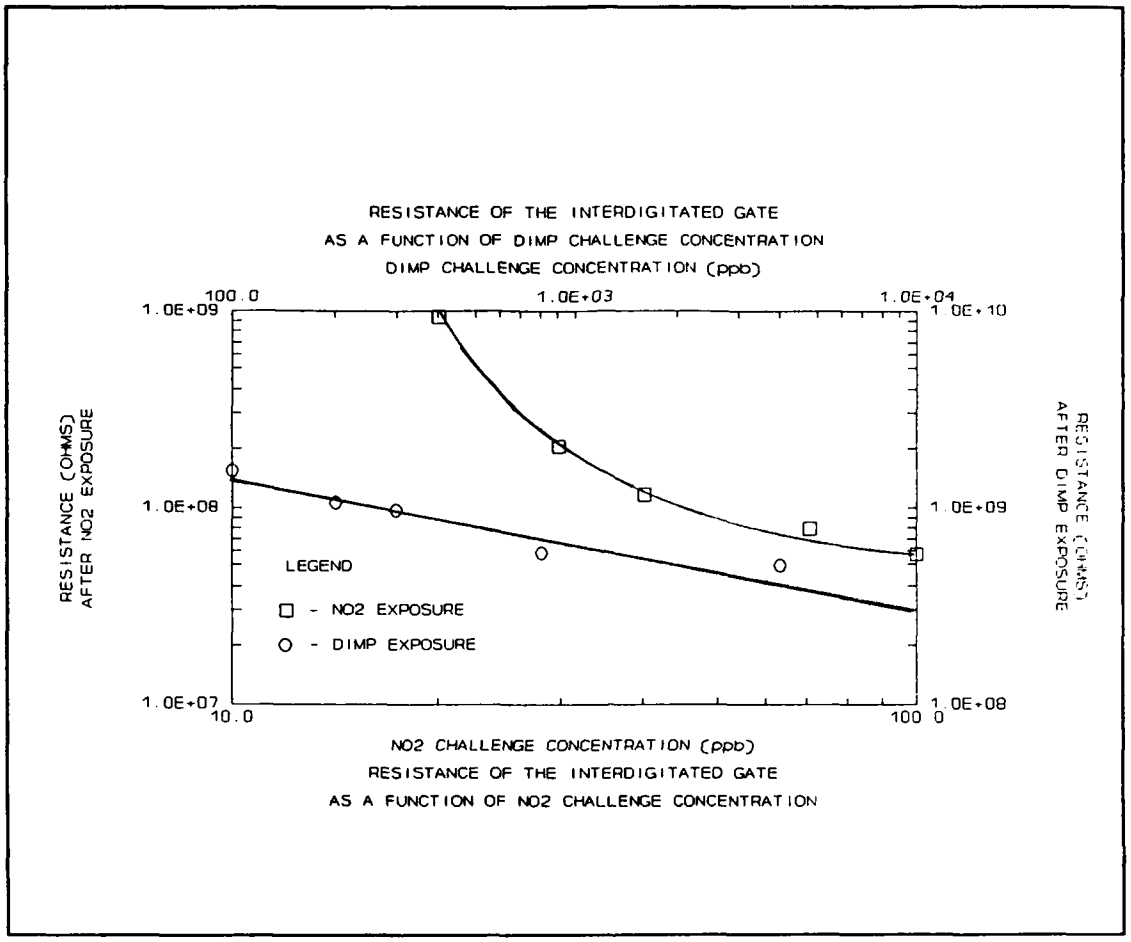

Figure V-14. Interdigitated Gate Resistance as a Function of Challenge Gas Concentration.

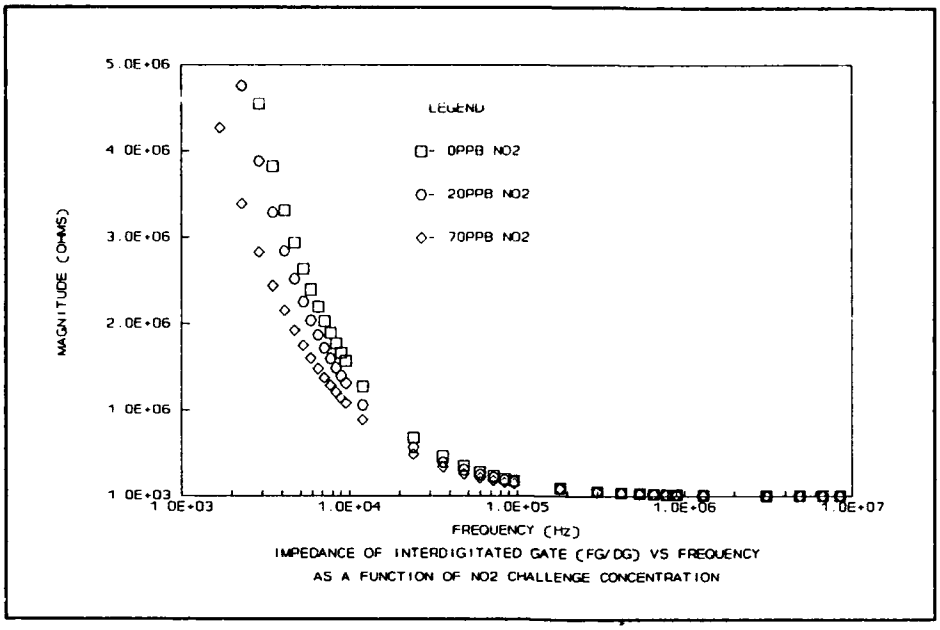

Figure V-15. Impedance of the Copper Phthalocyanine-Coated Interdigitated Gate vs Frequency as a Function of the Nitrogen Dioxide (NO_2) Challenge Concentration.

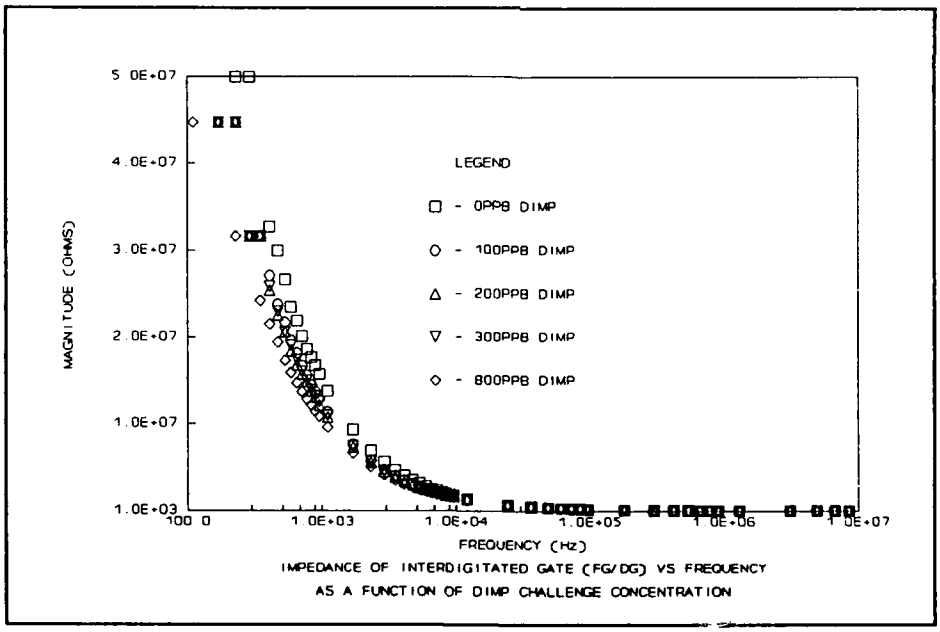

Figure V-16. Impedance of the Copper Phthalocyanine-Coated Interdigitated Gate vs Frequency as a Function of the Diisopropyl Methylphosphonate (DIMP) Challenge Concentration.

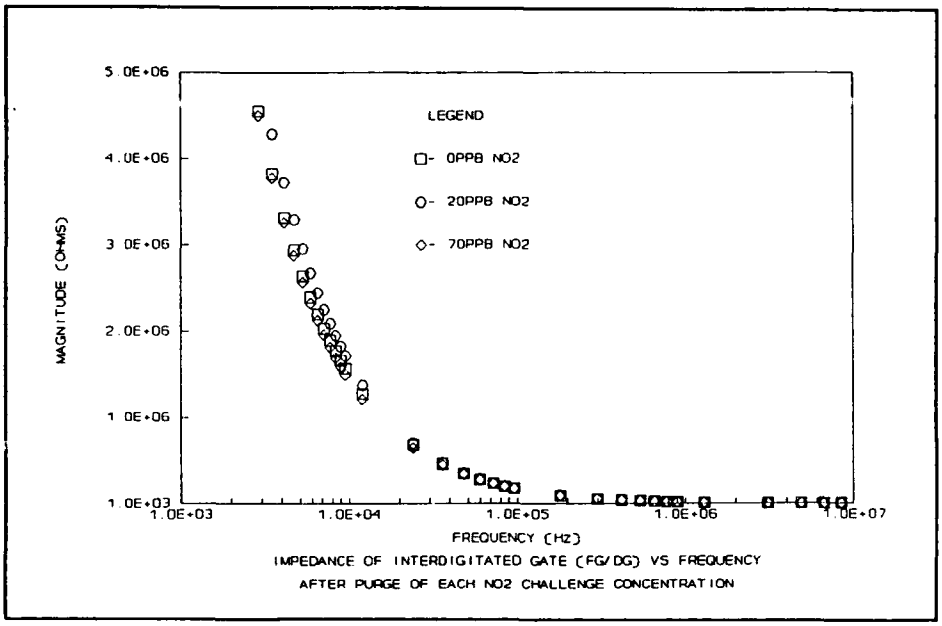

Figure V-17. Impedance of the Copper Phthalocyanine-Coated Interdigitated Gate vs Frequency after Purge of each Nitrogen Dioxide (NO_2) Challenge Concentration.

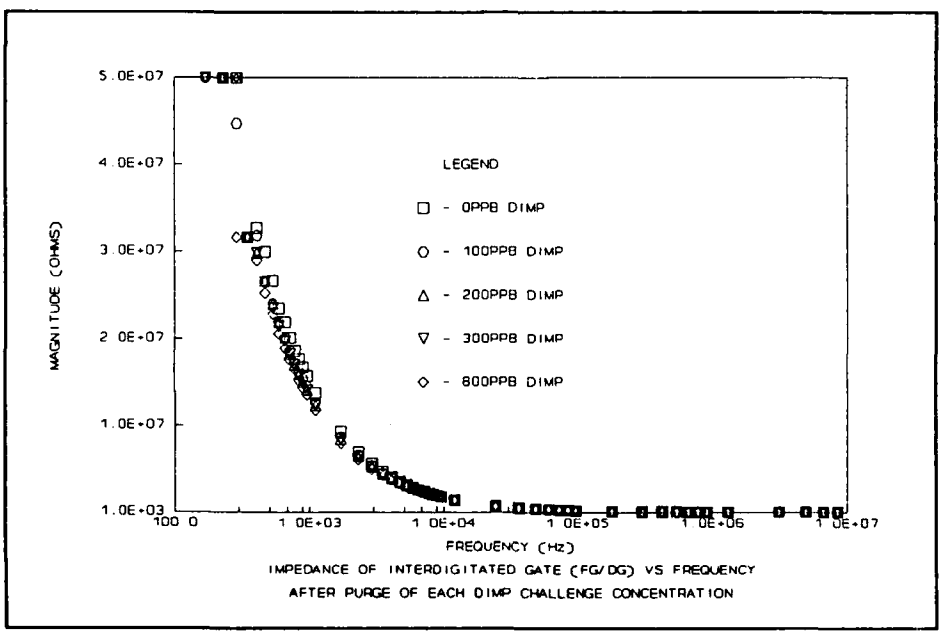

Figure V-18. Impedance of the Copper Phthalocyanine-Coated Interdigitated Gate vs Frequency after Purge of each Diisopropyl Methylphosphonate (DIMP) Challenge Concentration.

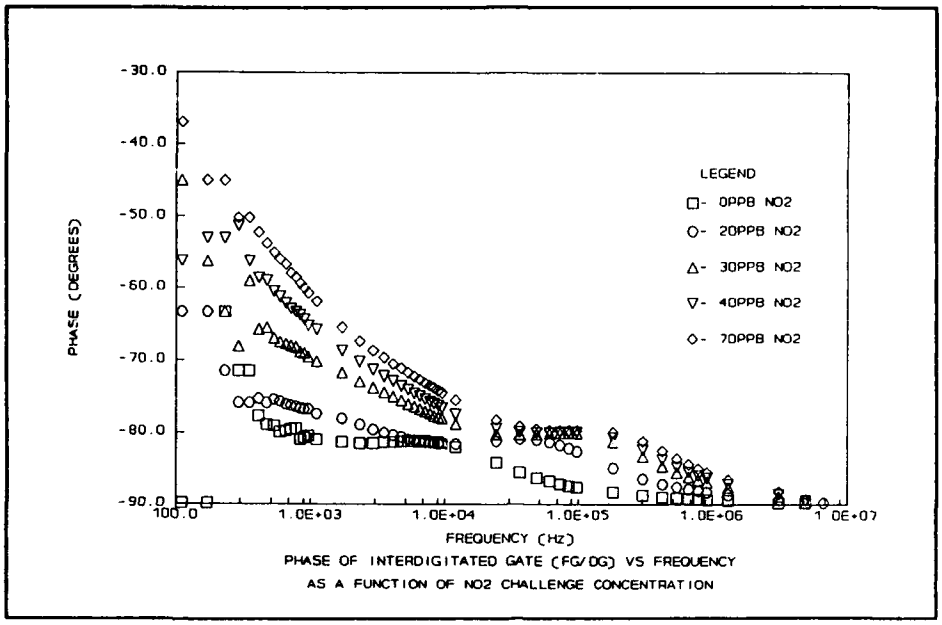

Figure V-19. Phase of the Copper Phthalocyanine-Coated Interdigitated Gate vs Frequency as a Function of the Nitrogen Dioxide (NO_2) Challenge Concentration.

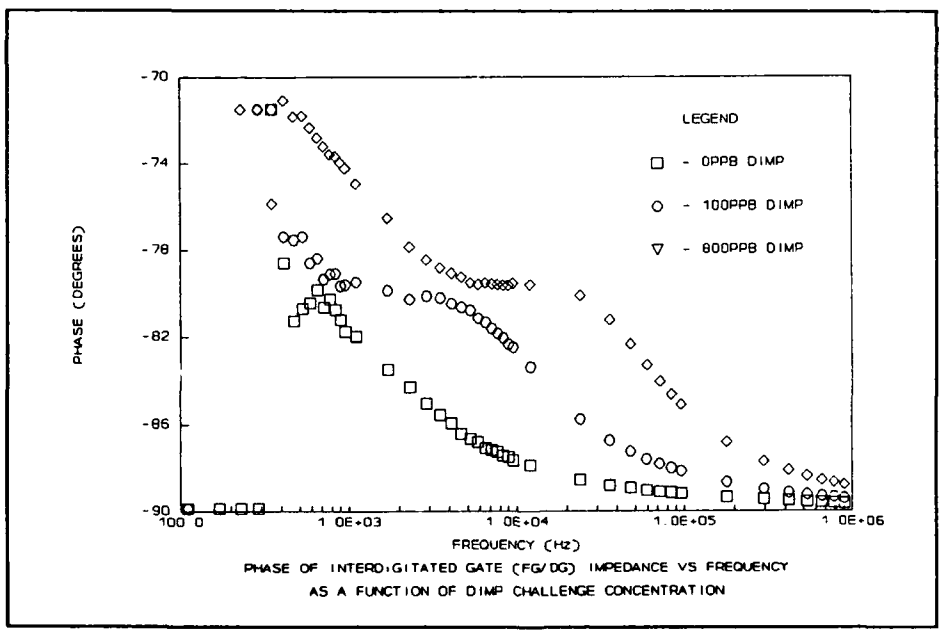

Figure V-20. Phase of the Copper Phthalocyanine-Coated Interdigitated Gate vs Frequency as a Function of the Diisopropyl Methylphosphonate (DIMP) Challenge Concentration.

observed; instead, the region of constant phase observed in the unexposed CuPc film, was shifted to higher frequencies (30 - 150 KHz at 70 ppb NO_2), and the phase increased to -78°. The phase response in the second experiment was similar to the results obtained when the epoxy was first applied to the interdigitated gate; that is, the phase increased and the increase shifted to higher frequencies. In the DIMP experiment, the no exposure phase curve did not exhibit a region of constant phase. This behavior suggests that the NO_2 was not completely removed by the overnight purge. When exposed to DIMP, the region of constant phase re-formed. As the DIMP challenge concentration was increased, the region of constant phase shifted to higher frequencies and increased in magnitude. Figures V-21, V-22 show the phase of the interdigitated gate impedance after it was purged of the NO_2 and the *DIMP challenge concentrations, respectively.*

Gain and Phase of the Interdigitated Gate.

The decrease in the magnitude of the impedance of the CuPc film upon exposure to NO_2 was also reflected in the gain/phase analysis of the interdigitated gate (Figure V-23). The magnitude of the impedance decrease resulted in a smaller voltage drop across the interdigitated gate, and therefore, the gain measured at the floating gate increased from -55 dB to -35 dB at 10 Hz when the CHEMFET was exposed to 70 PPB NO_2. The gain difference resulting from exposure to a challenge gas decreased with increasing frequency, in agreement in the smaller change in the impedance magnitude at higher frequencies. The corresponding phase of the interdigitated gate's transfer function, shown in Figure V-24, had its largest change

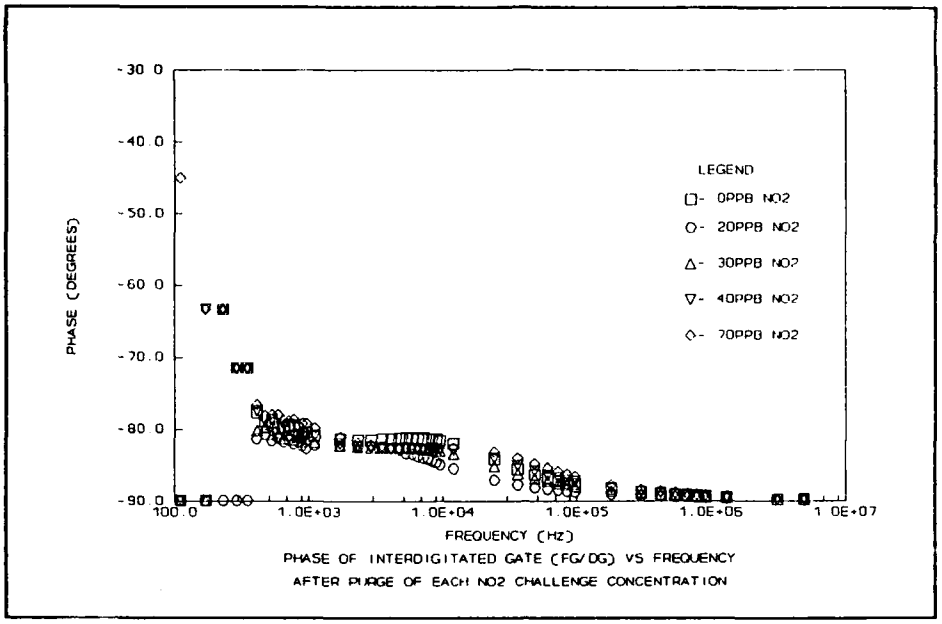

Figure V-21. Phase of the Copper Phthalocyanine-Coated Interdigitated Gate vs Frequency after Purge of each Nitrogen Dioxide (NO_2) Challenge Concentration.

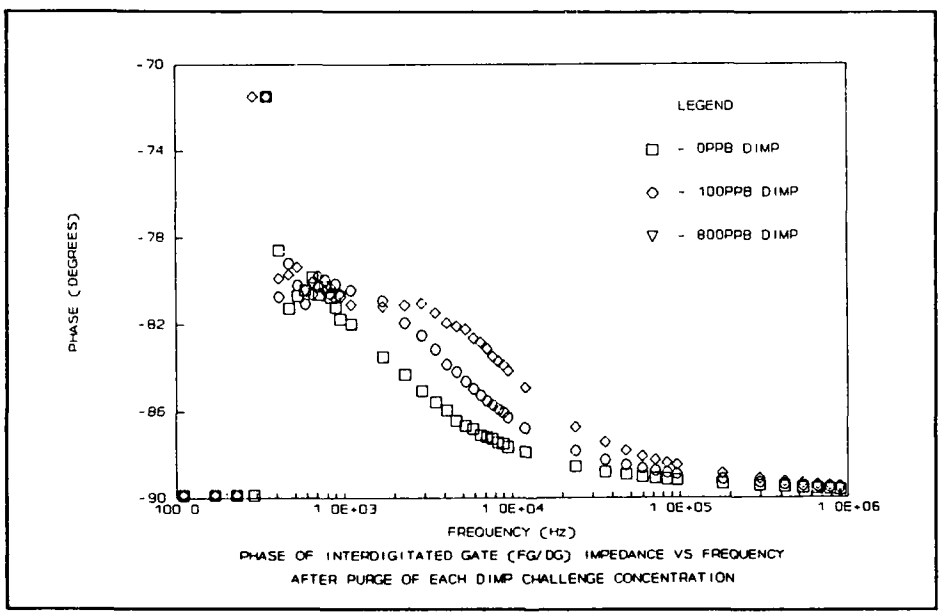

Figure V-22. Phase of the Copper Phthalocyanine-Coated Interdigitated Gate vs Frequency after Purge of each Diisopropyl Methylphosphonate (DIMP) Challenge Concentration.

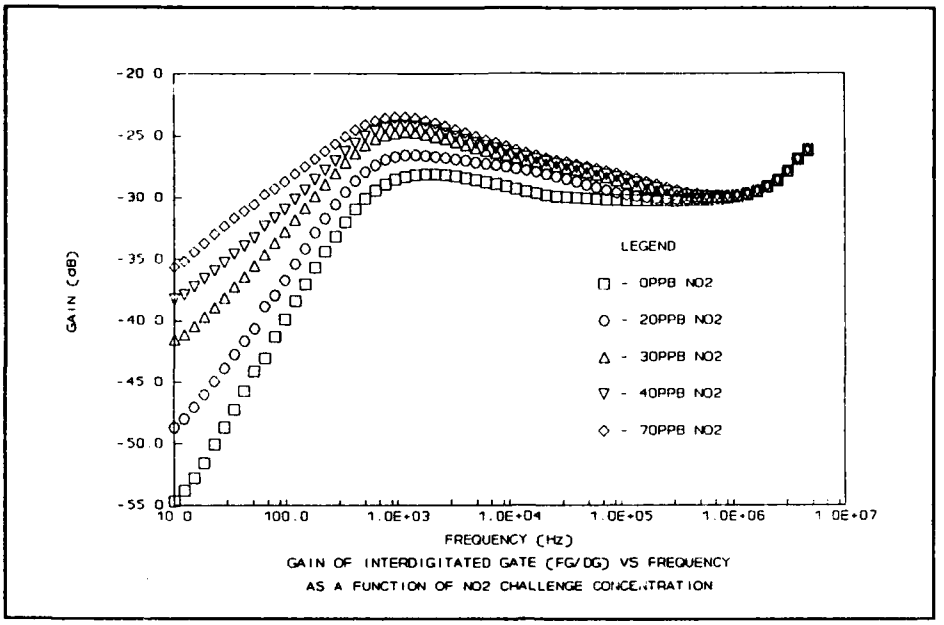

Figure V-23. Gain of the Copper Phthalocyanine-Coated Interdigitated Gate vs Frequency as a Function of the Nitrogen Dioxide (NO_2) Challenge Concentration.

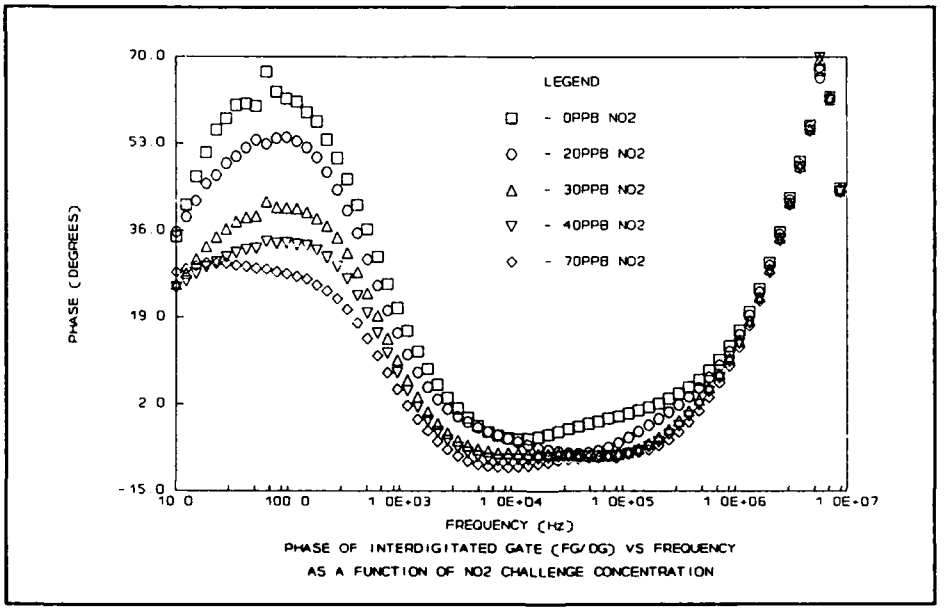

Figure V-24. Phase of the Copper Phthalocyanine-Coated Gate vs Frequency as a Function of the Nitrogen Dioxide (NO_2) Challenge Concentration.

at a frequency of 100 Hz, decreasing from 62^{o} to 28^{o}. The phase also has a significant change in the frequency range spanning 10 - 1000 KHz. At a concentration of 20 ppb NO_2, the phase decreased in the frequency range from 10 - 200 KHz, with the minimum (-8^{o}) occurring at approximately 40 KHz. With increasing NO_2 concentration, the phase at 40 KHz decreases only slightly. However, the phase above and below 40 KHz continued to decrease. A new minimum (-10^{o}) in the phase curve forms at 8 KHz, and a shoulder forms at 100 KHz. By comparison with the impedance measurements, an increase in the phase results in a decrease in the phase of the transfer function. Also, the small impedance change at 40 KHz, when the exposure concentration was increased from 20 to 70 ppb, correlates with the small gain change observed at this frequency for NO_2 concentrations above 20 ppb. These behavioral trends in the gain and phase were also observed in the first NO_2 experiment (see Appendix G). It is not totally clear why the gain and phase of the interdigitated gate's transfer function for both experiments agree, while the phase of the interdigitated gate's impedance measurement does not.

Gain and Phase of the CHEMFET Sensor.

The increased signal on the floating gate resulting from a reduction in the interdigitated gate impedance when exposed to a NO_2 or DIMP challenge was amplified with the CHEMFET transistor. As shown in Figures V-25, V-26, V-27, and V-28, the trends observed in the interdigitated gate impedance and gain/phase measurements were also observed in the CHEMFET sensor's output. As the

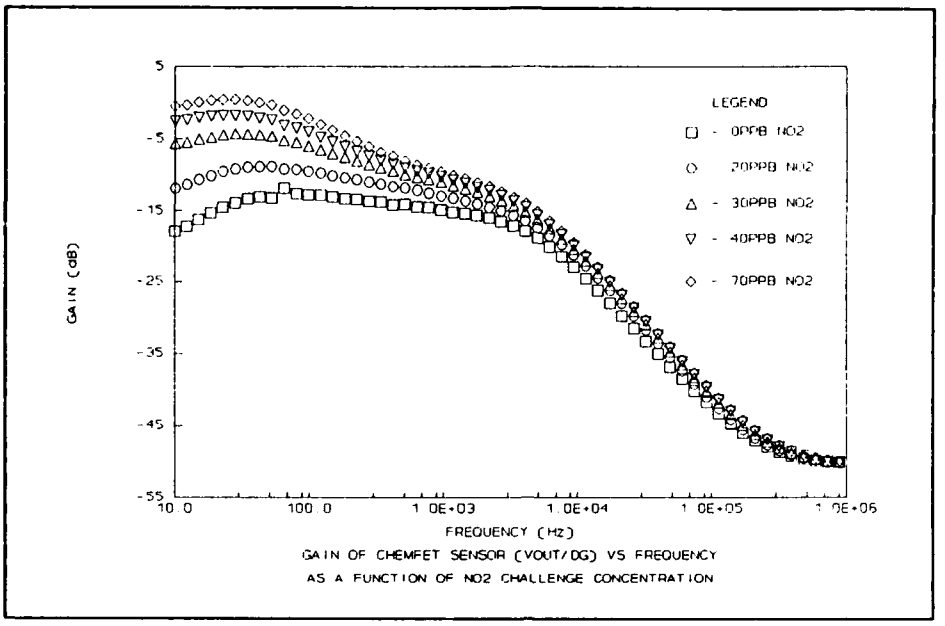

Figure V-25. Gain of the Copper Phthalocyanine-Coated CHEMFET Sensor vs Frequency as a Function of the Nitrogen Dioxide (NO_2) Challenge Concentration.

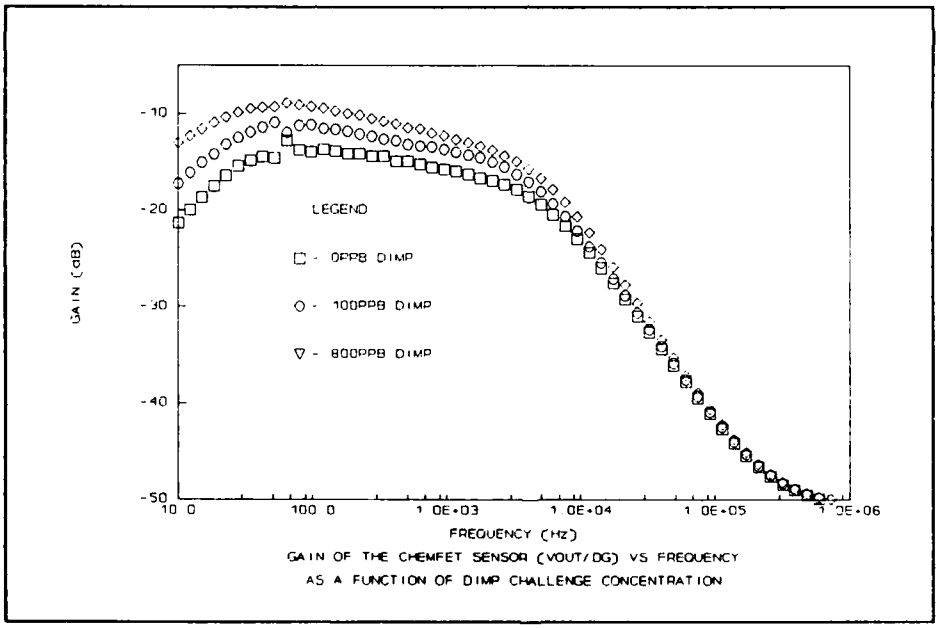

Figure V-26. Gain of the Copper Phthalocyanine-Coated CHEMFET Sensor vs Frequency as a Function of the Diisopropyl Methylphosphonate (DIMP) Challenge Concentration.

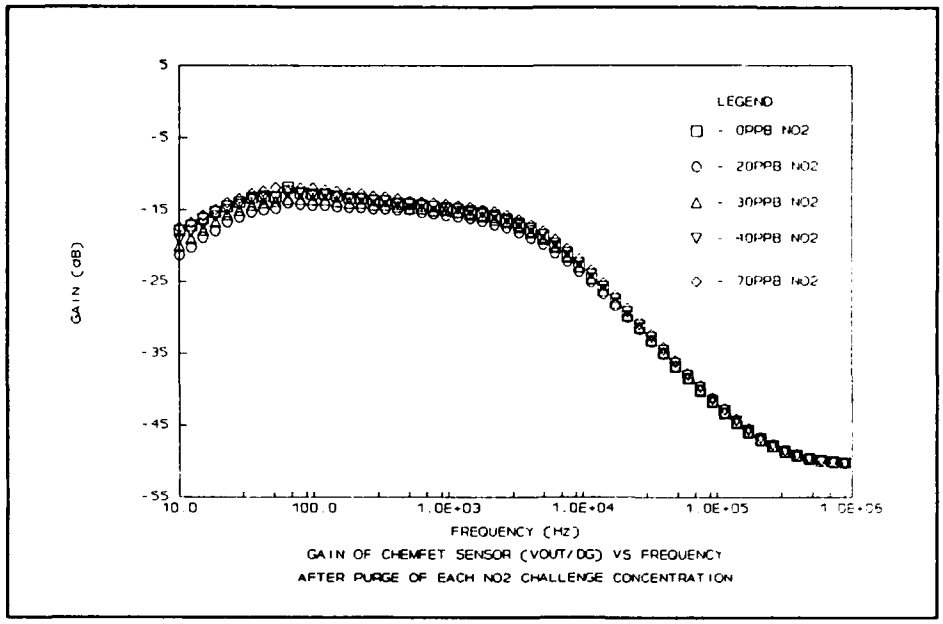

Figure V-27. Gain of the Copper Phthalocyanine-Coated CHEMFET Sensor vs Frequency after Purge of each Nitrogen Dioxide (NO_2) Challenge Concentration.

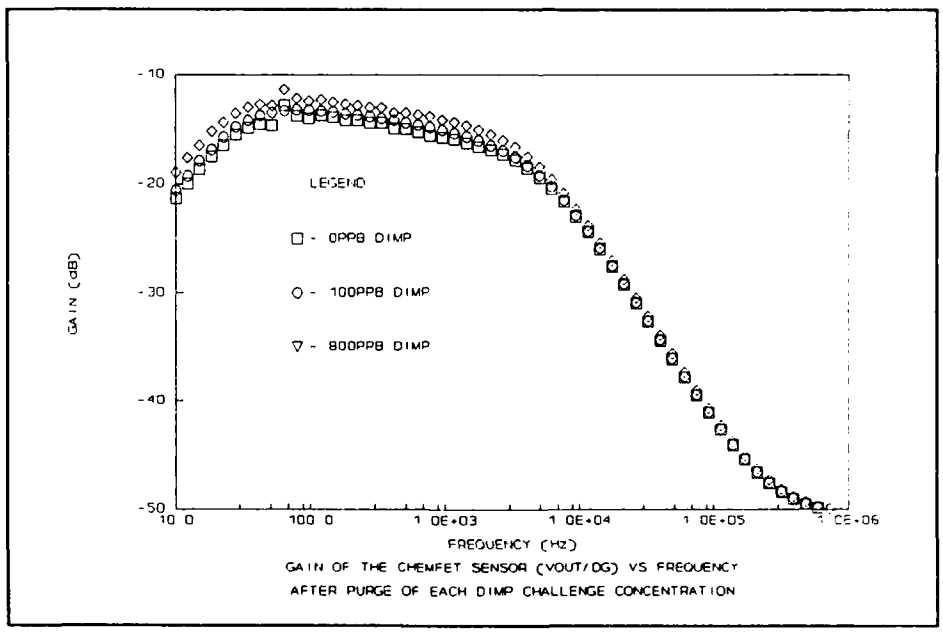

Figure V-28. Gain of the Copper Phthalocyanine-Coated CHEMFET Sensor vs Frequency after Purge of each Diisopropyl Methylphosphonate (DIMP) Challenge Concentration.

challenge concentration increased, the impedance of the interdigitated gate decreased. This resulted in a larger signal being applied to the floating gate of the CHEMFET sensor. In turn, this larger signal is then amplified by the transistor and there is an increase in the CHEMFET sensor's gain with increasing challenge concentrations. However, the gain increases nonlinearly in the frequency range spanning 0 to 10 KHz. For example, the measured interdigitated gate's gain with no gas exposure was -55 dB at 10 Hz and -40 dB at 100 Hz. The corresponding gain of the CHEMFET sensor was -18 dB and -13 dB, respectively. With a constant transistor gain of 9 dB below 10 KHz, the expected gain at the output would be -44 dB and -31 dB, respectively. The cause of this apparent nonlinearity is attributable to the loading effect of the gain/phase analyzer on the measurement of the interdigitated gate's gain and phase. The input impedance of the analyzer is 1 Mohm, with a 28 pF shunt capacitance (51:1-23). At low frequencies, the impedance of the interdigitated gate's circuit elements was greater than the input impedance of the analyzer. Thus, the measured voltage amplitude on the floating gate was less than its actual value. This behavior resulted in a measured gain that was less than its actual value. However, as the frequency increased, the impedance of the interdigitated gate decreased and the loading effects of the analyzer correspondingly decreased.

Although the loading effects of the analyzer similarly distort the phase measurements of the interdigitated gate, the trends observed in the phase of the impedance and gate transfer function were also observed in the output of the

CHEMFET sensor. Figures V-29 and V-30, show the phase of the CHEMFET sensor with respect to the driven gate's signal for exposure to NO_2 and DIMP. As observed in the interdigitated gate's gain and phase measurements the largest phase change due to NO_2 exposure occurs at 100 Hz. On an expanded scale (not shown), the phase also decreases over the frequency range of 10 - 200 KHz. Upon exposure to DIMP, the CHEMFET sensor revealed a smaller, but similar change in its phase. Figures V-31 and V-32 depict the CHEMFET sensor's phase following the purge of the challenge concentrations.

Frequency Response of the Interdigitated Gate to a Pulse Excitation Signal.

The response of the interdigitated gate to a pulse excitation signal depended upon the NO_2 challenge concentration. The signal waveforms appearing on the floating gate, when the driven gate was excited with a 256 Hz, 50 μs wide voltage pulse were captured on a dual trace oscilloscope (Tektronix Corp., model 475, Beaverton, OR). The amplitude of the excitation signal was 4 V. Figure V-33 shows the captured waveforms after exposure of the CHEMFET to several NO_2 challenge concentrations. The FFT of these waveforms were computed with the FFT analyzer (Bruel & Kjaer, model 2032, Marlborough, MA). Since the input impedance of the oscilloscope and the FFT analyzer were both 1 Mohm, these waveforms were also distorted by essentially the same loading effects of the instrumentation. Thus, only the trends observed in the waveforms have significance. The upper trace corresponds to the 4 V excitation signal applied to the driven gate. The lower trace is associated with the output signal appearing on the floating gate. With no exposure to NO_2

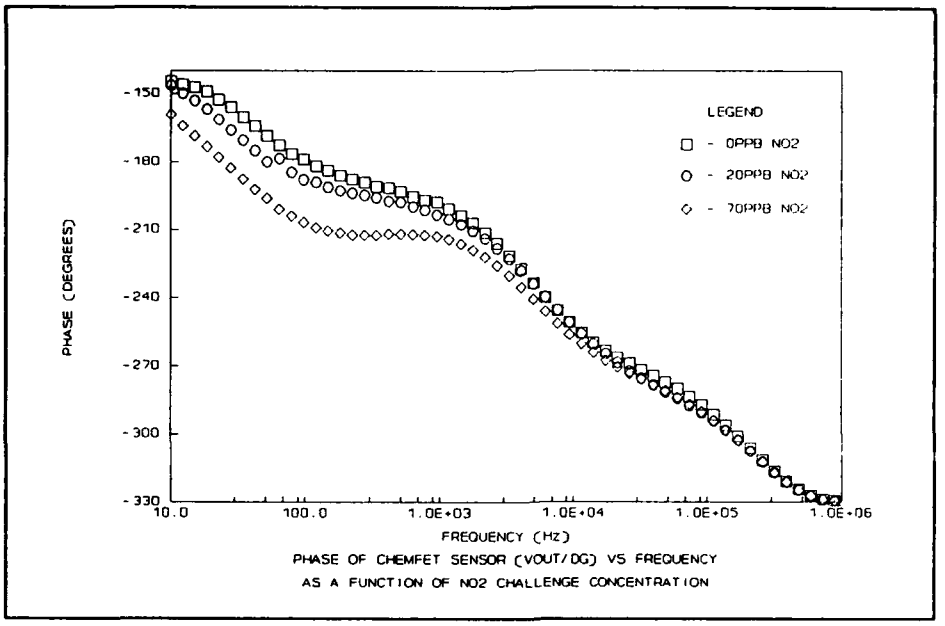

Figure V-29. Phase of the Copper Phthalocyanine-Coated CHEMFET Sensor vs Frequency as a Function of the Nitrogen Dioxide (NO_2) Challenge Concentration.

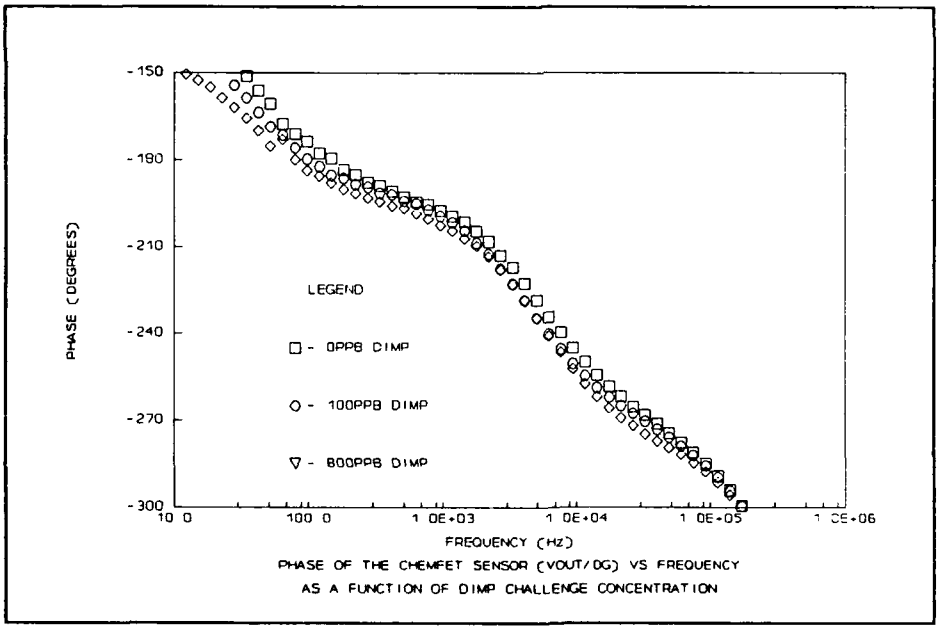

Figure V-30. Phase of the Copper Phthalocyanine-Coated CHEMFET Sensor vs Frequency as a Function of the Diisopropyl Methylphosphonate (DIMP) Challenge Concentration.

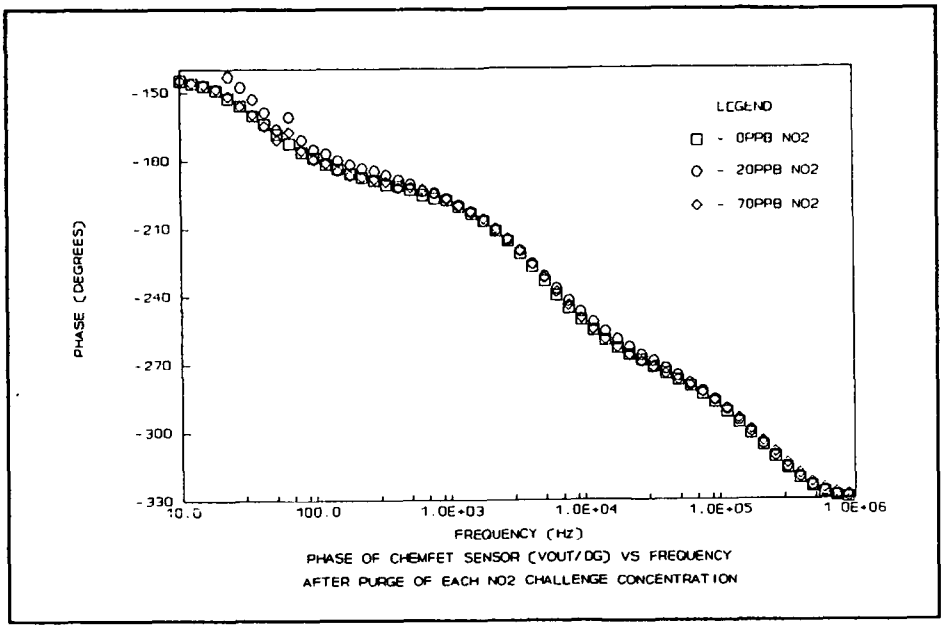

Figure V-31. Phase of the Copper Phthalocyanine-Coated CHEMFET Sensor vs Frequency after Purge of each Nitrogen Dioxide (NO_2) Challenge Concentration.

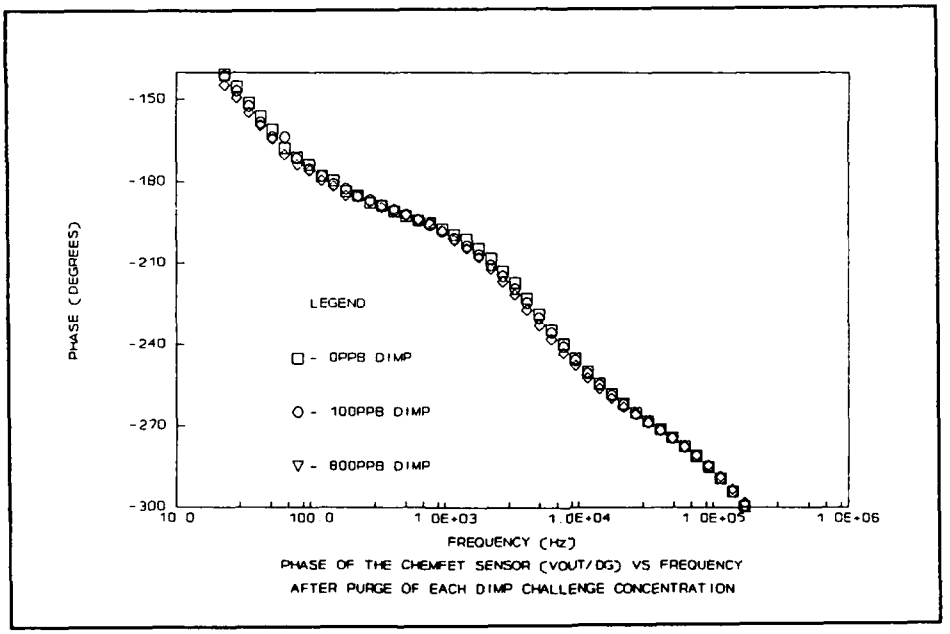

Figure V-32. Phase of the Copper Phthalocyanine-Coated CHEMFET Sensor vs Frequency after Purge of each Diisopropyl Methylphosphonate (DIMP) Challenge Concentration.

(Figure V-33a), the floating gate's signal is highly attenuated (0.1 V), but is not significantly distorted. Exposure of the CHEMFET to NO_2 (Figures V-33 b),d),f),and h) produced a significant change in both the amplitude and the shape of the floating gate's time-domain response. After NO_2 exposure, a greater proportion of the low frequency content of the excitation signal reaches the floating gate, and the response of the interdigitated gate resembles that of a low pass filter. Figures V-33 c),e), and g) depict the interdigitated gate's response after it returns to its initial state following a 30 minute purge of the challenge concentration. As the NO_2 concentration was increased, the amplitude of the response signal increased from 0.1 V, with no NO_2 exposure, to approximately 0.18 V, with an exposure concentration of 70 ppb.

The FFT spectra of the floating gate waveforms also reflected the changes observed in the time-domain response. Figure V-34 illustrates the normalized difference spectra obtained from the FFT spectrum at each NO_2 challenge concentration with respect to the unexposed FFT spectrum. As a result of the normalization process (see Chapter IV, Data Reduction and Analysis Software) Figure V-34 does not show the absolute change in the harmonic amplitudes, but rather, it shows the relative change in the shape of the spectral envelope. A large change in the spectral envelope, as a result of NO_2, exposure occurs at frequencies below 512 KHz and at frequencies near 5 KHz.

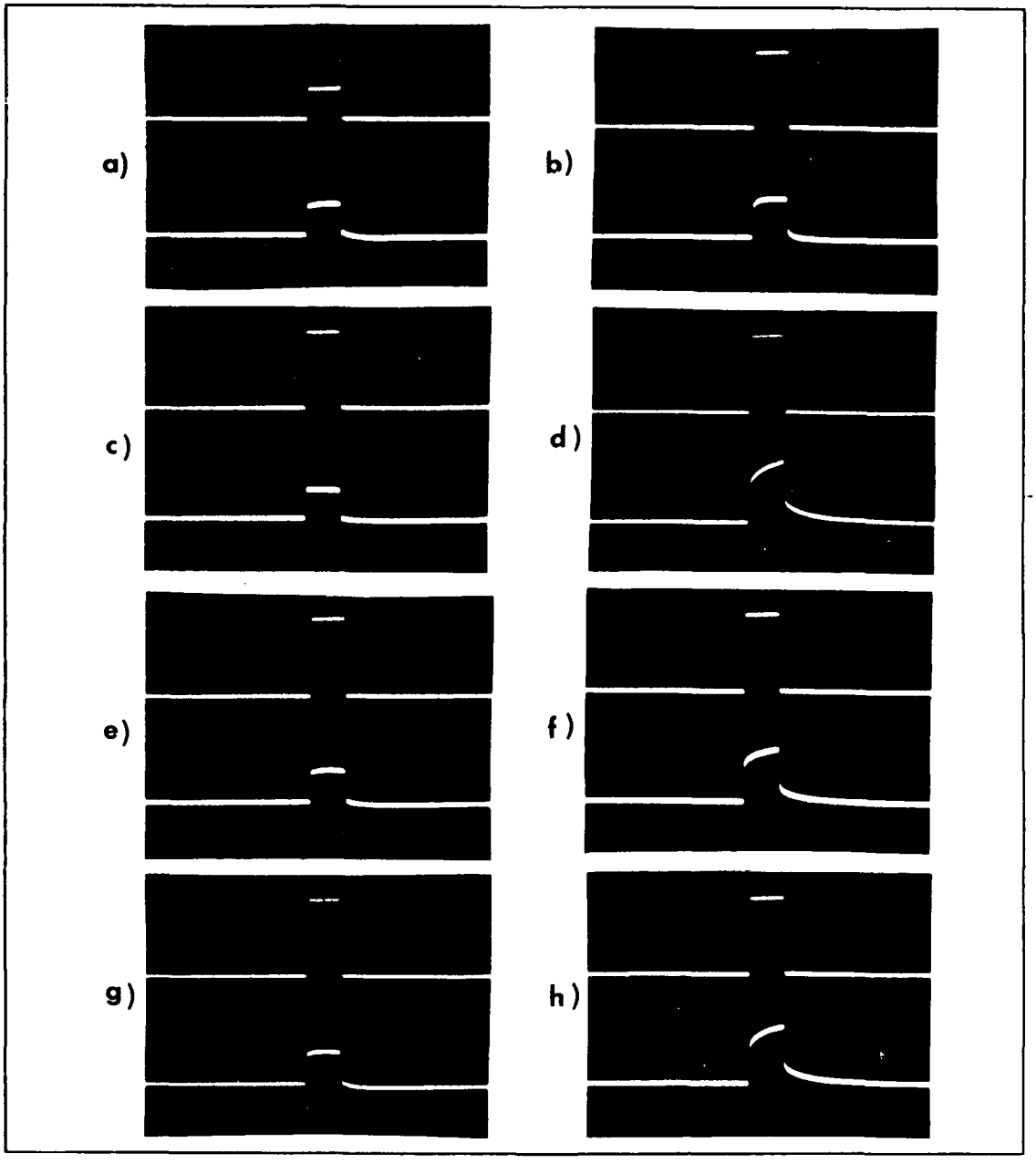

Figure V-33. Time-Domain Response of the Interdigitated Gate to a Pulse Excitation Signal as a Function of the Nitrogen Dioxide (NO_2) Challenge Concentration.

NO_2 Challenge Concentrations: a) No Gas, b) 20 ppb, c) 20 ppb/purge, d) 40 ppb, e) 40 ppb/purge, f) 70 ppb, g) 70 ppb/purge, h) 100 ppb. Upper Trace: 4V, 50μs Wide Excitation Signal (a: 5V/div, all others: 2V/div). Lower Trace: Floating Gate Voltage (0.1V/div). Horizontal Scale: 50μs/div.

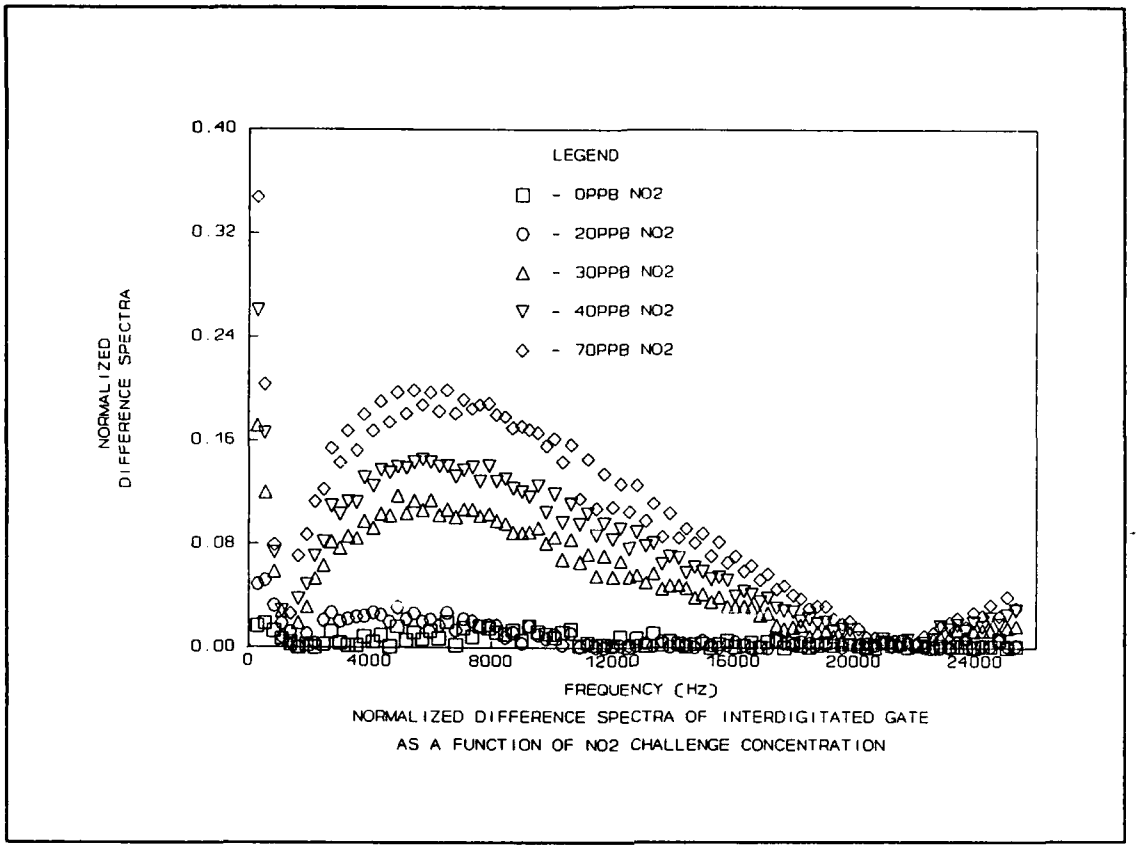

Figure V-34. Normalized Difference Spectra of the Copper Phthalocyanine-Coated Interdigitated Gate as a Function of the Nitrogen Dioxide (NO_2) Challenge Concentration.

Frequency Response of the CHEMFET Sensor to a Pulse Excitation Signal.

The effect of NO_2 and DIMP exposure on the frequency response of the CHEMFET sensor was more pronounced compared to that measured with respect to the interdigitated gate alone. Figures V-35 and V-36 show the time-domain waveforms measured at the drain of the CHEMFET sensor after the cyclical exposure and purge to the NO_2 and DIMP challenge concentrations, respectively. The same CHEMFET sensor was used to measure the effect both NO_2 and DIMP exposure. The CHEMFET sensor was first used to measure the response of the CuPc film to NO_2. After the 100 ppb NO_2 exposure, the CHEMFET sensor was purged overnight with the carrier gas. By comparison, Figures V-35a and V-36a reveal that the CHEMFET's response prior to exposure with NO_2 was essentially identical to its response following the overnight purge with the carrier gas. In addition, the CHEMFET sensor's response following exposure to the 20 - 40 ppb NO_2 challenge concentrations (Figure V-35 b), and d) was similar to the response of the 100 - 4000 ppb DIMP challenge concentrations (Figure V-36 b), d), f), and h). However, at the large NO_2 exposure concentrations (70 and 100 ppb), a significant redistribution of the harmonic content of the FFT waveform was observed (Figure V-35 f), and h). Based upon the shape of the time-domain output signal, the low frequency content of the signal increased with exposure to DIMP or small NO_2 concentrations. With large NO_2 concentrations, a proportional amount of the low frequency content decreased relative to the high frequency content. This behavior at high concentrations was also reflected in the measured FFT spectra. The

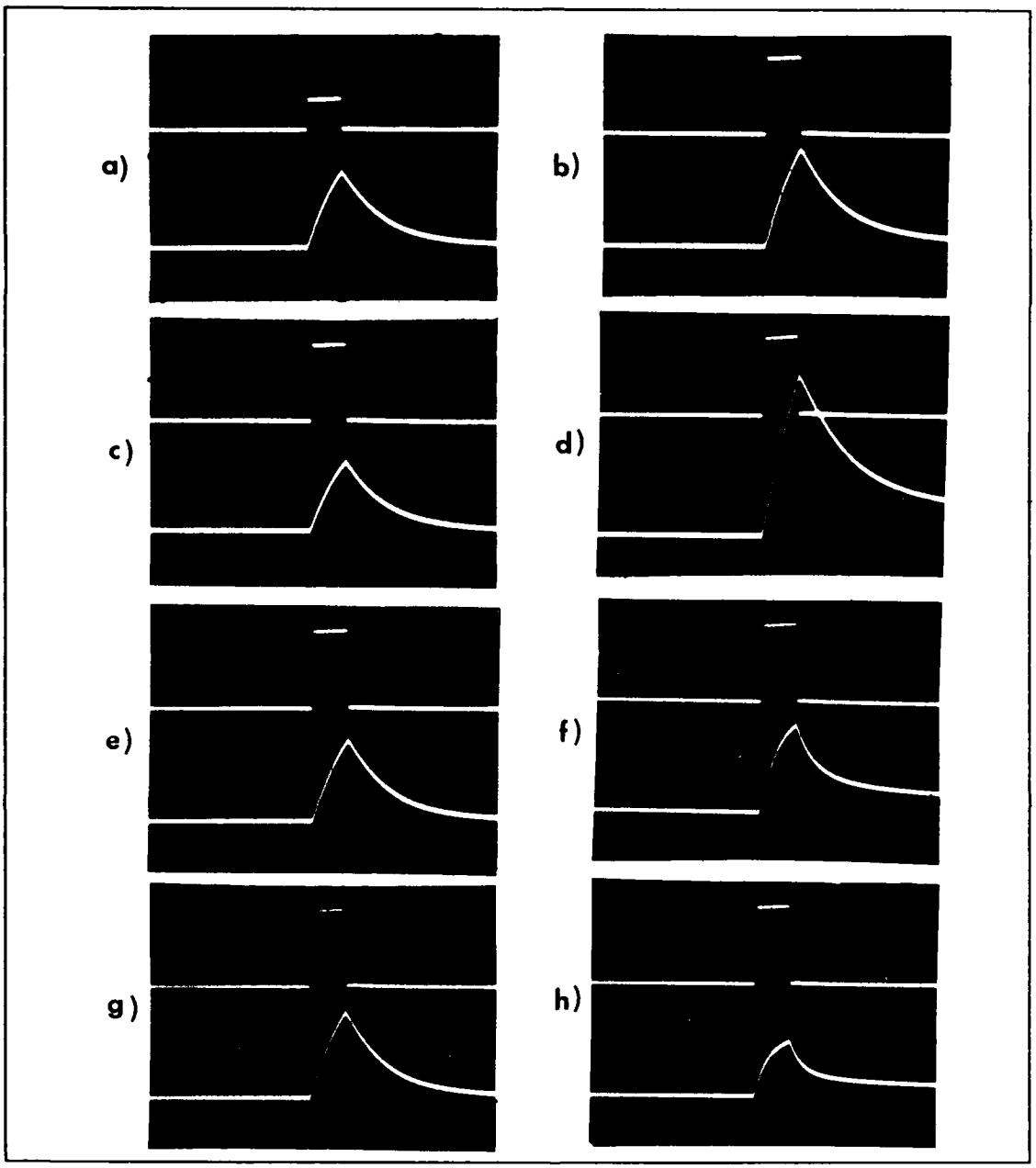

Figure V-35. Time-Domain Response of the CHEMFET Sensor to a Pulse Excitation Signal as a Function of the Nitrogen Dioxide (NO_2) Challenge Concentration.

NO_2 Challenge Concentrations: a) No Gas, b) 20 ppb, c) 20 ppb/purge, d) 40 ppb, e) 40 ppb/purge, f) 70 ppb, g) 70 ppb/purge, h) 100 ppb. Upper Trace: 4V, 50μs Wide Excitation Signal (a: 5V/div, all others: 2V/div). Lower Trace: Sensor Output Voltage (0.2V/div). Horizontal Scale: 50μs/div.

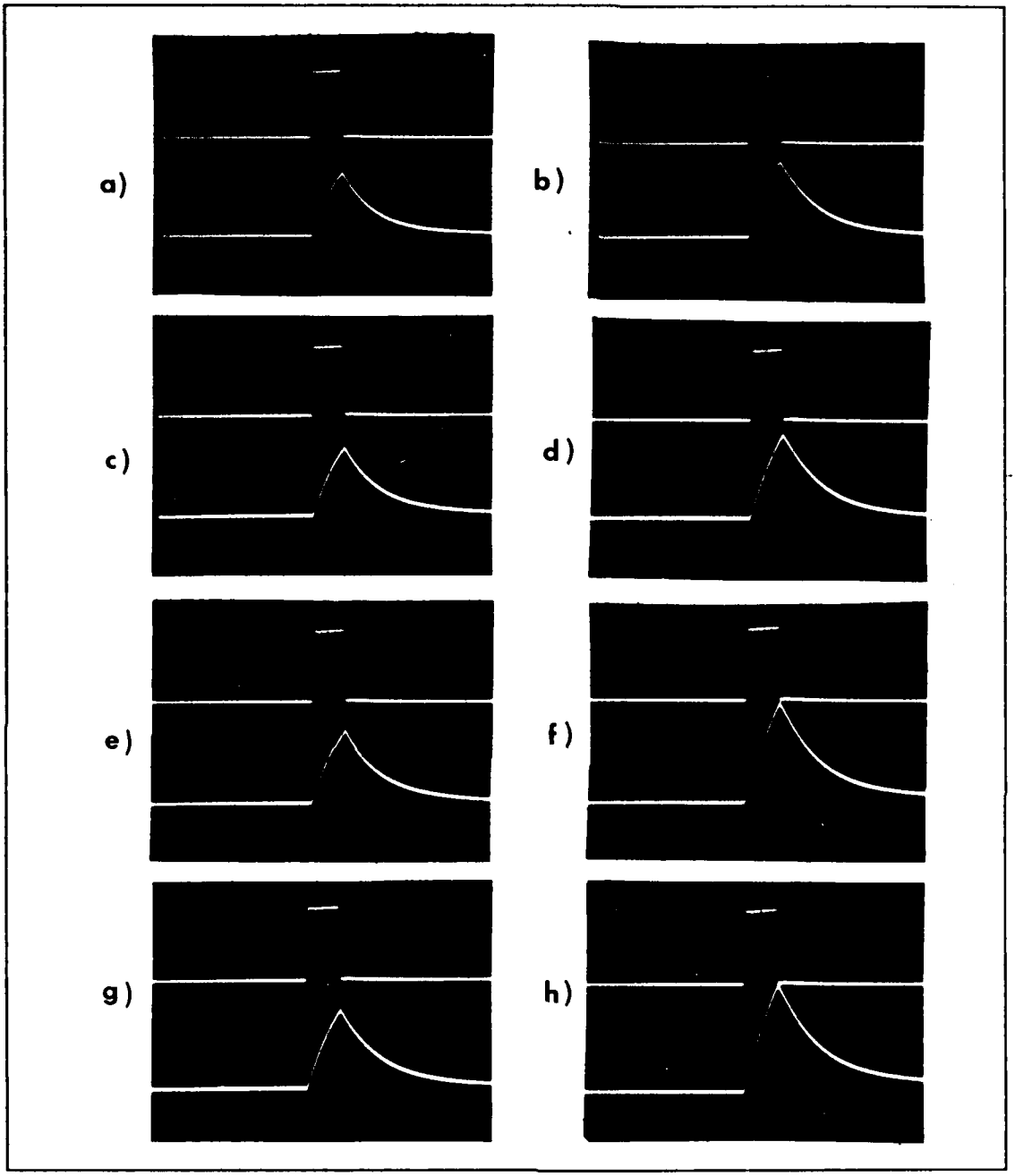

Figure V-36. Time-Domain Response of the CHEMFET Sensor to a Pulse Excitation Signal as a Function of the DIMP Challenge Concentration.

DIMP Challenge Concentrations: a) No Gas, b) 100 ppb, c) 100 ppb/purge, d) 200 ppb, e) 200 ppb/purge, f) 800 ppb, g) 800 ppb/purge, 4000 ppb. Upper Trace: 4V, 50μs Wide Excitation Signal (a: 5V/div, all others: 2V/div). Lower Trace: Sensor Output Voltage (0.2V/div). Horizontal Scale: 50μs/div.

amplitude of the highest harmonic in the FFT spectra of the unexposed CHEMFET sensor's response was 14 millivolts. This amplitude increased to 49 millivolts when the CHEMFET was exposed to 40 ppb NO_2. Similarly, the amplitude of the highest harmonic decreased to 28 millivolts at 70 ppb NO_2 and to 16.4 millivolts at 100 ppb NO_2. This trend was not observed in any of the other electrical measurements. Furthermore, this behavior in the CHEMFET sensor's waveform was not observed in a separate experiment with NO_2 concentrations as large as 400 ppb (See Appendix G). As shown in Figures V-35 c), e), g), and V-36 c), e), g), the CHEMFET sensor returned to its initial "no exposure" response following a 30 minute purge of each exposure concentration.

The normalized difference spectra associated with the CHEMFET output following exposure to either a NO_2 or DIMP challenge, and its output prior to exposure, are shown in Figures V-37 and V-38. The difference in the spectral envelopes increased at low frequencies as the challenge concentration was increased. Despite the abrupt switch in the characteristics of the CHEMFET's time-domain response at high NO_2 concentrations, a consistent change in the spectral envelope was obtained. The largest change in the spectral envelope as a result of either NO_2 or DIMP exposure occurred at low frequencies: 1 KHz for NO_2 and 2 KHz for DIMP. As illustrated in Figure V-39, the manner in which the envelopes change are significantly different between the two challenge gases.

The large difference between the spectral envelope changes in the CHEMFET's output voltage upon exposure to NO_2 and DIMP suggests that, in

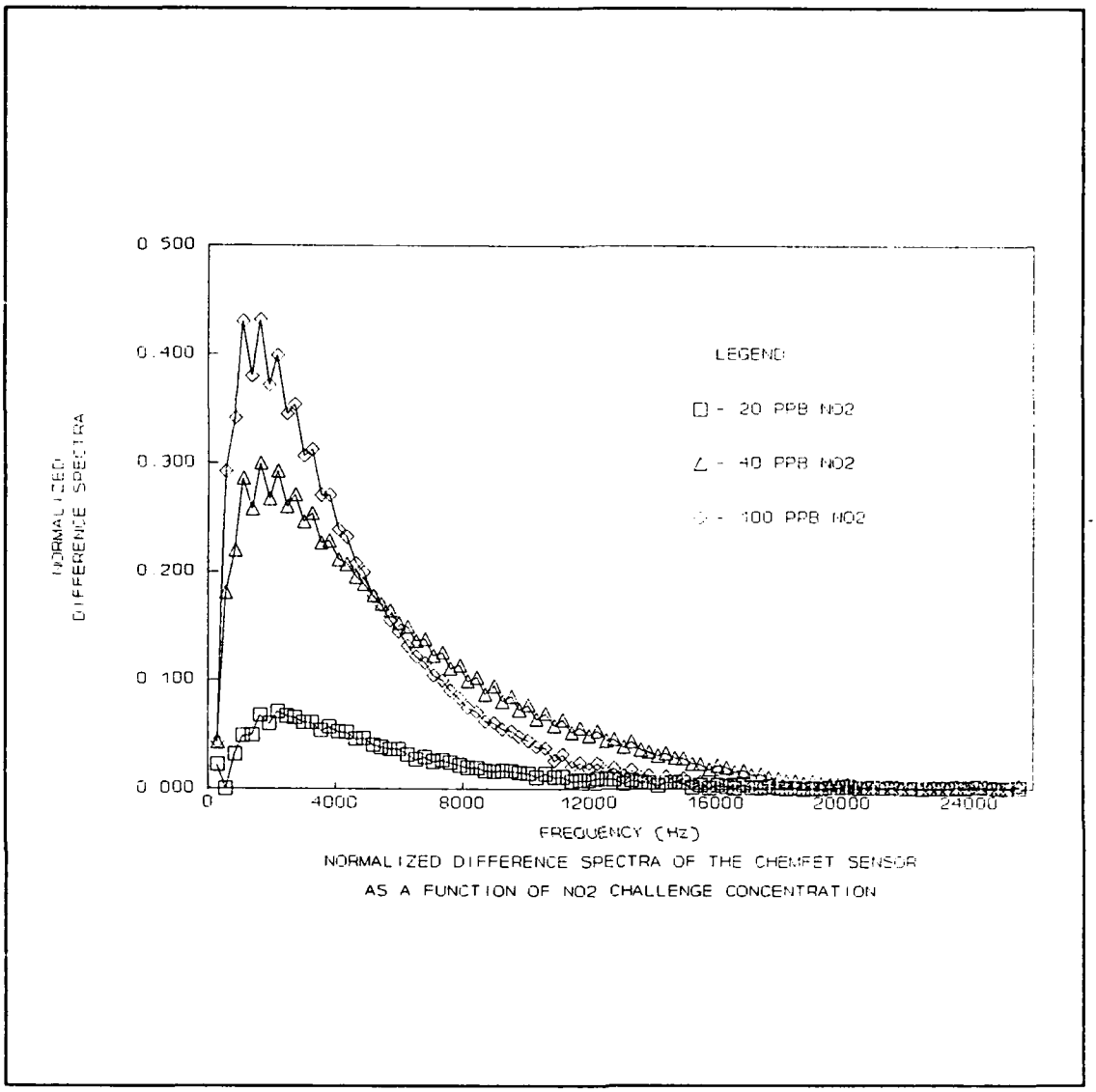

Figure V-37. Normalized FFT Response of the CHEMFET Sensor as a Function of the Nitrogen Dioxide (NO_2) Challenge Concentration.

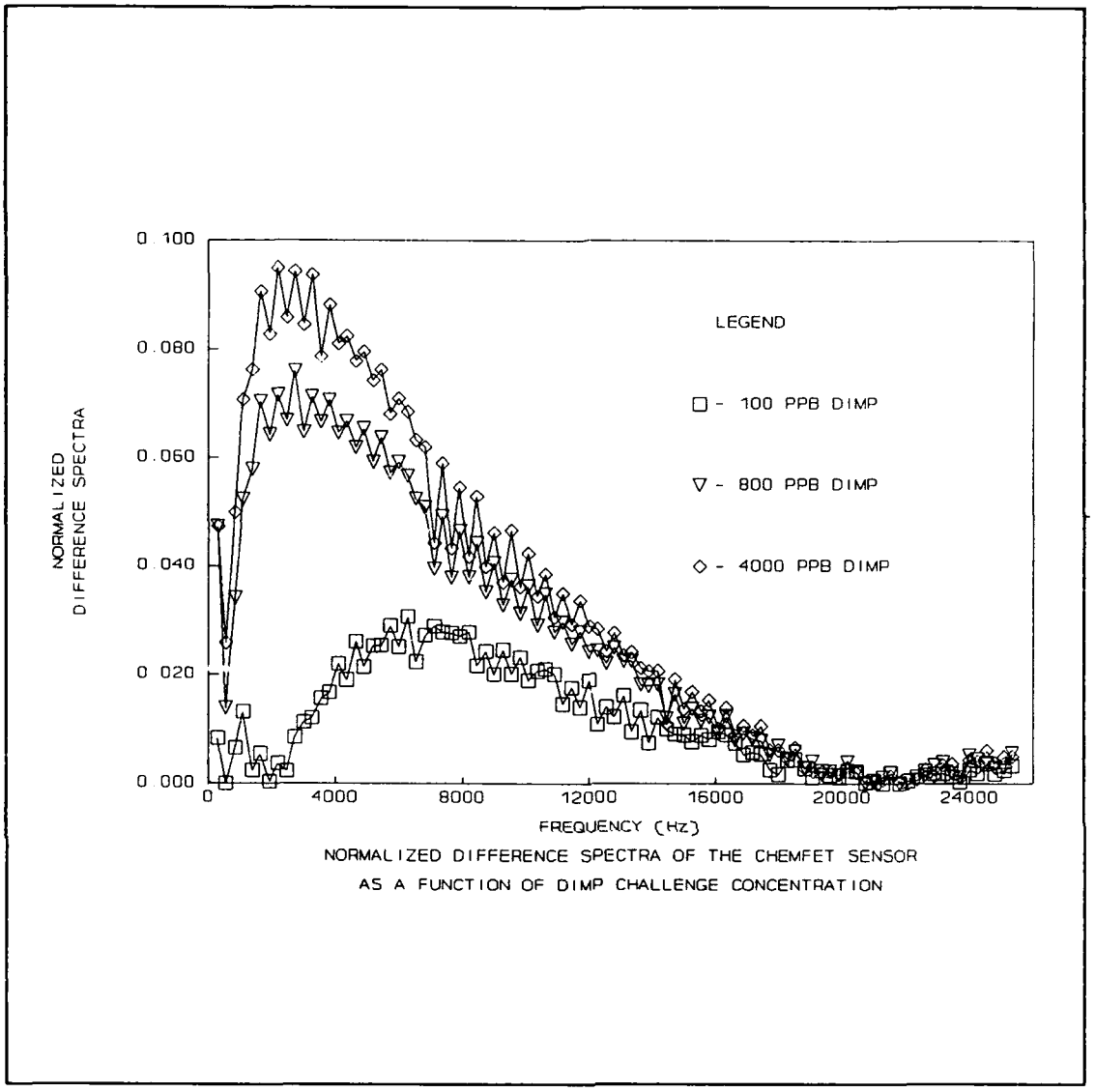

Figure V-38. Normalized FFT Difference Spectra of the CHEMFET Sensor as a Function of the Diisopropyl Methylphosphonate (DIMP) Challenge Concentration.

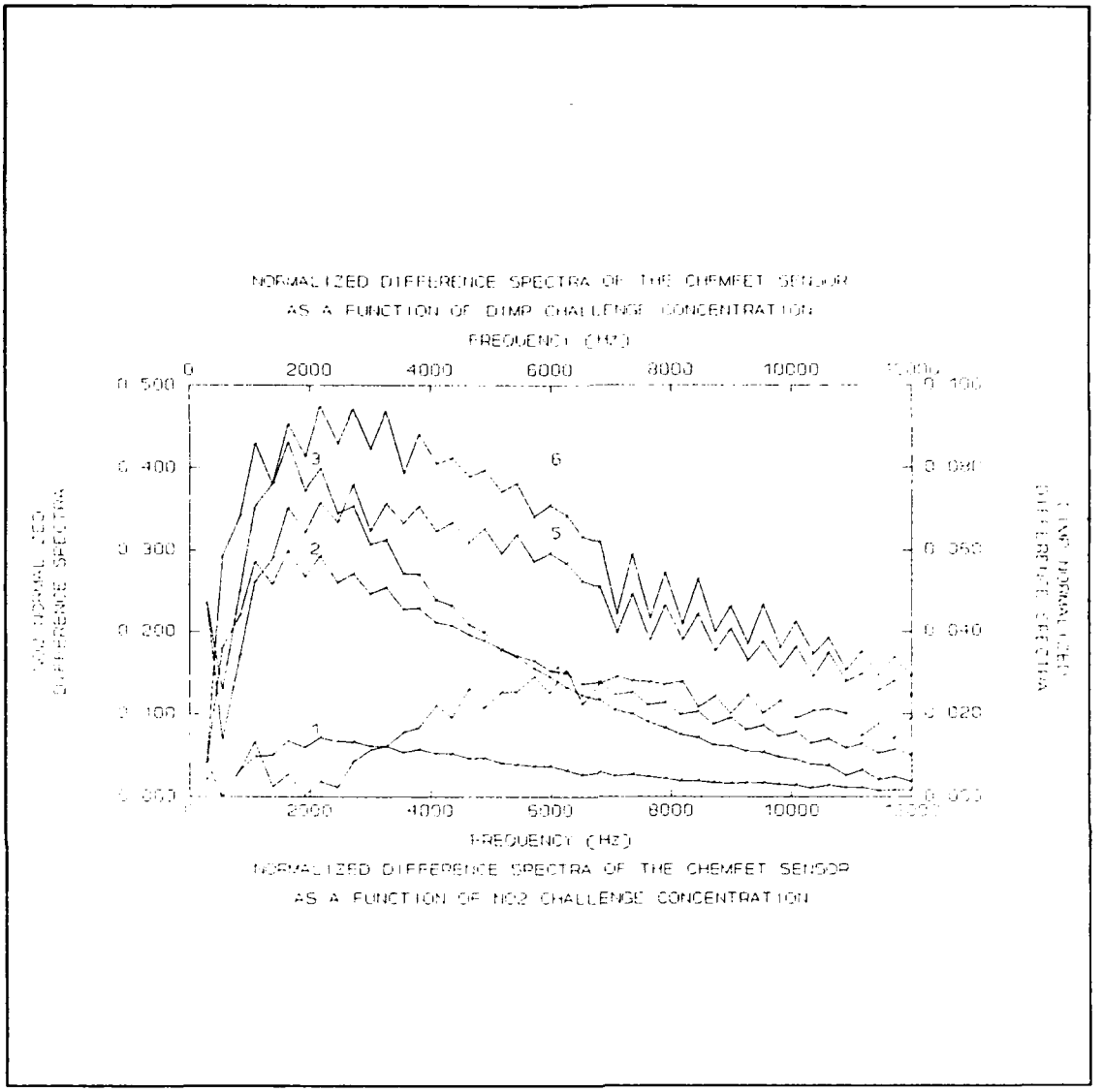

Figure V-39. Comparison of the FFT Envelope Changes Resulting From Exposure to Nitrogen Dioxide (NO_2) and Diisopropyl Methylphosphonate (DIMP) Challenge Concentrations.

contrast to the resistance measurements, the sensor's AC electrical properties can distinguish between the two challenge gases. That is, the CHEMFET has a unique selectivity feature that is manifested in the frequency dependent response to a challenge gas. Thus, by examining the relative changes in the electrical properties at different frequencies, the CHEMFET can be utilized to determine the type of challenge gas present. To illustrate this capability, Table V-1 summarizes the percentage change in the CHEMFET's gain at selected frequencies within the range spanning 256 Hz - 5 KHz after exposure to 30 ppb NO_2 and 800 ppb DIMP. At these concentrations the two challenge gases caused approximately the same percentage change in the interdigitated gate resistance. However, as shown in Table V-1, the CHEMFET's frequency response was clearly different for the two challenge gases. At low frequencies the change in the CHEMFET sensor's gain is greater with respect to a given NO_2 challenge concentration. As the frequency increases, the NO_2 induced gain change decreases rapidly, eventually becoming less than the gain change produced by the DIMP challenge at approximately 3 KHz. These results are consistent with the changes observed in the spectral envelope of the CHEMFET's output voltage when excited with a pulse signal.

ACHE Response to DIMP Exposure

ACHE Experiment Number 1.

In the first ACHE experiment, the ACHE film was exposed to a 500 ppb DIMP challenge for a 150 minute duration. The baseline electrical measurements were then accomplished after 30, 90, and 150 minutes of exposure duration. The

Table V-1
Percentage Change in the CHEMFET Gain as a Function of Frequency for 30 ppb NO_2 and 800 ppb DIMP Challenge Concentrations

	Percent Change In the CHEMFET Gain	
Frequency (Hz)	30 ppb NO_2	800 ppb DIMP
250	38.5	27.8
500	31.5	23.9
1000	25.8	21.9
2000	20.6	19.3
3000	17.0	17.1
4000	15.3	15.7
5000	13.7	14.2

sample cell temperature was constant at 37 ± 1 ^{o}C, and the relative humidity was 58 ± 2 percent. The baseline electrical measurements revealed no change in the impedance properties of the film as a result of the exposure (data not shown). A slow increase in the resistance of the film was noted during both the initial purge and the DIMP exposure. The rate of the resistance increase was not observed to change upon exposure to DIMP (data not shown).

ACHE Experiment Number 2.

In the second ACHE experiment, the DIMP challenge concentration was increased to 1 ppm and the humidity within the sample cell was increased. The

humidity was increased to more accurately simulate the normal aqueous environment associated with active enzymes. The measured humidity at the outlet of the sample cell was 108 percent. The reason the digital hygrometer reading was above 100 percent was attributed to the temperature difference between the sample cell (37 ^{o}C) and the hygrometer's sensor (22 ^{o}C). As a consequence the relative humidity within the cell was assumed to be near 100 percent under these conditions. The baseline electrical measurements were performed after 30, 90, and 150 minutes of exposure to the challenge gas. Once again, there was no observed change in the film's electrical properties associated with DIMP exposure (data not shown). However, the long term drift in the film's resistance observed during the first ACHE experiment was also observed. To further investigate the long term resistance drift phenomenon, the interdigitated gate resistance was measured at 25 second intervals during an overnight purge of the sample with the carrier gas. Figure V-40 reveals the resistance drift which occurred during the DIMP exposure and the overnight purge. The slope of both least square lines was 1.7×10^{7} ohms/minute, which indicates that the resistance change was independent of the DIMP exposure.

ACHE Experiment Number 3.

Since the dry ACHE film did not respond to a DIMP challenge, an alternative approach was considered where the ACHE could be exposed to a DIMP challenge while in solution. A 5 μl aliquot of the ACHE solution was the maximum volume which could be deposited on the CHEMFET's interdigitated gate. This small volume rapidly evaporates (less than 30 minutes), and thus, the electrical properties of the

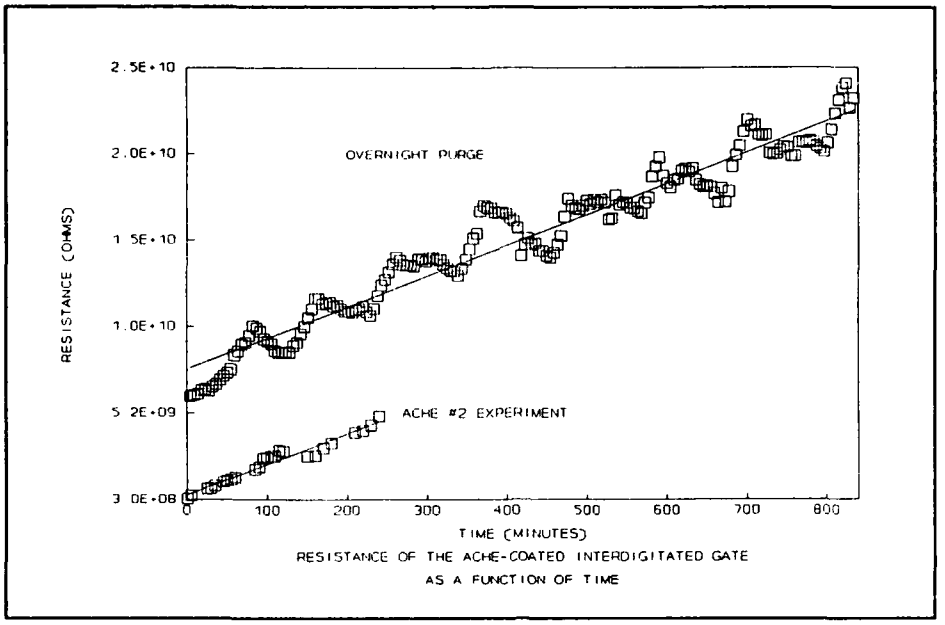

Figure V-40. Long Term Drift in the Interdigitated Gate Resistance with the Acetylcholinesterase (ACHE) Film.

film are unstable. The variation in the interdigitated gate resistance during repeated film application and evaporation cycles is shown in Figure V-41. The resistance decreased upon application of the ACHE solution and increased as the water evaporated. However, an overall decrease in the resistance was observed after repeated applications. This reduction in the resistance was attributed to an accumulation of a thicker ACHE film and higher ionic contamination on the interdigitated gate's surface.

ACHE Experiment Number 4.

In the fourth experiment, the possibility that the transient response of the interdigitated gate observed in the third ACHE experiment was indeed sensitive to a prior exposure of the ACHE solution to DIMP was investigated. Figure V-42

shows the response of the interdigitated gate resistance to two separate applications of both DIMP-exposed and unexposed ACHE solutions. The transient reduction in the resistance upon deposition of the ACHE solutions was highly variable. However, after the initial transient, the rate at which the resistance increased depended upon the prior DIMP exposure of the ACHE solution. That is, the interdigitated gate's resistance increased much more rapidly with the unexposed ACHE solution. Additional data for the rate of resistance increase for the unexposed ACHE film was obtained during the third ACHE experiment. Excluding the data measured during the first ten minutes after a film was deposited, the slope of the least square line (plotting resistance versus time) was computed for the DIMP-exposed and the unexposed ACHE films. Table V-2 summarizes the rate of resistance increase for

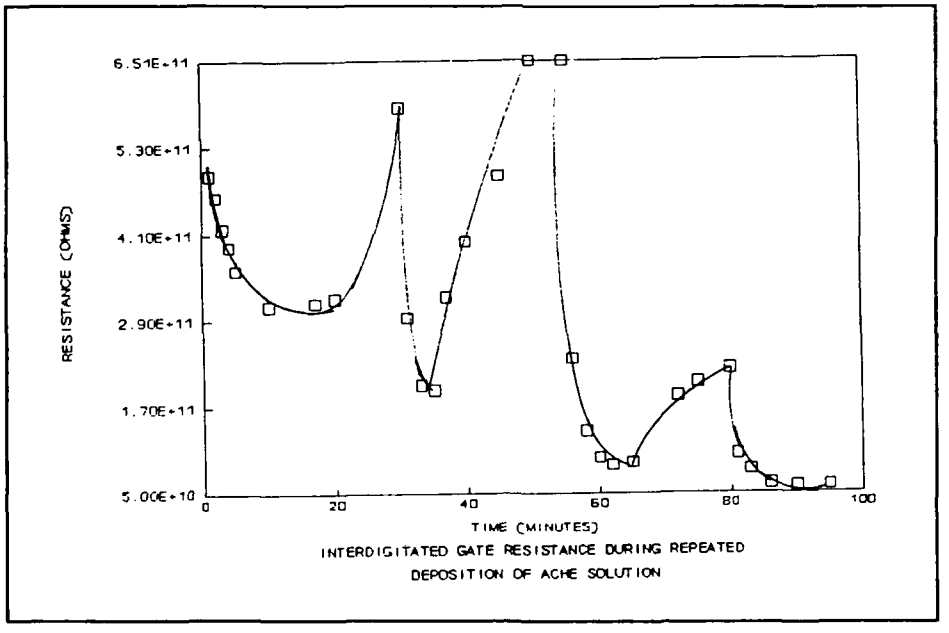

Figure V-41. Resistance Of the Interdigitated Gate with Consecutive 5μl Applications of the Acetylcholinesterase (ACHE) Solution.

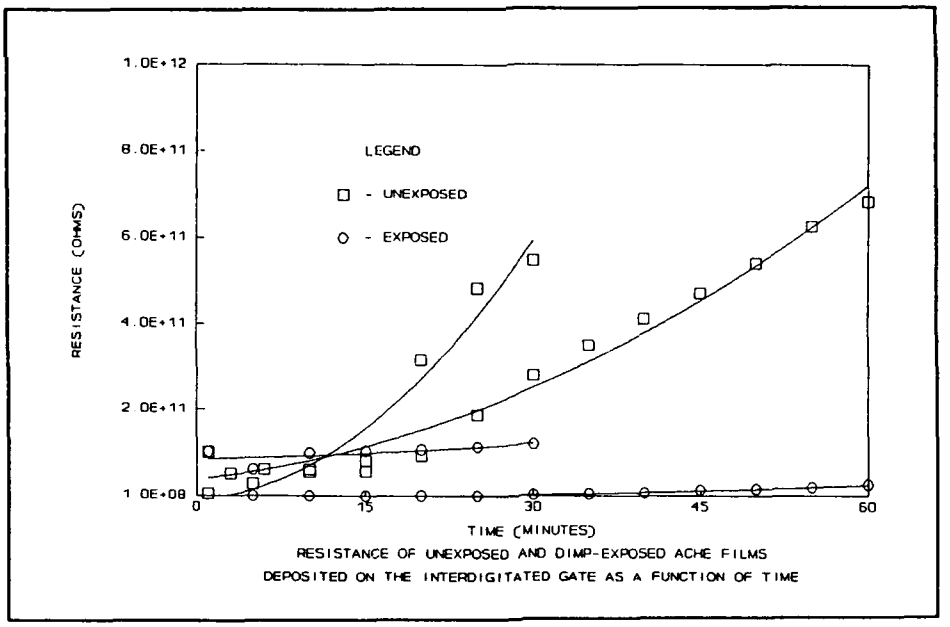

Figure V-42. Resistance of the Unexposed and DIMP-Exposed Acetylcholinesterase (ACHE) Films Deposited on the Interdigitated Gate as a Function of Time.

the unexposed and exposed ACHE films. The rate at which the resistance increased with the unexposed film was approximately one order of magnitude greater than the rate observed with the DIMP-exposed ACHE film.

Summary

The electrical performance of the CHEMFET as a sensor was evaluated for detecting changes in the chemical state of three different films: an epoxy, copper phthalocyanine, and acetylcholinesterase. The change in the electrical properties of each film and its effect on the CHEMFET sensor's response were analyzed in relation to either the epoxy's cure time or with respect to a gaseous challenge concentration.

Table V-2
Rate of the Interdigitated Gate Resistance Increase for
DIMP Exposed and Unexposed Acetylcholinesterase Films

	Resistance of the Unexposed ACHE Film (ohms)	Resistance of the Exposed ACHE Film (ohms)
	1.4×10^{10}	5.1×10^{8}
	2.8×10^{10}	1.0×10^{9}
	1.4×10^{10}	
	1.8×10^{10}	
	1.0×10^{10}	
	1.0×10^{8}	
Average	1.0×10^{10}	7.6×10^{8}

VI. Conclusions and Recommendations

Conclusions

An interdigitated gate electrode CHEMFET was designed and its electrical performance, both in the time-domain and frequency-domain, was evaluated for detecting changes in the molecular structure or chemical composition of three thin films: an epoxy, copper phthalocyanine (CuPc), and acetylcholinesterase (ACHE). The change in the chemical state of a film was manifested as a change in the electrical impedance of the interdigitated gate electrode structure. For the epoxy, its bulk molecular structure changed as a result of the curing reaction. To induce a change in the chemical state of the CuPc and ACHE films, they were exposed to a challenge gas, either nitrogen dioxide (NO_2) or diisopropyl methylphosphonate (DIMP).

The electrical performance of the CHEMFET transistors was verified. Typical MOSFET I-V characteristics were measured. The CHEMFET transistors had a gain of approximately 9 dB, and the - 3 dB cutoff frequency was 8 KHz.

The electrical changes observed in the epoxy film during cure were consistent with the results reported by Lee (34). The conductivity of the epoxy decreased as the cure reaction progressed. This behavior resulted in a smaller signal reaching the floating gate, and thus, decreased the CHEMFET's output voltage and gain. The effect of the conductivity change was observed in the gain/phase and pulse signal excitation response of the CHEMFET sensor. Of particular importance, was the

amplitude change in the harmonic content of the CHEMFET's output signal during cure when a pulsed signal excitation was applied to the driven gate. The largest change in the spectral envelope occurred at low frequencies, in agreement with the gain/phase and impedance measurements. In addition to this characteristic change at low frequency, the spectral envelope change peaked at frequencies centered at 500, 3000, 6500, and 10000 Hz. This additional information in the spectral envelope of the CHEMFET's output signal can be used to further characterize the material properties.

The CuPc-coated CHEMFET was able to detect and discriminate between NO_2 and DIMP challenge gases. Upon exposure to either challenge gas, the impedance of the film decreased. An 82 percent change in the interdigitated gate resistance occurred with exposure to a 20 ppb NO_2 challenge concentration. The impedance change in the CuPc film was much more sensitive to NO_2 than DIMP. A similar percent change in the interdigitated gate resistance required a 300 ppb DIMP challenge concentration. The observed changes in the interdigitated gate impedance were reflected in the gain and phase of the interdigitated gate and CHEMFET sensor. The measurement of the interdigitated gate's gain/phase response and its pulse signal excitation response were distorted by the loading effects of the instrumentation. The loading effects were reduced, but not eliminated when the measurements were made at the output of the CHEMFET transistor because its input impedance was reduced by the 20 Mohm gate bias resistor. Although the resistance change is consistently the highest-sensitivity measurement parameter

associated with a of the change in the chemical state of a film, it does not provide an explicit means of discriminating between NO_2 and DIMP exposures. However, the spectral changes in the CHEMFET's pulse signal excitation response were unique for each challenge gas, and by observing the CHEMFET's response at several frequencies, the specific challenge gas could be determined.

The sensitivity of the ACHE film to DIMP exposure was not unequivocally determined by the electrical measurements performed with the CHEMFET. No change in the electrical properties of a dry ACHE film was detected which could be attributed to DIMP exposure with challenge concentrations as large as 1 ppm. Since the dry ACHE film did not respond to DIMP exposure, an alternative approach was devised where the ACHE film could be exposed while in solution. The electrical properties of an ACHE solution deposited on the CHEMFET interdigitated gate electrode was unstable as a result of solvent evaporation. Thus, the ACHE solution was exposed to a 4 ppm DIMP challenge concentration prior to its deposition on the interdigitated gate. The electrical properties of the deposited ACHE solution were still unstable, but a difference in the rate at which the resistance increased was observed between the exposed and unexposed ACHE solutions. The rate of resistance increase for the exposed ACHE solution was approximately one order of magnitude less than that associated with the unexposed ACHE solution. This large difference suggests that the conductivity of the ACHE solution was increased by exposure to the DIMP challenge concentration.

In conclusion, the CHEMFET sensor concept was clearly demonstrated for detecting chemical and structural changes in an epoxy and CuPc films. Furthermore, exposure of the CHEMFET to a particular gas produces a unique change in its frequency domain response. The CHEMFET can eliminate the loading effects of the instrumentation on the measurement of the electrical properties of a high impedance film. The CHEMFET also provides signal amplification, which reduces problems associated with electrical noise. Since conventional solid state fabrication technology is used to fabricate the CHEMFET, a small, low mass, highly reliability sensor can be mass produced at relatively low cost.

Recommendations

The results of this research effort have demonstrated the feasibility of using an interdigitated gate CHEMFET to detect changes in the chemical composition and structure of a material, and it also can be used to detect trace quantities of NO_2 and DIMP. Future work should be directed towards improving the CHEMFET design for the long-range goal of developing a multifunctional sensor which can identify and quantify the components in a gas mixture. The specific recommendations for follow-on studies are:

1. Redesign the interdigitated CHEMFET to improve its electrical performance. The current CHEMFET design has limited gain and a relatively low cutoff frequency. The gain and cutoff frequency could be improved by designing a two stage amplifier. The cutoff frequency could also be extended by minimizing the transistor's gate capacitance via smaller geometrical features. The use of a

depletion-mode MOSFET eliminates the need for a high resistance gate bias resistor.

2. Perform an equivalent circuit analysis and computer simulation of the CHEMFET's interdigitated gate structure to predict the geometry that will yield optimum sensor performance.

3. Evaluate the performance of the CHEMFET sensor with respect to film thickness, temperature, and humidity.

4. Evaluate the sensitivity and the spectral response of the CHEMFET coated with other metal-substituted phthalocyanines (for example zinc, lead, cobalt, iron, and nickel phthalocyanines) to NO_2 and DIMP.

5. Determine if the ACHE electrical properties can be stabilized by using a suitable semi-permeable binder, such as agarose. The DIMP challenge can diffuse into the semi-permeable solid and interact with the ACHE to elicit a change in its electrical properties.

6. Determine if the increased isolation of the interdigitated gate from the CHEMFET transistor produced by applying a reverse bias across the p-well/substrate junction can improve the electrical performance of the CHEMFET.

7. Collect and examine the real and imaginary parts of the interdigitated impedance to explain the observed response of the CHEMFET sensor at high NO_2 challenge concentrations. A switch in the relative magnitude of the real and imaginary parts

Appendix A

Metal Oxide Semiconductor Implementation Service (MOSIS)

Process Characterization Data Sheet

This Appendix contains the MOSIS Process Characterization Data Sheet associated with the interdigitated gate CHEMFET's fabrication. The data sheet includes the performance of MOSIS test transistors and a comparison with the predicted performance from an associated SPICE model analysis. The data sheet also includes information concerning the critical fabrication process parameters (such as gate oxide thickness).

MOSIS PARAMETRIC TEST RESULTS

RUN: N85R / RALPH
TECHNOLOGY: SCP

VENDOR: HP
FEATURE SIZE: 3.0um

I. INTRODUCTION. This report contains the lot average results obtained by MOSIS from measurements of the MOSIS test structures on the selected wafers of this fabrication lot. The SPICE and/or BSIM parameters obtained from similiar measurements on these wafers are also attached.

COMMENTS: This looks like a typical HP 3.0um run.

II. TRANSISTOR PARAMETERS:	W/L	N-CHANNEL	P-CHANNEL	UNITS
Vth (Vds=.05V)	4.5/3	.852	-.896	V
Vth (Vds=.05V)	27/3	.891	-.938	V
Idss (Vgds=5V)	27/3	2609.0	-1172.0	uA
Vpt (Id=1.0uA)	27/3	17.96	-17.41	V
Vth (Vds=.05V)	50/50	.918	-.983	V
Vbkd (Ij=1.0uA)	50/50	17.4	-18.7	V
Kp (Uo*Cox/2)	50/50	24.2	8.99	uA/V**2
Gamma (2.5v,5.0v)	50/50	1.084	.537	V**0.5
Delta Length		.723	.771	um
Delta Width		.443	.953	um
(Effective=Drawn-Delta)				

COMMENTS: These parameters look normal.

III. FIELD OXIDE TRANSISTOR PARAMETERS:	GATE	SOURCE/DRAIN N - ACTIVE	SOURCE/DRAIN P - ACTIVE	UNITS
Vth (Vbs=0,I=1uA)	Poly	19.6	-11.0	V
Vth (Vbs=0,I=1uA)	Metal1	19.3	-22.0	V
Vth (Vbs=0,I=1uA)	Metal2	19.2	-15.1	V

COMMENTS: These parameters look normal.

IV. PROCESS PARAMETERS:	N POLY	P POLY	N DIFF	P DIFF	P WELL	METAL 1	METAL 2	UNITS
Sheet Resistance	17.2	26.8	29.5	113.7	2472.0	.039	.030	Ohm/sq
Width Variation (Measured - Drawn)	-.131	.097	-.116	.092	----	.356	.077	um
Contact Resist. (Metal1 to Layer)	7.35	12.06	40.49	37.02	----	----	.019	Ohms
Gate Oxide Thickness:	----	----	438.	----	----	----	----	Angst.

COMMENTS: These parameters look normal.

V. CAPACITANCE

PARAMETERS:	POLY	N DIFF	P DIFF	METAL 1	METAL 2	UNITS
Area Cap (Layer to subs)	.055	.376	.242	.035	.023	fF/um**2
Area Cap (Layer to Poly)	----	.769	.594	.053	.022	fF/um**2
Area Cap (Layer to Metal1)	----	----	----	----	.034	fF/um**2
Fringe Cap (Layer to subs)	----	.516	.293	----	----	fF/um

COMMENTS: These parameters look normal.

VI. CIRCUIT PARAMETERS:

Vinv,	K = 1	2.11	V
Vinv,	K = 1.5	2.31	V
Vlow,	K = 2.0	0.00	V
Vhigh,	K = 2.0	5.01	V
Vinv,	K = 2.0	2.46	V
Gain,	K = 2.0	-20.35	
Ring Oscillator Frequency		15.72	MHz (31 stages @ 5.0V)

COMMENTS: The ring oscillator frequency is typical.

N85R SPICE PARAMETERS

```
.MODEL CMOSN NMOS LEVEL=2 LD=0.400000U TOX=418.00000E-10
+ NSUB=2.97056E+16 VTO=0.881794 KP=5.49941E-05 GAMMA=1.20205
+ PHI=0.6 UO=665.699 UEXP=0.240761 UCRIT=73478.7
+ DELTA=0.001 VMAX=64117.6 XJ=0.400000U LAMBDA=0.0292501
+ NFS=2.89619E+12 NEFF=1.001 NSS=1E+12 TPG=1.000000
+ RSH=29.370003 CGDO=3.30431E-10 CGSO=3.30431E-10 CGBO=2.47823E-10
+ CJ=0.0003789 MJ=0.528300 CJSW=4.15E-10 MJSW=0.320000 PB=0.840000
* Weff = Wdrawn - Delta_W
* The suggested Delta_W is 0.30 um
.MODEL CMOSP PMOS LEVEL=2 LD=0.325645U TOX=418.00000E-10
+ NSUB=7E+15 VTO=-0.822049 KP=1.73164E-05 GAMMA=0.583813
+ PHI=0.6 UO=209.614 UEXP=0.214077 UCRIT=72408.3
+ DELTA=0.734324 VMAX=100000 XJ=0.400000U LAMBDA=0.0374271
+ NFS=1.34086E+12 NEFF=1.001 NSS=1E-12 TPG=-1.000000
+ RSH=112.300010 CGDO=2.69008E-10 CGSO=2.69008E-10 CGBO=7.43469E-10
+ CJ=0.0002376 MJ=0.475000 CJSW=3.652E-10 MJSW=0.274700 PB=0.720000
* Weff = Wdrawn - Delta_W
* The suggested Delta_W is 0.90 um
```

Appendix B

Permeation Tube and Flowmeter Calibration Information

This Appendix contains vendor-supplied calibration information for the permeation tubes (GC Industries, model 23-7392 for DIMP and model 23-7502 for NO_2, Chatsworth, CA) and the precision flowmeters (Gilmont Instruments, model F-7660, Great Neck, NY). Flowmeter model F-7660 is a kit of three separate flowmeters with the following model numbers: F-1100, F-1200, and F-1300. These charts are required for determining the operational conditions required to generate a specific gas challenge concentration. The first section contains the calibration information and charts for the NO_2 and DIMP permeation tubes. The second section contains the calibration charts for the 12 flowmeters (four F-7660 kits were used, and each flowmeter is individually calibrated). Each flowmeter can use either a stainless steel float or a glass float. If a glass float is used, the flow rate can be read directly from the calibration charts in Figures B-7 to B-19. The conversion scales in Figures B-20 to B-22 are provided if the stainless steel float is used.

Permeation Tube Calibration Information

INSTRUCTION SHEET

G-CAL TYPE NO_2 S/N G-4767 MODEL 23-7052

WEIGHT OF G-CAL (LESS SCRUBBER) AT SHIPMENT 252.255 gms. G-CAL IS EMPTY WHEN WEIGHT REACHES 250-300 gms. or LOWER

SHIPMENT DATE 5-26-88

CAUTION: G-CAL CONTAINS GAS OR LIQUID UNDER HIGH PRESSURE. THE MATERIAL CONTAINED MAY BE FLAMMABLE AND/OR HIGHLY TOXIC. USE EXTREME CAUTION DURING USE. DO NOT EXPOSE TO TEMPERATURES ABOVE 122°F (50°C) OR BELOW 0°F (-18°C). DO NOT EVER OPEN END FITTINGS AS THIS WILL RESULT IN RELEASE OF GAS.

CAUTION: WHEN EXPIRED, THIS DEVICE SHOULD ONLY BE DISCARDED THROUGH AN INDUSTRIAL WASTE SERVICE. GENERAL PURPOSE DISPOSAL IS NOT RECOMMENDED.

WARRANTY: Each G-CAL device, except for Chlorine gas, is warranted to have a useful life of 12 months* of normal use and service from the date of shipment. G-CAL for Chlorine is warranted for 6 months from the date of shipment. Defective G-CAL returned prepaid to factory with prior approval, will be repaired or replaced free within the first six months (3 months for Chlorine) of shipment. A pro-rated fee will be charged for G-CAL repaired after this period. The warranty is void if the G-CAL assembly is taken apart or opened in any way other than for normal use.

The liability of Seller to the Buyers arising out of the supplying of G-CAL assembly on its use, whether on warranty, contract, or otherwise, shall not in any case exceed the cost of the original purchase and upon the expiration of warranty period, all such liability shall terminate. In no event shall G C Industries, Inc. be liable for incidental or consequential damage.

INTRODUCTION: G-CAL assembly is a permeation device designed to continuously release a fixed rate of material at a given temperature. The material released is continuously mixed with the carrier gas (to be provided by the user at a known flow rate) and will result in a calibration mixture of known concentration in parts per million (ppm) by volume. Due to the negligible temperature dependence (see Graph) of the permeation rate, the G-CAL may be conveniently and accurately used as a portable field calibration device. All that is required to generate a known concentration is to pass carrier gas (typically air or nitrogen) at a known flow rate through one side end of the Tee assembly while the G-CAL device is connected to the middle end of the Tee and the calibration mixture is available at the other side end of the Tee.

The concentration of pollutant obtained in ppm (by volume) may be computed for the following formula:

$$C = \frac{K \times P}{F}$$

Where C = concentration in ppm volume
K = 0.532
F = Carrier gas flow rate in ml/minute
P = Permeation rate of the G-CAL assembly obtained from graph in nanograms/minute at the temperature of the G-CAL

INSTALLATION: The G-CAL assembly is shipped with a scrubber cartridge attached to the permeating end-fitting of ¼" stainless steel nut with ferrules (Gyrolok). Remove the cartridge to attach the Tee assembly provided in the bag. Normally the Tee assembly supplied is made from polypropylene material and will make an adequate leak-free connection. However, for applications requiring frequent removal of the Tee assembly or requiring completely leak-free connection, a ¼" stainless steel Tee assembly (Gyrolok or Swagelok) is recommended. The scrubber cartridge should be saved and replaced whenever G-CAL is not being used. The cartridge has a limited useful life and must be discarded whenever the pink powder turns to greenish black or gray in color. Extra scrubber cartridges are available from the factory. DO NOT EVER CLOSE THE PERMEATING-END OF G-CAL WITH ANY FITTING AS THIS MAY PERMANENTLY ALTER THE PERMEATION RATE.

SPECIAL NOTES FOR CHLORINE G-CALS: Due to the extreme corrosive properties of the Chlorine gas, the fittings and the ¼" nut assembly are made from Teflon. The polypropylene Tee assembly provided should not be used for more than 30 minutes at a time. We recommend the use of a ¼" Teflon Tee assembly for more frequent use (may be purchased from the factory). All tubing used should be Teflon only. Viton and rubber tubing must never be used as they will absorb Chlorine gas released from the G-CAL assembly. Teflon connections are to be made hand tight only.

*6 months for Gas Phase G-CALs.

Figure B-1. NO_2 Permeation Tube, Model 23-7502, Part Number G-4767, Information Sheet.

NOTE: The following graph represents the permeation rate of the G-CAL at various operating temperatures in degrees celsius of the G-CAL Assembly. This graph was individually obtained for the G-CAL, Model No. 23-7502, S/N G-4767 for NO_2.

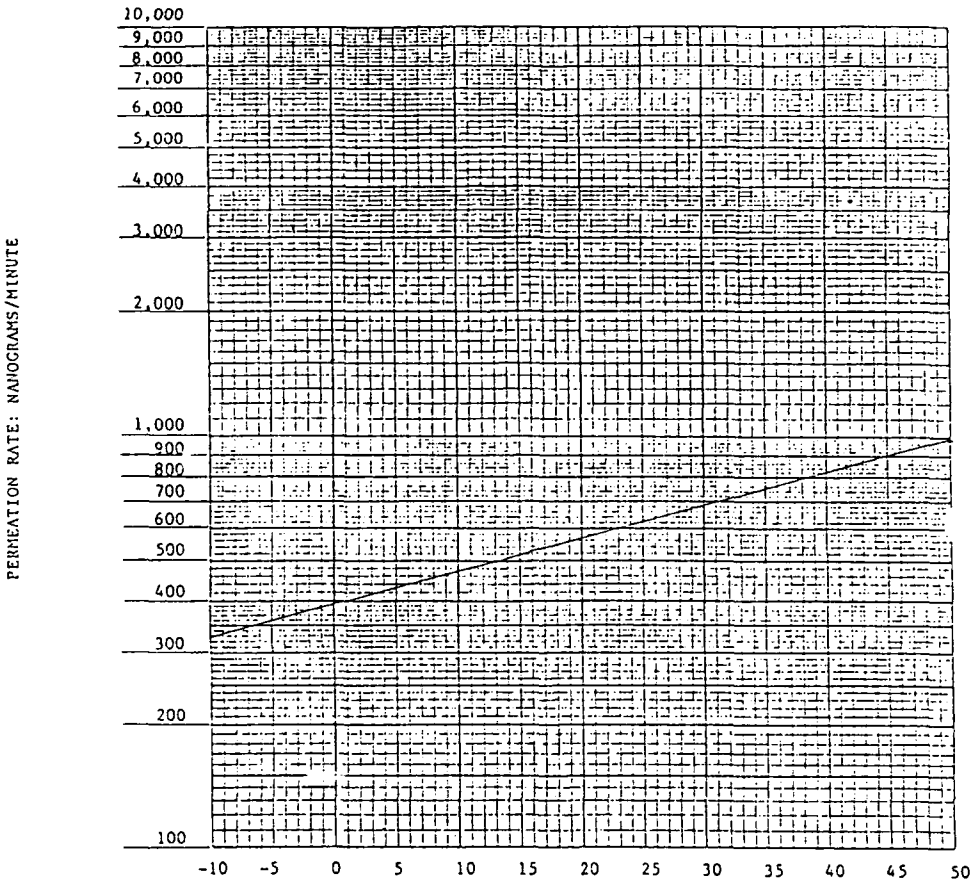

Permeation Rate @25°C 620

Permeation Rate @50°C 980

PERMEATION RATE Vs TEMPERATURE °C

G C INDUSTRIES, INC.
20361 Prairie Street, Unit 4
Chatsworth, CA 91311
213/701-7072

Figure B-2. NO_2 Permeation Tube, Model 23-7502, Part Number G-4767, Calibration Chart.

GC INDUSTRIES

G-CAL PERMEATION DEVICE

INSTRUCTION SHEET

G-CAL TYPE NO_2 S/N G-4766 MODEL 23-7052

WEIGHT OF G-CAL (LESS SCRUBBER) AT SHIPMENT 252.620 gms.

G-CAL IS EMPTY WHEN WEIGHT REACHES 250.620 gms. or LOWER

SHIPMENT DATE 5-26-88

CAUTION: G-CAL CONTAINS GAS OR LIQUID UNDER HIGH PRESSURE. THE MATERIAL CONTAINED MAY BE FLAMMABLE AND/OR HIGHLY TOXIC. USE EXTREME CAUTION DURING USE. DO NOT EXPOSE TO TEMPERATURES ABOVE 122°F (50°C) OR BELOW 0°F (-18°C). DO NOT EVER OPEN END FITTINGS AS THIS WILL RESULT IN RELEASE OF GAS.

CAUTION: WHEN EXPIRED, THIS DEVICE SHOULD ONLY BE DISCARDED THROUGH AN INDUSTRIAL WASTE SERVICE. GENERAL PURPOSE DISPOSAL IS NOT RECOMMENDED.

WARRANTY: Each G-CAL device, except for Chlorine gas, is warranted to have a useful life of 12 months* of normal use and service from the date of shipment. G-CAL for Chlorine is warranted for 6 months from the date of shipment. Defective G-CAL returned prepaid to factory with prior approval, will be repaired or replaced free within the first six months (3 months for Chlorine) of shipment. A pro-rated fee will be charged for G-CAL repaired after this period. The warranty is void if the G-CAL assembly is taken apart or opened in any way other than for normal use.

The liability of Seller to the Buyers arising out of the supplying of G-CAL assembly on its use, whether on warranty, contract, or otherwise, shall not in any case exceed the cost of the original purchase and upon the expiration of warranty period, all such liability shall terminate. In no event shall G C Industries, Inc. be liable for incidental or consequential damage.

INTRODUCTION: G-CAL assembly is a permeation device designed to continuously release a fixed rate of material at a given temperature. The material released is continuously mixed with the carrier gas (to be provided by the user at a known flow rate) and will result in a calibration mixture of known concentration in parts per million (ppm) by volume. Due to the negligible temperature dependence (see Graph) of the permeation rate, the G-CAL may be conveniently and accurately used as a portable field calibration device. All that is required to generate a known concentration is to pass carrier gas (typically air or nitrogen) at a known flow rate through one side end of the Tee assembly while the G-CAL device is connected to the middle end of the Tee and the calibration mixture is available at the other side end of the Tee.

The concentration of pollutant obtained in ppm (by volume) may be computed for the following formula:

$$C = \frac{K \times P}{F}$$

Where C = concentration in ppm volume
K = 0.533
F = Carrier gas flow rate in ml/minute
P = Permeation rate of the G-CAL assembly obtained from graph in nanograms/minute at the temperature of the G-CAL

INSTALLATION: The G-CAL assembly is shipped with a scrubber cartridge attached to the permeating end-fitting of ¼" stainless steel nut with ferrules (Gyrolok). Remove the cartridge to attach the Tee assembly provided in the bag. Normally the Tee assembly supplied is made from polypropylene material and will make an adequate leak-free connection. However, for applications requiring frequent removal of the Tee assembly or requiring completely leak-free connection, a ¼" stainless steel Tee assembly (Gyrolok or Swagelok) is recommended. The scrubber cartridge should be saved and replaced whenever G-CAL is not being used. The cartridge has a limited useful life and must be discarded whenever the pink powder turns to greenish black or gray in color. Extra scrubber cartridges are available from the factory. DO NOT EVER CLOSE THE PERMEATING-END OF G-CAL WITH ANY FITTING AS THIS MAY PERMANENTLY ALTER THE PERMEATION RATE.

SPECIAL NOTES FOR CHLORINE G-CALS: Due to the extreme corrosive properties of the Chlorine gas, the fittings and the ¼" nut assembly are made from Teflon. The polypropylene Tee assembly provided should not be used for more than 30 minutes at a time. We recommend the use of a ¼" Teflon Tee assembly for more frequent use (may be purchased from the factory). All tubing used should be Teflon only. Viton and rubber tubing must never be used as they will absorb Chlorine gas released from the G-CAL assembly. Teflon connections are to be made hand tight only.

*6 months for Gas Phase G-CALs.

Figure B-3. NO_2 Permeation Tube, Model 23-7502, Part Number G-4766, Information Sheet.

NOTE: The following graph represents the permeation rate of the G-CAL at various operating temperatures in degrees celsius of the G-CAL Assembly. This graph was individually obtained for the G-CAL, Model No. 23-7055, S/N G-4766 for NO2.

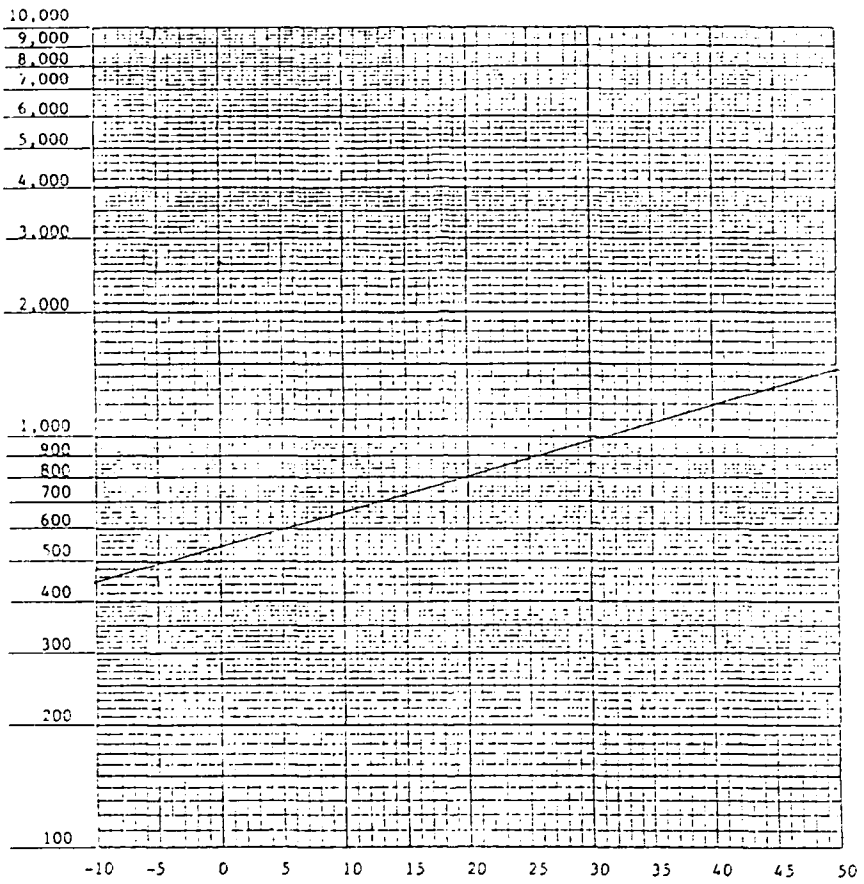

Permeation Rate @25°C 880

Permeation Rate @50°C 1050

PERMEATION RATE Vs TEMPERATURE °C

G C INDUSTRIES, INC.
20361 Prairie Street, Unit 4
Chatsworth, CA 91311
213/701-7072

Figure B-4. NO_2 Permeation Tube, Model 23-7502, Part Number G-4766, Calibration Chart.

G-CAL PERMEATION DEVICE

INSTRUCTION SHEET

G-CAL TYPE DIMP S/N G-4942 MODEL 23-7392

WEIGHT OF G-CAL (LESS SCRUBBER) AT SHIPMENT 143.712 gms. G-CAL IS EMPTY WHEN WEIGHT REACHES 143.100 gms. or LOWER

SHIPMENT DATE 7-26-88

CAUTION: G-CAL CONTAINS GAS OR LIQUID UNDER HIGH PRESSURE. THE MATERIAL CONTAINED MAY BE FLAMMABLE AND/OR HIGHLY TOXIC. USE EXTREME CAUTION DURING USE. DO NOT EXPOSE TO TEMPERATURES ABOVE 122°F (50°C) OR BELOW 0°F (-18°C). DO NOT EVER OPEN END FITTINGS AS THIS WILL RESULT IN RELEASE OF GAS.

CAUTION: WHEN EXPIRED, THIS DEVICE SHOULD ONLY BE DISCARDED THROUGH AN INDUSTRIAL WASTE SERVICE. GENERAL PURPOSE DISPOSAL IS NOT RECOMMENDED.

WARRANTY: Each G-CAL device, except for Chlorine gas, is warranted to have a useful life of 12 months* of normal use and service from the date of shipment. G-CAL for Chlorine is warranted for 6 months from the date of shipment. Defective G-CAL returned prepaid to factory with prior approval, will be repaired or replaced free withio the first six months (3 months for Chlorine) of shipment. A pro-rated fee will be charged for G-CAL repaired after this period. The warranty is void if the G-CAL assembly is taken apart or opened in any way other than for normal use.

The liability of Seller to the Buyers arising out of the supplying of G-CAL assembly on its use, whether on warranty, contract, or otherwise, shall not in any case exceed the cost of the original purchase and upon the expiration of warranty period, all such liability shall terminate. In no event shall G C Industries, Inc. be liable for incidental or consequential damage.

INTRODUCTION: G-CAL assembly is a permeation device designed to continuously release a fixed rate of material at a given temperature. The material released is continuously mixed with the carrier gas (to be provided by the user at a known flow rate) and will result in a calibration mixture of known concentration in parts per million (ppm) by volume. Due to the negligible temperature dependence (see Graph) of the permeation rate, the G-CAL may be conveniently and accurately used as a portable field calibration device. All that is required to generate a known concentration is to pass carrier gas (typically air or nitrogen) at a known flow rate through one side end of the Tee assembly while the G-CAL device is connected to the middle end of the Tee and the calibration mixture is available at the other side end of the Tee.

The concentration of pollutant obtained in ppm (by volume) may be computed for the following formula:

$$C = \frac{K \times P}{F}$$

Where C = concentration in ppm volume
K = 0.136
F = Carrier gas flow rate in ml/minute
P = Permeation rate of the G-CAL assembly obtained from graph in nanograms/minute at the temperature of the G-CAL

INSTALLATION: The G-CAL assembly is shipped with a scrubber cartridge attached to the permeating end-fitting of ¼" stainless steel nut with ferrules (Gyrolok). Remove the cartridge to attach the Tee assembly provided in the bag. Normally the Tee assembly supplied is made from polypropylene material and will make an adequate leak-free connection. However, for applications requiring frequent removal of the Tee assembly or requiring completely leak-free connection, a ¼" stainless steel Tee assembly (Gyrolok or Swagelok) is recommended. The scrubber cartridge should be saved and replaced whenever G-CAL is not being used. The cartridge has a limited useful life and must be discarded whenever the pink powder turns to greenish black or gray in color. Extra scrubber cartridges are available from the factory. DO NOT EVER CLOSE THE PERMEATING-END OF G-CAL WITH ANY FITTING AS THIS MAY PERMANENTLY ALTER THE PERMEATION RATE.

SPECIAL NOTES FOR CHLORINE G-CALS: Due to the extreme corrosive properties of the Chlorine gas, the fittings and the ¼" nut assembly are made from Teflon. The polypropylene Tee assembly provided should not be used for more than 30 minutes at a time. We recommend the use of a ¼" Teflon Tee assembly for more frequent use (may be purchased from the factory). All tubing used should be Teflon only. Viton and rubber tubing must never be used as they will absorb Chlorine gas released from the G-CAL assembly. Teflon connections are to be made hand tight only.

*6 months for Gas Phase G-CALs.

Figure B-5. DIMP Permeation Tube, Model 23-7392, Part Number G-4942, Information Sheet.

NOTE: The following graph represents the permeation rate of the G-CAL at various operating temperatures in degrees celsius of the G-CAL Assembly. This graph was individually obtained for the G-CAL, Model No. 23-7392, S/N G-4942 for DIMP.

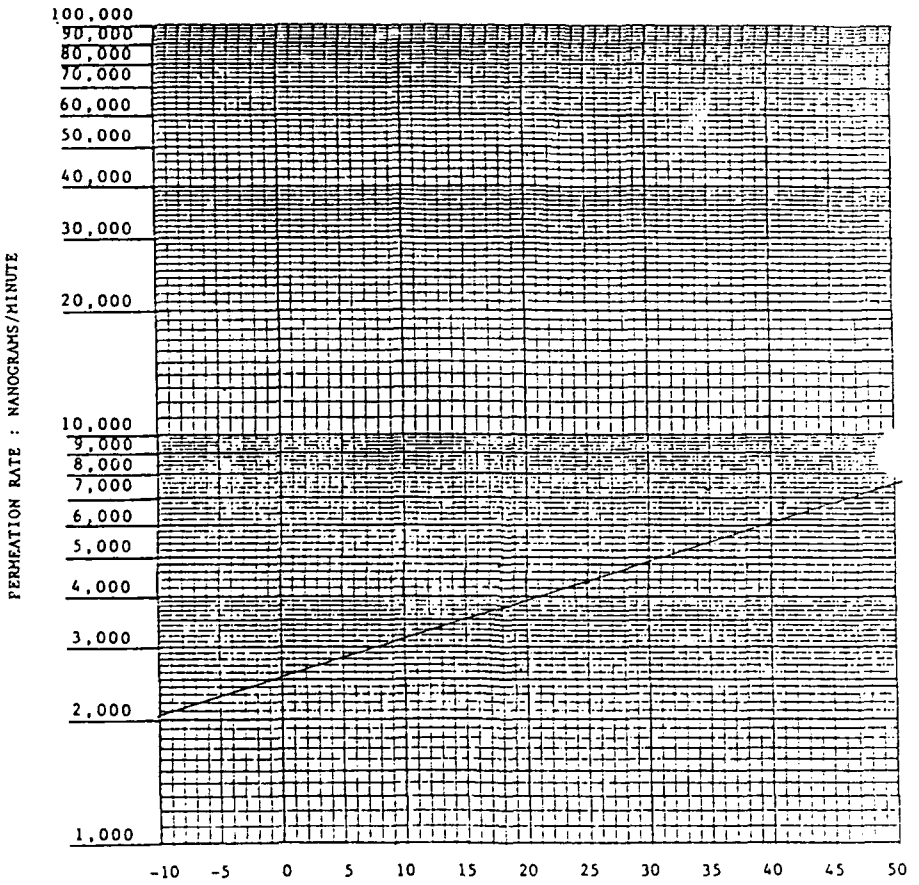

Permeation Rate @ 25°C 4300

Permeation Rate @ 50°C 7600

PERMEATION RATE Vs TEMPERATURE °C

G C INDUSTRIES
20361 Prairie St. Unit 4
Chatsworth, CA 91311
(213) 701-7072

Figure B-6. DIMP Permeation Tube, Model 23-7392, Part Number G-4942, Calibration Chart.

Flowmeter Calibration Charts

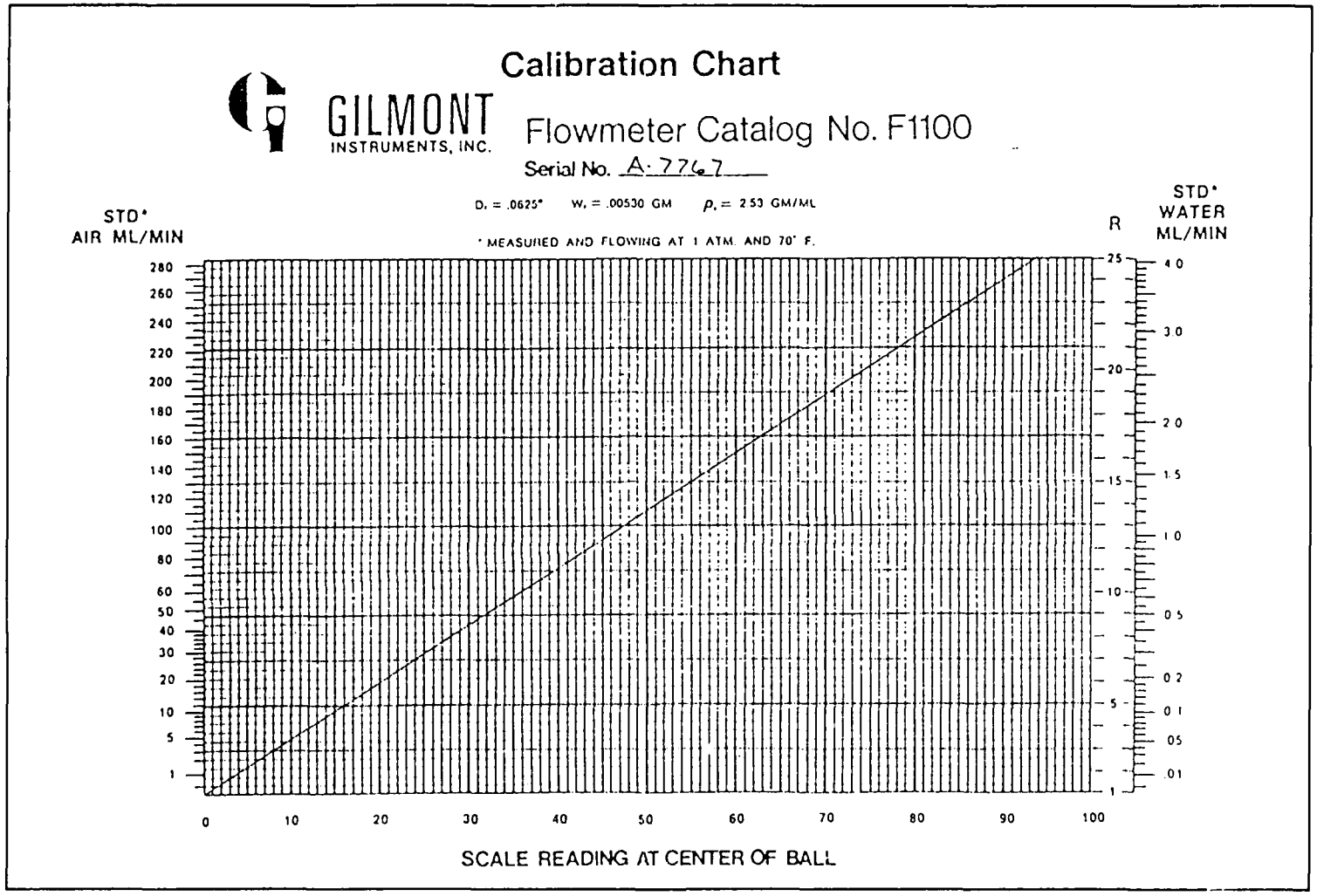

Figure B-7. Gilmont Instruments Flowmeter Model F-1100, Serial Number A-7767, Size 1 Calibration Chart.

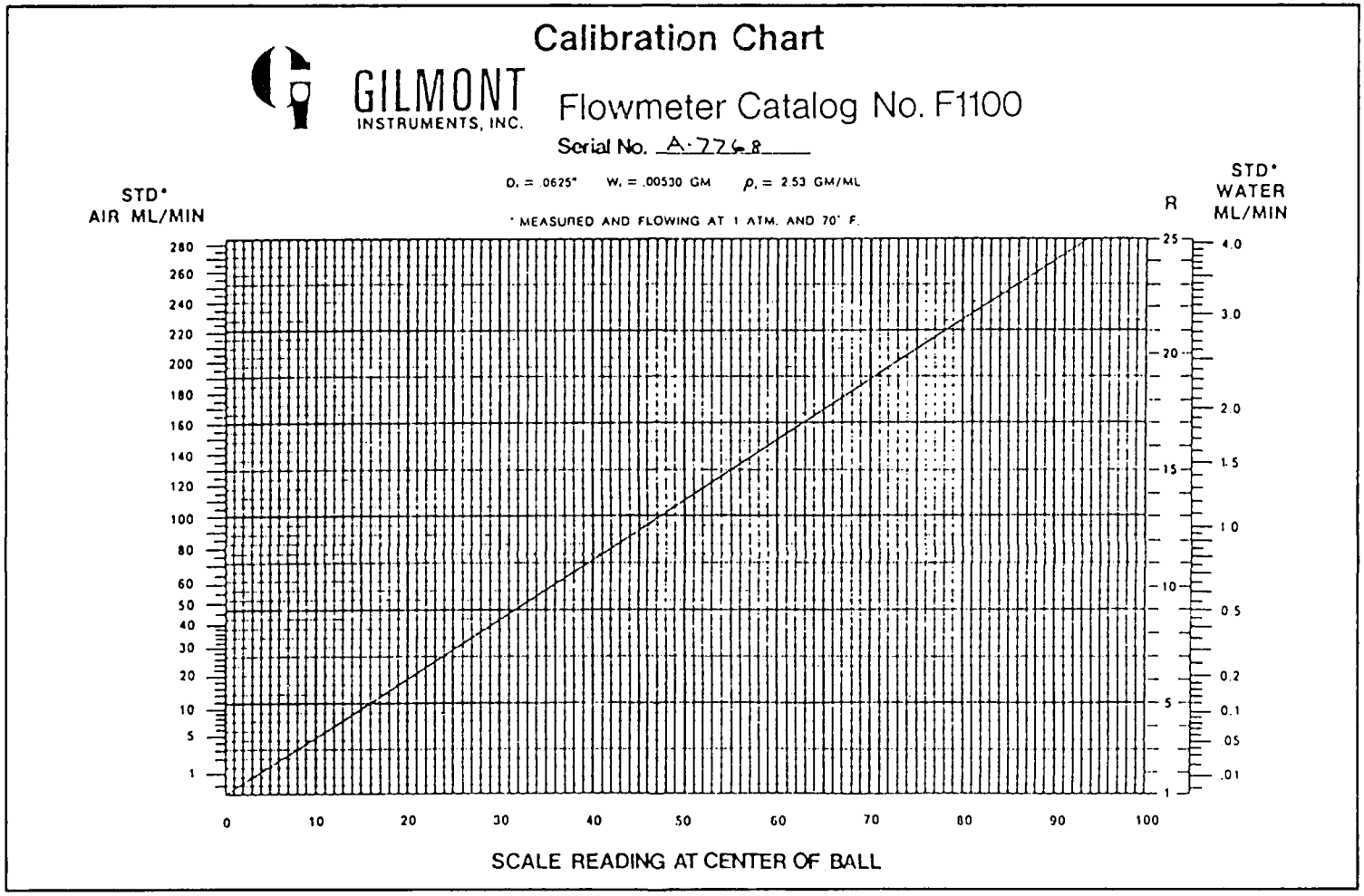

Figure B-8. Gilmont Instruments Flowmeter Model F-1100, Serial Number A-7768, Size 1 Calibration Chart.

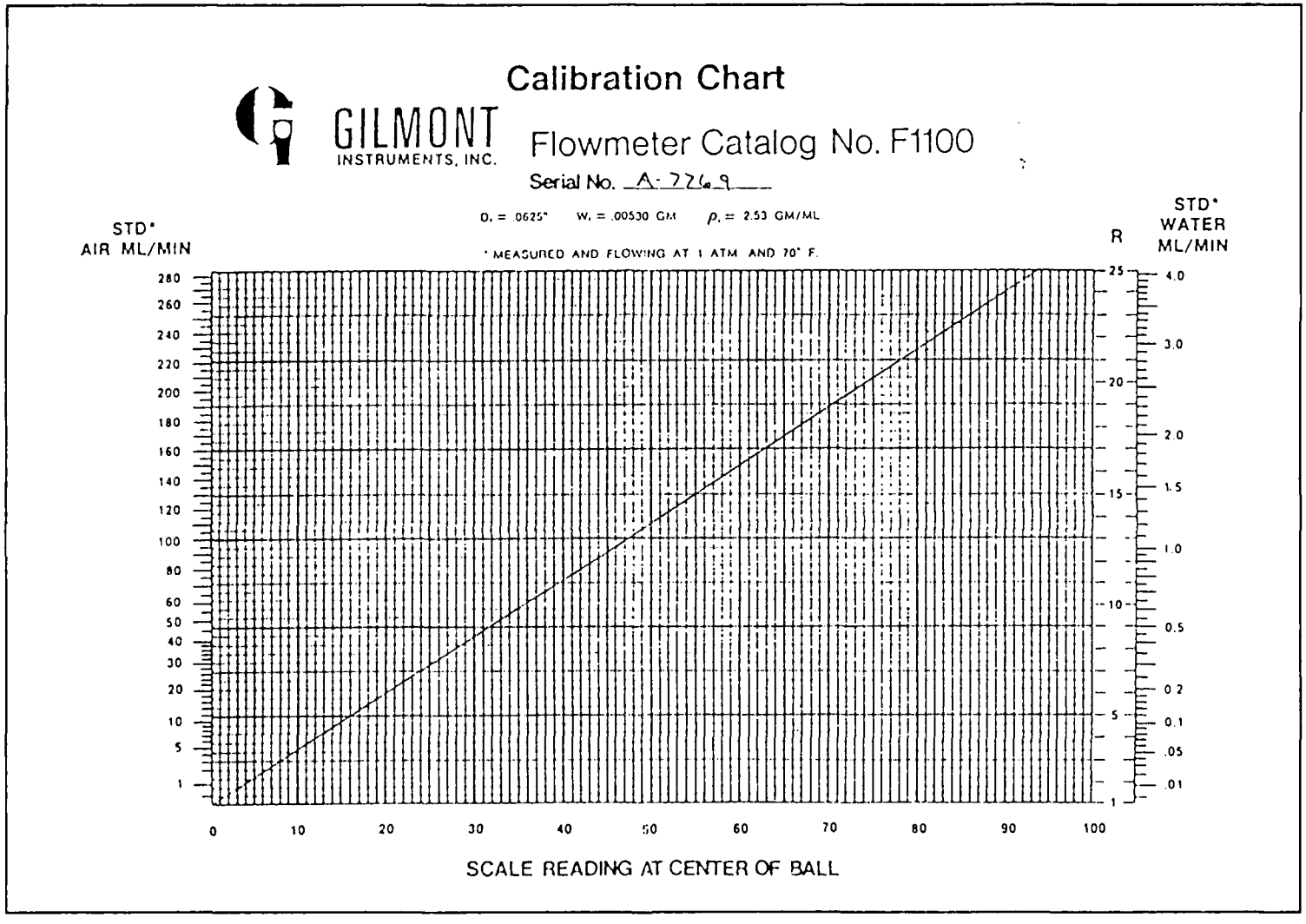

Figure B-9. Gilmont Instruments Flowmeter Model F-1100, Serial Number A-7769, Size 1 Calibration Chart.

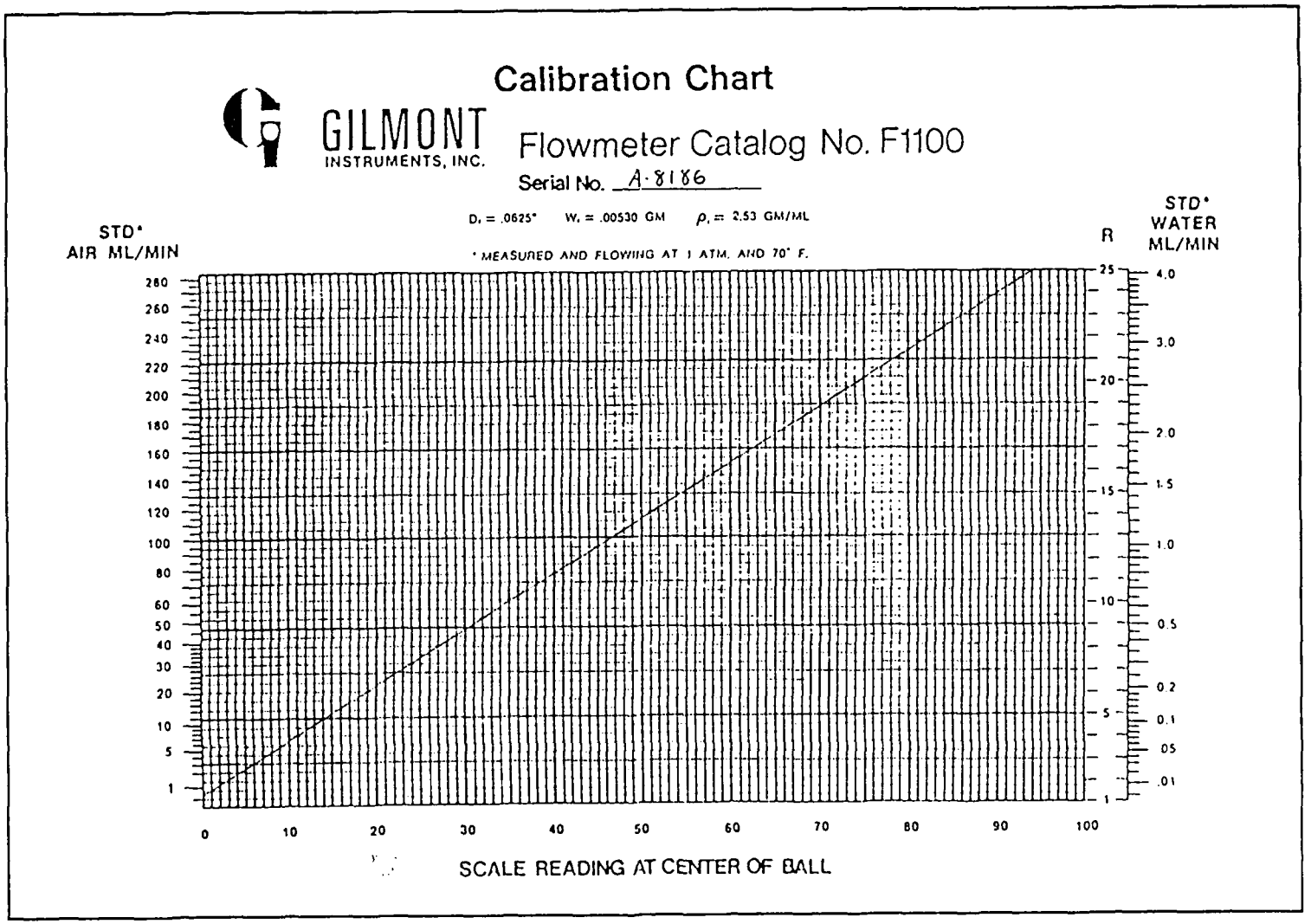

Figure B-10. Gilmont Instruments Flowmeter Model F-1100, Serial Number A-8186, Size 1 Calibration Chart.

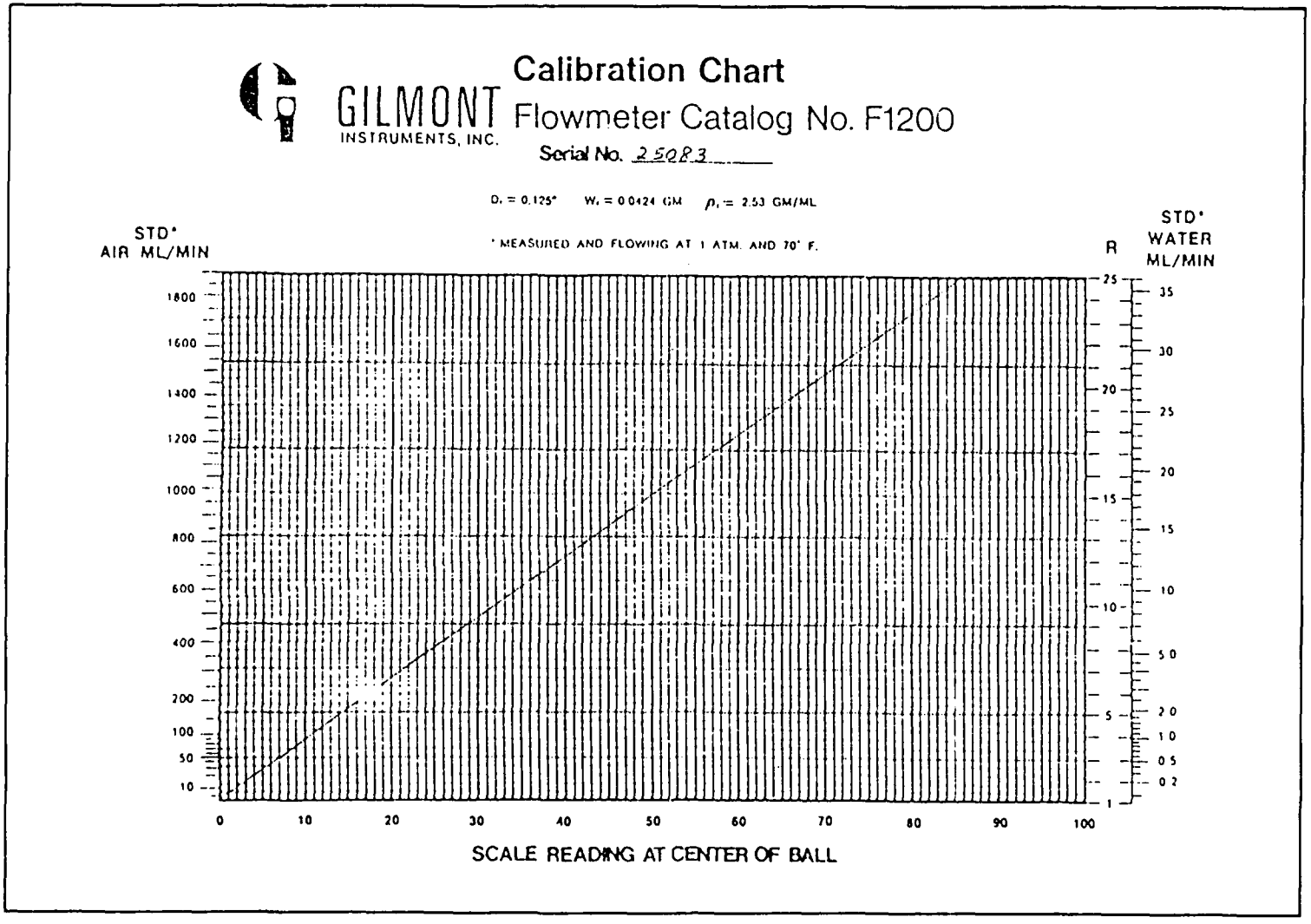

Figure B-11. Gilmont Instruments Flowmeter Model F-1200, Serial Number 25083, Size 2 Calibration Chart.

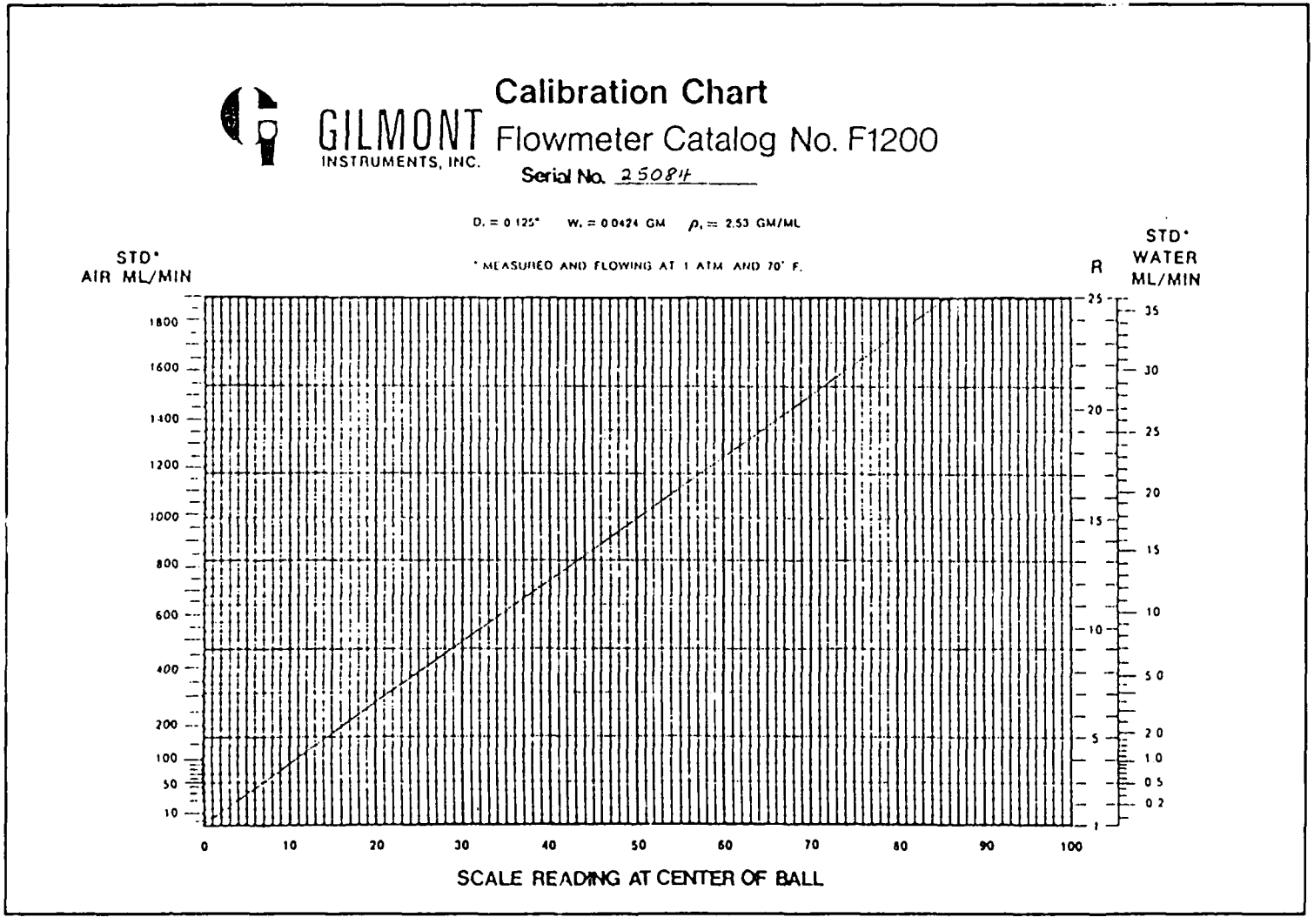

Figure B-12. Gilmont Instruments Flowmeter Model F-1200, Serial Number 25084, Size 2 Calibration Chart.

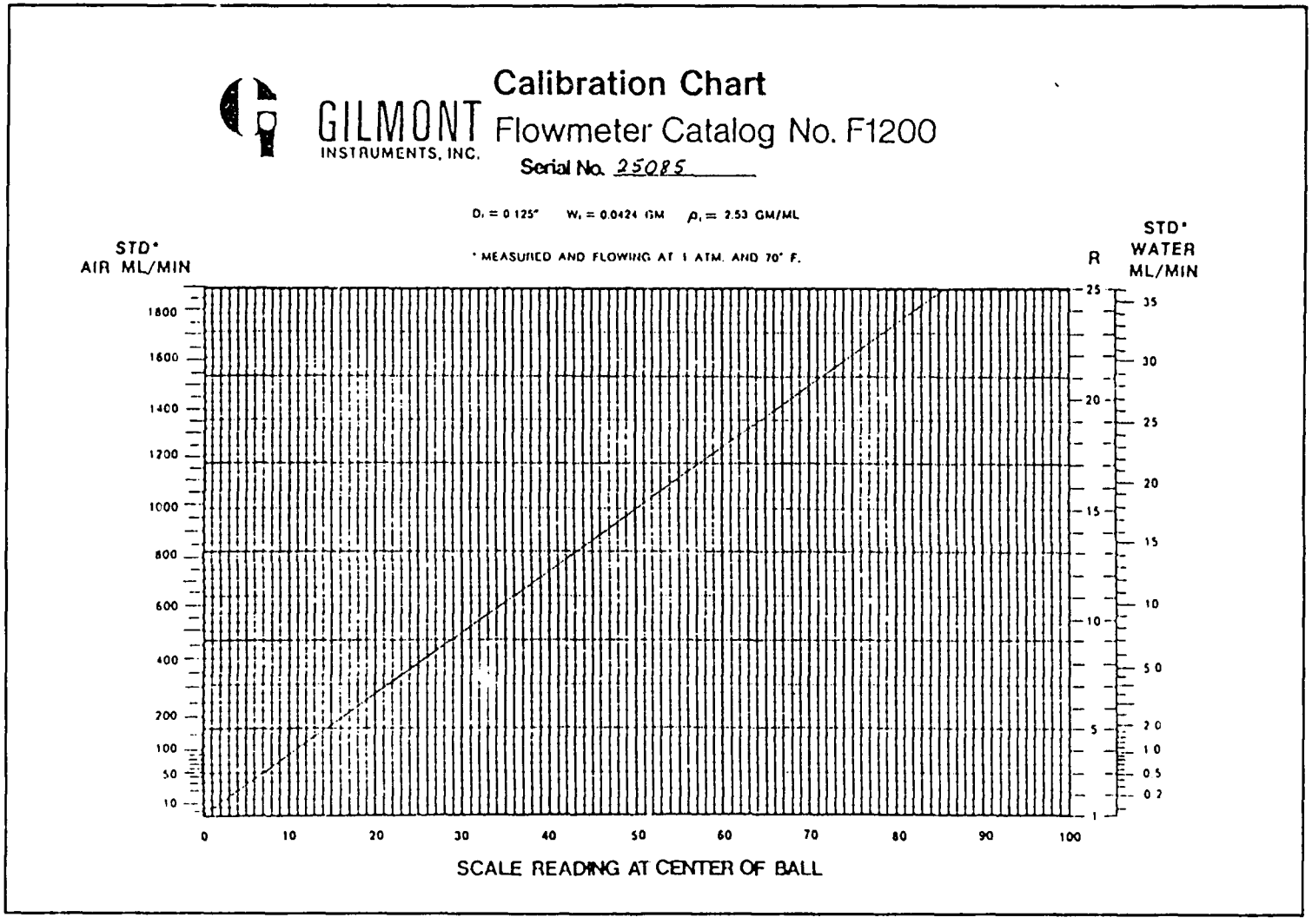

Figure B-13. Gilmont Instruments Flowmeter Model F-1200, Serial Number 25085, Size 2 Calibration Chart.

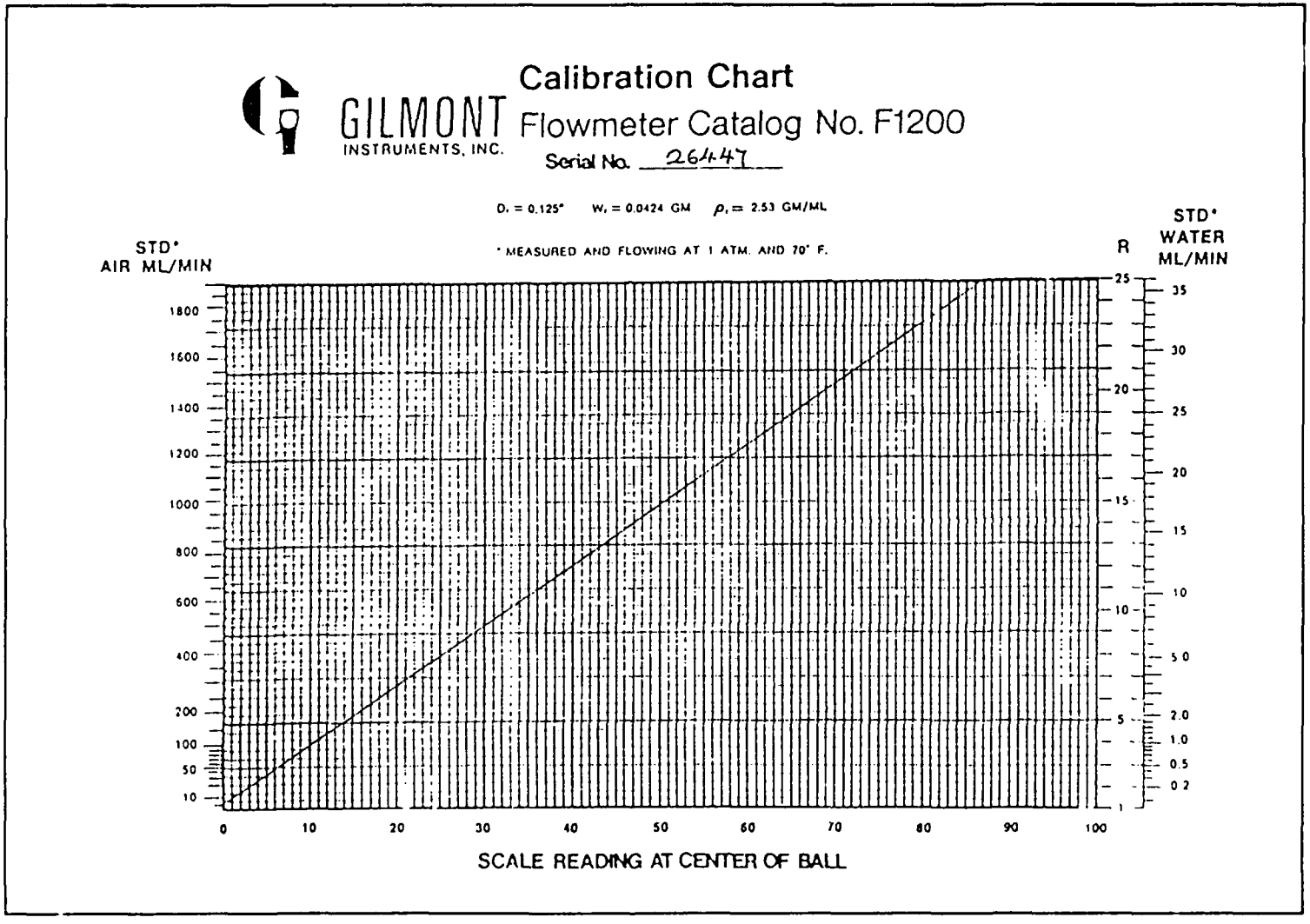

Figure B-14. Gilmont Instruments Flowmeter Model F-1200, Serial Number 26447, Size 2 Calibration Chart.

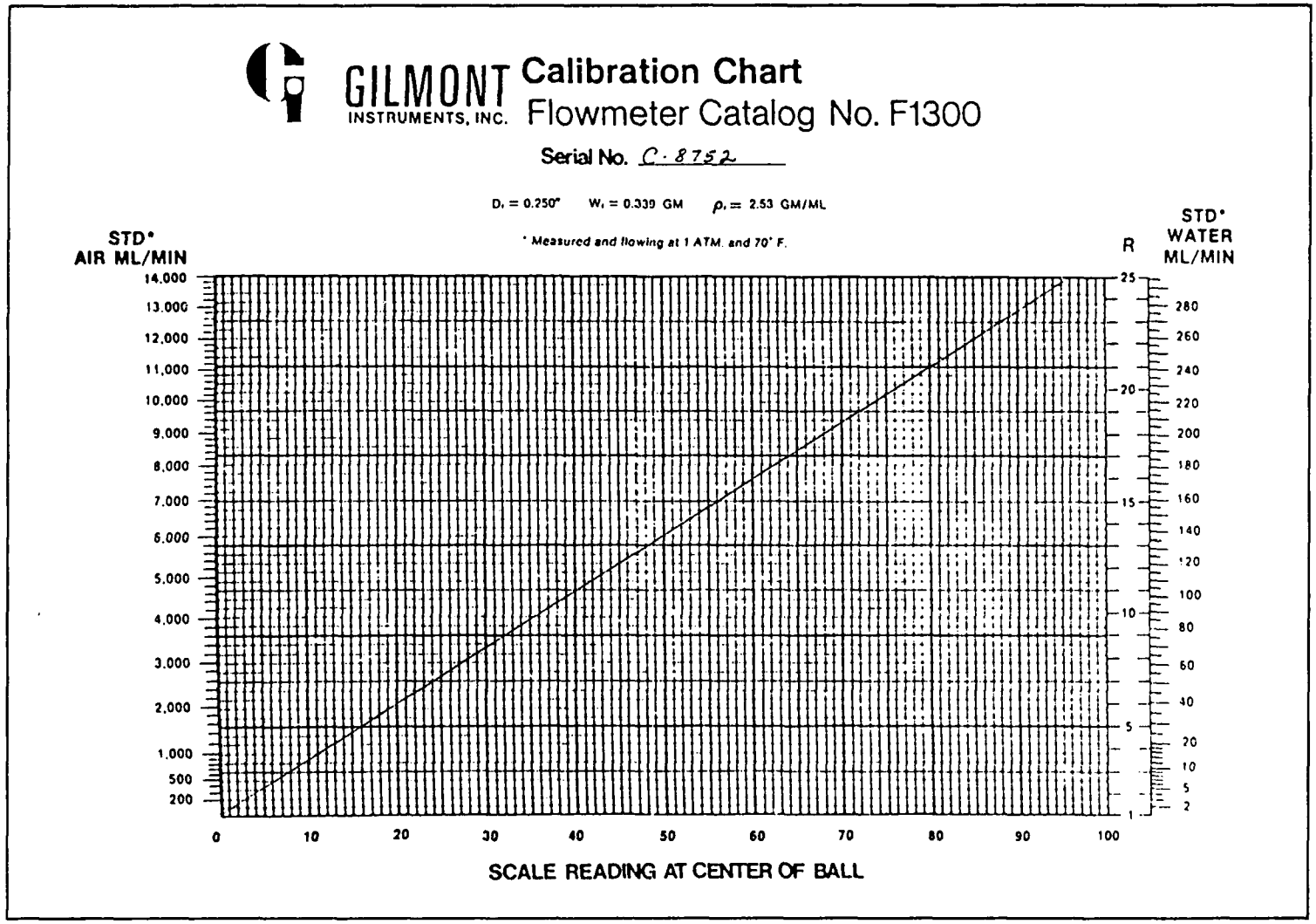

Figure B-15. Gilmont Instruments Flowmeter Model F-1300, Serial Number C-8752, Size 3 Calibration Chart.

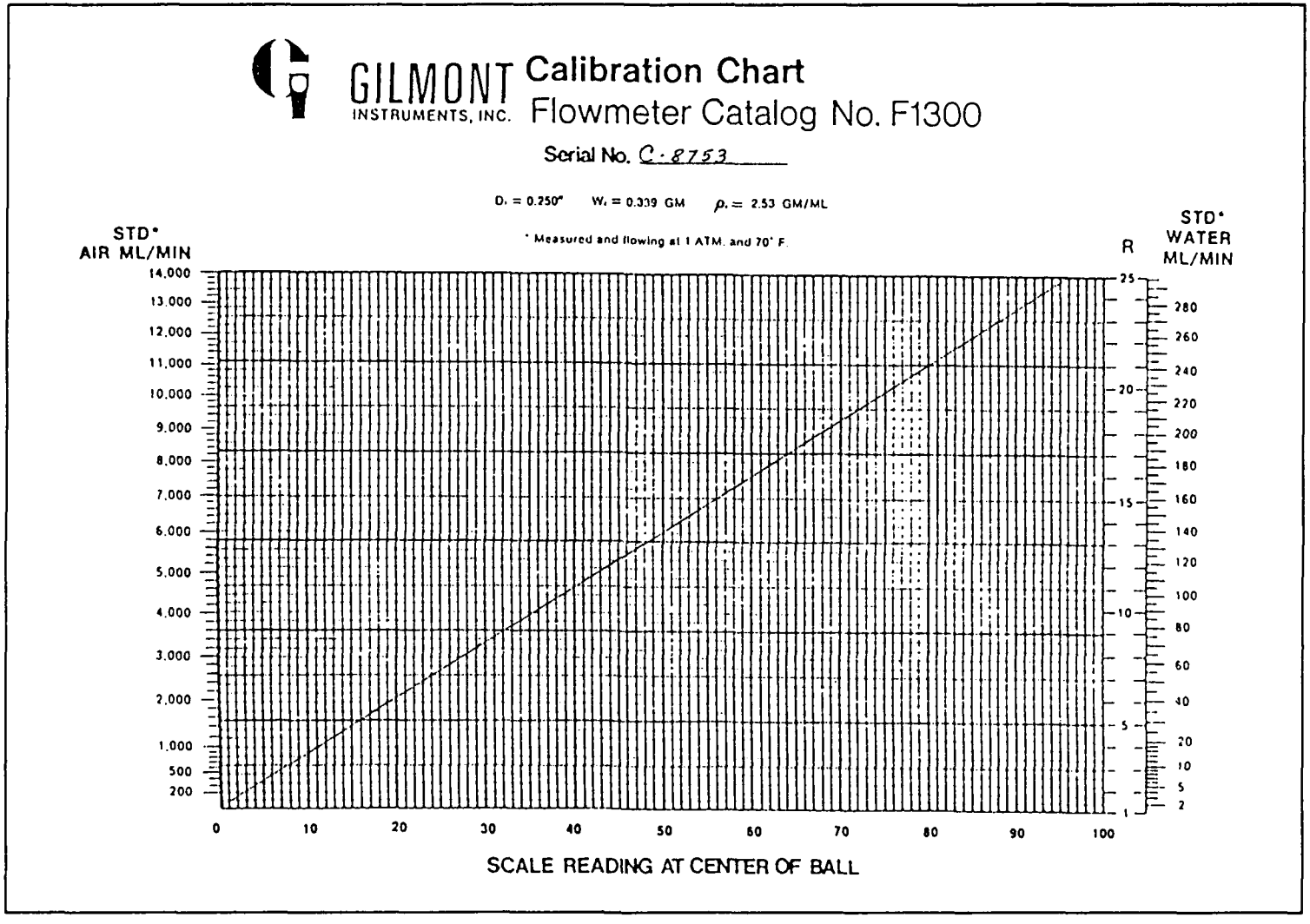

Figure B-16. Gilmont Instruments Flowmeter Model F-1300, Serial Number C-8753, Size 3 Calibration Chart.

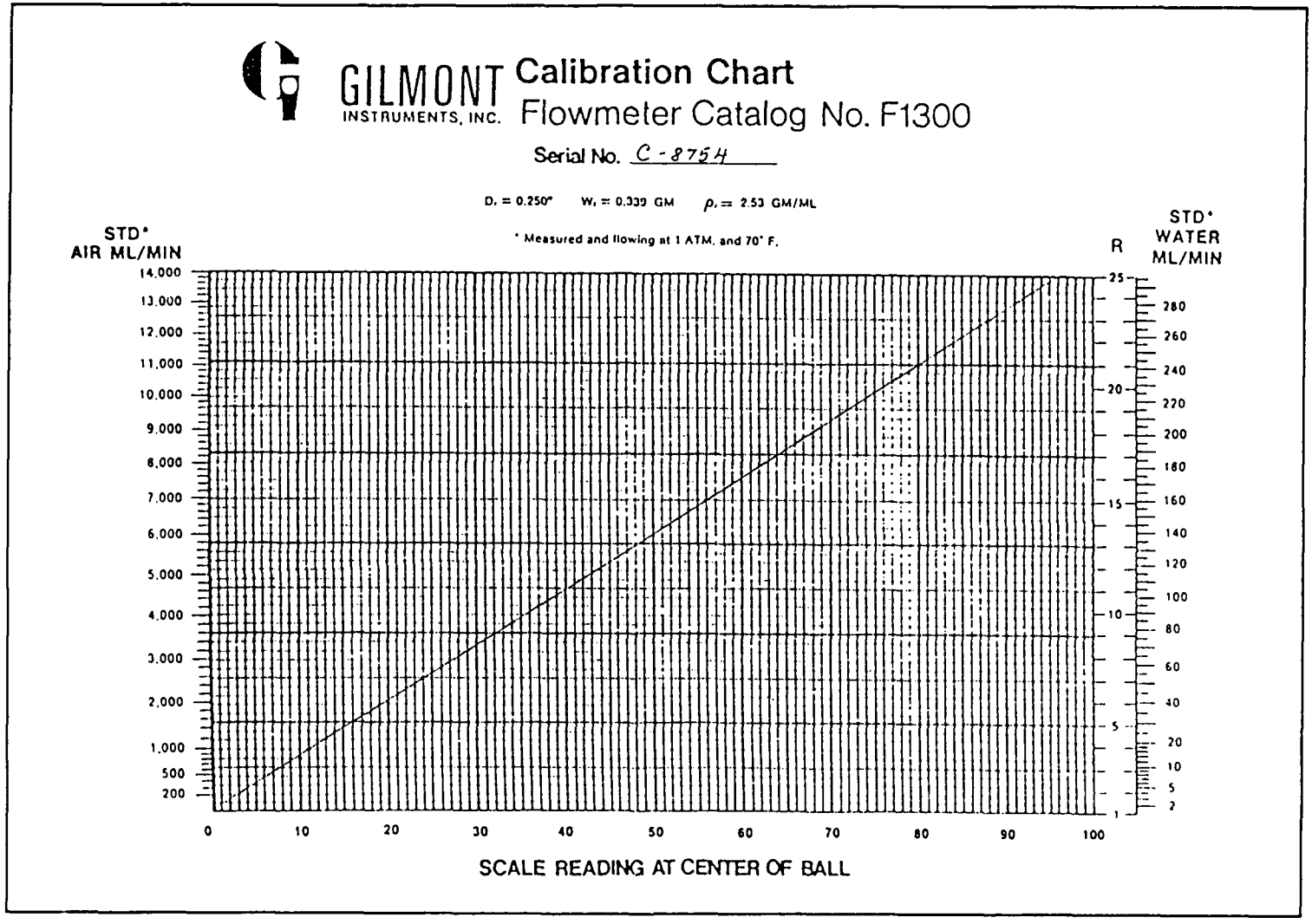

Figure B-17.Gilmont Instruments Flowmeter Model F-1300, Serial Number C-8754, Size 3 Calibration Chart.

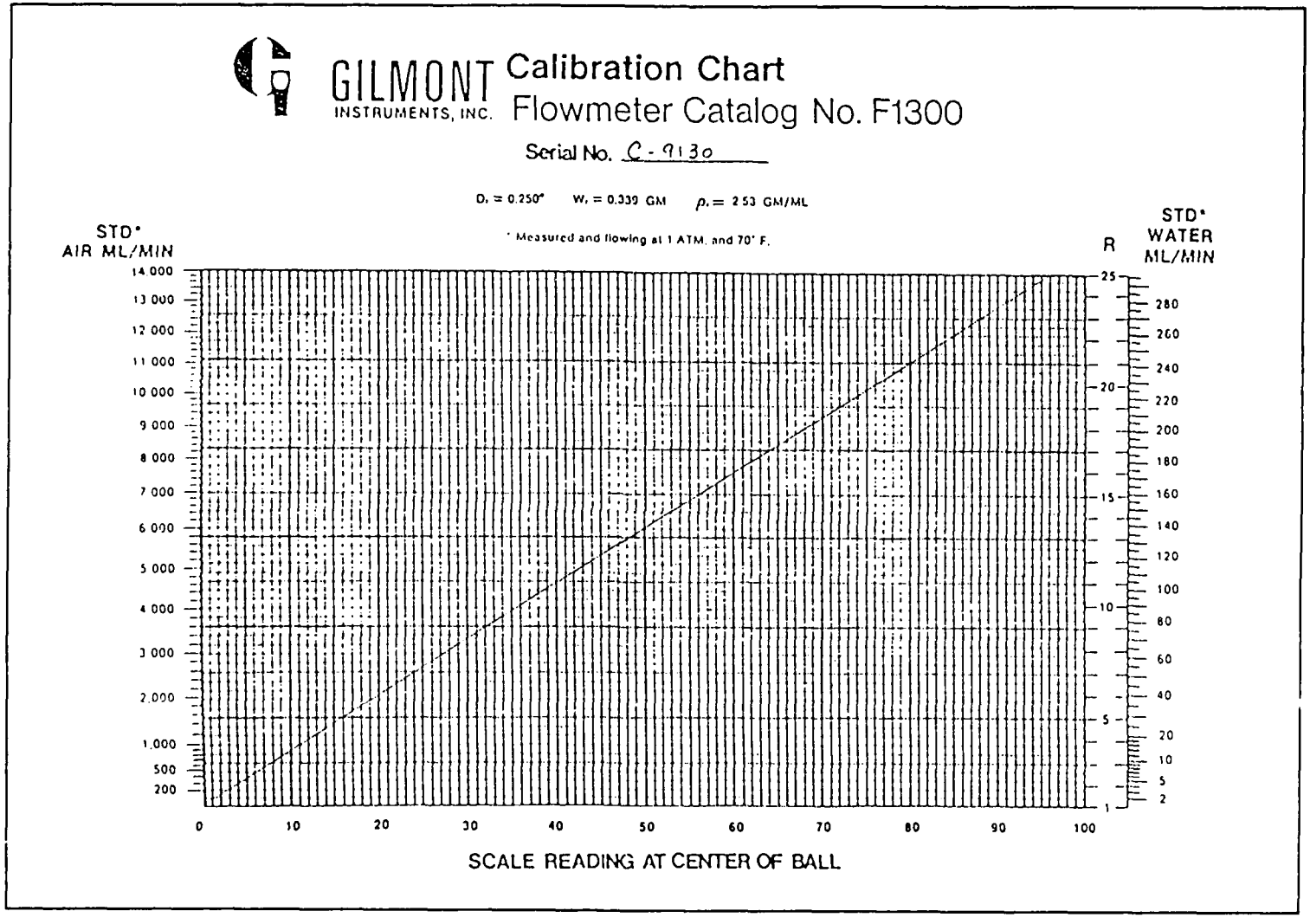

Figure B-18. Gilmont Instruments Flowmeter Model F-1300, Serial Number C-9130, Size 3 Calibration Chart.

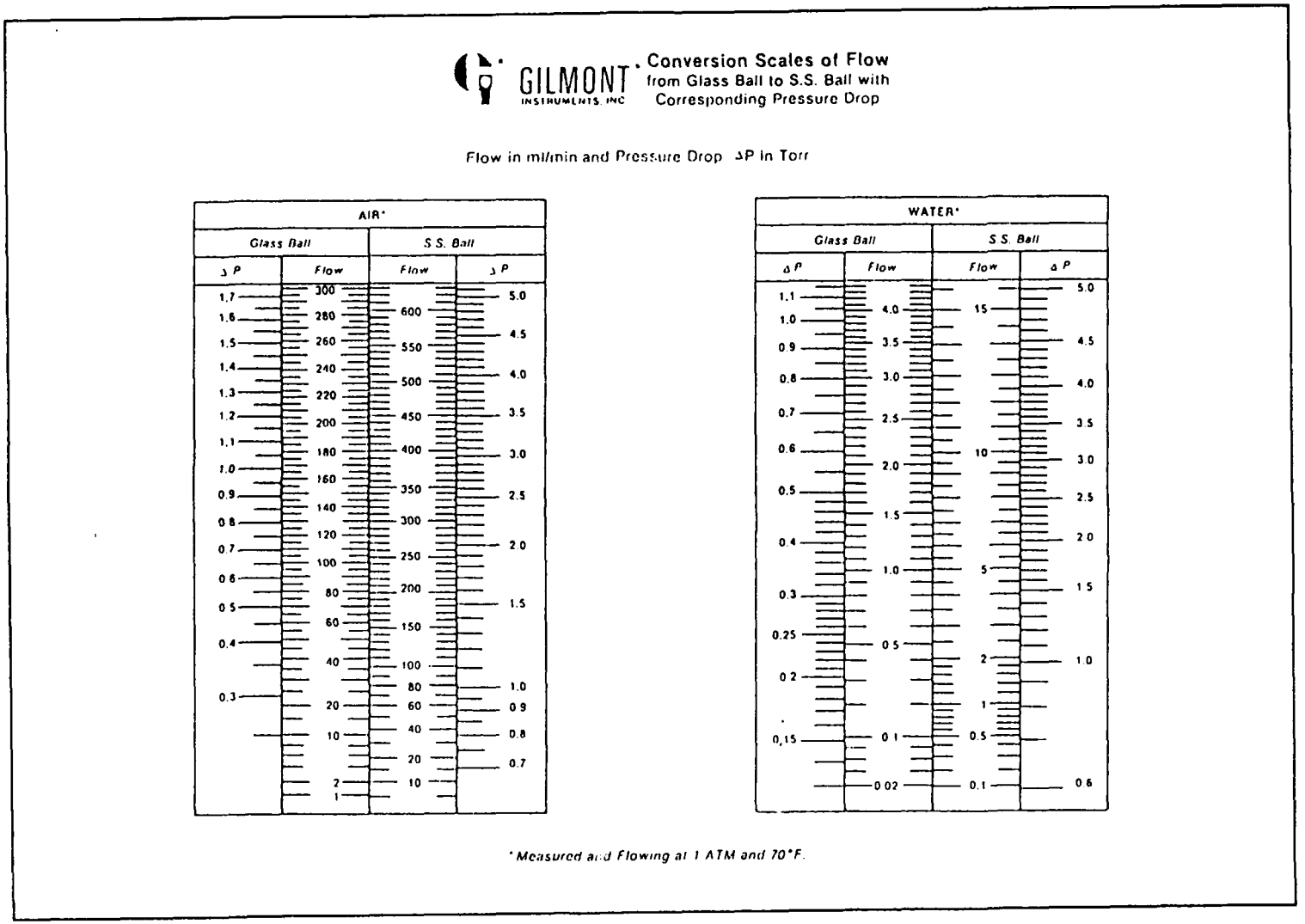

Figure B-19. Glass to Stainless Steel Float Conversion Scale for Size 1 Flowmeter.

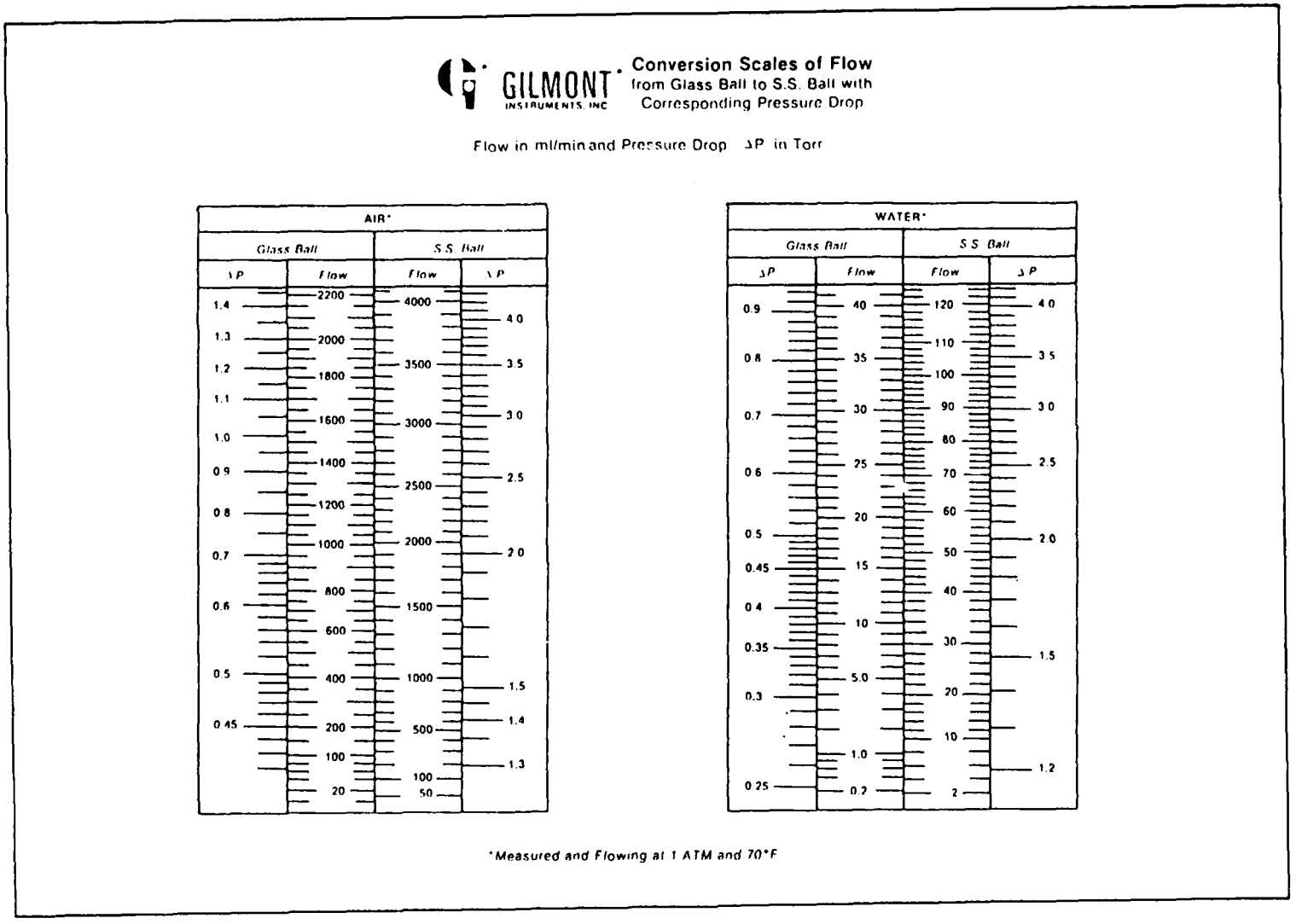

Figure B-20. Glass to Stainless Steel Float Conversion for Size 2 Flowmeter.

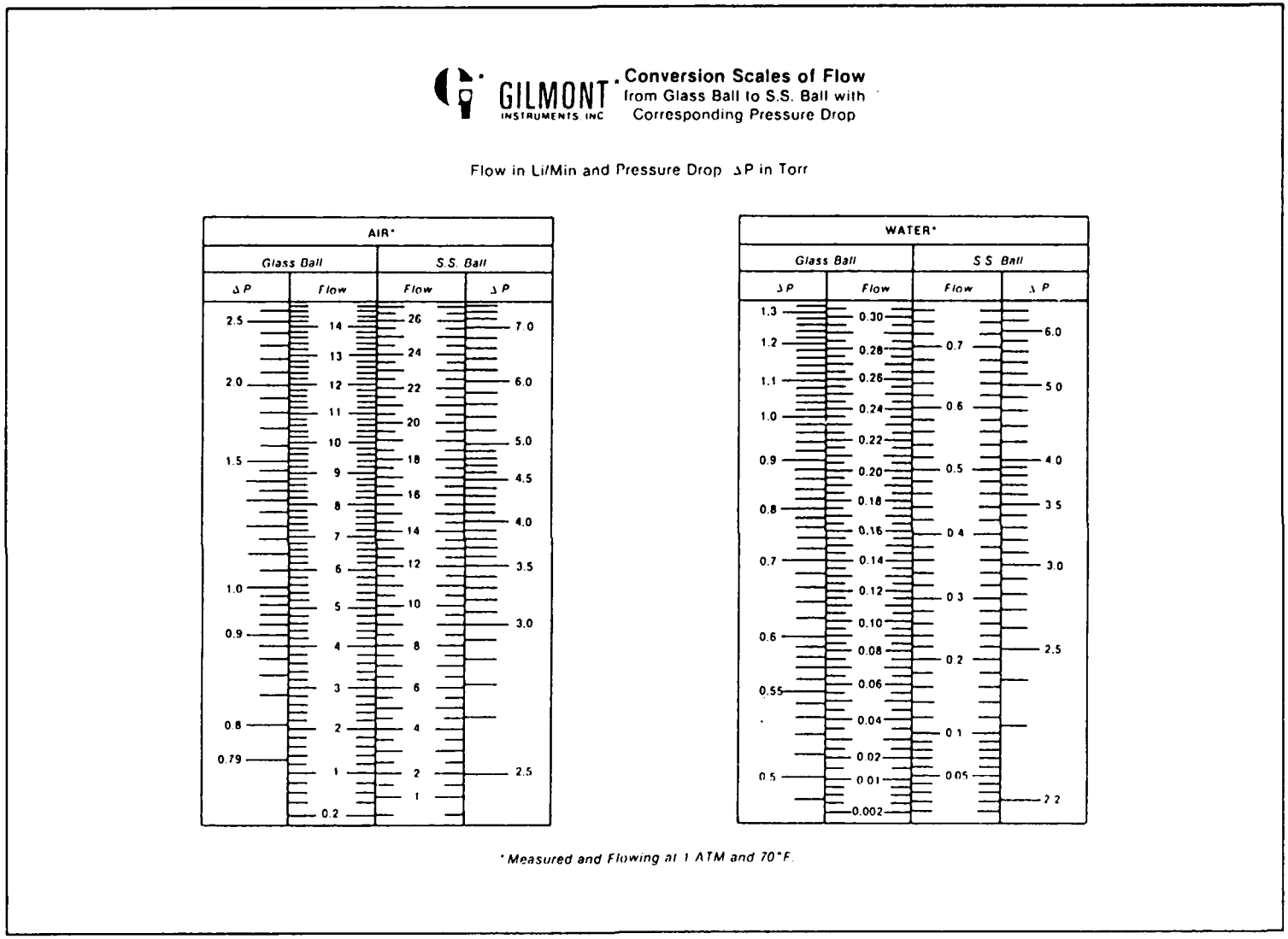

Figure B-21. Glass to Stainless Steel Float Conversion for Size 3 Flowmeter.

Appendix C

Detailed Instrumentation Schematic

for Evaluation of the CHEMFET Electrical Performance

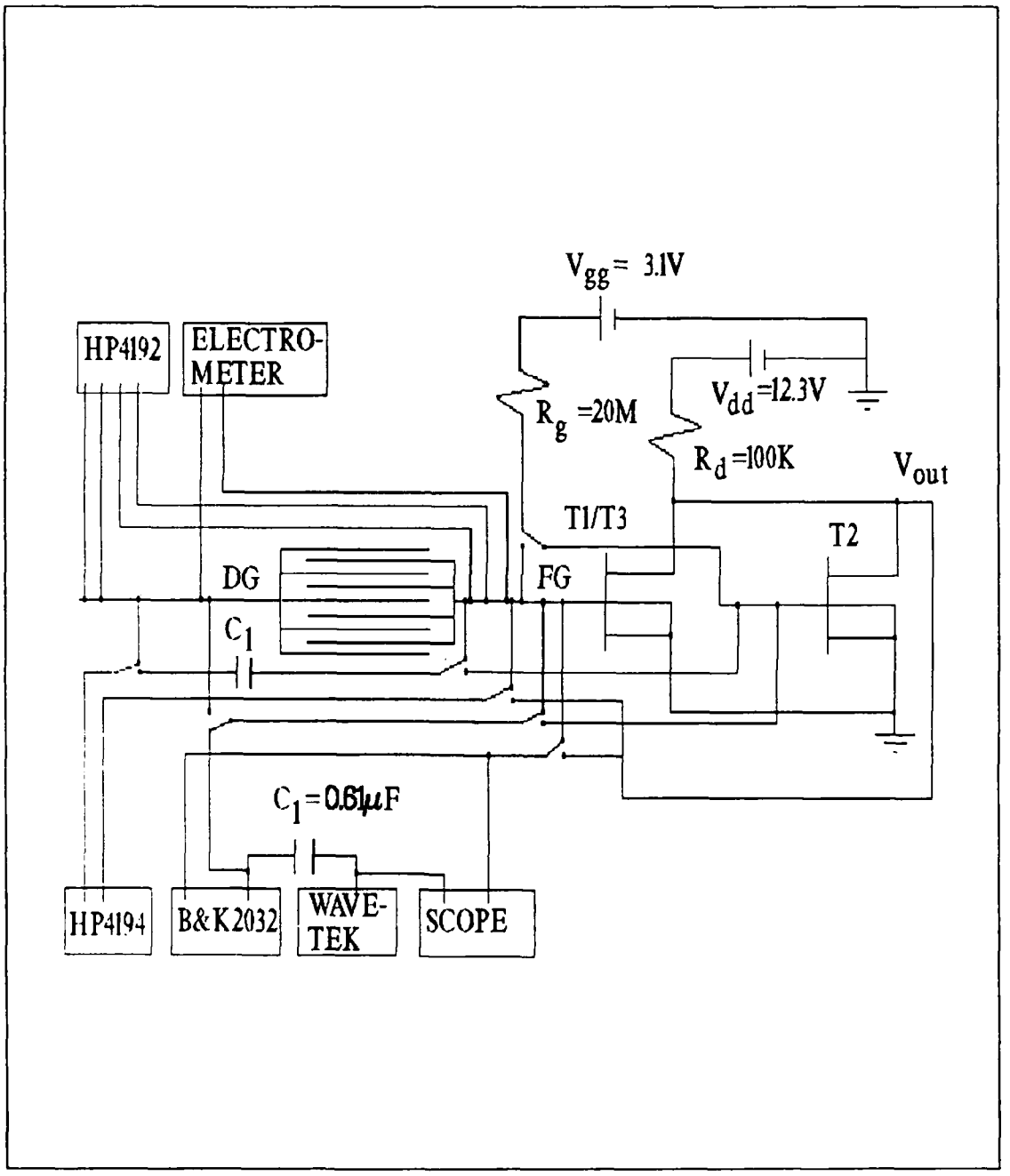

Figure C-1. Detailed Instrumentation Schematic used to Evaluate the CHEMFET's Electrical Performance.

Appendix D

Computer Programs

```
100 CLS
200 '
300 '
400 '                        IMPEDANCE MODULATION TEST SOFTWARE
500 '
600 ' FILENAME : IMPEDMOD.SOF
700 '
800 ' THIS PROGRAM WAS USED TO CONFIGURE THE TEST INSTRUMENTATION AND TO COLLECT
900 ' THE MEASURED DATA. THE PROGRAM ALSO PERFORMS THE IMPEDANCE SHORT CIRCUIT CALIBRATION
1000 ' AT EVERY MEASUREMENT FREQUENCY AND SUBTRACTS THIS VALUE FROM THE MEASURED IMPEDANCE.
1100 ' THE PROGRAM CHECKS THE MEASUREMENT MODE OF THE IMPEDANCE ANALYZER AND IF IN ADMITTANCE
1200 ' MODE THE DATA IS CONVERTED TO THE EQUIVALENT IMPEDANCE. THE DATA COLLECTED BY THE
1300 ' PROGRAM IS STORED IN SEVEN DATA FILES CORRESPOMDING TO THE IMPEDANCE DATA (BOTH DC AND AC),
1400 ' INTERDIGITATED GATE GAIN/PHASE, SENSOR GAIN/PHASE, CHEMFET TRANSISTOR GAIN/PHASE,
1500 ' REFERENCE TRANSISTOR GAIN/PHASE, INTERDIGITATED GATE FFT SPECTRUM, AND THE SENSOR
1600 ' FFT SPECTRUM. A ELAPSED TIMER IS ALSO PROVIDED. THE TIMER STARTS AFTER THE SET-UP
1700 ' MEASUREMENTS (LINE 19900).
1800 '
1900 ' PROGRAMMER'S NOTE: THE HP EQUIPMENT HAS A MINOR INCOMPATIBILITY WITH THE CEC IEEE-488
2000 ' INTERFACE. THE PROBLEM MANIFESTS ITSELF WHEN ATTEMPTING TO COLLECT DATA IN A LOOP USING
2100 ' THE SEND ENTER% COMMANDS. IF THE LOOP INCLUDES ADDITIONAL PROCESSING SUCH AS THE CASE  FOR
2200 ' THE IMEPDANCE MEASUREMENTS THE ERROR DOES NOT OCCUR. HOWEVER, THE PROBLEM DID OCCUR WHEN
COLLECTING
2300 ' DATA FROM THE GAIN/PHASE ANALYZER. THE PROBLEM WAS CORRECTD USING THE TRANSMIT% AND
2400 ' RECIEVE% COMMANDS.
2500 '
2600 '
2700 DIM REAL.REF(406), IMAG.REF(406), DATA1#(405), DATA2#(405), FREQ(405)
2800 DIM FFT.TEST(800), FFT.REF(800), DATA3(800), GAIN(400), PHS(400)
2900 DIM GFREQ(400), FFT.FREQ(800)
3000 DEF SEG=&HC400                          ' ADDRESS OF GP-IB INTERFACE
3100 INIT%=0                                 ' OFFSET OF INITIALIZE ROUTINE
3200 TRANSMIT%=3                            ' OFFSET OF TRANSMIT ROUTINE
3300 RECIEVE%=6                             ' OFFSET OF RECIEVE ROUTINE
3400 SEND%=9                                ' OFFSET OF SEND ROUTINE
3500 SPOLL%=12                              ' OFFSET OF SERIAL POLL ROUTINE
3600 ENTER%=21                              ' OFFSET OF ENTER ROUTINE
3700 '
3800 '
3900 '
4000 ' GP-IB ADDRESSES OF INSTRUMENTS
4100 '
4200 HP4194%=17: HP4192%=9: PRINTER%=1: MY.ADDR%=21: K617%=27
4300 BK2032%=26
4400 '
4500 SYSCON%=0                              'PC488 ACTS AS CONTROLLER
4600 '
4700 CALL INIT%(MY.ADDR%,SYSCON%)
4800 '
4900 EX$="EX"
5000 FREQ(0)=5
5100 ELAPSE.TIME$="00:00:00"
5200 HOURS =0
5300 MINUTES = 0
5400 SECONDS = 0
5500  '
5600 INPUT "NAME OF EXPERIMENT:", EXPERIMENT$
5700 INPUT "NAME OF IMPEDANCE DATA FILE:", IMPFILE$
5800 INPUT "NAME OF GATE GAIN/PHASE DATA FILE:", GATEGP.FILE$
5900 INPUT "NAME OF TEST TRANSISTOR GAIN/PHASE DATA FILE:",TESTGP.FILE$
6000 INPUT "NAME OF FLT GATE/DRAIN GAIN/PHASE DATA FILE:",FLTGP.FILE$
6100 INPUT "NAME OF REF TRANSISTOR GAIN/PHASE DATA FILE:",REFGP.FILE$
```

```
6200 INPUT "NAME OF GATE FFT DATA FILE:",GATE.FFT.FILE$
6300 INPUT "NAME OF DG-VOUT FFT DATA FILE:", DG.VOUT.FFT.FILE$
6400 '
6500 OPEN "O",#1, IMPFILE$
6600 OPEN "O",#2, GATEGP.FILE$
6700 OPEN "O", #3, TESTGP.FILE$
6800 OPEN "O", #4,FLTGP.FILE$
6900 OPEN "O",#5, REFGP.FILE$
7000 OPEN "O",#6,GATE.FFT.FILE$
7100 OPEN "O",#7, DG.VOUT.FFT.FILE$
7200 '
7300 '
7400 '              SET-UP ELECTROMETER FOR MEASUREMENT
7500 '
7600 S$="F1"                              'SET TO MEASURE AMPS
7700 CALL SEND%(K617%,S$,STATUS%)
7800 S$="R1X"                        'SET TO 2pA RANGE
7900 CALL SEND%(K617%,S$,STATUS%)
8000 S$="Z1X"                   'PERFORM ZERO CORRECT
8100 CALL SEND%(K617%,S$,STATUS%)
8200 S$="T0X"
8300 CALL SEND%(K617%,S$,STATUS%)
8400 '
8500 S$="F5X"                     'SET TO V/I OHMS MODE
8600 CALL SEND%(K617%,S$,STATUS%)
8700 S$="V100X"                   'SET INTERNAL VOLTAGE SOURCE TO 100V
8800 CALL SEND%(K617%,S$,STATUS%)
8900 '
9000 '
9100 '
9200 '              SET-UP HP4192 FOR MEASUREMENT
9300 '
9400 S$="A2B1T3F0"              'A=REAL, B=IMAGINARY, T3=MAN TRIGGER
9500 CALL SEND%(HP4192%,S$,STATUS%)
9600 '
9700 INPUT "CONNECT 4192 FOR ZERO SHORT OFFSET MEASUREMENT, HIT RETURN WHEN READY",NULL$
9800 '
9900 I=0
10000 GOSUB 31400                   'MAKE ZERO OFFSET MEASUREMENT
10100 FOR I=0 TO 405: REAL.REF(I)=DATA1#(I): IMAG.REF(I)=DATA2#(I): NEXT I
10200 '
10300 '
10400 '
10500 '                     SET-UP 4194 FOR G/P MEASUREMENTS
10600 '
10700 '
10800 S$="RST"                            'INITIALIZE 4194 TO POWER ON SETTING
10900 CALL SEND%(HP4194%,S$,STATUS%)
11000 S$="RQS2"                           'UNMASK AND ENABLE BIT1 FOR SRQ
11100 CALL SEND%(HP4194%,S$,STATUS%)
11200 S$="FNC2"                           'SET 4194 TO GAIN PHASE MODE
11300 CALL SEND%(HP4194%,S$,STATUS%)
11400 S$="PHS2"                           'SET PHASE SCALE TO EXPANSION MODE
11500 CALL SEND%(HP4194%,S$,STATUS%)
11600 S$="SWM2"                          'SET SWEEP MODE TO SINGLE
11700 CALL SEND%(HP4194%,S$,STATUS%)
11800 S$="SWT2"                           'SET TO LOG SWEEP
11900 CALL SEND%(HP4194%,S$,STATUS%)
12000 S$="OSC=-10DBM"                     'SET SWEEP OSCILLATOR TO -10 dBM
12100 CALL SEND%(HP4194%,S$,STATUS%)
12200 S$="MCF0"                           'TURN MARKERS OFF
12300 CALL SEND%(HP4194%,S$,STATUS%)
12400 S$="ZIR1"                          'SET REF CHANNEL INPUT IMP.=1Mohm
12500 CALL SEND%(HP4194%,S$,STATUS%)
12600 S$="ZIT1"                          'SET TEST CHANNEL INPUT IMP=1Mohm
12700 CALL SEND%(HP4194%,S$,STATUS%)
12800 S$="ITM2"                          'SET INTEGRATION TIME TO 5mSEC
```

```
12900 CALL SEND%(HP4194%,S$,STATUS%)
13000 S$="STOP=10000000HZ"                    'SWEEP TO 10MHz
13100 CALL SEND%(HP4194%,S$,STATUS%)
13200 '
13300 INPUT "CONNECT 4194 FOR OFFSET REF STORE, RETURN WHEN READY", NULL$
13400 '
13500 '
13600 S$="SWTRG"                              'PERFORM SINGLE SWEEP
13700 CALL SEND%(HP4194%,S$,STATUS%)
13800 CALL SPOLL%(HP4194%,POLL%,STATUS%)
13900 IF ((POLL% AND 64) <> 64) THEN 13800
14000 S$="OFSTR"                              'STORE OFFSET DATA
14100 CALL SEND%(HP4194%,S$,STATUS%)
14200 S$="AOF1"                               'OFFSET A ON
14300 CALL SEND%(HP4194%,S$,STATUS%)
14400 S$="BOF1"                               'OFFSET B ON
14500 CALL SEND%(HP4194%,S$,STATUS%)
14600 '
14700 S$="X?"                                 'READ IN FREQUENCY POINTS
14800 CALL SEND%(HP4194%,S$,STATUS%)
14900 S$="MLA TALK 17"                        '4194 TO OUTPUT
15000 CALL TRANSMIT%(S$,STATUS%)
15100 TEMP$=SPACE$(15)
15200 FOR I=0 TO 400
15300 CALL RECIEVE%(TEMP$,LENGTH%,STATUS%)
15400 GFREQ(I)=VAL(LEFT$(TEMP$,12))
15500 NEXT I
15600 '
15700 '
15800 '                  SET-UP FFT ANALYZER
15900 '
16000 '
16100 FOR O = 1 TO 3
16200 PRINT
16300 PRINT "INSTALL THE DUT INTO SAMPLE CELL AND"
16400 INPUT "CONNECT FFT ANALYZER ACROSS GATE, HIT RETURN WHEN READY", NULL$
16500 PRINT "MAKING INITIAL READING"
16600 S$="SR"
16700 CALL SEND%(BK2032%,S$,STATUS%)
16800 S$="DM 1"                               'SET STATUS BYTE FOR END OF AVERAGES
16900 CALL SEND%(BK2032%,S$,STATUS%)
17000 S$="DF UM"                              'DISPLAY FORMAT:UPPER MEASUREMENT SET-UP
17100 CALL SEND%(BK2032%,S$,STATUS%)
17200 S$="EM PA,0"                            'GO TO SPECIAL PARAMETER MAIN
17300 CALL SEND%(BK2032%,S$,STATUS%)
17400 S$="EM VA,2032"                         'SET MAIN TO 2032
17500 CALL SEND%(BK2032%,S$,STATUS%)
17600 S$="EM PA,88"                           'GOTO SPECIAL PARAMETER DUMP PLOT
17700 CALL SEND%(BK2032%,S$,STATUS%)
17800 S$="EM VA,1"                            'SET DUMP TO "THINK JET MODE"
17900 CALL SEND%(BK2032%,S$,STATUS%)
18000 MESSAGE$= EXPERIMENT$ + " " + DATE$ + " " + ELAPSE.TIME$
18100 WRITE #6, DATE$,ELAPSE.TIME$
18200 GOSUB 41000
18300 INPUT "FREQUENCY RESOLUTION:", FREQ.RES
18400 INPUT "LOWEST FREQUENCY:",FFT.FREQ(0)
18500 S$="LD"                                 'SET MAIN CURSOR TO LOWER DISPLAY
18600 CALL SEND%(BK2032%,S$,STATUS%)
18700 FOR I=0 TO 800                          'CALCULATE FREQ PTS, READ IN LOWER DISPLAY DATA, OUTPUT DATA
18800 S$="AF " +STR$(I)
18900 CALL SEND%(BK2032%,S$,STATUS%)
19000 CALL ENTER%(TEMP$,LENGTH%,BK2032%,STATUS%)
19100 FFT.REF(I)=VAL(MID$(TEMP$,2,9))
19200 FFT.FREQ(I)=FFT.FREQ(0) + I*FREQ.RES
19300 WRITE #6, FFT.FREQ(I),FFT.TEST(I), FFT.REF(I)
19400 NEXT I
19500 NEXT O
```

```
19600 S$="DF UL"                          'SET UPPER/LOWER DISPLAY FORMAT
19700 CALL SEND%(BK2032%,S$,STATUS%)
19800 '
19900 'TURN ON ELAPSE TIMER
20000 CLS
20100 BEGIN.TIME$=TIME$
20200 BEGIN.HRS= VAL(LEFT$(BEGIN.TIME$,2))
20300 BEGIN.MIN= VAL(MID$(BEGIN.TIME$,4,2))
20400 BEGIN.SEC= VAL(RIGHT$(BEGIN.TIME$,2))
20500 ON TIMER (1) GOSUB 49200
20600 TIMER ON
20700 '
20800 CLS
20900 PRINT "INITIAL SET-UP COMPLETE"
21000 '
21100 '
21200 '                          'DATA INPUT LOOP
21300 '
21400 '
21500 INPUT "CONNECT ELECTROMETER ACROSS GATE, HIT RETURN WHEN READY", NULL$
21600 S$="C0X"                            'ENABLE READING
21700 CALL SEND%(K617%,S$,STATUS%)
21800 TEMP$=SPACE$(16)
21900 FOR I=1 TO 1000: NEXT I             'LET ELECTROMETER SETTLE
22000 CALL ENTER%(TEMP$,LENGTH%,K617%,STATUS%)
22100 DC.RESIST= VAL(RIGHT$(TEMP$,12))
22200 WRITE #1, DATE$,ELAPSE.TIME$
22300 WRITE #1,"0",DC.RESIST
22400 S$="O0X"                            'TURN OFF VOLTAGE SOURCE
22500 CALL SEND%(K617%,S$,STATUS%)
22600 S$="C1X"                            'DISABLE READING
22700 CALL SEND%(K617%,S$,STATUS%)
22800 '
22900 INPUT "CONNECT HP4192 ACROSS GATE, HIT RETURN WHEN READY",NULL$
23000 I=0
23100 GOSUB 31400
23200 FOR I=0 TO 405
23300 REALOUT=DATA1#(I)-REAL.REF(I)
23400 IMAGOUT=DATA2#(I)-IMAG.REF(I)
23500 WRITE #1, FREQ(I),REALOUT,IMAGOUT
23600 NEXT I
23700 '
23800 CLS
23900 INPUT "CONNECT 4194 ACROSS GATE,RETURN WHEN READY", NULL$
24000 MESSAGE$=EXPERIMENT$+" GATE " + DATE$ + " " + ELAPSE.TIME$
24100 WRITE #2, DATE$, ELAPSE.TIME$
24200 GOSUB 43900
24300 FOR I= 0 TO 400
24400 WRITE #2, GFREQ(I), GAIN(I), PHS(I)
24500 NEXT I
24600 '
24700 INPUT "CONNECT 4194 ACROSS DG TO VOUT, RETURN WHEN READY", NULL$
24800 MESSAGE$= EXPERIMENT$ + " TEST TRANSISTOR " + DATE$ + " " + ELAPSE.TIME$
24900 WRITE #3, DATE$,ELAPSE.TIME$
25000 GOSUB 43900
25100 FOR I=0 TO 400
25200 WRITE #3, GFREQ(I), GAIN(I), PHS(I)
25300 NEXT I
25400 '
25500 '
25600 '
25700 '
25800 INPUT "CONNECT FFT ANALYZER ACROSS GATE, HIT RETURN WHEN READY", NULL$
25900 MESSAGE$=EXPERIMENT$ + " GATE FFT " + DATE$ + " " + ELAPSE.TIME$
26000 WRITE #6, DATE$, ELAPSE.TIME$
26100 GOSUB 40800
26200 FOR I=0 TO 800
```

```
26300 WRITE #6, FFT.FREQ(I), FFT.TEST(I)
26400 NEXT I
26500 S$="DF UL"                                    'SET UPPER/LOWER DISPLAY FORMAT
26600 CALL SEND%(BK2032%,S$,STATUS%)
26700 '
26800 INPUT "CONNECT FFT ANALYZER ACROSS DG TO VOUT,  HIT RETURN WHEN READY", NULL$
26900 MESSAGE$=EXPERIMENT$ + " FFT DG-VOUT" + DATE$ + " " + ELAPSE.TIME$
27000 WRITE #7, DATE$, ELAPSE.TIME$
27100 GOSUB 40800
27200 FOR I=0 TO 800
27300 WRITE #7, FFT.FREQ(I), FFT.TEST(I)
27400 NEXT I
27500 S$="DF UL"                                    'SET UPPER/LOWER DISPLAY FORMAT
27600 CALL SEND%(BK2032%,S$,STATUS%)
27700 '
27800 '
27900 '
28000 S$="OSC=-20DBM"                               'SET SWEEP OSCILLATOR TO -20DBM
28100 CALL SEND%(HP4194%,S$,STATUS%)
28200 INPUT "CONNECT 4194 FROM FLT GATE TO DRAIN, RETURN WHEN READY", NULL$
28300 MESSAGE$= EXPERIMENT$ + " FLT GATE TO DRAIN " + DATE$ + ELAPSE.TIME$
28400 WRITE #4, DATE$, ELAPSE.TIME$
28500 GOSUB 43900
28600 FOR I= 0 TO 400
28700 WRITE #4, GFREQ(I), GAIN(I), PHS(I)
28800 NEXT I
28900 '
29000 INPUT "CONNECT 4194 ACROSS REF TRANSISTOR, RETURN WHEN READY", NULL$
29100 MESSAGE$=EXPERIMENT$ + " REF TRANS " + DATE$ + " " + ELAPSE.TIME$
29200 WRITE #5,DATE$,ELAPSE.TIME$
29300 GOSUB 43900
29400 FOR I=0 TO 400
29500 WRITE #5, GFREQ(I), GAIN(I), PHS(I)
29600 NEXT I
29700 S$="OSC=-10DBM"                               'SET SWEEP OSCILLATOR TO -10DBM
29800 CALL SEND%(HP4194%,S$,STATUS%)
29900 '
30000 '
30100 '
30200 INPUT "COLLECT MORE DATA, Y OR N:", MOREDATA$
30300 IF MOREDATA$="N" THEN 30600
30400 GOTO 21200
30500 '
30600 CLOSE #1
30700 CLOSE #2
30800 CLOSE #3
30900 CLOSE #4
31000 CLOSE #5
31100 CLOSE #6
31200 CLOSE #7
31300 STOP
31400 '
31500 '
31600 '
31700 '
31800 '                          HP4192 FREQUENCY SCAN CONTROL ROUTINE
31900 '
32000 '
32100 S$="SF.001ENTF.005ENPF.1EN"       'STEP=1Hz, START=5Hz, STOP=100Hz
32200 IMPSTEP=1
32300 GOSUB 35200
32400 '
32500 S$="SF.01ENTF.110ENPF1EN"         'STEP=10Hz, START=110Hz, STOP=1KHz
32600 IMPSTEP=10
32700 GOSUB 35200
32800 '
32900 S$="SF.1ENTF1.1ENPF10EN"          'STEP=100Hz, START=1.1KHz, STOP=10KHz
```

```
33000 IMPSTEP=100
33100 GOSUB 35200
33200 '
33300 S$="SF2ENTF12ENPF100EN"           'STEP=2KHz, START=12KHz, STOP=100KHz
33400 IMPSTEP=2000
33500 GOSUB 35200
33600 '
33700 S$="SF20ENTF120ENPF1000EN"        'STEP=20KHz, START=120KHz, STOP=1000KHz
33800 IMPSTEP=20000
33900 GOSUB 35200
34000 '
34100 S$="SF300ENTF1300ENPF13000EN"     'STEP=300KHz, START=1300KHz, STOP=13000KHz
34200 IMPSTEP=300000!
34300 GOSUB 35200
34400 RETURN
34500 '
34600 '
34700 '
34800 '
34900 '                          HP4192 DATA INPUT ROUTINE
35000 '
35100 '
35200 CALL SEND%(HP4192%,S$,STATUS%)
35300 '
35400 S$="W1 W2"                        'AUTO SWEEP, SWEEP UP
35500 CALL SEND%(HP4192%,S$,STATUS%)
35600 '
35700 '
35800 'LOOP FOR COLLECTION OF DATA
35900 '
36000 J$=SPACE$(31)
36100 S$=EX$                            'EXECUTE INCREMENTS THE FREQUENCY OF 4192
36200 CALL SEND%(HP4192%,S$,STATUS%)
36300 CALL ENTER%(J$,LENGTH%,HP4192%,STATUS%)
36400 CALL SPOLL%(HP4192%,POLL%,STATUS%)
36500 IF (POLL%=0) THEN 40400           'IS SWEEP COMPETE?
36600 '
36700 'CHECK FOR VALID DATA
36800 '
36900 VALID.REAL$=LEFT$(J$,1):VALID.IMAG$=MID$(J$,17,1)
37000 IF (VALID.REAL$="N" AND VALID.IMAG$="N") THEN 37600
37100 IF (VALID.REAL$="O" OR VALID.IMAG$="O") THEN 37300
37200 DATA2#(I)=0: GOTO 37800             'IMAG UNMEASURABLE
37300 DATA1#(I)=9E+36: DATA2#(I)=9E+36     'REAL AND IMAGINARY TOO LARGE
37400 GOTO 39900
37500 '
37600 TEMP$=RIGHT$(J$,11)                 'EXTRACT REAL DATA FROM DATA STRING
37700 DATA2#(I)=VAL(TEMP$)
37800 TEMP$=MID$(J$,5,11)                 'EXTRACT IMAGINARY DATA FROM DATA STRING
37900 DATA1#(I)=VAL(TEMP$)                'CONVERT STRING TO NUMBER
38000 '
38100 ' CHECK CIRCUIT MODE
38200 '
38300 MODE$=MID$(J$,2,2)
38400 IF MODE$<>"GF" THEN 39900           'MODE NOT PARALLEL THEN 32900
38500 '
38600 TEMP1#= DATA1#(I)^2 + DATA2#(I)^2     'OTHERWISE CONVERT G+jB TO R+jX
38700 IF TEMP1#<>0! THEN 39000
38800 TEMP1#=9E+36
38900 GOTO 39100
39000 TEMP1#=1/SQR(TEMP1#)
39100 IF DATA1#(I)<>0! THEN 39400
39200 TEMP2#= -1.5707963#
39300 GOTO 39600
39400 TEMP2#= DATA2#(I)/DATA1#(I)
39500 TEMP2#= -(ATN(TEMP2#))
39600 DATA1#(I)= TEMP1#* COS(TEMP2#)
```

```
39700 DATA2#(I)= TEMP1# * SIN(TEMP2#)
39800 '
39900 IF I=0 THEN 40100                    'CALCULATE MEASUREMENT FREQUENCIES
40000 FREQ(I)=FREQ(I-1) + IMPSTEP
40100 I=I+1
40200 GOTO 36100                           ' READ IN MORE DATA
40300 '
40400 RETURN
40500 '
40600 '
40700 '
40800 '                          'FFT ANALYZER DATA INPUT ROUTINE
40900 '
41000 S$= "UNL MTA LISTEN 26 DATA 'KP  ' 03 13 10"  'INPUT AUTORANGE
41100 CALL TRANSMIT%(S$,STATUS%)
41200 S$="KP A"                                    'START AVERAGING
41300 CALL SEND%(BK2032%,S$,STATUS%)
41400 CALL SPOLL%(BK2032%,POLL%,STATUS%)
41500 IF (POLL% AND 1) <> 1 THEN 41400             'IF AVERAGING NOT COMPLETE THEN POLL
41600 S$="KP I"                                    'STOP RECORDING OF DATA
41700 CALL SEND%(BK2032%,S$,STATUS%)
41800 S$="KP D"                                    'AUTO SCALE GRAPH A OR B
41900 CALL SEND%(BK2032%,S$,STATUS%)
42000 S$="KP R"                                    'SWITCH TO OTHER GRAPH
42100 CALL SEND%(BK2032%,S$,STATUS%)
42200 S$="KP D"                                    'AUTOSCALE THE OTHER GRAPH
42300 CALL SEND%(BK2032%,S$,STATUS%)
42400 S$="PR '"+ MESSAGE$ + "'"
42500 CALL SEND%(BK2032%,S$,STATUS%)
42600 S$="UNL UNT LISTEN 01"                       'PREPARE FOR MANUAL DUMP
42700 CALL TRANSMIT%(S$,STATUS%)
42800 INPUT "PERFORM MANUAL DUMP TO PRINTER, HIT RETURN WHEN FINISHED",NULL$
42900 TEMP$=SPACE$(12)
43000 S$="UD"                                      'SET TO UPPER DISPLAY
43100 CALL SEND%(BK2032%,S$,STATUS%)
43200 FOR I=0 TO 800
43300 S$="AF " + STR$(I)                           'READ IN UPPER DISPLAY DATA
43400 CALL SEND%(BK2032%,S$,STATUS%)
43500 CALL ENTER%(TEMP$,LENGTH%,BK2032%,STATUS%)
43600 FFT.TEST(I)=VAL(MID$(TEMP$,2,9))
43700 NEXT I
43800 RETURN
43900 '
44000 '
44100 '                          HP4194 DATA INPUT ROUTINE
44200 '
44300 '
44400 CALL SPOLL%(HP4194%,POLL%,STATUS%)           'MAKE SURE SRQ IS NOT SET
44500 S$="SWTRG"                                   'PERFORM SINGLE SWEEP
44600 CALL SEND%(HP4194%,S$,STATUS%)
44700 CALL SPOLL%(HP4194%,POLL%,STATUS%)           'IS SWEEP COMPLETE?
44800 IF ((POLL% AND 64) <> 64) THEN 44700                 'IF NOT CONTINUE POLL
44900 '
45000 S$="AUTOA"                                   'AUTOSCALE DISPLAY A
45100 CALL SEND%(HP4194%,S$,STATUS%)
45200 S$="AUTOB"                                   'AUTOSCALE DISPLAY B
45300 CALL SEND%(HP4194%,S$,STATUS%)
45400 S$= "CMT '" + MESSAGE$ + "'"                 'PLACE MESSAGE ON 4194 DISPLAY
45500 CALL SEND%(HP4194%,S$,STATUS%)
45600 S$= " UNL UNT LISTEN 01"
45700 CALL TRANSMIT%(S$,STATUS%)
45800 INPUT "PERFORM MANUAL DUMP TO PRINTER, SET 4194 TO ADDRESSABLE, RETURN WHEN READY", NULL$
45900 '
46000 '    NOTE MANUAL DUMP REQUIRES MANUAL EXECUTION OF THE FOLLOWING 4194 COMMANDS:
46100 '    GOTO LOCAL; MORE MENUS; HPIB DEFINE; TALK ONLY; COPY
46200 '    WHEN DUMP COMPLETE: MORE MENUS; HPIB DEFINE; ADDRESSABLE
46300 '    RETURN TO CONTINUE PROGRAM EXECUTION
```

```
46400 '
46500 S$="A?"                                   'READ IN GAIN FROM ARRAY REGISTER A
46600 CALL SEND%(HP4194%,S$,STATUS%)
46700 '
46800 IF STATUS%=0 THEN 47200                   'IS 4194 SET TO ADDRESSABLE?
46900 INPUT "SET 4194 TO ADDRESSABLE, RETURN WHEN READY", NULL$
47000 GOTO 46500
47100 '
47200 S$= "MLA TALK 17"
47300 CALL TRANSMIT%(S$,STATUS%)
47400 TEMP$= SPACE$(13)
47500 FOR I = 0 TO 400
47600 CALL RECIEVE%(TEMP$,LENGTH%,STATUS%)
47700 GAIN(I)=VAL(LEFT$(TEMP$,12))              'EXTRACT GAIN VALUE
47800 NEXT I
47900 '
48000 S$="B?"                                   'READ IN PHASE FROM ARRAY REGISTER B
48100 CALL SEND%(HP4194%,S$,STATUS%)
48200 S$= "MLA TALK 17"
48300 CALL TRANSMIT%(S$,STATUS%)
48400 FOR I= 0 TO 400
48500 CALL RECIEVE%(TEMP$,LENGTH%,STATUS%)
48600 PHS(I)= VAL(LEFT$(TEMP$,12))              'EXTRACT PHASE VALUE
48700 NEXT I
48800 '
48900 '
49000 CALL SPOLL%(HP4194%,POLL%,STATUS%)        'MAKE SURE SRQ NOT SET
49100 RETURN
49200 '                  TIMER ROUTINE
49300 '
49400 Y=CSRLIN
49500 X=POS(0)
49600 TIME.NOW$=TIME$
49700 NOW.HRS= VAL(LEFT$(TIME.NOW$,2))
49800 NOW.MIN= VAL(MID$(TIME.NOW$,4,2))
49900 NOW.SEC= VAL(RIGHT$(TIME.NOW$,2))
50000 SECONDS= NOW.SEC-BEGIN.SEC
50100 IF SECONDS >= 0 THEN 50300
50200 SECONDS=SECONDS+60: NOW.MIN=NOW.MIN-1
50300 MINUTES=NOW.MIN-BEGIN.MIN
50400 IF MINUTES >= 0 THEN 50600
50500 MINUTES=MINUTES+60: NOW.HRS=NOW.HRS-1
50600 IF NOW.HRS<BEGIN.HRS THEN NOW.HRS=NOW.HRS+24
50700 HOURS=NOW.HRS-BEGIN.HRS
50800 IF SECONDS<10 THEN SECONDS$="0" + RIGHT$(STR$(SECONDS),1)
50900 IF SECONDS >= 10 THEN SECONDS$=RIGHT$(STR$(SECONDS),2)
51000 IF MINUTES<10 THEN MINUTES$="0" + RIGHT$(STR$(MINUTES),1)
51100 IF MINUTES >= 10 THEN MINUTES$=RIGHT$(STR$(MINUTES),2)
51200 ELAPSE.TIME$= STR$(HOURS) + ":" + MINUTES$ +":" + SECONDS$
51300 LOCATE 20,45: PRINT "ELAPSED TIME: "; ELAPSE.TIME$
51400 LOCATE Y,X
51500 RETURN
```

```
100 ' FILENAME = IMPCOMP
200 '
300 '                                    IMPEDANCE DATA COMPRESSION SOFTWARE
400 '
500 '
600 ' THIS PROGRAM ENTERS THE RESISTANCE AND REACTANCE DATA STORED IN THE FILE IMP AND
700 ' COMPUTES THE MAGNITUDE AND PHASE OF THE IMPEDANCE. THE PROGRAM OUTPUTS THE DC RESISTANCE
800 ' IN THE FILE DCRES. tHE MAGNITUDE AND PHASE ARE COMPUTED FOR EVERY SIXTH FREQUENCY AT
900 ' EACH MEASUREMENT TIME AND OUTPUT IN THE FILES MGPHSXX.PRN.
1000 '
1100 '
1200 I=1                                          'I = OUTPUT FILE COUNTER
1300 ON ERROR GOTO 5800
1400 OPEN "I",#1,"A:IMP"
1500 OPEN "O",#3,"C:DCRES"
1600 '
1700 '
1800 IF I<10 THEN 2100
1900 OPEN "O",#2, "C:MGPHS" + RIGHT$(STR$(I),2) + ".PRN"
2000 GOTO 2500
2100 OPEN "O",#2, "C:MGPHS" + RIGHT$(STR$(I),1) + ".PRN"
2200 '
2300 ' INPUT MEASUREMENT DATE AND TIME, AND ELECTROMETER RESISTACNE MEASUREMENT
2400 '
2500 INPUT #1,EXP.DATE$,EXP.TIME$
2600 INPUT #1, FREQ,DC
2700 PRINT #3,DC
2800 '
2900 ' LOOP FOR MAGNITUDE AND PHASE COMPUTATION, ASSUMES EACH MEASUREMENT TIME
3000 ' DATA SET CONTAINS 406 FREQUENCY POINTS
3100 '
3200 K=0                          ' INITIALIZE COUNTER
3300 FOR J= 0 TO 405
3400 INPUT #1, FREQ, REAL#, IMAG#
3500 IF K<>0 THEN 5000            ' COMPUTE AND SAVE ONLY WHEN K=0 (EVERY SIXTH FREQUENCY
3600 '
3700 IF (REAL#< 1E+18) AND (IMAG#<1E+18) THEN 4000      ' DATA VALID?
3800 MAG#= 1E+18
3900 GOTO 4200
4000 MAG#=REAL#^2 + IMAG#^2                             ' COMPUTE MAGNITUDE
4100 MAG#= SQR(MAG#)
4200 IF REAL#<>0# THEN 4500
4300 PHAS#=90
4400 GOTO 4900
4500 PHAS#= IMAG#/REAL#                                 ' COMPUTE PHASE
4600 PHAS#=ATN(PHAS#)
4700 PHAS#= (PHAS#*360)/(2*3.145926#)
4800 MAGOUT!=MAG#: PHASOUT!=PHAS#
4900 PRINT #2, FREQ,MAGOUT!, PHASOUT!
5000 K=K+1                                              ' INCREMENT DATA REDUCTION COUNTER
5100 IF K=6 THEN K=0
5200 NEXT J
5300 CLOSE #2
5400 '
5500 '
5600 I=I+1                                              ' NEXT OUTPUT FILE
5700 GOTO 1800
5800 IF ERR=62 THEN PRINT "END OF DATA"
5900 CLOSE #1
6000 CLOSE #2
6100 STOP
6200 END
```

```
100 ' FILENAME = GPCOMP.BAS
200 '
300 '
400 '                                    GAIN/PHASE DATA REDUCTION SOFTWARE
500 '
600 I=1                                              ' I = FILE COUNTER
700 ON ERROR GOTO 4300
800 '
900 ' ASK FOR INPUT FILENAME: GP12, GP13, GP23, OR GP43
1000 '
1100 INPUT "INPUT DATA FILE NAME", IFILE$
1200 OPEN "I",#1,"A:" + IFILE$
1300 '
1400 ' OPEN OUTPUT FILE
1500 '
1600 IF I<10 THEN 1900
1700 OPEN "O",#2, "C:" + IFILE$ + RIGHT$(STR$(I),2) + ".PRN"
1800 GOTO 2200
1900 OPEN "O",#2, "C:" + IFILE$ + RIGHT$(STR$(I),1) + ".PRN"
2000 '
2100 '
2200 INPUT #1,EXP.DATE$,EXP.TIME$
2300 K=0
2400 FOR J= 0 TO 400                    ' ASSUMES EACH TIME MEASUREMENT DATA SET
2500 '                                    CONTAINS 401 FREQUENCY POINTS
2600 '
2700 INPUT #1, FREQ, GAIN, PHASE
2800 '
2900 ' OUTPUT WHEN K=0 (EVERY SIXTH FREQUENCY POINT)
3000 '
3100 IF K<>0 THEN 3500
3200 PRINT J,FREQ,GAIN,PHASE
3300 PRINT #2, FREQ, GAIN, PHASE
3400 '
3500 K=K+1                              ' INCREMENT DATA REDUCTION COUNTER
3600 IF K=6 THEN K=0
3700 NEXT J
3800 CLOSE #2
3900 I=I+1                              ' NEXT OUTPUT FILE
4000 GOTO 1600
4100 '
4200 '
4300 IF ERR=62 THEN PRINT "END OF DATA"
4400 CLOSE #1
4500 CLOSE #2
4600 STOP
4700 END
```

```
100 'FILENAME = EDFFT13.BAS
200 '
300 '
400 '                          DIFFERENCE SPECTRA ALGORITHM FOR EPOXY FFT13 DATA
500 '
600 '
700 DIM RACH(800), RBCH(800)
800 OPEN "I",#1,"A:FFT12"
900 IF EOF(1) THEN 3400
1000 '
1100 ' READ IN REFERENCE SPECTRA IN THIRD MEASUREMENT SET OF FFT12
1200 '
1300 FOR K=1 TO 3
1400 INPUT #1, EXPDATE$,EXPTIME$
1500 FOR I= 0 TO 800
1600 INPUT #1, FREQ, RACH(I), RBCH(I)
1700 NEXT I
1800 NEXT K
1900 CLOSE #1
2000 '
2100 '
2200 OPEN "I",#1, "A:FFT13"
2300 FILENUM=1
2400 COUNT =0
2500 IF FILENUM<10 THEN OPEN "O",#2,"C:DFFT13" + RIGHT$(STR$(FILENUM),1) ELSE OPEN
"O",#2,"C:DFFT13"+ RIGHT$(STR$(FILENUM),2)
2600 INPUT #1, EXPDATE$,EXPTIME$
2700 FOR I=0 TO 800
2800 INPUT #1, FREQ, ACH
2900 GOSUB 4100
3000 NEXT I
3100 FILENUM=FILENUM+1
3200 CLOSE #2
3300 GOTO 2400
3400 CLOSE #1
3500 END
3600 '
3700 '
3800 ' SUBROUTINE TO LOCATE THE HARMONIC AND COMPUTE THE DIFFERENCE IN HARMONIC
3900 ' AMPLITUDE BETWEEN THE SENSOR OUTPUT AND THE EXCITATION SIGNAL.
4000 '
4100 IF FREQ < (COUNT -32) THEN 5500
4200 TDIFF= RBCH(I)-ACH
4300 IF I<>0 THEN 4700
4400 DIFF=TDIFF
4500 GFREQ=FREQ
4600 GOTO 5000
4700 IF RBCH(I-1)> RBCH(I) THEN 5000
4800 DIFF=TDIFF
4900 GFREQ=FREQ
5000 IF FREQ<COUNT +32 THEN 5500
5100 COUNT =GFREQ
5200 COUNT=COUNT+256
5300 PRINT #2,GFREQ,DIFF
5400 PRINT GFREQ,DIFF
5500 RETURN
```

```
10 'FILENAME = NDFFT12.BAS
15 '
16 '
20 '                                NORMALIZED DIFFERENCE SPECTRA SOFTWARE FOR
25 '                                  INTERDIGITATED GATE
26 '
27 '
30 DIM FREQ(800),REF(800), TEST(800),TMAX(800)
40 OPEN "I", #1, "A:FFT12"
50 IF EOF(1) THEN 480
60 '
70 ' READ IN UNEXPOSED DATA
80 '
90 FOR K=1 TO 3
100 INPUT #1, EXPDATE$, EXPTIME$
110 FOR I=0 TO 800
120 INPUT #1, FREQ (I), REF(I), DUMMY
130 TMAX(I) = REF(I)
140 NEXT I
150 NEXT K
160 '
170 '
190 GOSUB 710                          'FIND THE MAX HARMONIC AMPLITUDE: MAXA
195 '
200 FOR I=0 TO 800: REF(I)=REF(I)/MAXA  'NORMALIZE THE UNEXPOSED SPECTRA
210 NEXT I
220 '
230 FILENUM=1
240 COUNT = 256
250 IF FILENUM<10 THEN OPEN "O",#2,"C:DFFT12" + RIGHT$(STR$(FILENUM),1) ELSE OPEN "O",#2,"C:DFFT12"+
RIGHT$(STR$(FILENUM),2)
260 '
270 ' READ IN TEST FFT SPECTRA
280 INPUT #1, EXPDATE$,EXPTIME$
290 FOR I=0 TO 800
300 INPUT #1, FREQ(I), TEST(I)
310 TMAX(I)=TEST(I)
320 NEXT I
330 GOSUB 710                          'FIND THE MAX HARMONIC AMP:MAXA
340 '
350 FOR I=0 TO 800                     'NORMALIZE THE TEST DATA
360 TEST(I)=TEST(I)/MAXA
370 NEXT I
380 '
390 ' FIND HARMONIC AND CALCULATE DIFFERENCE ; FIRST HARMONIC KNOWN TO
400 ' OCCUR ABOVE THE 7TH DATA POINT
410 '
420 FOR I=7 TO 800
430 GOSUB 530
440 NEXT I
450 FILENUM=FILENUM+1
460 CLOSE #2
470 GOTO 240
480 CLOSE #1
490 END
500 '
510 'SUBROUTINE TO LOCATE HARMONIC AND CALCULATE DIFFERENCE
520 '
530 IF FREQ(I) < (COUNT -32) THEN 670
540 TDIFF= ABS(TEST(I)-REF(I))
550 IF I<>0 THEN 590
560 DIFF=TDIFF
570 GFREQ=FREQ(I)
580 GOTO 620
590 IF REF(I-1) > REF(I) THEN 620
600 DIFF=TDIFF
610 GFREQ=FREQ(I)
```

```
620 IF FREQ(I)<COUNT +32 THEN 670
630 COUNT =GFREQ
640 COUNT=COUNT+256
650 PRINT #2,GFREQ,DIFF
660 PRINT GFREQ,DIFF
670 RETURN
680 '
690 ' SUBROUTINE TO LOCATE MAX HARMONIC: KNOWN TO OCCUR WITHIN FIRST 200 POINTS
700 '
710 MAXA=TMAX(0)
720 FOR L=1 TO 200
730 IF MAXA>= TMAX(L) THEN 750
740 MAXA= TMAX(L)
750 NEXT L
760 RETURN
```

```
100 'FILENAME = DFFT13.BAS
200 '
300 '
400 '                                          NORMALIZED DIFFERENCE SPECTRA SOFTWARE
500 '                                                FOR CHEMFET SENSOR
600 '
700 '
800 '
900 DIM FREQ(800),REF(800), TEST(800),TMAX(800)
1000 '
1100 'READ IN UNEXPOSED FFT SPECTRA
1200 '
1300 OPEN "I",#1,"A:FFT13"
1400 IF EOF(1) THEN 5100
1500 INPUT #1, EXPDATE$,EXPTIME$
1600 FOR I= 0 TO 800
1700 INPUT #1, FREQ(I), REF(I)
1800 TMAX(I)=REF(I)
1900 NEXT I
2000 '
2100 GOSUB 7400                              'FIND THE MAX HARMONIC AMPLITUDE: MAXA
2200 '
2300 FOR I=0 TO 800: REF(I)=REF(I)/MAXA   'NORMALIZE THE UNEXPOSED SPECTRA
2400 NEXT I
2500 '
2600 FILENUM=1
2700 COUNT = 256
2800 IF FILENUM<10 THEN OPEN "O",#2,"C:DFFT13" + RIGHT$(STR$(FILENUM),1) ELSE OPEN
"O",#2,"C:DFFT13"+ RIGHT$(STR$(FILENUM),2)
2900 '
3000 ' READ IN TEST FFT SPECTRA
3100 INPUT #1, EXPDATE$,EXPTIME$
3200 FOR I=0 TO 800
3300 INPUT #1, FREQ(I), TEST(I)
3400 TMAX(I)=TEST(I)
3500 NEXT I
3600 GOSUB 7400                               'FIND THE MAX HARMONIC AMP:MAXA
3700 '
3800 FOR I=0 TO 800                          'NORMALIZE THE TEST DATA
3900 TEST(I)=TEST(I)/MAXA
4000 NEXT I
4100 '
4200 ' FIND HARMONIC AND CALCULATE DIFFERENCE ; FIRST HARMONIC KNOWN TO
4300 ' OCCUR ABOVE THE 7TH DATA POINT
4400 '
4500 FOR I=7 TO 800
4600 GOSUB 5600
4700 NEXT I
4800 FILENUM=FILENUM+1
4900 CLOSE #2
5000 GOTO 2700
5100 CLOSE #1
5200 END
5300 '
5400 'SUBROUTINE TO LOCATE HARMONIC AND CALCULATE DIFFERENCE
5500 '
5600 IF FREQ(I) < (COUNT -32) THEN 7000
5700 TDIFF= ABS(TEST(I)-REF(I))
5800 IF I<>0 THEN 6200
5900 DIFF=TDIFF
6000 GFREQ=FREQ(I)
6100 GOTO 6500
6200 IF REF(I-1) > REF(I) THEN 6500
6300 DIFF=TDIFF
6400 GFREQ=FREQ(I)
6500 IF FREQ(I)<COUNT +32 THEN 7000
6600 COUNT =GFREQ
```

```
6700 COUNT=COUNT+256
6800 PRINT #2,GFREQ,DIFF
6900 PRINT GFREQ,DIFF
7000 RETURN
7100 '
7200 ' SUBROUTINE TO LOCATE MAX HARMONIC: KNOWN TO OCCUR WITHIN FIRST 200 POINTS
7300 '
7400 MAXA=TMAX(0)
7500 FOR L=1 TO 200
7600 IF MAXA>= TMAX(L) THEN 7800
7700 MAXA= TMAX(L)
7800 NEXT L
7900 RETURN
```

Appendix E

Electron Beam Thermal Evaporation Procedure

The following procedure was implemented to evaporate the copper phthalocyanine (CuPc) films onto the interdigitated gate electrode structures of the CHEMFET integrated circuit. A 1000 angstrom thick CuPc film was deposited over the interdigitated gate electrode structures using a vacuum electron beam evaporation system in conjunction with an appropriately sized mask. The film thickness was monitored with a pre-calibrated piezoelectric quartz crystal microbalance detector. The calibration of the piezoelectric detector is described in Appendix F. The entire deposition procedure was accomplished utilizing the mask fabrication equipment and the vacuum deposition system located in the AFIT Electronic and Materials Cooperative Laboratory (Building 125). This procedure is described in two parts: i) the steps implemented to fabricate the evaporation masks and ii) the steps implemented to evaporate the CuPc film onto the interdigitated gate structure of the CHEMFET.

Fabrication of the Evaporation Mask

The masks were fabricated from 6 mil thick beryllium copper (BeCu) stock. A 2 foot sample of the BeCu stock was provided by NGK Metals Corporation (21412 Protecta Drive, Elkhart IN 46516). The trade name for the BeCu stock is Berylco and it is a 25 alloy with XHM temper (52).

The steps for fabricating the evaporation mask were:

1. The evaporation mask pattern shown in Figure E-1 was printed on a High Resolution Plate (HRP) reticle using the procedure described by Pirolo (53). The evaporation mask pattern consisted of four rectangles corresponding to the two large and two small interdigitated gate electrode structures in the CHEMFET integrated circuit. One additional large and small rectangle was included on the same HRP reticle. These two rectangles were sufficiently separated from the four rectangular patterns and each other, such that they could be used to mask a single interdigitated gate electrode structure.

2. The BeCu stock was cut into a 2.25 inch square piece with a sheet metal shear located in the AFIT machine shop.

3. The BeCu square was polished and cleaned before it was coated with photoresist. Both surfaces were polished on a slurry table and then cleaned with a 1:10 mixture of a 50% sodium hydroxide solution and deionized water for 1 minute. The BeCu square was then rinsed for several minutes in deionized water and dried with compressed nitrogen gas.

4. Two coats of negative photoresist (Waycoat Type 3, 28 cps) was applied on one side of the BeCu square. This photoresist coating was utilized to protect the unpatterned side of the stock from the chemical etching process. The photoresist was spun-on at 2000 rpm for 15 seconds. After each photoresist application, the BeCu square was hard-baked at 150 ^{o}C for 45 minutes.

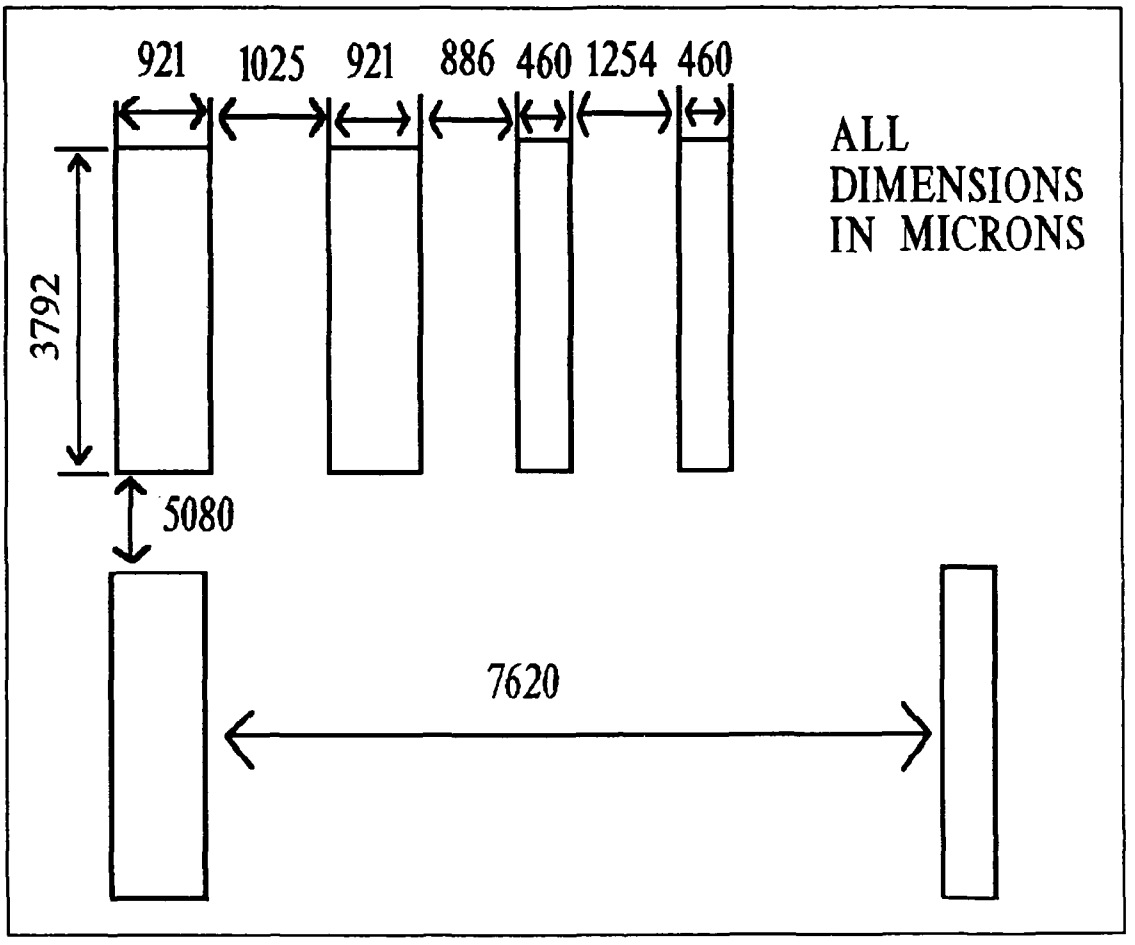

Figure E-1. Evaporation Mask Pattern.

5. The side of the BeCu square to be patterned was then coated with negative photoresist. The photoresist was spun-on at 2000 rpm for 15 seconds. The BeCu square was pre-baked at 70 ^{o}C for 30 minutes.

6. The rectangular structures were patterned in the negative photoresist using a mask aligner and the High Resolution Plate reticle. The High Resolution Plate reticle was centered over the photoresist coated BeCu square. The emulsion surface of the HRP reticle was contacted to the BeCu square. This sandwiched

configuration was then exposed to ultraviolet light via the mask aligner for 6 seconds.

7. The photoresist pattern printed on the BeCu square was developed by spinning the substrate at 2000 rpm and rinsing it for 30 seconds with xylene, followed by a 30 second purge with butyl acetate. The BeCu square was spun dry at 4000 rpm for 40 seconds.

8. The photoresist pattern was inspected under an optical microscope for pin-hole defects, and edge definition.

9. The unwanted BeCu was chemically etched in ferric chloride. The etching process took approximately 3 hours.

10. The BeCu square was rinsed for 5 minutes to remove the ferric chloride after the etching process was completed.

Electron Beam Evaporation of CuPc Films

The process utilized to evaporate the CuPc films onto the interdigitated gate electrode structures in the CHEMFET integrated circuit were:

1. The CHEMFET integrated circuit was affixed to a blank silicon wafer with double-sided cellophane tape. Two slices of a second blank silicon wafer were positioned next to the CHEMFET integrated circuit. The CuBe mask was then manually aligned with the CHEMFET's interdigitated gate electrode structures using a micromanipulator probe station (The Micromanipulator Company, model 6200, Carson City, NV) and held in place with small office binder clips. Figure E-2 shows a schematic of this arrangement.

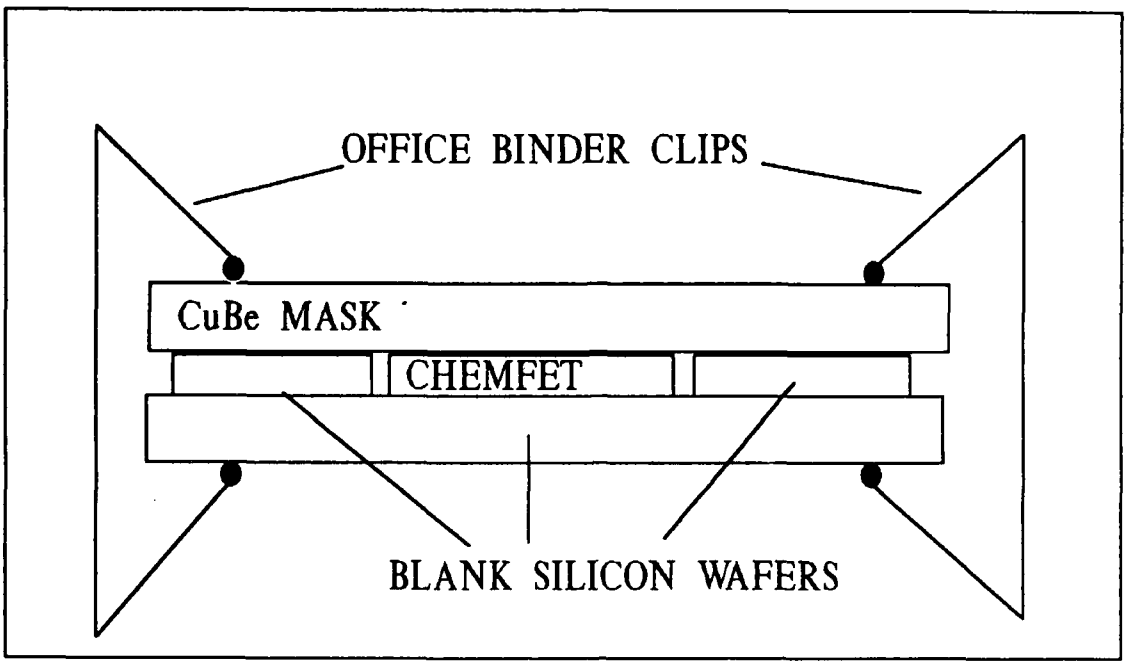

Figure E-2. CHEMFET Die Masking Arrangement For Copper Phthalocyanine Evaporation.

2. The masked CHEMFET integrated circuit was positioned in the vacuum deposition system (Denton Vacuum Corporation, model DV-602, Cherry Hill, NJ) chamber coplanar with the piezoelectric quartz crystal microbalance film thickness detector. The tooling factor on the thickness monitor electronics was set at 99.81 percent. The copper phthalocyanine was placed in a crucible. The chamber was evacuated and the electron beam moved into the crucible. The electron beam power source supplied a filament current of 0.55 - 0.6 amperes at a DC voltage of 2.5 - 3 KV. These settings were manually adjusted during the evaporation process to obtain an evaporation rate, measured with the piezoelectric detector, on the order of 1-10

angstroms/second. A stable evaporation rate was difficult to achieve and continuous adjustment of the electron beam supply voltage was required.

3. The film thickness was monitored with the calibrated piezoelectric detector (See Appendix F), and the evaporation process was stopped when the film thickness reached 1000 angstroms.

Appendix F

Piezoelectric Quartz Microbalance Detector Calibration

Two different methods were investigated for calibrating the piezoelectric quartz crystal microbalance detector to measure the thickness of the deposited copper phthalocyanine (CuPc) films. The first method calibrated the detector with the film thickness determined utilizing an independent ellipsometric measurement. The results obtained from this technique indicated that the ellipsometric method was unsuitable for specifying the thickness of CuPc films. The second method calibrated the detector with the film thickness measured with a profilometer. The procedure for performing the calibrations is discussed in the first section and the results of the two calibration methods are discussed in the second and third sections.

Piezoelectric Quartz Microbalance Detector Calibration Procedure

The calibration procedure was accomplished by evaporating copper phthalocyanine (CuPc) films with three different thicknesses onto a blank silicon wafer. The wafer was cleaned for 20 minutes in a freshly prepared 3:2 mixture of sulfuric acid and hydrogen peroxide. The wafer was rinsed with deionized water and then cleaned for 10 minutes with a 10:1 hydrofluoric acid and deionized water solution. The wafer was then rinsed with deionized water and dried with nitrogen gas. An evaporation mask was positioned on top of the cleaned wafer and held in place with small office binder clips. The fabrication of the evaporation mask is described in Appendix E. The film thickness of each CuPc film was measured with

the piezoelectric quartz crystal microbalance detector, an ellipsometer (Gaertner Scientific Corporation, model L-117, Chicago, IL), and a profilometer (Sloan Technology Corporation, model Dek-Tak 900051, Santa Barbara, CA). The published density of CuPc is 1.50 g/cm^3 and it has a refractive index of 2.08 - 2.5, depending on crystal orientation (54). The true density of CuPc crystals range from 1.59 - 1.62 g/cm^3 depending on crystal orientation (54). A refractive index of 2.5 was used in the ellipsometric measurements. The material's density is required to obtain a film thickness determination from the piezoelectric quartz crystal microbalance detector. Initially, a density of 1.62 g/cm^3 was assumed. The density is a parameter which is entered into the piezoelectric detector electronics and is used to determine the film's thickness. The density was adjusted after each evaporation process based on the film thickness determined from the profilometry measurements. After performing an evaporation, the piezoelectric thickness measurement was adjusted by changing the value of the density entered into the detector. Thus, the density of the film was determined empirically by adjusting the detector to read the thickness of the film determined by an independent method. The thickness of the three evaporated CuPc films, as measured with the piezoelectric quartz crystal microbalance detector, were 2270, 10300, and 7392 angstroms. The assumed density for each evaporation was 1.62, 1.62 ,and 1.45 gm/cm^3. The difference in the densities results from the amorphous properties of evaporated films.

Ellipsometry Results

An ellipsometer with a red laser source (λ=6328 angstroms) was used to measure the evaporated CuPc film thickness. The measured thickness of all three films were approximately 360 angstroms plus the periodicity thickness. The probability of all three films having the same baseline thickness was considered to be extremely small. The reason the film thickness was the same for all three films was subsequently attributed to the absorbance of CuPc at the laser wavelength. CuPc is a blue material, and therefore, absorbs red light. Since the same thickness was obtained for the three different films, this result suggests that only the light reflected from the first 360 angstroms of the CuPc film reached the ellipsometer's detector. The light which penetrates deeper into the film is absorbed. Thus, the resulting measured film thickness would always be the same for films greater than 360 angstroms thick, and it was concluded that this method was unsuitable for measurement of the CuPc film thickness.

Profilometry Results

The thickness of each evaporated CuPc film was measured at several locations on the wafer. The measured thicknesses for each film are listed in Table F-1. The thicker films provided more reliable results since a larger step provides a larger measurement signal. Measurement of film thicknesses less than 2000 angstroms with the profilometer was difficult because of the small signal and comparatively large instrument drift. The density used with the piezoelectric detector was adjusted to 1.45 gm/cm^3 to obtain thickness readings equal to the

Table F-1
Profilometer CuPc Film Thickness Measurements

	Thickness Measurements (angstroms)		
Piezoelectric Detector Thickness	2270	10300	7392
Profilometer Thickness	2300	11200	7400
	2800	11000	8000
	2300	11800	7700
	2700	11800	7500
	2300	11400	7400
	2700	11400	8000
	2300	11200	7900
	2300	12400	7700
		11400	
		12000	
		11800	
		11800	
		11600	
		11600	
		11400	
		11400	
		11600	
		11200	
		11400	
		11200	
		11400	
		11400	
		11200	
Average Thickness (angstroms)	2460	11500	7700

profilometer measurement. This density was selected for the evaporation of the CuPc onto the CHEMFET integrated circuit.

A possible source of error with profilometry measurements is that the measurement stylus may burrow into the film and produce a film thickness measurement that is actually less than the true value. To determine if the burrowing effect was occurring with the measurement of the CuPc films, the films were examined under a scanning electron microscope following the profilometry measurements. As shown in Figure F-1 and F-2, the profilometer stylus did burrow into the CuPc films. The burrowed depth was not determined, but it was considered to be relatively small based upon the close agreement (within 10 percent) between the profilometer and piezoelectric quartz crystal microbalance measurements. Nevertheless, this result indicates that the profilometer thickness measurements underestimate the true film's thickness.

Conclusions

The CuPc film thickness measured in this research is only an estimate of the true thickness. Ellipsometry was found to be unsuitable for measuring the film thickness at a wavelength of 6238 angstroms. The profilometer measurement slightly underestimates the true film thickness since the profilometer's stylus burrows into the CuPc film. Despite this problem, a relatively good estimate of the film thickness was obtained based upon the agreement between the piezoelectric quartz crystal microbalance detector and the profilometer measurements, along with the agreement

between the empirically determined CuPc film density and that reported in the literature.

Figure F-1. Scanning Electron Micrograph of Burrow in the Copper Phthalocyanine Film Produced by the Profilometer Stylus.

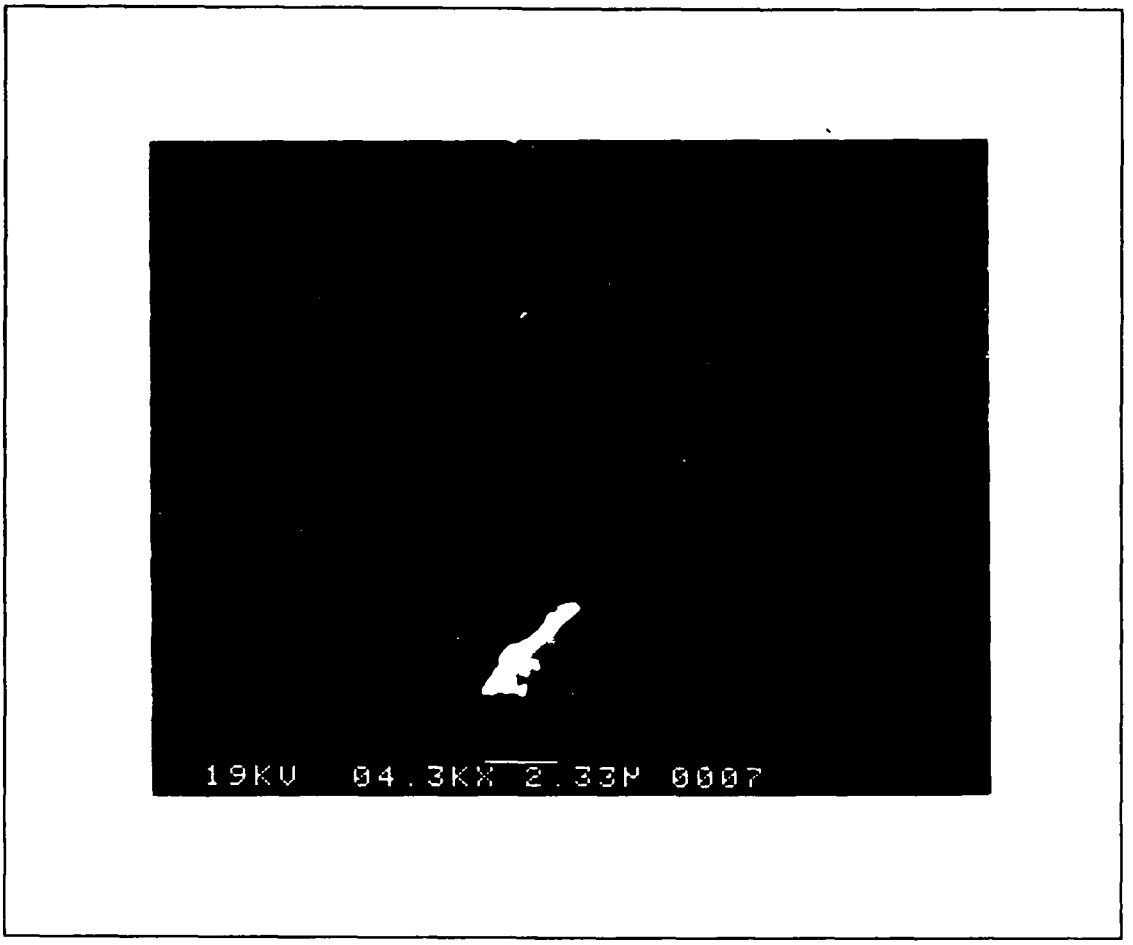

Figure F-2. Enlargement of the Burrow in the Copper Phthalocyanine Film Produced by the Profilometer Stylus.

Appendix G

Electrical Performance Data for the Copper Phthalocyanine-Coated CHEMFET upon Exposure to 40-400 ppb Nitrogen Dioxide

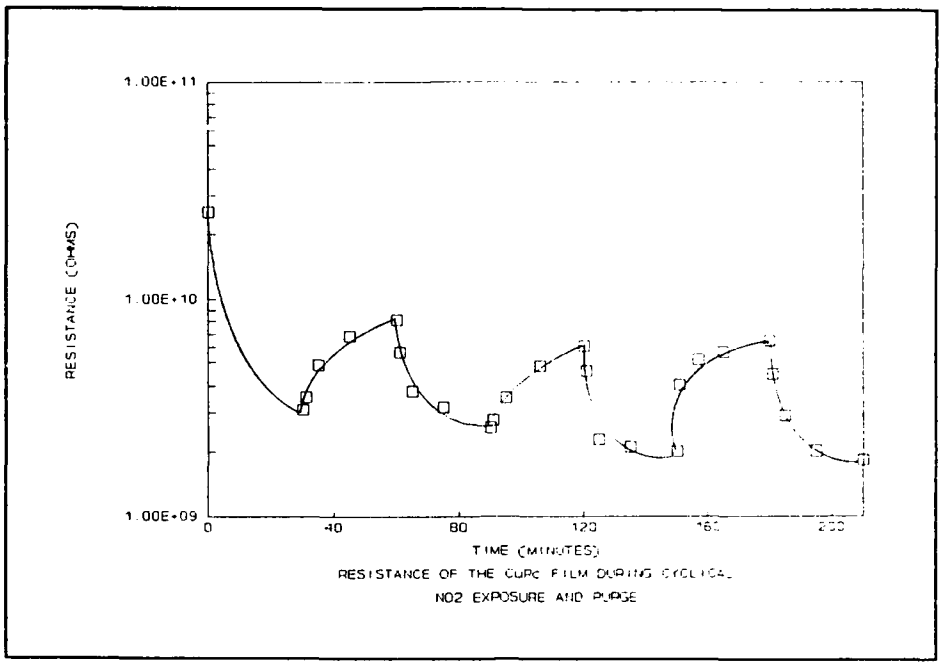

Figure G-1. Resistance of the Copper Phthalocyanine (CuPc) Film During Cyclical Nitrogen Dioxide (NO_2) Exposure and Purge.

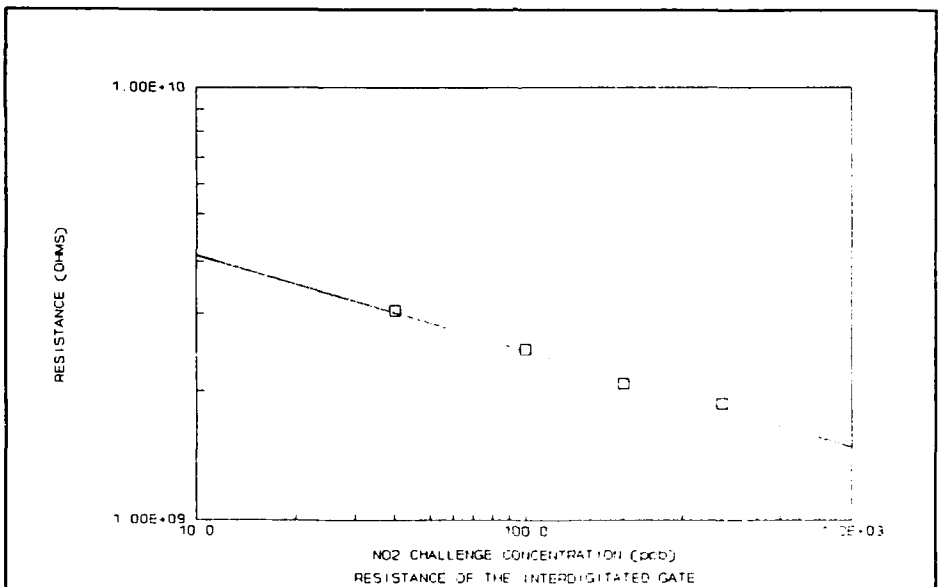

Figure G-2. Interdigitated Gate Resistance as a Function of the Nitrogen Dioxide (NO_2) Challenge Concentration.

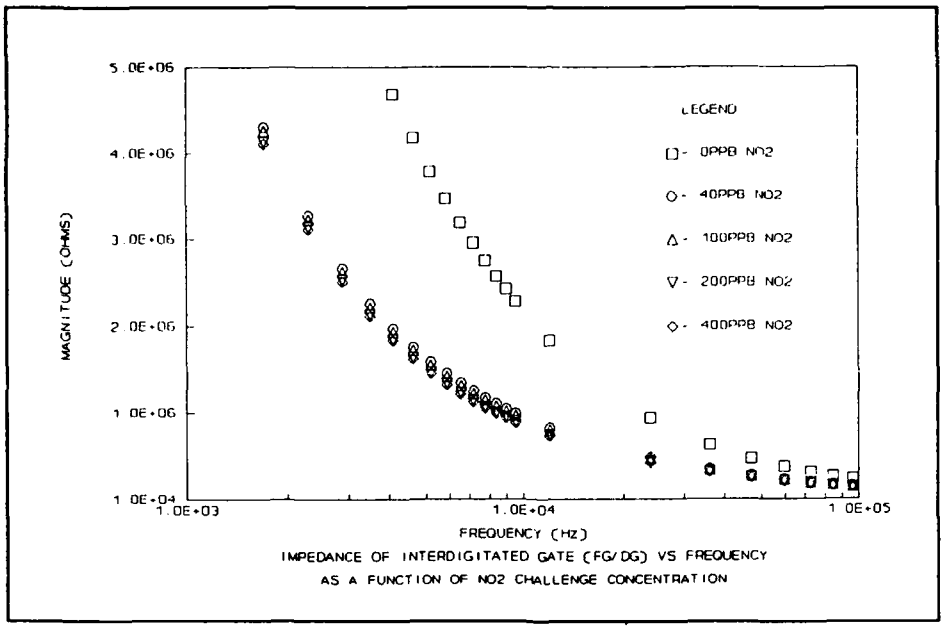

Figure G-3. Impedance of the Copper Phthalocyanine-Coated Interdigitated Gate vs Frequency as a Function of the Nitrogen Dioxide (NO_2) Challenge Concentration.

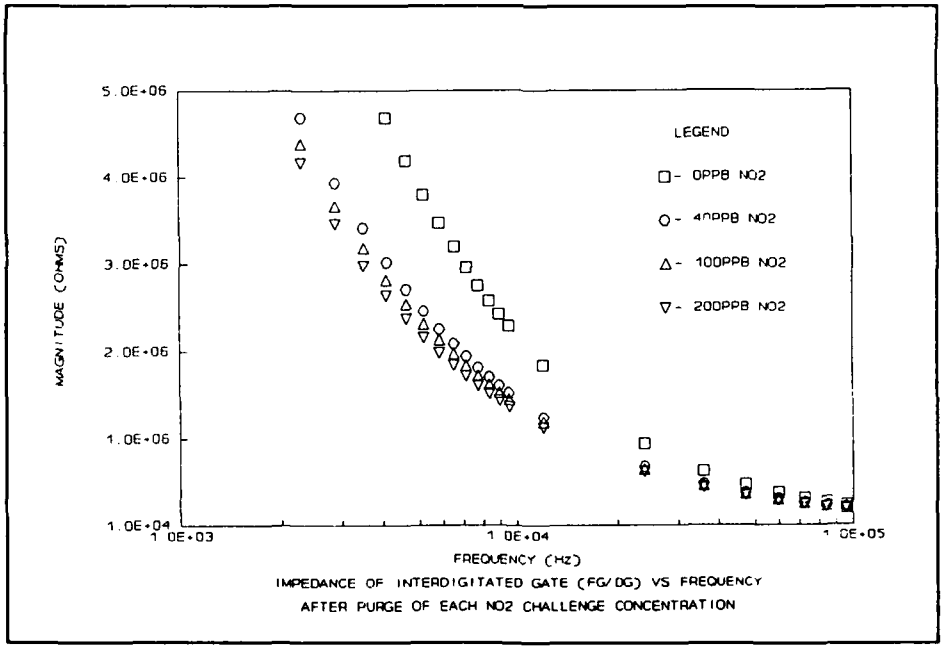

Figure G-4. Impedance of the Copper Phthalocyanine-Coated Interdigitated Gate vs Frequency after Purge of Each Nitrogen Dioxide (NO_2) Challenge Concentration.

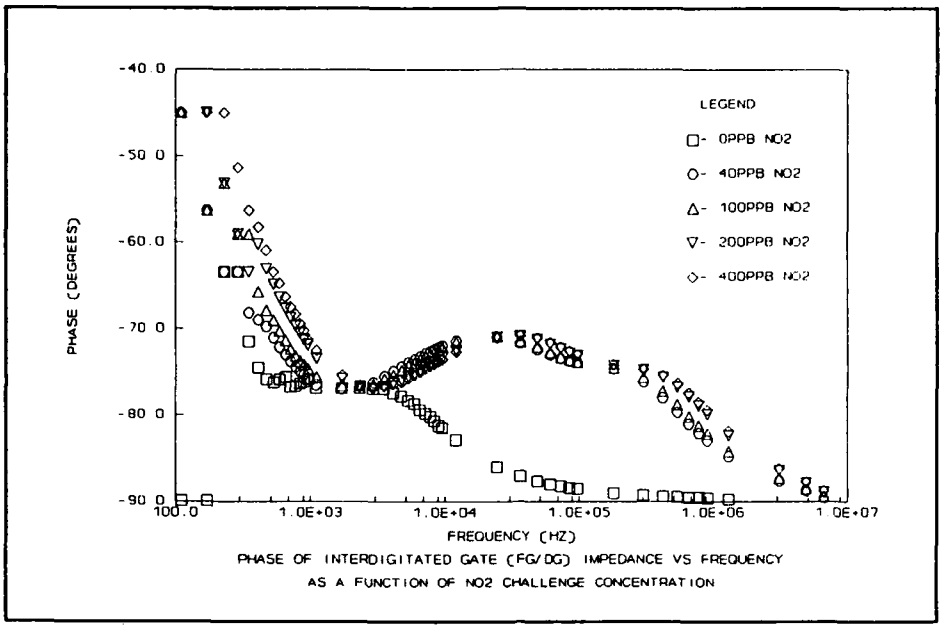

Figure G-5. Phase of the Copper Phthalocyanine-Coated Interdigitated Gate vs Frequency as a Function of the Nitrogen Dioxide (NO_2) Challenge Concentration.

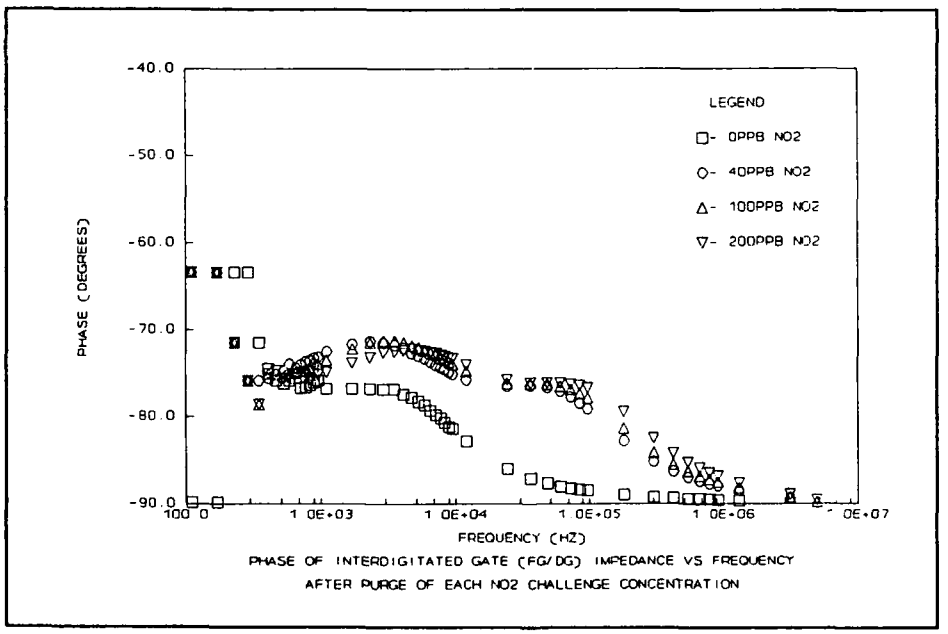

Figure G-6. Phase of the Copper Phthalocyanine-Coated Interdigitated Gate vs Frequency after Purge of each Nitrogen Dioxide (NO_2) Challenge Concentration.

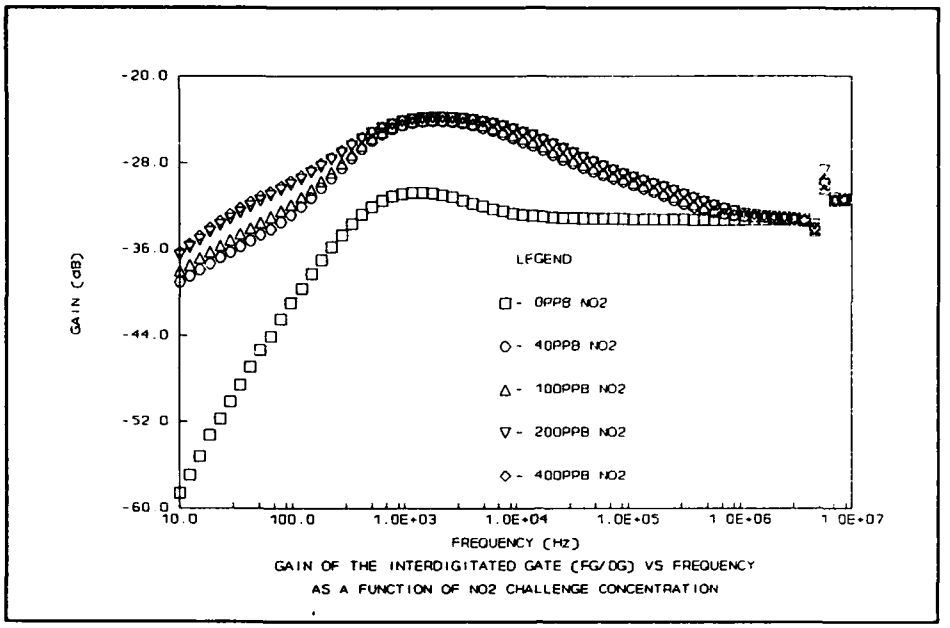

Figure G-7. Gain of the Copper Phthalocyanine-Coated Interdigitated Gate vs Frequency as a Function of the Nitrogen Dioxide (NO_2) Challenge Concentration.

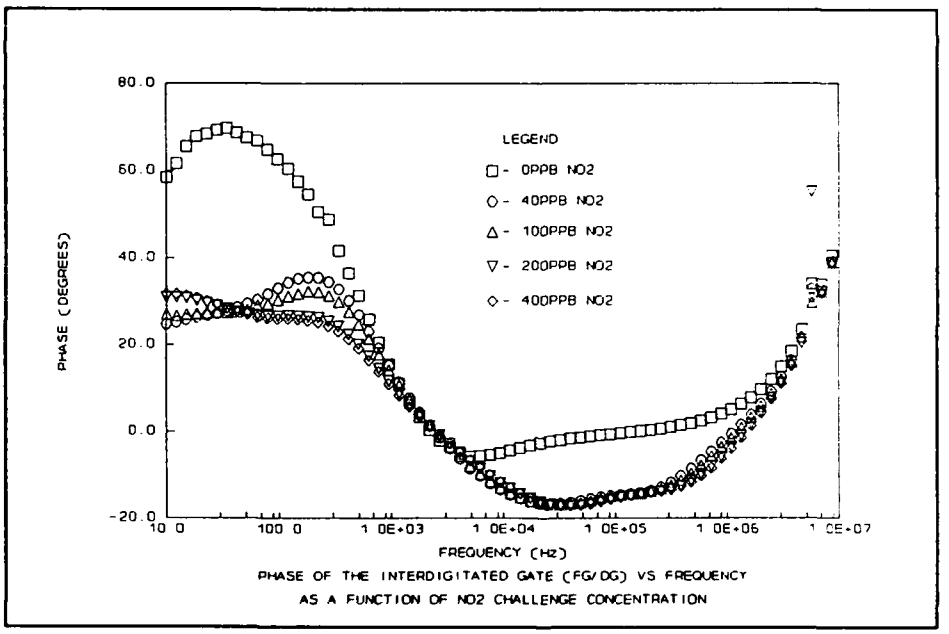

Figure G-8. Phase of the Copper Phthalocyanine-Coated Interdigitated Gate vs Frequency as a Function of the Nitrogen Dioxide (NO_2) Challenge Concentration.

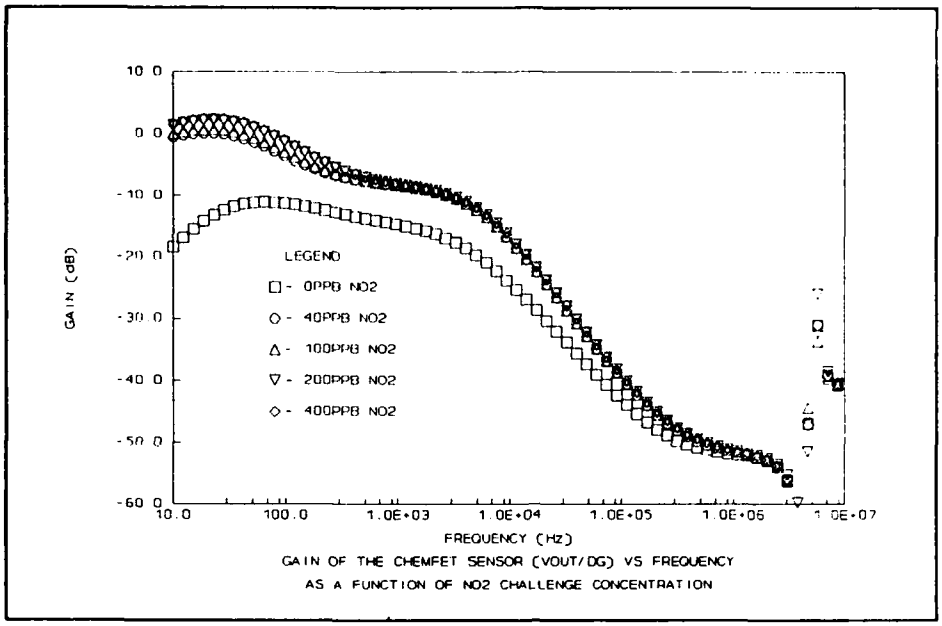

Figure G-9. Gain of the Copper Phthalocyanine-Coated CHEMFET Sensor vs Frequency as a Function of the Nitrogen Dioxide (NO_2) Challenge Concentration.

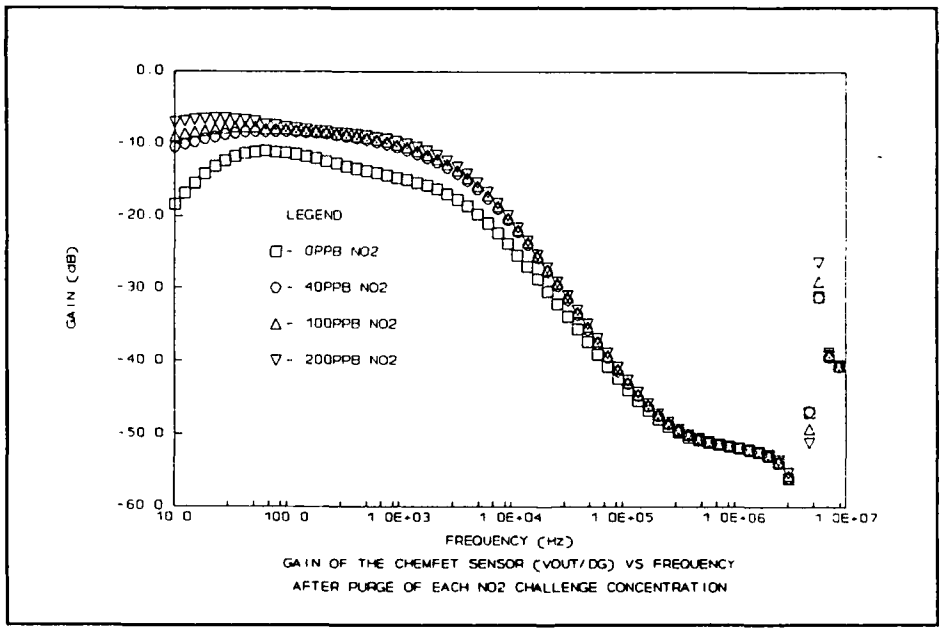

Figure G-10. Gain of the Copper Phthalocyanine-Coated CHEMFET Sensor vs Frequency after Purge of each Nitrogen Dioxide (NO_2) Challenge Concentration.

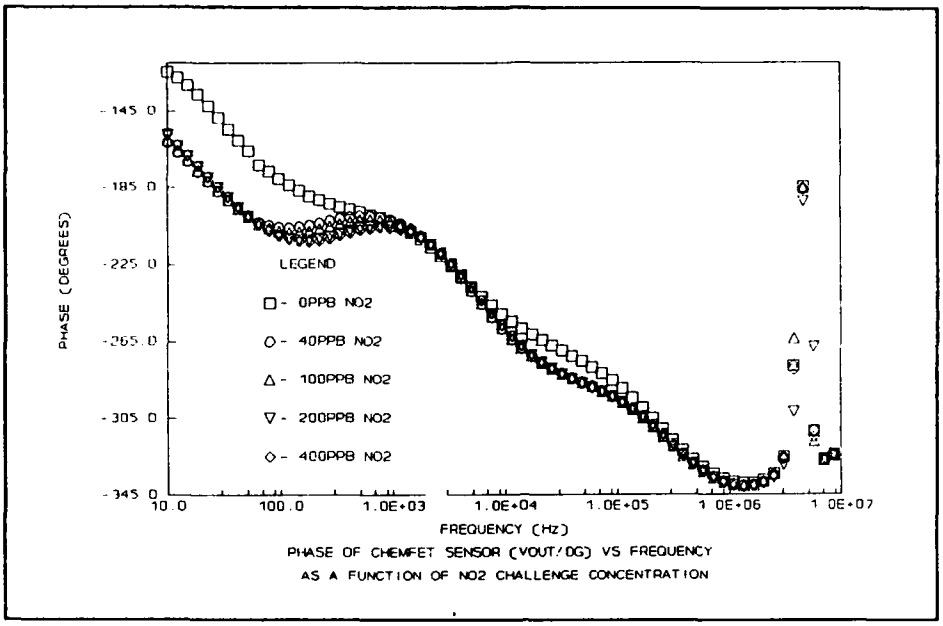

Figure G-11. Phase of the Copper Phthalocyanine-Coated CHEMFET Sensor vs Frequency as a Function of the Nitrogen Dioxide (NO_2) Challenge Concentration.

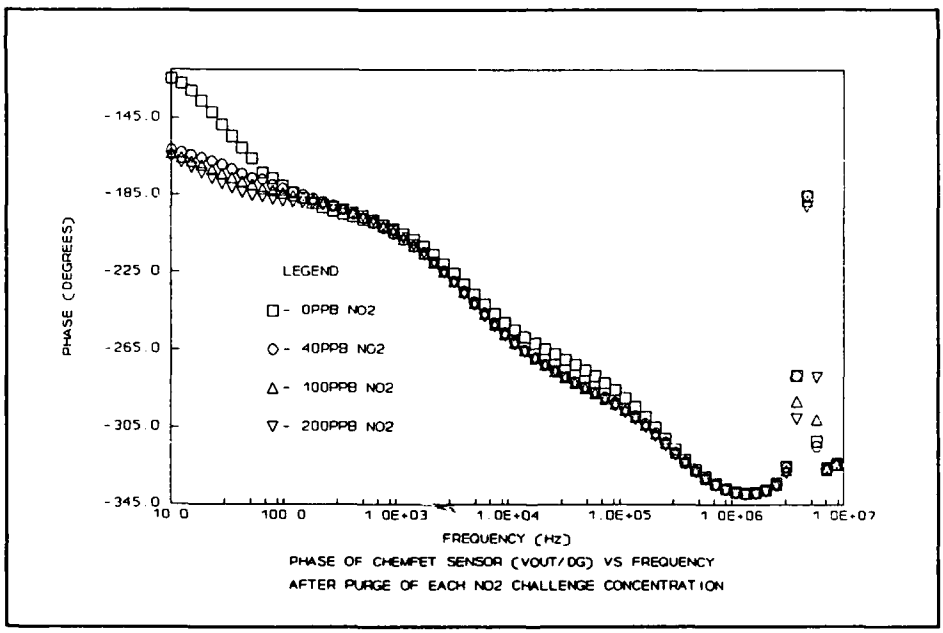

Figure G-12. Phase of the Copper Phthalocyanine-Coated CHEMFET Sensor vs Frequency after Purge of each Nitrogen Dioxide (NO_2) Challenge Concentration.

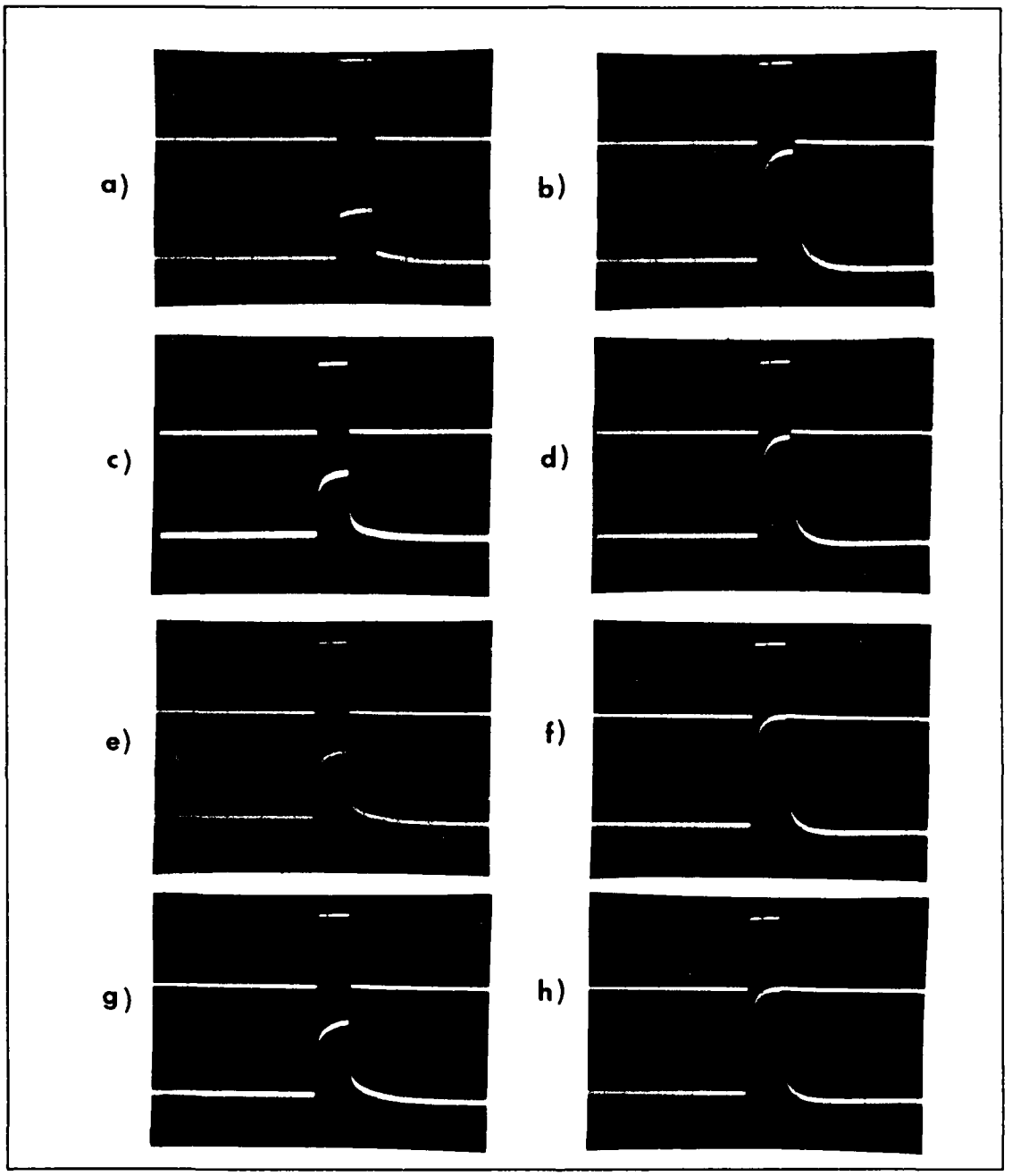

Figure G-13. Time-Domain Response of the Interdigitated Gate to a Pulse Excitation as a Function of the Nitrogen Dioxide (NO_2) Challenge Concentration.

NO_2 Challenge Concentrations: a) No Gas, b) 40 ppb, c) 40 ppb/purge, d) 100 ppb, e) 100ppb/purge, f) 200 ppb, g) 200 ppb/purge, h) 400 ppb. Upper trace: 4V, 50μs Wide Excitation Signal (2V/div). Lower Trace: Floating Gate Voltage (0.2V/div); Horizontal Scale: 50μs/div.

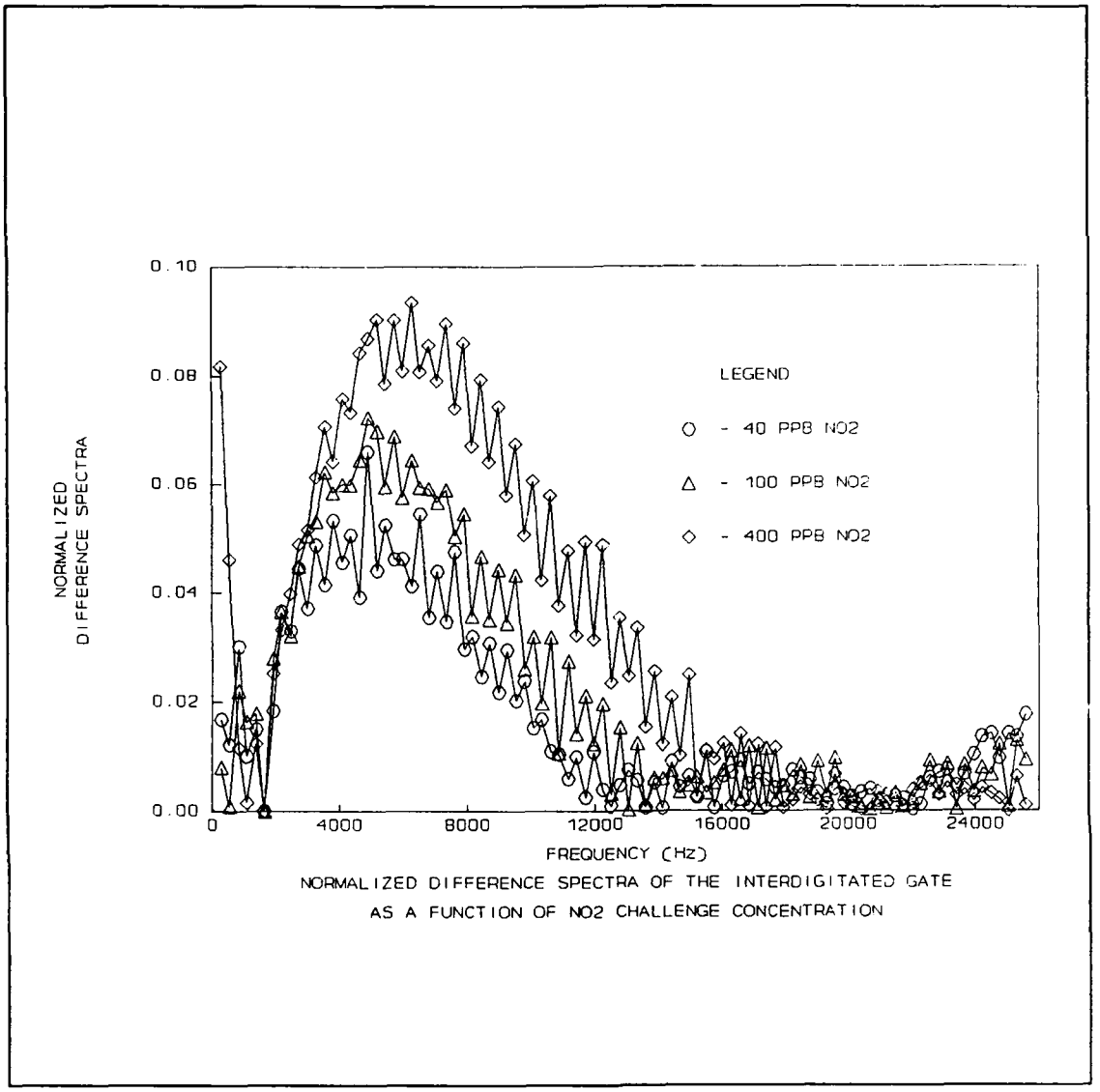

Figure G-14. Normalized Difference Spectra of the Copper Phthalocyanine-Coated Interdigitated Gate as a Function of the Nitrogen Dioxide (NO_2) Challenge Concentration.

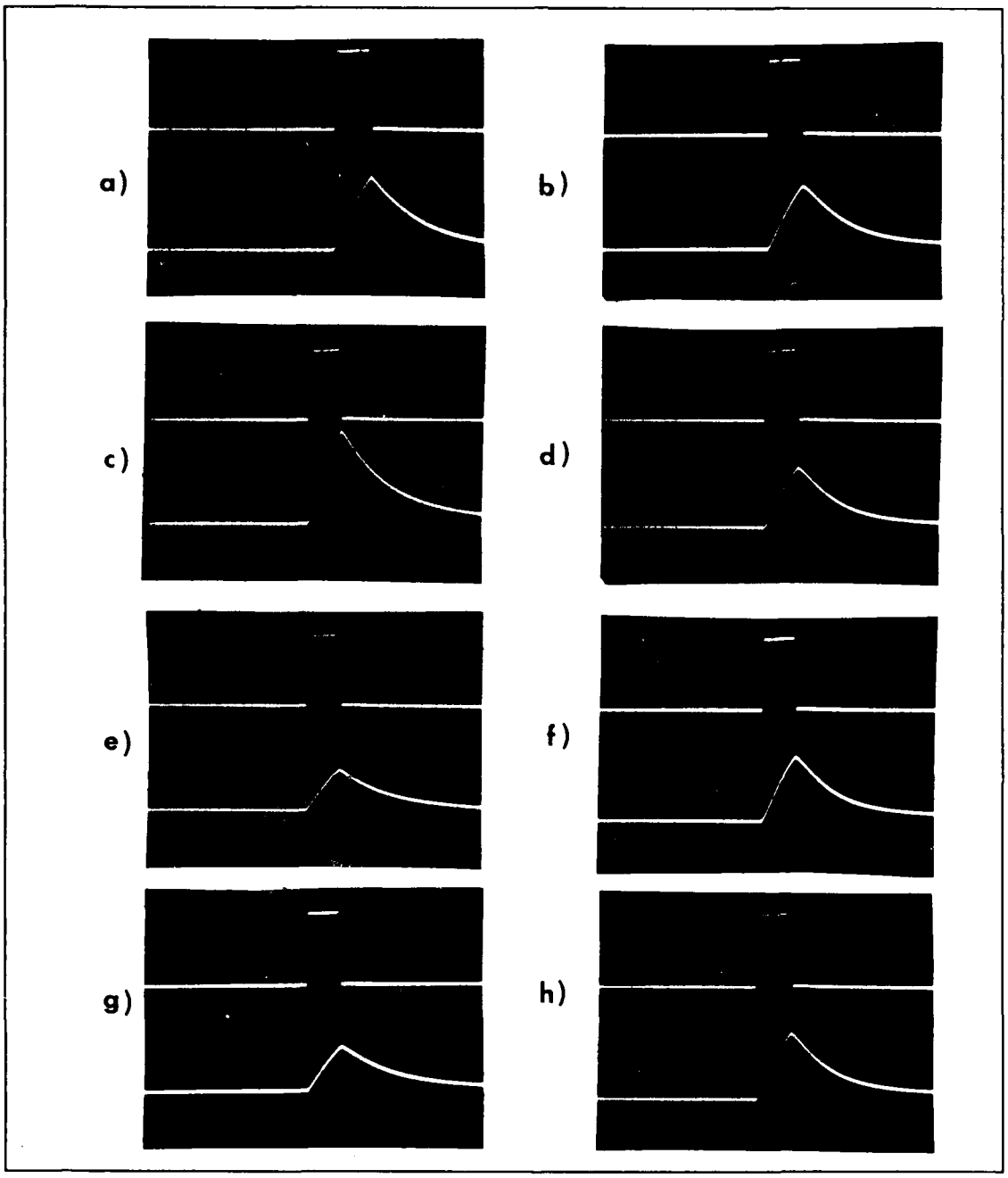

Figure G-15. Time-Domain Response of the CHEMFET Sensor to a Pulse Excitation as a Function of the Nitrogen Dioxide (NO_2) Challenge Concentration.

NO_2 Challenge Concentrations: a) No Gas, b) 40 ppb, c) 40 ppb/purge, d) 100 ppb, e) 100ppb/purge, f) 200 ppb, g) 200 ppb/purge, e) 400 ppb). Upper trace: 4V, 50μs Wide Excitation Signal (2V/div). Lower Trace: Sensor Output Voltage (0.5V/div). Horizontal Scale: 50μs/div.

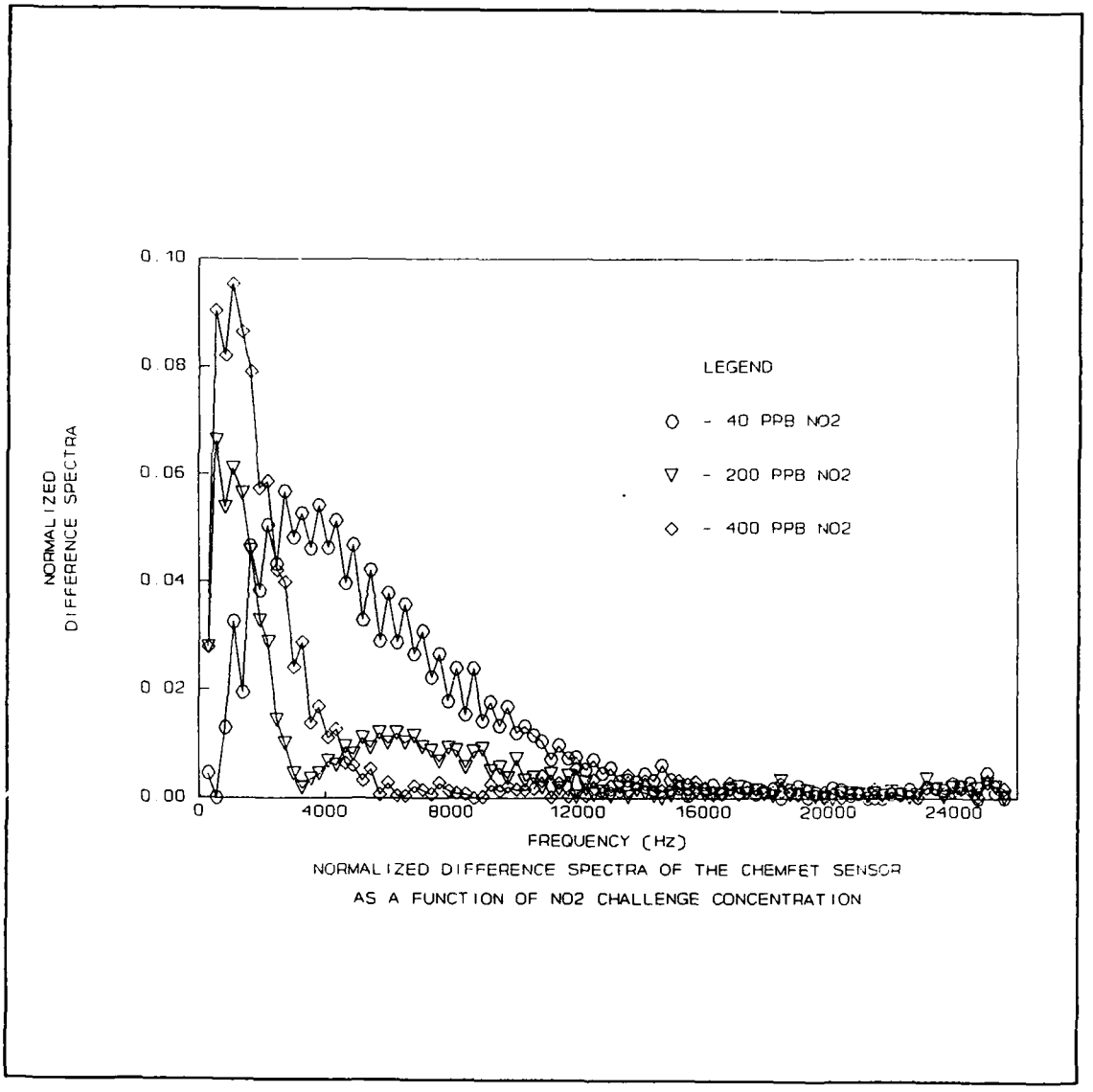

Figure G-16. Normalized FFT Response of the CHEMFET Sensor as a Function of the Nitrogen Dioxide (NO_2) Challenge Concentration.

Bibliography

1. Department of Defense. Design and Acquisition of Nuclear, Biological, Chemical (NBC) Contamination-Survivable Systems. DoD Instruction 4245.13. Washington: Government Printing Office, 15 Jun 1987.

2. Ancman, 2Lt Eileen G. "Weapon System Vulnerability/Survivability in a Chemical Warfare Environment". Presented at the Air University's Symposium on Low Intensity Conflict. Maxwell AFB AL, 11-13 Mar 1985.

3. LaVoie, J., Senior Scientist. Personal Interview. Monsanto Research Corporation, Inorganic Materials and Compatibility Group, Miamisburg OH, 10 Feb 1988.

4. Kolesar, E., Associate Professor of Electrical and Computer Engineering. Personal Interview. Air Force Institute of Technology, Wright-Patterson AFB OH, 2 May 1988.

5. Goldberg, B. and M. Semmel. Dielectric Cure Monitoring: Preliminary Studies. NASA-TM-86452. Huntsville AL: George C. Marshall Space Flight Center, NASA, May 1984 (N64 31378).

6. Janata, J. and R. Huber. Solid State Chemical Sensors. Orlando Florida: Academic Press, 1985.

7. Schuetzle, D. and R. Hammerle. Fundamentals and Applications of Chemical Sensors. ACS Symposium Series 309. Washington D. C.: American Chemical Society, 1986.

8. Senturia, S. et al. Microdielectrometry, Cambridge MA: Massachusetts Institute of Technology, Office of Naval Research, Dec 1979 (AD-A100649).

9. Sheppard, N. Dielectric Analysis of the Cure of Thermosetting Epoxy/Amine Systems. PhD Dissertation. Massachusetts Institute of Technology, Cambridge MA, 1986.

10. Jones, T. and B. Bott. "Gas-Induced Electrical Conductivity in Metal Phthalocyanines", Sensors and Actuators 9: 27-37, 1986.

11. Bergveld, P. "The Impact of MOSFET-Based Sensors", Sensors and Actuators, 8: 109-127, 1985.

12. Schiede E. and G. Guilbault. "Piezoelectric Detectors for Organophosphorus Compounds and Pesticides", Analytical Chemistry, 44: 1764-1768, Sep 1972.

13. Guilbault, G., Y. Tomita, and E. Kolesar. "A Coated Piezoelectric Crystal Coating for Detection of Organophosphorus Compounds and Pesticides", Sensors and Actuators, 2: 43-47, 1981.

14. Guilbault, G. et al. "Piezoelectric Crystal Coating for Detection of Organophosphorus Compounds", Analytical Chemistry 53: 2057-2060, 1981.

15. Kolesar, E. Electronic Detection of Low Concentrations of Organophosphorus Compounds with a Solid State Device Utilizing Supported Copper and Cuprous Oxide Island Films. PhD Dissertation. University of Texas, Austin TX, May 1985 (AD-A158181).

16. Barger, W., H. Wohltjen, and A. Snow, "Chemiresistor Transducers Coated with Phthalocyanine Derivatives by the Langmuir-Blodgett Technique", IEEE International Conference on Solid State Sensors and Actuators, 410-413, 1985.

17. Janata, J. et al. "Chemically Sensitive Field-Effect Transistor to Detect Organophosphorus Compounds and Pesticides", Aviation, Space, and Environmental Medicine, 666-671, Nov 1981.

18. Janata, J. and D. Gehmlich. CHEMFET Chemical Warfare Agent Detector, USAFSAM-TR-83-47. Salt Lake City UT: University of Utah, Dec 1983 (AD-A139636).

19. Smith, A. and J. Cooper. Elements of Physics (Eighth Edition). New York: McGraw-Hill Book Company, 1972.

20. King, W. "Piezoelectric Sorption Detector", Analytical Chemistry 36: 1735-1739, Aug 1964.

21. Wohltjen, H. et al. "A Vapor-Sensitive Chemiresistor Fabricated with Planar Microelectrodes and a Langmuir-Blodgett Organic Semiconductor Film", IEEE Transactions On Electron Devices ED-32: 1170-1174, July 1985.

22. Janata, J. and R. Huber. "Chemically Sensitive Field-Effect Transistors", Ion-Selective Electrodes in Analytical Chemistry 2: 107-174, Modern Analytical Chemistry Series, New York: Plenum Press, 1980.

23. Gutierrez-Monreal, F. and C. Mari. "The Use of Polymer Materials as Sensitive Elements in Physical and Chemical Sensors", Sensors and Actuators 12: 129-144, 1987.

24. Hampel, C. and G. Hawley. The Encyclopedia of Chemistry (Third Edition). New York: Van Nostrand Reinhold Company, 1973.

25. Tredgold, R. et al. "Gas Sensors made from Langmuir-Blodgett films of Porphyrins", IEEE Proceedings 132: 151-156, June 1985.

26. Baker, S. et al. "Phthalocyanine Langmuir Blodgett-film gas detector", IEEE Proceedings 130: 260-263, Oct 1983.

27. Khanna, S. et al. Thin-Film Chemical Sensors Based on Electron Tunneling. DOE/ER/13007-1. JPL-Pub-85-85. Pasadena CA: Jet Propulsion Laboratory, California Institute of Technology, Nov 1985.

28. Nieuwenhuizen, M. and A. Barendsz. "Processes Involved at the Chemical Interface of a SAW Chemosensor", Sensors and Actuators 11: 45-62.

29. Venema, A. et al. "NO_2 Gas-Concentration Measurement with a SAW-Chemosensor", IEEE Transactions on Ultrasonics, Ferroelectrics, and Frequency Control UFFC-34: 148-154, Mar 1987.

30. Nieuwenhuizen, M., A. Nederlof, and A. Barendsz. "Metallophthalocyanines as Chemical Interfaces on a Surface Acoustic Wave Gas Sensor for Nitrogen Dioxide", Analytical Chemistry 60: 230-235, 1988.

31. Burr, P. et al. "A Gas-Sensitive Field-Effect Transistor Utilizing a Thin Film of Lead Phthalocyanine as the Gate Material", Thin Solid Films 151: L111-L113, 1987.

32. Senturia, S. et al. "Cure Monitoring and Control with Combined Dielectric/Temperature Probes", SAMPE Journal 19: 22-26, Jul/Aug 1983.

33. Senturia, S., C. Sechen, and J. Wishneusky. "The Charge-Flow Transistor: A New MOS Device", Applied Physics Letters 30: 106-108, Jan 1977.

34. Lee, H. Optimization of a Resin Cure. MS thesis, Massachusetts Institute of Technology, Cambridge MA, 1982.

35. Senturia, S. et al. The Feasibility of Electrical Monitoring of Resin Cure with the Charge-Flow Transistor. Cambridge MA: Massachusetts Institute of Technology, Office of Naval Research, Dec 1979 (AD-A081977).

36. Sheppard, N. et al. "Microdielectrometry: A New Method for In-Situ Cure Monitoring", Proceedings of the 26th National SAMPE Symposium, 65-76, Apr 1981.

37. Senturia, S. and N. Sheppard. "Dielectric Analysis of Thermoset Cure", Epoxy Resins and Composites IV, edited by K. Dusek. Springer-Verlag Berlin Heidelberg, 1986.

38. Anderson, J. Dielectrics. New York: Reinhold Publishing Company, 1964.

39. Blythe, A. Electrical Properties of Polymers. Cambridge: Cambridge University Press, 1979.

40. Macdonald, J. Impedance Spectroscopy: Emphasizing Solid Materials and Systems. New York: John Wiley & Sons, 1987.

41. Stremler, F. Introduction to Communication Systems (2nd Edition). Reading MA: Addison-Wesley Publishing Company, 1982.

42. Gade, S. and H. Herlufsen. "Windows to FFT Analysis", Sound and Vibration, Instrumentation Reference Issue: 14-22, March 1988.

43. Senturia, S. et al. "In-Situ Measurement of the Properties of Curing Systems with Microdielectrometry", J. Adhesion 15: 69-90, 1982.

44. Sze, S. Physics of Semiconductor Devices (2nd Edition). New York: John Wiley & Sons, 1981.

45. Kiethley Instruments, Incorporated. Instruction Manual, Model 617 Programmable Electrometer. Cleveland OH, 1984.

46. Miller-Stephenson Chemical Company, Incorporated. Epoxy Systems: Technical Information. Danbury CT, Undated.

47. White, A., P. Handler, E. Smith. Principles of Biochemistry (4th Edition). New York: McGraw-Hill Book Company, 1968.

48. Lehninger, A. Biochemistry (2nd Edition), New York: Worth Publishers, 1975.

49. Kolesar, E. and R. Walser. "Organophosphorus Compound Detection with a Supported Copper + Cuprous Oxide Island Film. 1. Gas-Sensitive Film Physical Characteristics and Direct Current Studies", Analytical Chemistry 60: 1731-1736, 1988.

50. Fluka Chemical Corporation. Catalog 15. Ronkonkoma NY, 1986.

51. Hewlett Packard, Incorporated. Operation Manual: Model 4194A Impedance/Gain-Phase Analyzer. Palo Alto CA, 1986.

52. NGK Metals Corporation. Packaging Material: Report of Analysis. Elkhart IN, May 1988.

53. Pirolo, D. Piezoelectric Polymer Tactile Sensor Arrays for Robotics. MS Thesis, AFIT/GE/ENG/87D-52. School of Engineering, Air Force Institute of Technology (AU), Wright-Patterson AFB OH, December, 1987.

54. Renyuan, Q., S. Zurong, and C. Zhongfu. "Refractive Index and Apparent Density of the Evaporated Film of Copper Phthalocyanine", Kexue Tanbao Vol. 26. No.6, 522-525, June 1981.

VITA

Captain John M. Wiseman was born [redacted] He graduated from high school in [redacted] in 1974 and attended the University of Texas at Arlington, from which he received the degree of Bachelor of Science in Biochemistry in June 1978. He was employed at the University of Texas Health Science Center in Dallas, Texas as a research assistant in the field of molecular biology. He joined the United States Air Force in 1981. He attended Officer Training School from November 1981 through February 1982. Under the undergraduate degree conversion program, he attended Louisiana Tech University from which he received the degree of Bachelor of Science in Electrical Engineering in November 1983. He served in the Program Management Division of the Air Force Space Technology Center, Kirtland AFB, New Mexico as a electrical engineer and program manager from Dec 1983 through May 1987. At the end of May 1987, he entered the School of Engineering, Air Force Institute of Technology.

[redacted]

REPORT DOCUMENTATION PAGE

Form Approved
OMB No. 0704-0188

1a. REPORT SECURITY CLASSIFICATION UNCLASSIFIED	1b. RESTRICTIVE MARKINGS
2a. SECURITY CLASSIFICATION AUTHORITY	3. DISTRIBUTION/AVAILABILITY OF REPORT Approved for public release; distribution unlimited.
2b. DECLASSIFICATION/DOWNGRADING SCHEDULE	
4. PERFORMING ORGANIZATION REPORT NUMBER(S) AFIT/GE/ENG/88D-61	5. MONITORING ORGANIZATION REPORT NUMBER(S)
6a. NAME OF PERFORMING ORGANIZATION School of Engineering 6b. OFFICE SYMBOL (If applicable) AFIT/ENG	7a. NAME OF MONITORING ORGANIZATION
6c. ADDRESS (City, State, and ZIP Code) Air Force Institute of Technology Wright-Patterson AFB OH 45433-6583	7b. ADDRESS (City, State, and ZIP Code)
8a. NAME OF FUNDING/SPONSORING ORGANIZATION Andy Jeffers 8b. OFFICE SYMBOL (If applicable) AFWAL/FIE	9. PROCUREMENT INSTRUMENT IDENTIFICATION NUMBER
8c. ADDRESS (City, State, and ZIP Code) Wright-Patterson AFB OH 45433	10. SOURCE OF FUNDING NUMBERS PROGRAM ELEMENT NO. / PROJECT NO. / TASK NO. / WORK UNIT ACCESSION NO.
11. TITLE (Include Security Classification) See Box 19	
12. PERSONAL AUTHOR(S) John M. Wiseman, B.S.E.E., Captain, USAF	
13a. TYPE OF REPORT MS Thesis 13b. TIME COVERED FROM _____ TO _____ 14. DATE OF REPORT (Year, Month, Day) 1988 December 15. PAGE COUNT 240	
16. SUPPLEMENTARY NOTATION	

17. COSATI CODES			18. SUBJECT TERMS (Continue on reverse if necessary and identify by block number)
FIELD	GROUP	SUB-GROUP	Chemically-Sensitive Field Effect Transistor, CHEMFET, Dielectric Spectroscopy, Sensors, Epoxy Cure, Organophosphorus Compound, Nitrogen Dioxide
09	01		

19. ABSTRACT (Continue on reverse if necessary and identify by block number)

Title: INVESTIGATION OF THE IMPEDANCE MODULATION OF THIN FILMS WITH A CHEMICALLY-SENSITIVE FIELD-EFFECT TRANSISTOR

Thesis Chairman: Edward S. Kolesar, Jr. Major, USAF
Associate Professor of Electrical Engineering

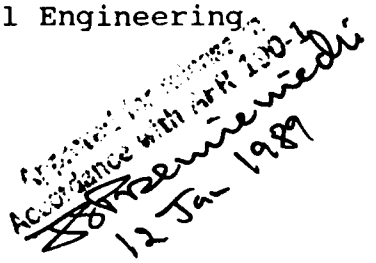

20. DISTRIBUTION/AVAILABILITY OF ABSTRACT ☐ UNCLASSIFIED/UNLIMITED ☒ SAME AS RPT. ☐ DTIC USERS	21. ABSTRACT SECURITY CLASSIFICATION UNCLASSIFIED	
22a. NAME OF RESPONSIBLE INDIVIDUAL Edward S. Kolesar, Jr., Major, USAF	22b. TELEPHONE (Include Area Code) (513) 255-3576	22c. OFFICE SYMBOL AFIT/ENG

Abstract: This study resulted in the design and fabrication of a Chemically-Sensitive Field-Effect Transistor (CHEMFET) with an interdigitated gate electrode structure. The electrical performance of the CHEMFET, both in the time-domain and frequency domain, was evaluated for detecting changes in the molecular structure and chemical composition in three thin films: an epoxy, copper phthalocyanine (CuPc), and acetylcholinesterase (ACHE). The change in the chemical state of a film was manifested as a change in the electrical impedance of the interdigitated gate electrode structure. For the epoxy, its molecular structure changed as a result of the curing reaction. To induce a change in the chemical state of the CuPc and ACHE films, they were exposed to part-per billion concentrations of a challenge gas, either nitrogen dioxide (NO_2) or the organophosphorus compound, diisopropyl methylphosphonate (DIMP). The results clearly show that the CHEMFET can detect chemical and structural changes in an epoxy and CuPc film. The sensitivity of the ACHE film was not unequivocally determined due to long term drift in the ACHE film's electrical properties. The most remarkable result of this effort was the demonstration of a unique selectivity feature in the CHEMFET's frequency dependent response to a challenge gas. The examination of the relative changes in the electrical properties of the CHEMFET at different frequencies showed that the CHEMFET can be used to distinguish between NO_2 and DIMP exposure.